Performance measurement of mobile manipulators

Roger Bostelman

UNIVERSITY OF BURGUNDY

U.F.R. SCIENCES ET TECHNIQUES

THESIS

presented by

Roger BOSTELMAN

to obtain the degree of

DOCTOR OF THE UNIVERSITY

Specialty : COMPUTER SCIENCE

PERFORMANCE MEASUREMENT OF MOBILE MANIPULATORS

Présentée le 16 mars 2018, devant le Jury composé de:

Prof. Lionel ROUCOULES, ENSAM Aix-en-Provence, Rapporteur (Président)

Prof. Rochdi MERZOUKI, Polytech Lille, Rapporteur

Prof. Abdelaziz BOURAS, University Lyon 2, Examinateur

Frédéric SEGONDS, Maître de Conférences ENSAM Paris, Examinateur

Prof. Sebti FOUFOU, Université de Bourgogne, Directeur de Thèse

Prof. Dominique MICHELUCCI, Université de Bourgogne, Coencadrant

Abstract

An advanced approach to flexible manufacturing is to move robotic manipulators, using an AGV or mobile robot, called mobile manipulators, between workstations. The use of mobile manipulators can be advantageous in a number of situations. It can result in cost savings when a single mobile manipulator can be used to replace several stationary manipulators. However, mobile manipulators are "a relatively young discipline within robotics." An extensive literature review of the research leading to commercial mobile manipulators and mobile robots was performed. The performance measurement of mobile manipulators, including a mobile base with an onboard robot arm, is virtually non-existent. However, mobile manipulators are beginning to appear in manufacturing, healthcare, and possibly other industries and therefore, a method to measure their performance is critical to both manufacturers and users of these relatively complex systems. Measurements of mobile manipulators performing standard tasks (poses and motions) are also non-existent except for simply ensuring that the task has been more or less completed. The task chosen for this thesis is assembly due to its requirement for relatively precise system posing.

Performance test methods have lagged behind safety test methods for mobile manipulators which is progressing towards development of a new safety standard in the US. Metrics for safety and performance of mobile manipulators include many areas, such as: safe operation, task completion, time to complete the task, quality, and quantity (i.e., accuracy and repeatability, respectively) of tasks completed. Prior to industrial acceptance and standards development for mobile manipulators, users of these new systems will expect manufacturers to provide real performance data to guide their procurement and assure suitability for given application tasks. Due to the relatively high cost to procure and setup motion tracking systems to measure systems performance, an alternative method for use by manufacturers and users is ideal. A new test method concept that uses an artifact, called the Reconfigurable Mobile Manipulator Artifact (RMMA), is described in this thesis and compared to an optical tracking system that was used as ground truth for the RMMA and mobile manipulator.

System modeling the mobile manipulator system, components, and the associated measurements can help to improve the understanding of these relatively complex systems. Systems Modeling Language (SysML) was chosen and used throughout this thesis because of SysML has reusable software modules for structure, behavior, requirements and parametrics off the mobile manipulator. The models describe the many aspects of measuring mobile manipulator performance also as new research area. The models were evaluated through experiments on an example mobile manipulators' components and the entire system. SysML was used to describe the theoretical basis of the performance through propagation of uncertainty where mathematical equations are also modeled.

A use case is modeled and described where the concepts researched to measure mobile manipulator performance are applied to a manufacturing implementation. The simplistic nature of the measurement process using the RMMA can be directly applied to today's manufacturing processes, and extended beyond the contributions of this research to other even more complex measurement needs. The research is also discussed to even apply to cross-industry test methods for exoskeletons worn by humans.

Résumé

Une approche avancée de la fabrication flexible consiste à déplacer les manipulateurs robot entre les postes de travail, en utilisant un véhicule autonome ou un robot mobile, appelé manipulateurs mobiles. L'utilisation de manipulateurs mobiles peut être avantageuse dans plusieurs situations. Par exemple, cette utilisation peut entraîner des économies de coûts lorsqu'un seul manipulateur mobile est utilisé pour remplacer plusieurs manipulateurs stationnaires. Cependant, les manipulateurs mobiles sont «relativement jeune dans la robotique». Une étude approfondie a été réalisée sur les travaux de recherche qui ont menée au développement de manipulateurs mobiles commerciaux. Cependant, la mesure de la performance des manipulateurs mobiles, y compris une base mobile avec un bras de robot à bord, est pratiquement inexistante. Les manipulateurs mobiles commencent à paraître dans les secteurs de la fabrication, de la santé et éventuellement d'autres industries et, par conséquent, une méthode pour mesurer leur performance est essentielle pour les fabricants et les utilisateurs de ces systèmes relativement complexes. Les mesures des manipulateurs mobiles exécutant des tâches classiques (poses et déplacements) sont également inexistantes, sauf pour s'assurer que la tâche a été plus ou moins complétée. Pour ce travail de thèse, nous nous concentrons sur les manipulateurs mobile exécutant une tâche d'assemblage. Cette tâche est choisie car elle exige un système de pose très précis.

Les méthodes de mesure de performances des manipulateurs mobiles n'ont pas connu les mêmes avancées que les méthodes de test de sécurité qui progressent vers le développement d'une nouvelle norme de sécurité aux États-Unis. Les mesures pour la sécurité et les performances des manipulateurs mobiles incluent de nombreux domaines, tels que: l'usage sécurisé, l'achèvement de la tâche, le temps nécessaire pour compléter la tâche, la qualité (en terme de précision) et la quantité (en terme de répétabilité) des tâches réalisées. En attendant l'adoption des manipulateurs par l'industrie et le développement des normes appropriées, les utilisateurs de ces nouveaux systèmes s'attendront à ce que les fabricants fournissent des données de performance réelles pour guider leurs choix d'investissement et assurer l'adéquation pour les tâches à réaliser. En raison du coût relativement élevé pour l'achat et la mise en place d'un outil de suivi mouvements pour mesurer les performances des manipulateurs mobiles, il est nécessaire de proposer une méthode alternative pour les fabricants et les utilisateurs. En effet, nous avons conçu et mis en œuvre une nouvelle de méthode de test qui utilise un composant, appelé Reconfigurable Mobile Manipulator Artifact (RMMA). Cette méthode est décrite dans cette thèse et comparée à un système de suivi optique.

La modélisation des composants, des mesures associées, et du flux d'informations d'un système de manipulation mobile peut aider à mieux comprendre ces systèmes relativement complexes. Le langage de modélisation des systèmes (SysML) a été choisi et utilisé tout au long de cette thèse pour représenter le système manipulateur mobile. Le choix de SysML est motivé par le fait qu'il offre des modules logiciels réutilisables pour représenter la structure, le comportement, les exigences et les paramètres du manipulateur mobile. Les modèles ont été évalués à travers des expériences sur un exemple de composants de manipulateurs mobiles et l'ensemble du système. SysML a été utilisé pour décrire la base théorique de la performance par propagation de l'incertitude où les équations mathématiques sont également modélisées.

Un cas d'utilisation est modélisé et décrit où les outils que nous avons développé pour mesurer la performance du manipulateur mobile sont appliqués dans un contexte de fabrication. La nature simpliste de la méthode de mesure proposée, qui utilise le RMMA, permet son application directe aux processus de fabrication actuels et son extension pour mesurer des processus encore plus complexes. L’application de la méthode proposées à d’autres domaines est également discutée.

Table of Contents

LIST OF TABLES

LIST OF FIGURES

1. INTRODUCTION

Industry is making increasing use of robotics for material transport and processing. These robotic systems make use of many innovative sensing technologies [1][2][3][4] and control techniques [5][6][7][8] to improve their versatility and agility. The traditional approach to flexible manufacturing is to use mobile robots to transport materials [7][9] between workstations containing stationary robotic manipulators [5]. Another approach is to move the robotic manipulators between the workstations [10] using an automatic guided vehicle (AGV). This configuration is referred to, as in this thesis, as a mobile manipulator. The use of mobile manipulators can be advantageous in a number of situations. It can result in cost savings when a single mobile manipulator can be used to replace several stationary manipulators. The use of mobile manipulators is also useful in cases where the item being worked on is too large to be easily moved. Throughout this paper the term manipulator will refer to the robotic manipulator arm mounted on the mobile base, and the mobile base will be referred to as the AGV, or in some cases a mobile robot which is typically more autonomous than an AGV. The combination is referred to as a mobile manipulator.

The performance measurement of mobile manipulators, including a mobile base with an onboard robot arm, is virtually non-existent. However, mobile manipulators are beginning to appear in manufacturing, healthcare, and possibly other industries and therefore, a method to measure their performance is critical to both manufacturers and users of these relatively complex systems. Modeling the mobile manipulator can help to reduce the understanding of system complexity and is an overarching computer science theme to this thesis research. Additionally, this thesis: presents the challenges of measuring performance of mobile manipulators; discusses research that defines appropriate methods to measure performance of these systems; and simplifies the measurement method with a novel approach using artifacts to be extended to standard test methods and even measurement beyond mobile manipulators to exoskeletons worn by humans. Section 1.1 states the motivations for performance measurement of mobile manipulators. Section 1.2 provides an overview of the current performance measurements that have occurred for these systems. Section 1.3 presents the challenges related to measuring performance of mobile manipulators as most are currently non-existent. Finally, Section 1.4 presents the structure of this document and briefly describes the proposed approach to address these problems.

1.1. Motivation for Performance Measurement of Mobile Manipulators

The importance and popularity of research toward mobile robots and mobile manipulators (robotic arms on mobile bases) has grown in recent years [11]. This emphasis on research and development has also spiked in recent years due to advances in technology that have enabled broad use of automation and robotics while simultaneously reducing costs. In general, mobile manipulators have been more recently researched and are now becoming commercial tools for industrial use [12][13][14]. In research, considerations have focused on the coordination of movements of the robot and the base to perform tasks since redundant degrees of freedom (DoF) are created by adding the moving base. However, measurements of mobile manipulators performing standard tasks (poses and motions) are non-existent except for simply ensuring that the task has been more or less completed. Safety test methods for mobile manipulators is beginning in the research [15] and is progressing towards development of a new safety standard in the US [16]. Performance

test methods have lacked the same research push. Although mobile manipulators have been researched for use in many areas including marine [17], undersea [18], agriculture [19], and space [20] applications, this thesis mainly focuses on manufacturing, specifically assembly operations, and industrial applications where measurements are performed inside a facility. However, similar performance measurement methods, such as using artifacts described throughout this thesis, could potentially be applied to mobile manipulators used in other industries as well. As shown above, the application of mobile manipulators can be vast and measuring their performance across all applications could appear to be unending. Therefore, it is important for this thesis research to narrow the focus and pose a specific case study to set the context. As assembly is a relatively new and difficult application for mobile manipulators, this shall be the task.

The case study for this thesis therefore includes:

- repeatedly measuring any mobile manipulator to perform assembly tasks,
- a fixtureless mobile base,
- a rapid, non-contact measurement test method for in-situ use,
- a relatively inexpensive measurement system for vast adoption by manufacturers and users.

Associated with this case study is the fact that mobile manipulators must, for example, navigate (e.g., path plan, be controlled, remain stable, etc.) to and dock with an assembly station. Hence, to be thorough, this thesis covers metrics and measurement systems that are useful for all aspects of the case study, including the mobile manipulator components, mobile base, and manipulator.

An example mobile manipulator consists of a six DoF robot arm mounted onboard a wheeled base (e.g., AGV or mobile robot) with two translational and one rotational DoF in the horizontal plane for a total of nine DoF [21]. Some mobile manipulators have more or fewer DoF and may also be equipped with vertical axis motion control of the robot arm base. Holonomic and non-holonomic are frequently used terms throughout mobile robot research to describe system kinematics. Mobile manipulator control can range from manual teleoperation to full autonomy (i.e., an operator or facility management system controls the mobile manipulator using typically high level remote commands to the onboard controller with no direct operator interface).

Two motivations for this thesis research are therefore, mobile manipulator metrics to measure and the measurement system and/or method to do so. Metrics for safety and performance of mobile manipulators include many areas, such as: safe operation, task completion, time to complete the task, quality, and quantity of tasks completed. Inherent in "quality" and "quantity" are the mobile manipulator accuracy and repeatability, respectively. These metrics not only include task completion but also focus on how well and how many times the task was completed.

Prior to industrial acceptance and standards development for mobile manipulators, users of these new systems will expect manufacturers to provide real performance data to guide their procurement and assure suitability for given application tasks. Robot performance measurements typically include the difference in position and orientation (pose), of the end of arm tooling (EOAT) from the commanded robot pose. Without tested measurement methods to ensure mobile manipulator performance, system users must rely on manufacturers specifications that may or may not be valid. Ground truth measurement, used to compare to a system-under-test (SUT), or the mobile manipulator in this case, is "evaluated with respect to a device whose accuracy is well-known and at least one order of magnitude higher than that of the device to be evaluated." [22]

Ground truth measurement using motion tracking systems provides static and dynamic and relatively accurate robot joint, segment, or tool point position information, enabling comparisons with the commanded pose. Review of robot, mobile robot, and mobile manipulator performance measurement research shows that use of motion tracking systems is a relatively new technique for performance evaluation within the research community. However, assurance from these tracking systems also requires that their accuracy meets or exceeds the ground truth, order of magnitude requirement. Therefore, another motivation is to ensure that the motion tracking system is acceptable as a ground truth system and moreover, that it can be used to measure the performance of mobile manipulators.

Due to the relatively high cost to procure and setup motion tracking systems to measure a SUT performance, an alternative method for use by manufacturers and users is ideal. Machined artifacts are not typically used to measure complex systems such as mobile manipulators and rather only sub-components, such as only the robot arm. However, a novel approach is presented in this thesis proving that artifacts can possess the tolerances and system measurement required of ground truth systems while being an order of magnitude higher in accuracy (i.e., less uncertainty) than the SUT. Should the artifact be feasible for such measurements, measurements cost could be dramatically lower, implementation could be much simpler, and a variety of use case scenarios could be tested. Also noted is that the artifacts could potentially be even less expensive to produce through additive manufacturing (i.e., three-dimensional (3D) printing).

1.2. Overview of Current Performance Measurements

Metrics

This section includes references that suggest metrics and benchmarks as being useful and yet lacking in robotics. However, as will be shown, the many metrics and the test methods are lacking that describe and test the functionality of mobile manipulators, including the mobile base and robot arm (manipulator) that makeup a mobile manipulator. Albus [23] wrote: "A major barrier to the development of intelligent systems is the lack of metrics and quantifiable measures of performance. There cannot be a science of intelligent systems without standard units of measure. There are few benchmarks or standardized tests wherein performance can be compared."

Benchmarks play an important role in various aspects. Some see it related to roadmaps where benchmarks may guide developments and make progress in the right directions measurable. Another important aspect is the relation to standards [24]. Benchmarks are the framework leading to standards and alternatively, standards can foster the requirement for benchmarks in a field. This section describes the metrics for mobile manipulators and research that has occurred in this area. Besides the development of a three-dimensional, statistical, evaluation framework for performance measurement of robotic systems [25] dated 1998, the majority of references date research in this area within only the last 14 years (i.e., 2002 – 2016) implying that there is a relatively new thrust in measuring robot performance.

Here are eleven examples from mobile robot and mobile manipulator researchers in references [26] through [36], dating relatively recently from 2002, citing usefulness to directly compare measured results, as well as how the results are obtained (i.e., test methods). Mobile robot navigation is a highly researched robotics challenge and one of the key capabilities for robot autonomy. Navigation techniques have become more and more reliable, but evaluation mainly focuses on individual navigation components (i.e., mapping, localization, and planning) using

datasets or simulations. As an example, performance measures are often neglected in the mobile robot navigation research for applications such as: vacuuming, surface coating, and systematic foraging. In 2002, Wong et al. [26] presented two metrics for measuring performance of robot coverage (i.e., volume accessed by the robot) tasks and applied them to a real robot coverage experiment: percentage of coverage and distance traveled by the robot. The study found that the percentage of coverage is a good performance indicator if physical limitations of the robot are considered. On the other hand, distance traveled alone is a poor indicator because it completely ignores the amount of area (mobile base plus onboard manipulator) covered by the mobile manipulator. In 2014, Sprunk et al. [27] defined an experimental protocol to evaluate the whole navigation system, deployed in a real environment. To ensure repeatability and reproducibility of experiments, their benchmark protocol provided detailed definitions and controls for the environment dynamics (i.e., variations in different environments). They defined standardized environments and introduced the concept of a reference robot to allow comparison between different navigation systems at different experimentation sites. Wong and Sprunk references established one or more metrics (e.g., work volume) and benchmarks (e.g, navigation repeatability/reproducibility), respectively, and therefore begin to uncover measurement aspects that can be applied to mobile manipulators.

Ioan et al. [28] focused on mobile manipulator motion planning and wrote that the robotics community is seeing a growing awareness of the difficulty to compare, in a rigorous quantitative way, the many research results obtained from many different robotic application areas. Further towards comparison of results, Bonsignorio et al. [29] focused on the issues raised by the replication/reproducibility of results. They suggest that one aspect of these results is "a cornerstone of any scientific methodology," versus being "a basic prerequisite to compare different methods for common problems" previously proposed. In 2003, Jacoff et al. [30] discussed the development and proliferation of metrics in the form of robot test arenas that provide tangible, realistic, and challenging environments for mobile robot researchers interested in (teleoperated) search and rescue applications and other unstructured environments. The concept of test arenas with defined apparatus' or artifacts may also apply to mobile manipulator performance evaluation for industrial environments.

Lampe and Chatila [31] simulated an approach to qualify robot autonomy by measuring robot performance in completing a task as compared to the robot environment complexity. Steinfeld et al. [32] attempted to identify common metrics for task-oriented, human-robot interaction (HRI). HRI can also pertain to mobile manipulators where it is expected that future smart manufacturing systems will work collaboratively with humans. More recently, specific aspects of robot measurements were considered for smart manufacturing implementation. Two examples were in mobile robots used for welding and in dynamic pose estimation, both of which are critical to also consider for mobile manipulator use. Welding requires process validation prior to use in the manufacturing process. However, there is a lack of industry standards for mechanized or robotic welding that can impede the introduction of mobile robotic welding systems in the market place. There is also a lack of generalized fitness measures that gauge the suitability of mobile robot topologies or dimensional designs to a set of tasks and can be used in the design or verification process. Canfield et al. [33] proposed such a metric and demonstrated its use in evaluating mobile robot designs for welding tasks. Similarly, Eastman et al. [34] reported that an unsolved but important problem in intelligent manufacturing is dynamic pose estimation under complex environmental conditions, i.e., tracking an object's pose as it moves in an environment with uncontrolled lighting and background. This is a central task in robotic perception, and a robust,

highly-accurate solution would be of use in a number of manufacturing applications.

As an example of metrics suggested in research for mobile manipulators, Ilnicki and Zadarnowska [35] researched the problem of defining performance measures of doubly non-holonomic mobile manipulators. Results consisted of a definition of the following local performance characteristics: the dexterity ellipsoid, the local dexterity, the energy efficiency, and the motion efficiency.

Accuracy and repeatability, two common metrics considered in robotics, were described in [36]. Here, Shiakolas et al., identified the factors that affect accuracy and repeatability and developed an error tree. They established what they term the "degree of influence" that qualitatively assesses the relative contribution of each kinematic parameter variation to the accuracy and repeatability of rigid manipulators. However, these two metrics are only part of the overall performance criteria of mobile manipulators.

A common 'metrics and test methods are needed' theme was described in references [26] through [36], although each was described referring to only one or more metrics. Based on these few metrics and listed from the writers past research in robotics for industrial use, several other metrics are defined when considering performance of mobile manipulators where the importance of each metric is determined by the commanded task:

- time/task duration – the time for the mobile manipulator to complete a commanded task
- distance traveled – the distance that the mobile manipulator has traveled
- repeatability - the variation in measurements taken of the mobile manipulator with the same conditions per trial
- accuracy - the amount that a mobile manipulator measurement conforms to the correct value
- task completion/effectiveness – how successful the mobile manipulator is in performing a commanded task
- efficiency - the ratio of the expected mobile manipulator performance to the total performance.
- dexterity – the agile or nimble performance of a mobile manipulator
- autonomy – independent control performance of the mobile manipulator
- stability – the firmly established performance of the mobile manipulator
- obstacle detection and avoidance - the ability of the manipulator, mobile base or combined system to perceive and avoid objects in the environment
- exploration of unknown environments - the ability of the manipulator, mobile base or combined system to perceive and navigate the environment that is not currently within the system's map

Measurement Systems

Given the above metrics to consider for mobile manipulators, a survey of performance measurement systems to achieve these metrics as a ground truth tool is therefore necessary. Some examples of metrology methods for measuring performance of mobile manipulators, with technologies used to access parts or assemblies in manufacturing processes, include: physical contact using a touch probe [37], cameras detecting fiducials [38][39], laser interferometry [40][41], theodolites [42] and coordinate measuring arms [43]. An example uncertainty (position accuracy) for the camera calibration system in [39] was 0.1 mm and 0.2 mm for 650 mm and 950 mm target distances, respectively. Metrology methods in accordance with ISO 9283 [44] for

manipulator-only measurement include, mainly, path accuracy and repeatability, and are listed above, which inherently include: overshoot, drift, exchangeability, reorientation, posing time, static compliance, and deviations scoped in the standard.

Contact and non-contact sensors are readily available to measure various aspects of machine performance and are listed below. Each measurement system is numbered and listed in Table 1 and Table 2 where their suggested usefulness in measuring performance of mobile manipulators based on the metrics is also shown. Table 1 shows the usefulness to measure mobile manipulator performance where the systems used to measure mobile manipulator performance "may be constrained" by the measurement system and Table 2 shows the measurement "not constrained" by the measurement system. Not-constrained means only the distance, not the accuracy measurement capability which could also be affected by a minimal distance measurement capability. The "x" means usefulness in measuring performance, the yellow box means that the system has little use in measurement, and the red box means that the system cannot measure performance of the metric. Some limitations are also cited below for measurement systems to measure unconstrained performance of mobile manipulators.

1. Touch probes: contact measurement of positioning systems (e.g., computer numerical controlled machine backlash error measurement) [45].
   [limitations may occur from touch probe measurement distance and digital vs. variable response]
2. Wireless indoor position measurement systems: three typical location estimation schemes - triangulation, scene analysis, and proximity performance comparisons include: accuracy, precision, complexity, scalability, robustness [46].
3. Tools for mechanical design and performance evaluation of robots: Dynamics-based local performance evaluation of manipulator global, open- or closed-chain, and alternative dexterity, link and joint deflections, acceleration radius, elasto-static performance (i.e., robot response to applied loads), and elasto-dynamic performance (i.e., link and moments of inertia) [47].
4. Perception sensing systems: six DoF position and motion capture measurement systems, typically used to track people or other objects, are currently being used for assessing static [48] and dynamic [49] robot performance.
5. Motion tracking camera systems:
   a) using passive fiducial targets [50] affixed to the subjects being tracked with sub-millimeter accuracy;
   b) using active fiducial targets [51] affixed to the subjects being tracked;
   c) two camera opto-electronics measuring system tracks the 3D location of infrared light emitting diodes (LEDs) attached to a robot with resolution of approximately 0.01 % and absolute accuracy of 0.05 % [39].
6. Active camera mounted on a pan/tilt platform: image mapping is used to align images of different viewpoints so that static camera motion detection could be applied. The system extracts moving edges from dynamic images [52].
7. Acoustic and inertial motion tracking systems: obtain two types of measurements, acoustic and inertial, associated with the motion of a body and used extensively for measuring performance of robot systems [53][54].
8. Laser tracking systems (LTS): long range laser, relatively high accuracy, non-contact

measurement system, used extensively to measure robot performance. System use examples are:

[limitations may occur from complex or high-speed motions breaking the line-of-sight beam]

a) Real-time 3D static and dynamic positioning accuracy of a robot end-effector at 12.5 μm –50 μm and wrist orientations to within 2 s of arc [41];
b) LTS used with a vision system for six DoF, dynamic, real-time robot measurement for high-accuracy straightness measurement, precision leveling, and absolute distance metrology [55][56];
c) LTS with an automatic routine to reinsert calibrated parameters into robot/machine calibration tables to improve system accuracy to approximately 10 μm or higher [57].

9. Multiple sensors:
   a) Two lasers: static and dynamic 3D performance measurement using two laser beams to track an optical target attached to the robot end-effector, where target position coordinates are estimated using triangulation [58].
   b) LTS, a laser interferometer system, and a telescopic metrology bar: an LTS and the laser interferometer system are used to measure linear errors along a linear path of motion and angular errors about axes orthogonal to the path of motion, and a telescopic metrology bar is a low-cost, high-precision tool for assessing the static and dynamic positioning performance of industrial robots [59].

   [limitations may occur from complex or high-speed motions breaking the line-of-sight beam]
10. Laser diode with a position-sensitive detector: a non-linear, coupled, and measurement-based dynamic system model, a Lyapunov-type controller based on the deflection feedback to measure the tip oscillations and regulate the endpoint of the flexible robot [60].

    [limitations may occur for dexterity measurement since manipulator endpoint (i.e., three DoF, not six DoF) is measurement]
11. Indoor global positioning system (iGPS): multiple rotating, angled, laser scanners detect the triangulated position of transmitters with measurement accuracy of approximately 200 μm [61][62].

Table 1. Metrics and the corresponding numbered measurement systems to measure mobile manipulator performance where the systems used to measure mobile manipulator performance may be constrained by the measurement system. Boxes marked with an “x” indicate utility in performance measurements, while

boxes highlighted in yellow or red indicate limited or no utility, respectively toward measuring the specified metrics.

metric	1	2	3	4	5a	5b	5c	6	7	8a	8b	8c	9a	9b	10	11
(R)esearch or (C)ommerial	C	C	R	C	C	C	R	R	R	C	R	R	R	R	R	C
time/task duration		x	x	x	x	x	x	x	x	x	x	x	x	x	x	x
distance traveled	x	x	x	x	x	x	x	x	x	x	x	x	x	x	x	x
repeatability	x	x	x	x	x	x	x	x	x	x	x	x	x	x	x	x
accuracy	x	x	x	x	x	x	x	x	x	x	x	x	x	x		x
task completion/effectiveness	x	x	x	x	x	x	x	x	x	x	x	x	x	x	x	x
efficiency		x	x	x	x	x	x	x	x	x	x	x	x	x	x	x
dexterity	x	x	x	x	x	x	x	x	x	x	x	x	x		x	x
autonomy	x	x	x	x	x	x	x	x	x	x	x	x	x	x	x	x
stability		x	x	x	x	x	x	x	x	x	x	x	x	x	x	x
obstacle detection and avoidance		x	x	x	x	x	x	x	x	x	x	x	x			x
exploration of unknown environments	x	x	x	x	x	x	x	x	x	x	x	x	x			x

Table 2. Metrics and the corresponding numbered measurement systems to measure mobile manipulator performance where the systems used to measure mobile manipulator performance are not constrained by the measurement system.

metric	1	2	3	4	5a	5b	5c	6	7	8a	8b	8c	9a	9b	10	11
(R)esearch or (C)ommerial	C	C	R	C	C	C	R	R	R	C	R	R	R	R	R	C
time/task duration		x	x	x	x	x	x	x	x				x		x	x
distance traveled		x	x	x	x	x	x	x	x				x		x	x
repeatability		x	x	x	x	x	x	x	x				x		x	x
accuracy		x	x	x	x	x	x	x	x				x			x
task completion/effectiveness		x	x	x	x	x	x	x	x				x		x	x
efficiency		x	x	x	x	x	x	x	x				x		x	x
dexterity		x	x	x	x	x	x	x	x				x		x	x
autonomy		x	x	x	x	x	x	x	x				x		x	x
stability		x	x	x	x	x	x	x	x				x		x	x
obstacle detection and avoidance		x	x	x	x	x	x	x	x				x			x
exploration of unknown environments		x	x	x	x	x	x	x	x				x			x

If it is considered that measurement systems not marked in red (i.e., 2 through 7, 9a, and 11) are appropriate tools for measuring the metrics listed in Table 2, then a closer look is required to narrow which measurement system is ideal for performance measurement of mobile manipulators.

In near future smart manufacturing, a more flexible, automated environment is expected where mobile manipulators will be ideal tools. This advanced scenario is already being considered as a priority research area to minimize risk to manufacturers and users [63]. Specifically, a chosen task for measurement, therefore, is the advanced application of mobile manipulators used for assembly (see thesis case description in section 1.2) – a task that currently utilizes only workers, fixtured parts in relatively expensive jigs, and fixed robots typically in relatively expensive workcells. Given the system-under-test (mobile manipulator), the assembly task, will therefore be considered to choose the appropriate ground truth performance measurement system. Each of the measurement systems in the tables above are considered for performance measurement of mobile manipulators used in assembly applications towards an ideal measurement system:

- # 2 (Wireless indoor position measurement systems): As described in [46], "the high accuracy measurements in wireless networks may be limited by shadowing, by multipath reflections arriving from misleading directions, or by the directivity of the measuring aperture" and this system is not listed in the sub-millimeter range requirements for assembly (e.g., 0.5 m – 50 m accuracy in most indoor environments). As mobile manipulators would create shadows and cause multipath situations, and continuous sub-millimeter measurement is required, this measurement system is not valid for performance measurement ground truth of mobile manipulators for the thesis case.

- # 3 (Tools for mechanical design and performance evaluation of robots): In this case, they limited their scope to stationary, serial-linked robots, not on mobile systems with metrics of acceleration radius, elasto-static performance (i.e., robot response to applied loads), and elasto-dynamic performance (i.e., link and moments of inertia). Hence, this measurement system is not valid for performance measurement ground truth of mobile manipulators for the thesis case.

- # 4 (Perception sensing systems - *standards*) and 5 (Motion tracking camera systems - *research*): This system is ideal for performance measurement of mobile manipulators since markers are small, the system has a high update rate (currently up to 240 Hz), accuracy is proven with a new artifact presented in this thesis (section 4.1.2) and camera viewing can be setup for any configuration of mobile manipulator application. The differences in 4 and 5a versus 5b and 5c are that active individual targets [51] provide complications due to battery size and battery positioning and active frame targets [39] are cumbersome for measuring small system components (e.g., EOAT with respect to an assembly target). Therefore, measurement systems described in #4 and #5a are considered the most appropriate measurement system for this thesis.

- # 6 (Active camera mounted on a pan/tilt platform) This approach only measures from one vantage point requiring new system setup at each reconfigured system pose. Additionally, off-angles can contribute to accuracy measurement where early research in [52] provided an initial compensation for angular errors down to 3^0 - a relatively large error when the camera is perhaps one to several meters away from the assembly area. Hence, this measurement system is not valid for performance measurement ground truth of mobile manipulators for the thesis case.

- #7 (Acoustic and inertial motion tracking systems) High accuracy acoustic measurement can be disrupted in manufacturing environments due to ambient noise. "Typical drawbacks are latency, update rate, and sensitivity to ultrasonic noises in the environment." [53] Also, drift from inertial systems (e.g., gyros) also cause absolute measurement uncertainty. Hence, this measurement system is not valid for performance measurement ground truth of mobile manipulators for the thesis case.

- # 9a (Multiple sensors: Two lasers): Although potentially high accuracy, beams are broken as the system moves from one pose to another and loses tracking capability. Additionally, each laser measures range and azimuth of a single point where both position and orientation

measurements are required to fully characterize the SUT. Hence, this measurement system is not valid for performance measurement ground truth of mobile manipulators for the thesis case.

- # 11 (Indoor global positioning system - iGPS) Although potentially high accuracy, receivers are very large to place onto the EOAT and assembly. Hence, this measurement system is not valid for performance measurement ground truth of mobile manipulators for the thesis case.

Motion tracking systems (i.e., # 4 and #5) that use perception (i.e., cameras and markers) are therefore defined as the ideal performance measurement ground truth tool for mobile manipulators.

1.3. Challenges of Measuring Performance of Mobile Manipulators

The case study for this thesis is in repeatedly measuring mobile manipulators to perform assembly tasks from a fixtureless base using a rapid, non-contact measurement test method. Associated with this case study, however, is the fact that mobile manipulators must, for example, navigate (path plan, be controlled, remain stable, etc.) and dock with an assembly station. Hence, to be thorough, this thesis covers metrics and measurement systems that are useful for all aspects of the case study, including the mobile manipulator components, mobile base, and manipulator.

The shortcomings of existing research are that there have been relatively minimal performance measures considered for robots and mobile robots with regards to industrial applications where few measures have been published for mobile manipulators. As stated in section 1.2, measures are deeply influenced by the task, the environment, and their specific representation. In 2007, Zadarnowska and Tchon [64] noted that there are challenges in the performance evaluation of mobile manipulators and they considered the controllability of its theoretical configuration. They stated: "It seems that this area has not been explored systematically in the literature." For example, they reference motion generation, coordinated tasks, locomotion, and manipulation, kinematics to drive design, and trajectory planning. In section 2, example planning and control will be discussed where the literature only describes the proposed control concepts and reports results from simulation or physical systems as either having worked or not worked. In other words, there has been no generic measurement technique or test method to compare various mobile manipulator control methods performance nor to compare many of the other metrics described in section 1.2 to the case at hand. This leaves much room for development of an ideal solution for performance measurement of mobile manipulators, a main thrust of this thesis research, where the solution, as suggested by the author, must:

A. Be reconfigurable to measure a variety of mobile manipulator poses;
B. Measure the performance of any mobile manipulator;
C. Be cost effective to manufacturers and users;

The solution suggests reconfigurability as a key point for representing the many assembly situations that occur in industry. Measuring the mobile manipulator performance is the key thrust of the research. And as with solution A, the cost effectiveness of a viable solution will no doubt allow increased adoption by manufacturers and users of mobile manipulators.

The challenges of measuring the performance of mobile manipulators for use in assembly and other applications are therefore:

1. To model the subcomponents-through-the entire system, system and propagation of uncertainties, and use cases applicable to any mobile manipulator;
2. To measure a ground truth system to ensure that it is capable of measuring static and dynamic performance of the mobile manipulator and its subcomponents to at least one order of magnitude better than their manufacturer specifications;
3. To use the ground truth system to measure subcomponents of a mobile manipulator, namely the mobile base and the onboard robot arm (manipulator), to determine their uncertainties;
4. To use the ground truth system to measure a mobile manipulator as a combined system (i.e., mobile base with onboard manipulator) to determine their uncertainties;
5. To develop an ideal solution for measuring the performance of mobile manipulators and to develop a performance measurement test method for manufacturers and users;
6. To simultaneously measure, using a ground truth system, the mobile manipulator performance and the relative pose of the ideal solution that can cost-effectively replace the ground truth system.

Based on these challenges, the models and systems shown in Figure 1 were developed and used where Figure 1 (a) shows a Systems Modeling Language (SysML) package diagram of the systems that are detailed in this thesis. Figure 1 (b) shows a photo of the systems and Figure 1 (c) shows a SysML model block diagram of the mobile manipulator which breaks out the components of each system and the interconnections. These diagrams and the concepts within these diagrams and photo will be discussed further and referred to within this thesis.

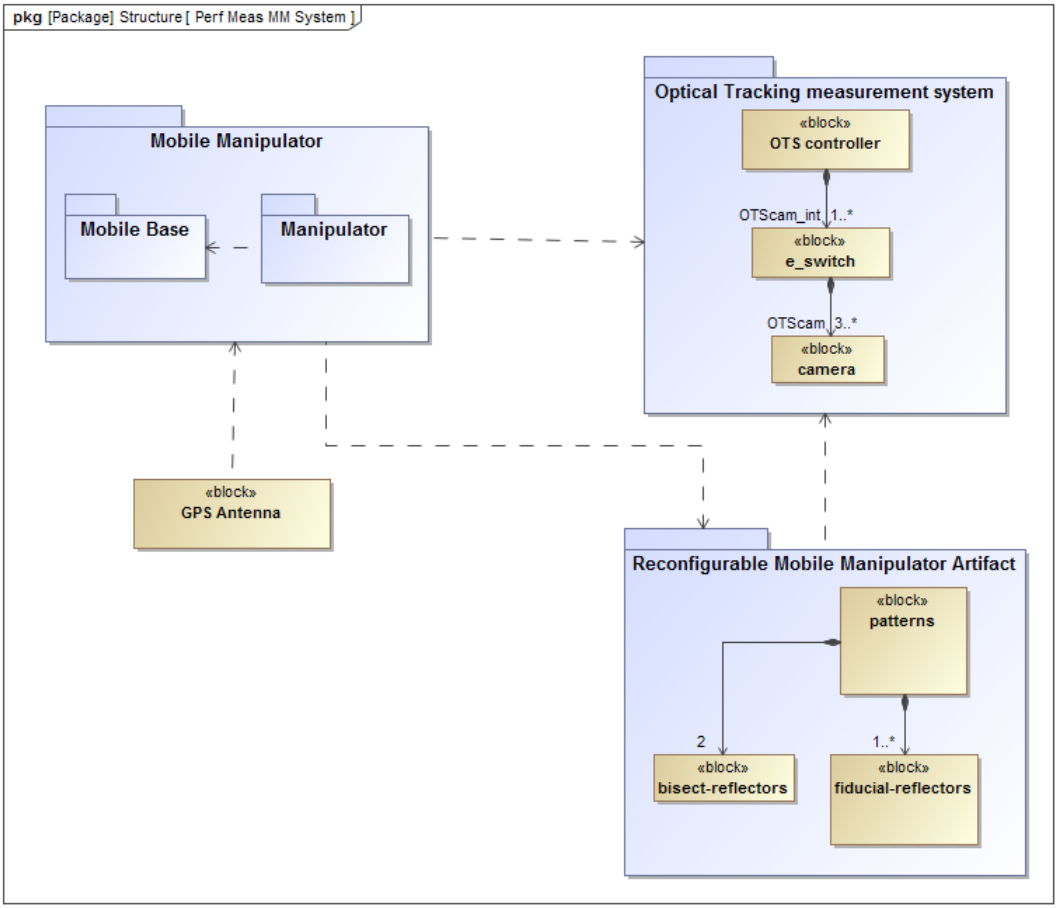
pkg [Package] Structure [Perf Meas MM System]
Mobile Manipulator
Mobile Base
Manipulator
Optical Tracking measurement system
«block»
OTS controller
OTScam_int 1..*
«block»
e_switch
OTScam 3..*
«block»
camera
«block»
GPS Antenna
Reconfigurable Mobile Manipulator Artifact
«block»
patterns
2
1..*
«block»
bisect-reflectors
«block»
fiducial-reflectors

a

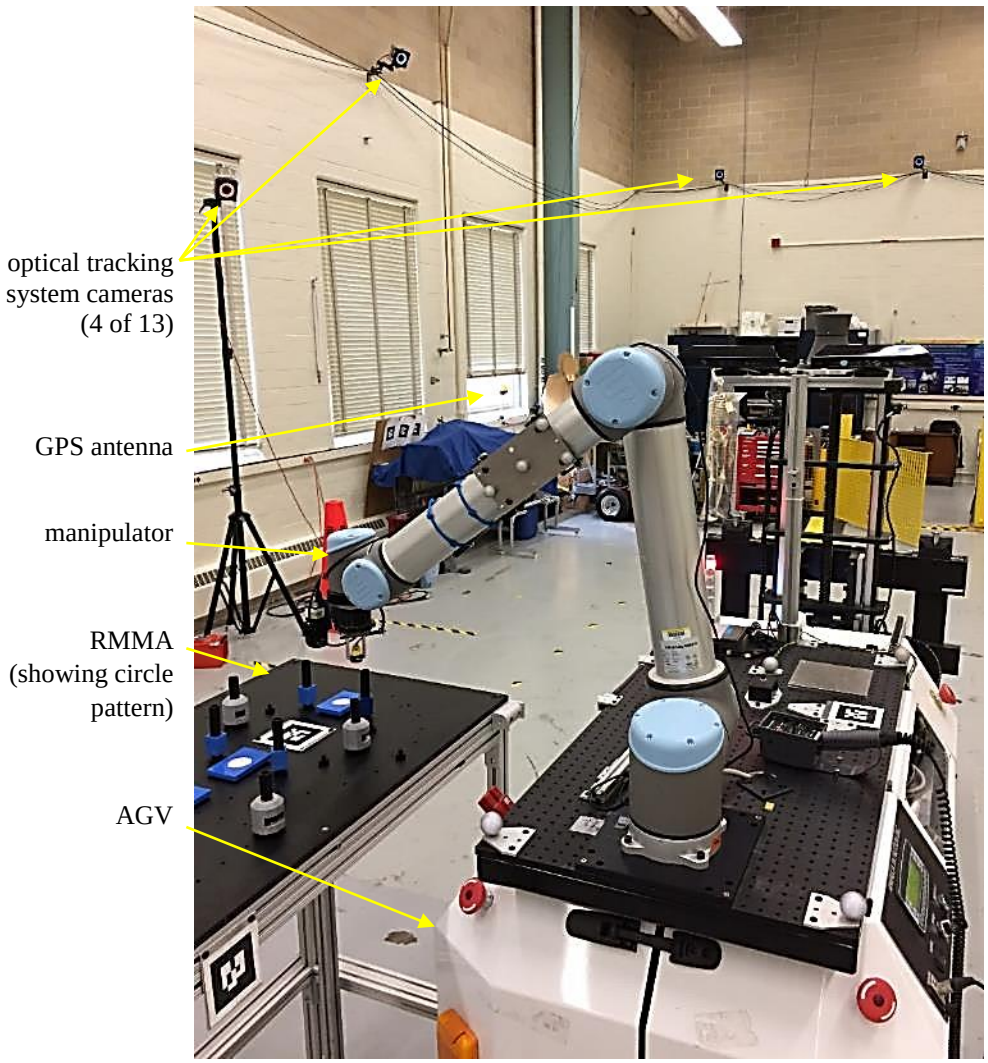
optical tracking system cameras (4 of 13)
GPS antenna
manipulator
RMMA (showing circle pattern)
AGV

b

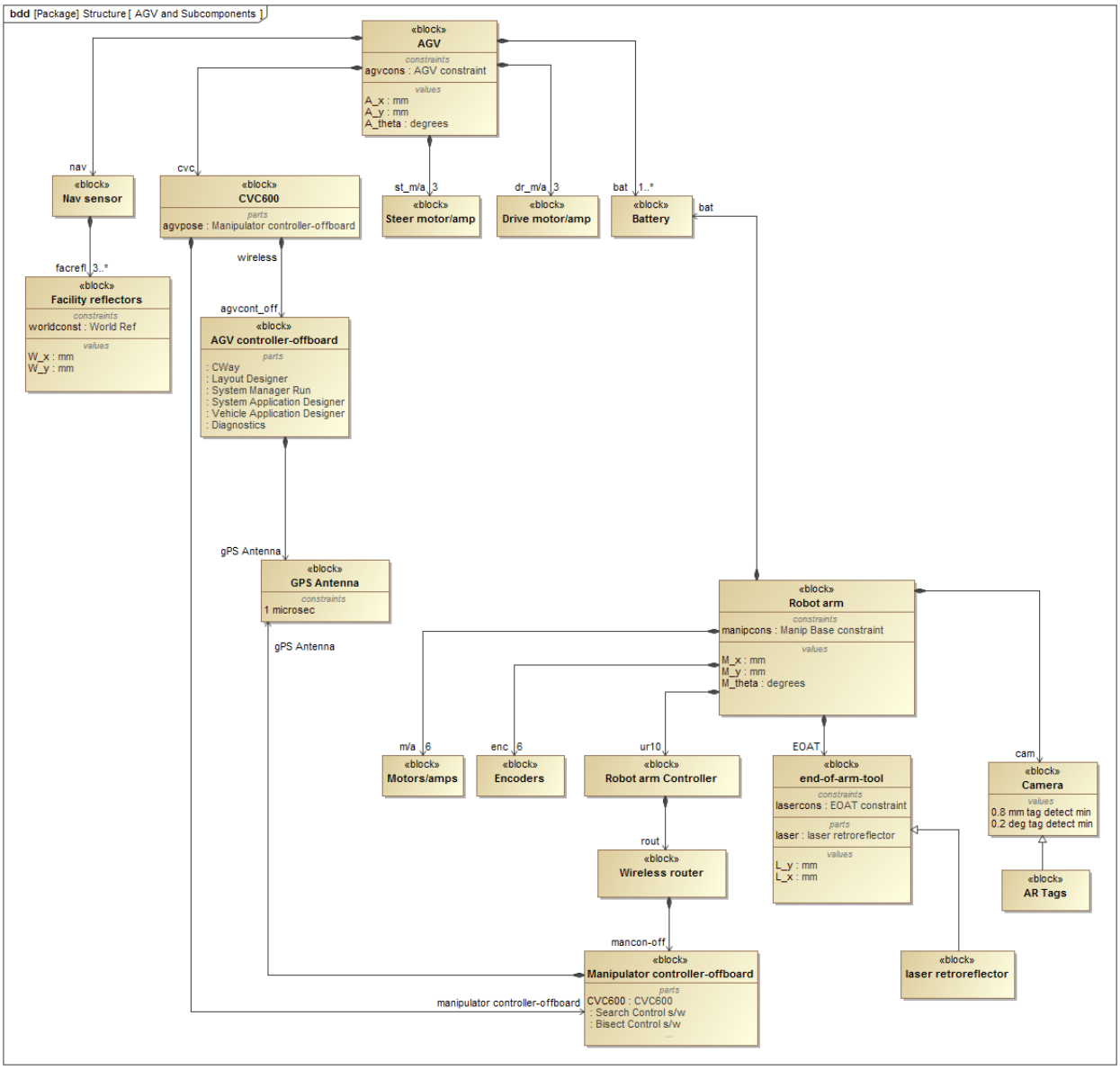

c

Figure 1. (a) SysML package diagram showing the mobile manipulator and measurement system structure. (b) Mobile manipulator and measurement systems used for this thesis. (c) SysML block diagram of mobile manipulator components and interconnections.

1.4. Structure of the Document

In addition to this introductory chapter, this thesis manuscript is organized into six other chapters and a conclusion. As briefly discussed in section 1.3, system modeling is a part of an ideal solution for measuring performance of mobile manipulators since there can be many types of mobile manipulators. Systems Modeling Language (SysML) was used to develop generic models describing the mobile manipulator software and hardware, system uncertainties, use case, as well

as the measurement systems. SysML models are therefore used to describe each section of the mobile manipulator and the performance measurement systems.

Chapter 2 Related Work provides an in-depth literature survey of mobile manipulator research, experimental applications, planning and control, and performance measurements of mobile bases, robots, and mobile manipulators. Also highlighted are calibration, standards, artifacts to evaluate performance.

Chapter 3 Systems Modeling and Measurement Systems describes the use of SysML to provide generic illustration of the mobile manipulator systems and subsystems, measurement systems, systems uncertainties, and a use case. This overarching viewpoint can, not only provide illustration here, but also provide the generic views for performance standards development beyond this thesis. Additionally, this section describes the measurement system models for an optical tracking system (OTS) that is used as ground truth for performance measurements. The chapter continues with description of research performed to measure the uncertainty of the OTS, as well as a description of a novel, reconfigurable mobile manipulator apparatus (RMMA) that is shown throughout the remaining chapters as part of the measurement concept.

Chapter 4 Mobile Base describes the mobile base (automatic guided vehicle or AGV) model, calibration, control program, and navigation performance evaluation. This system provides the highest uncertainty in the mobile manipulator system and therefore defines the key measurement criteria under which the remaining measurements are based.

Chapter 5 Manipulator describes the robot arm onboard the AGV by first describing its model followed by the manipulator control algorithm and performance evaluation. The combination of the mobile base and manipulator are then detailed in Chapter 6.

Chapter 6 Mobile Manipulator Performance Measurement describes the concept and model, the system registration, the system control for both the base and manipulator, the time correspondence between systems, the propagation of uncertainty among all associated systems, and the use case of the system.

Finally, Chapter 7 Thesis Contributions and Future Work describes efforts already in progress to apply concepts learned within the thesis effort to exoskeleton performance measurements and mobile manipulator performance standards. There is an active standards community and research and development from the mobile base, manipulator, and mobile manipulator areas can provide necessary input to develop generic test methods for both safety and performance standards already being developed.

2. RELATED WORK

This chapter provides a literature review of mobile manipulator research representing the state-of-the-art, beginning with examples of experimental applications. [65] The chapter also provides an extensive list of planning and control references as this has been the major research focus for mobile manipulators which factors into performance measurement of the system. The chapter then reviews performance metrics considered for mobile robots, robot arms, and mobile manipulators and the systems that measure their performance. Emphasis is placed on tracking systems for dynamic measurements as needed for mobile manipulators. Lastly, the chapter includes a section on performance measurement research for robots, mobile robots, and mobile manipulators, beginning with calibration, standards, and mobile manipulator artifacts being considered for evaluation of mobile manipulator performance. However, this chapter does not include grasping and in-hand manipulation of objects as the notion of performance measurement includes non-contact measurements. As noted in section 1.1, the case study for this thesis will be compared to the current state-of-the-art demonstrating the lack of performance measurements and replicable performance measurement test methods for mobile manipulators, which include the following:

1. Complete (demonstrate) the commanded (assembly) task, including navigation to the task area,
2. Fixtureless mobile manipulator,
3. Non-contact measurement,
4. Rapid measurement
5. Relatively inexpensive measurement system.

2.1. Mobile Manipulator Research

Expert researchers reported in 2005: "Autonomous mobile manipulation is a relatively young discipline within robotics." [66] As is shown in this chapter, much research on mobile manipulation occurred over the last 20 years and much of the research is task specific. The United States (U.S.) National Science Foundation (NSF)/National Aeronautics and Space Administration (NASA) Workshop on Autonomous Mobile Manipulation wrote that mobile manipulation combines a wide variety of research areas, ranging from force control to mechanism design to computer vision. Workshop recommendations for U.S. research laboratories included creating technological foci in the area of dexterous manipulation and physical interaction, among other critical areas. Programmatic recommendations included development of a simple integrated mobile manipulator aimed at a much lower price point so that it could be widely disseminated.

Mobile manipulators are capable of moving about—and interacting mechanically with—environments, and may be designed specifically to assist human beings in factories and in homes. The Introduction (Section I) references examples of commercial mobile manipulators [1][2][3][6] developed and being used for industrial purposes. An extensive literature review of the research leading to commercial mobile manipulators is provided in this section. As a precursor to mobile manipulator research, a literature review of mobile robot research was performed [11], which also includes a few examples of research on mobile manipulators. An earlier work by Bogh et al. [67] at Aalborg University, Denmark, provided a timeline of mobile manipulators that spans 30 years (see Figure 2). The timeline shows relatively lightweight manipulators on a variety of mobile robots used for research, and effectively concludes with the authors' own platform designed as a

proof-of-concept for general-purpose applications (such as material handling) within an industrial environment.

Many mobile manipulator applications are suggested throughout the research and discussed within this survey, for example:

1. Processing or assembly of large-scale parts such as wind turbine blades or towers
2. Welding of large-scale parts and components
3. Large-scale rapid prototyping
4. Surface processing (sanding, coating removal, or painting) of large systems such as aircraft or ships
5. Conveyor tending
6. Material handling
7. Flexible manufacturing

Processes 1 through 3 include or may include assembly and require, perhaps relatively more accuracy and repeatability than processes 4 through 7. This section provides an in-depth literature mobile manipulator research review divided into sections on: experimental applications and planning and control. Because of the major research efforts in mobile manipulator planning and control, this section is further divided into subsections on: unified motion, trajectory planning, configuration optimization, multiple tasks, stability, obstacle avoidance, outdoor use, and miscellaneous areas.

2.2. Experimental Applications

Through direct experimental applications, several researchers have improved the capabilities of mobile manipulators solving potential future, large volume, robot arm applications. Hamner et al. [5] developed an autonomous mobile manipulator system that was demonstrated experimentally to achieve "peg-in-hole" type of insertion assembly tasks. The system overcame inherent system uncertainties and exceptions by using control strategies that employ coordinated control, combined visual and force servoing, and incorporated reactive task control. A force-controlled, spiral search was used to overcome the positioning uncertainty of the system relative to the assembly environment. This research is similar to this thesis' focus on assembly applications, although the research includes only a demonstration that the mobile manipulator can perform a "peg-in-hole" task and does not provide an ideal, generic solution for performance measurement applicable to any mobile manipulator.

Researchers at Aalborg University described in [68] and demonstrated in [69] how their mobile manipulators initially calibrated to a fixture and then performed peg-in-hole assembly of a rotary shaft for a pump. This research aligns with the thesis assembly case and was fixtureless to the assembly workstation. However, the research required a long period of time (15 min) to achieve the calibration to the workstation. Also, the demonstration shows contact measurement is required for robot arm registration to the workstation. Flannigan et al. [70] developed a mobile manipulator system that utilized remote position sensing of the end-effector to accurately operate over a large work envelope, for example an aircraft wing or fuselage. The goal was to utilize an off-the-shelf, industrial, seven DoF robot arm, an omni-directional mobile platform, and a metrology system. The metrology system tracked multiple objects within a large work space with relatively high accuracy (200 μm) and in real-time. This research also aligns with the thesis to be fixtureless mobile manipulation to a workstation and to position as if performing assembly. However, the research required a relatively expensive indoor GPS measurement system to close-the-loop on end

effector positioning and measurement.

Chen et al. [71] designed a hierarchical intelligent controller using a neural network for the coordinated control of a mobile manipulator that identified and remedied leakage points of jugs filled with dangerous chemicals. The controller consisted of decision, processing, and execution levels. Peterson et al. [72] and Nagatani et al. [73] developed force/torque control of a mobile manipulator to open a door. Alternatively, Chitta et al. [74] showed how to overcome the high-dimensionality of the planning problem by identifying a graph-based representation that was small enough for efficient planning yet contained coordinated arm and base motions to open varying type doors. Pin and Culioli [75] studied a particular aspect of the mobile manipulator kinematic redundancy resolution for material handling tasks. Specifically, they studied the system's utility to optimize its position and configuration during task commutations to handle changes in task requirements or constraints. Basic optimization schemes were developed for cases when load and position constraints are applied at the end-effector. The research in the above references only provided task completion where the task was not assembly.

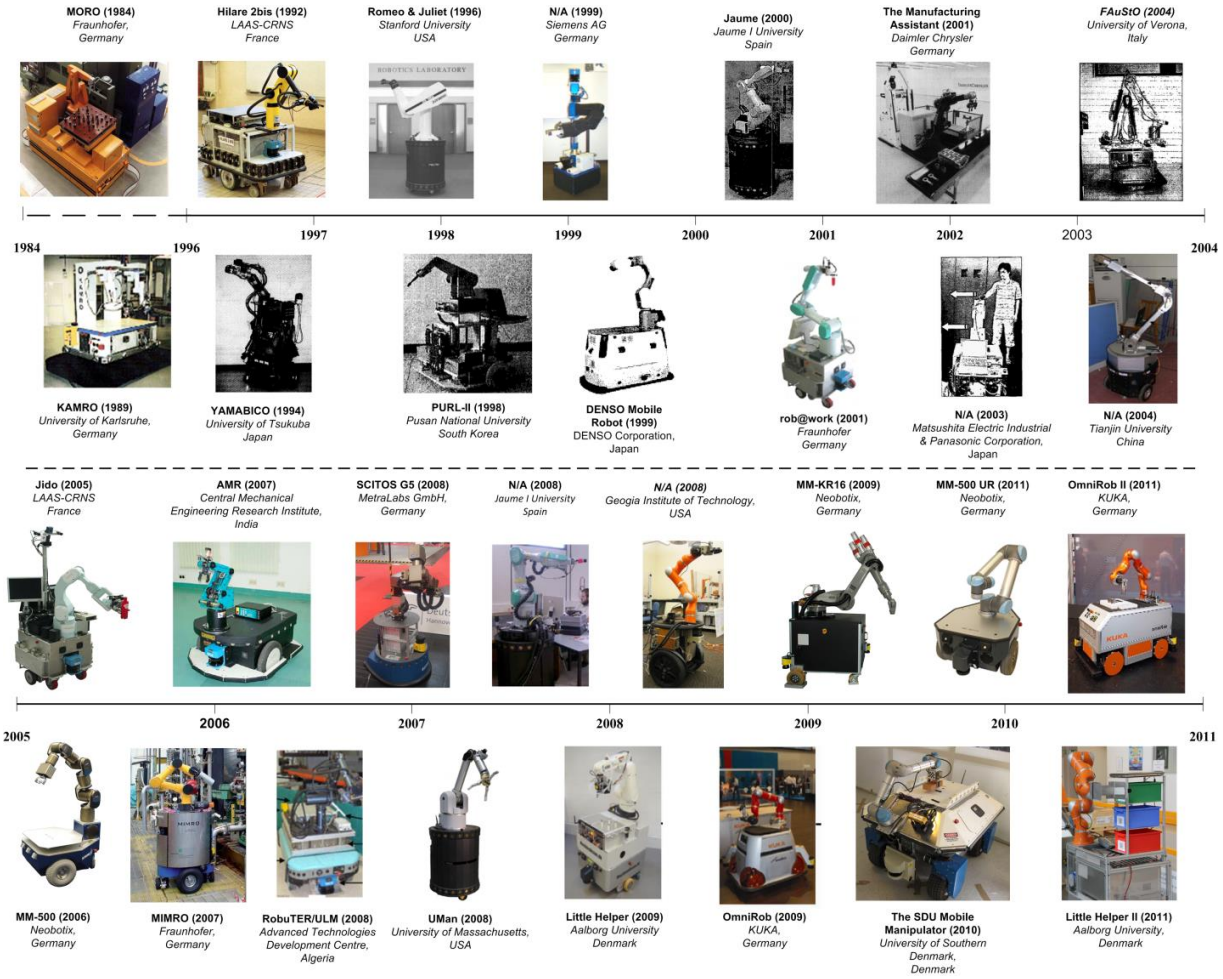

Figure 2. Timeline of mobile manipulator development.

Various optimization criteria have been investigated for task requirements including obstacle

avoidance, maneuverability, and several torque functions. Similarly, although for human assistance, Advait and Kemp [76] developed EL-E (see Figure 3). Once provided with a three-dimensional (3D) location via brief illumination with a laser pointer, the robot autonomously approached the location and then either grasped the nearest object or placed an object. This research is similar to the thesis case with fixtureless mobile manipulation and only demonstrated completion of the task, although not assembly, without repeatable measures of performance.

Agah and Tanie [77] discussed control issues for a service mobile manipulator delivering and handing objects to a human, although not having assembly accuracy requirements. In [78], Tomizawa et al. described a system which used a mobile manipulator as a remotely teleoperated tool to help humans browse books located in a library via the Internet. A voice-guided mobile manipulator was presented by Bort and Pobil [79]. The user could interact verbally with the system to help it localize, identify, database, and pick up objects. Neither of [78] or [79] match the thesis case requirements.

Holmberg and Khatib [80] designed and developed a powered caster vehicle (PCV) which provided the desired smooth, accurate motion and coordination with an onboard manipulator, a holonomic vibration-free wheel system that can be dynamically controlled. They proposed a new approach for modeling and controlling the dynamics of this parallel redundant system. The method for control was demonstrated, although not aligned with this thesis case.

Dual manipulators have also been researched, mainly for material handling. In 1996, Khatib et al. [81][82] developed multiple mobile manipulation systems and the basic models and methodologies for their analysis and control. They extended four fixed base manipulation methodologies to mobile manipulation systems, called Stanford Assistant Mobile Manipulators (SAMM). The methodologies included: "1) the Operational Space Formulation for task-oriented robot motion and force control; 2) the Dexterous Dynamic Coordination of Macro/Mini structures for increased mechanical bandwidth of robot systems; 3) the Augmented Object Model for the manipulation of objects in a robot system with multiple arms; and 4) the Virtual Linkage Model for the characterization and control of internal forces in a multi-arm system." Figure 4 shows a graphical depiction of the SAMM carrying a pipe. As in [80], these two references do not align with the thesis case.

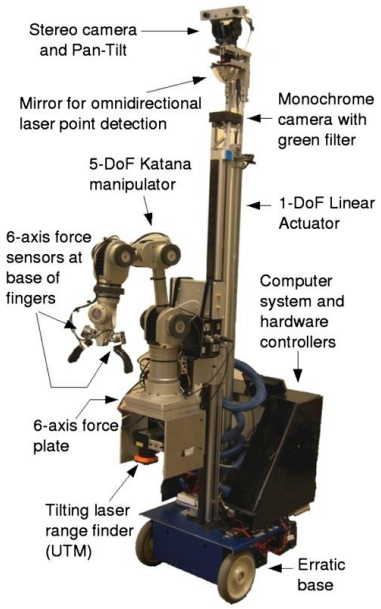

Figure 3. EL-E mobile manipulator

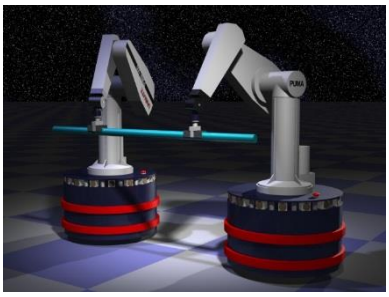

Figure 4. Graphical depiction of the Stanford Assistant Mobile Manipulators (SAMM) carrying a pipe.

Cooperating control (a derivation of force control) of multiple mobile manipulators was later studied by Osumi et al. [83] and Sugar and Kumar [84]. In 2005, Stroupe et al. [85], demonstrated a behavior-based system in which two mobile-base robots perform assembly tasks. One robot served as a master and the other as a slave in the assembly of beams into a structure. Stereo vision was used to locate fiducial marks on the components and force-torque sensing was used during transportation and assembly. The assembly task aligns with this thesis, however no repeatable performance measurement aspects were considered in the research, only that the task was completed.

Beyond the laboratory, Madsen et al. [67] evaluated two autonomous mobile manipulators in a real-world, industrial pump, manufacturing environment. The objective was to integrate the mobile manipulators with existing equipment to increase the technology-readiness-level for industrial use. The two robots worked together to produce rotors over a period of 10 days and were set up in less than a day. The experiment included workspace adaptation, safety regulations, rapid robot instruction and running production. Not included in the Figure 1 timetable is the Meka M1 Mobile Manipulator [13], pictured in Figure 5 which also included a vertical axis for the manipulator. The Meka M1 is being further developed by Alphabet and includes a humanoid system equipped with two compliant manipulators with 6-axis force-torque sensors at the wrist, compliant grippers, a "head" with a 3D sensor, and an omnidirectional wheel base. This interesting experiment aligns with the thesis case, although only through demonstrated of task completion without performance measurements and via a relatively slow setup and assembly.

Figure 5. Meka M1 Mobile Manipulator.

Design of mobile manipulators has also been researched for specific or generic use. Towards design of a mobile manipulator for a specific application, namely automated highway construction and maintenance, Gardner and Velinsky [86] described a systematic, unified, kinematic analysis for manipulator arms mounted to mobile platforms. The differential kinematics for the combined system was used, along with an extended definition of manipulability, to generate a design tool for this class of systems. An example was presented in which a three DoF anthropomorphic manipulator was mounted on a platform powered by two independent drive wheels. Scaled manipulability ellipses were used to visualize the effect of manipulator mounting position on the overall mobility of the system. This research is not aligned with this thesis case, although provides an interesting pre-mobile manipulator design methodology.

2.3. Planning and control

Most mobile manipulator research has been in planning and control due to the redundant DoF, such as the stability of the system with a moving manipulator onboard. This aligns with only the thesis case points regarding navigation to the assembly area and/or stability and manipulation during assembly operations (i.e., measurements). The research is included in this thesis only to be thorough and to align with the metrics listed in section 1.2. However, all of the research published and cited in this section would be ideal to apply to the thesis case and measure the improved performance associated with their research. As such, sections 4.3 and 4.4 describe experiments for navigation and docking performance evaluation, respectively, as they factor into the assembly process.

While complicating planning and control, the kinematic redundancy of mobile manulators is desirable since it allows them to operate under many modes of motion and to perform a wide variety of tasks. The chapter of planning and control, is therefore divided into several areas where research was published, including: unified motion of the manipulator with the base, trajectory planning and coordinated control of the system, the system performing multiple tasks, stability, obstacle avoidance of the manipulator combined with the base, the system use outdoors, and other miscellaneous mobile manipulator research.

2.3.1. Unified Motion

To plan a mobile manipulator's motion, some researchers considered the onboard manipulator as extra joints of the mobile base, where the locomotion controller is part of the manipulator

controller. However, it is difficult to implement both controllers as one since the controllers are typically manufactured by two different companies. In 2000, Papadopoulos and Poulakakis [87] described a planning and control methodology for mobile manipulators, allowing them to follow simultaneously-desired end-effector and platform trajectories without violating the non-holonomic constraints. In 2002, Kim et al. [88] formulated a combined approach for the mobile manipulator mobility and manipulation using a redundant scheme which used zero moment point. In the same year, Nagatani et al. [89] developed a path planning algorithm where the locomotion controller was independent from the manipulator controller, and cooperative motion occurred using communication between controllers. Further, in 2006, Katz, et al [66] considered end-effector-centric, integrated mobility with manipulation, or simply, tool-point control. The combination resulted in an experimental platform that allowed researchers to focus only on end-effector behavior without having to worry about the motion of the remaining DoF. Mailah et al. [90] proposed in 2006 the resolved acceleration control (RAC) and proportional-integral active force control (PIAFC) as an approach for the robust mobile manipulator motion control. The concept utilized a differentially-driven, wheeled, mobile platform with an onboard two-link planar arm. The study emphasized the integrated kinematic and dynamic control strategy in which the RAC was used to manipulate the kinematic component while the PIAFC compensated for dynamic effects, including disturbances and uncertainties. Unified motion of the mobile base and manipulator could provide efficient and fluid motion for assembly processes.

2.3.2. Trajectory Planning

Several researchers have studied trajectory planning. In 1997, Chen and Zalzala [91] developed an approach for the modeling and motion trajectory planning of a mobile manipulator system with a non-holonomic constraint. Tanner and Kyriakopoulos [92], in 2001, used Kane's dynamic equations. Mohri et al. [93], also in 2001, developed a trajectory planning method to optimally control the combined system of a mobile manipulator with the end-effector's specified path. Shin et al. [94], in 2003, presented a motion planning method for mobile manipulators where the base was moved to discrete poses from which the manipulator could be deployed to cover a prescribed trajectory. Finally, in 2011, Tang et al. [95] presented differential-flatness-based, integrated, point-to-point trajectory planning and control. Optimal trajectory planning applied to assembly tasks would be very useful to manufacturers that require efficient assembly processes.

2.3.3. Configuration Optimization

In 1992, Yamamoto and Yun [96] studied a planning and control algorithm for a mobile manipulator so that the manipulator was always positioned at the preferred configurations measured by its manipulability. Simulation results initially proved the intended algorithm result followed by implementation and verification on a real mobile manipulator system. In 1997, Chen and Zalzala [97] described a genetic algorithm approach to multi-criteria motion planning of mobile manipulator systems. Least-torque norm, manipulability, torque-distribution, and obstacle avoidance were considered for multi-criteria, mobile manipulator position and configuration optimization. The emphasis of the simulated study was placed on using genetic algorithms to search for global, optimal solutions and solve the minimax problem for manipulator torque distribution. Both references describe simulated research that could perhaps be applied to assembly, although was not demonstrated as such.

2.3.4. Multiple Tasks

In 1994, Pin et al. [98] focused on minimax planning the positions and configurations in which the system needed to be at task commutation in order to assure that it could properly initiate the next task to be performed. An implementation of the algorithms was performed using the HERMIES-III mobile manipulator. In 1997, Lee and Cho [99] proposed a new motion planning method for mobile manipulators to sequentially execute multiple tasks where, the final simulated configuration of each task was the initial configuration of the subsequent task. The multi-task mobile manipulator research could apply to efficient assembly operations.

2.3.5. Stability

As mentioned in the previous section, stability has been a large area for mobile manipulator research. As a mobile manipulator moves at high speeds and/or if the manipulator carries a non-centric load, the manipulator can dynamically disturb the vehicle, even causing a vehicle to tip over. Mobile manipulators operating in industrial or field environments will be required to apply forces, manipulate loads, and to perform such tasks on uneven terrain which may cause the system to approach, or reach, a dangerous tip over instability. For rapid assembly tasks, navigation from one assembly area to another while carrying nothing or carrying assembly parts or subsystems must abide by stability criteria of the mobile manipulator. Basically, the criteria is to ensure that the mobile manipulator with load center of gravity remains, even instantaneously, within the stable region on the system. To avoid tip over in an automatic system, or to provide a human operator with an indication of proximity to tip-over, a variety of control methods have been researched.

In 1989, Dubowsky and Vance [100] presented a planning method for mobile manipulators which insured that dynamic disturbances did not exceed the capabilities of the vehicle, and compromise its stability, while permitting the mobile manipulator to perform its tasks rapidly. Dubowsky et al. [101] later derived the dynamic equations of a fully spatial mobile manipulator with link flexibility. Huang et al. provided seven works [102][103][104][105][106][107][108] that researched stability of mobile manipulators - two examples are provided here. In 1994, Huang et al. [102] presented a control scheme for maintaining or recovering stability, called the method of zero motion path (ZMP) planning by a stability potential field, considering goal and prohibitive stability states. In 2000, Huang et al. [108] considered both stabilization and manipulation simultaneously while coordinating vehicle motion and manipulator motion. In 2001, Inoue et al. [109] verified their stability control strategy for a mobile manipulator when an external force exists and confirmed this through several experimental results. In 2003, Furuno et al. [110] presented methods of trajectory planning for a mobile manipulator with stability considerations. The proposed planning method was to generate a mobile manipulator trajectory from a given end-effector path when considering stability. Then, a dynamic model of the mobile manipulator was derived considering it as the combined system of the manipulator and the mobile platform. Zero motion point criterion was used as an index for the system stability demonstrated in simulation. In 2007, Shibata and Murakami [111] described a control strategy of mobile manipulator null space motion which used passivity-based stabilization of end-effector position. The research was verified by simulations and experiments of a two-wheeled mobile manipulator.

In 1996, Papadopoulos and Rey [112] defined a measure of available stability margin and in 2000 [113], they applied the force-angle stability measure which: had a simple geometric interpretation, was easily computed, and was sensitive to changes in center of mass height. Force-angle performance measurement was compared with that of other stability margin measures using a forestry vehicle simulation. In 2006, Thibodeau et al [114] compared whole body postural control

of humanoid robots to mobile manipulators, i.e., robot arms mounted onboard mobile robots having a reduced footprint and raising the center of mass of a robot. The results suggested that for pushing, pulling, or carrying tasks, using whole body postural control could lead to higher performance by allowing a platform to apply more force to the environment.

None of the stability research directly targets the case study of this thesis, although stability affects the mobile manipulator performance, even for assembly operations. As will be shown in section 4.5, the author completed stability experiments to demonstrate effects on the system.

2.3.6. Obstacle Avoidance

Some research, expanded from mobile robots, focused on obstacle avoidance for mobile manipulators. Since mobile manipulators can change their volumetric profile by protruding the manipulator beyond the base, the manipulator can potentially collide with obstacles that are outside of the mobile base volume. This has the effect on the thesis case where the volume of the mobile manipulator must be known to allow navigation to and docking with the assembly workstation. As such, not only does section 4.5.3 provide a stability view of obstacle avoidance, but more closely related here is section 6 which describes thesis case experiments performed where the manipulator adds no additional volume during navigation. Once docked, it will be shown that it is necessary for the manipulator to pass perform pre-moves to ensure collision avoidance with the assembly workstation.

Referring independently to robot arms and mobile bases, in 1986, Khatib [115] presented a very well referenced and unique real-time obstacle avoidance approach for manipulators and mobile robots based on the artificial, potential-field concept. This research also has bearing to the mobile manipulator research area since the principles of collision avoidance, traditionally considered a high-level planning problem, can be effectively distributed between different levels of control for both the manipulator and base.

In 1995, Yamamoto and Yun [116] developed a control method and discussed simulation results for mobile manipulators that integrated an obstacle avoidance scheme with a coordination scheme. The obstacle avoidance scheme was based on superquadric potential functions with coordination in preferred operating regions. The controller allowed a mobile manipulator to retain optimal or sub-optimal configurations while avoiding obstacles. Yamamoto and Fukuda [117] also investigated multiple, wheeled mobile manipulators coordinating with each other under a collision avoidance situation. Their earlier research in 1995 derived kinematic and dynamic manipulability for multiple mobile manipulators simultaneously transporting a single object. The later effort in 2002 extended the previous approach to a system consisting of two mobile manipulators avoiding a collision while carrying an object. The two mobile manipulators dynamically changed their configurations so that they did not collide with each other while not only maintaining the support for the object, but also keeping the arm's configuration away from singularities.

Reactive obstacle avoidance for mobile robots and sample-based motion planning for mobile manipulators were outlined in 2010 in Nowak et al. [118]. In their report, they aimed to develop a methodology for identifying and providing best practice algorithms in a range of robotics fields. The methodology found objective performance comparison measures, and finally resulted in a number of open source, best practice libraries. Suggested performance criteria are:

- Mission success
- Path length

- Time taken
- Number of collisions
- Obstacle clearance
- Robustness in narrow spaces

This thesis research could be expanded to include any of the obstacle detection and avoidance approaches described in this section for safe mobile manipulator operations, again towards efficient assembly tasks.

2.3.7. Outdoor Use

The case study posed for this thesis does not necessarily rely on indoor assembly applications. Therefore, it is useful to also review the mobile manipulator research for outdoor applications, although none of the research includes assembly. Researchers have studied the mobile manipulator control algorithm including dynamic motions caused by onboard manipulator motion, especially in undulating terrain [119]. A significant amount of research was also done and continues in mobile manipulators for use outdoors. In 2007, Najjaran and Goldenberg [120] presented real-time motion planning for an autonomous mobile manipulator that scanned outdoor terrain to detect landmines. In their systems, a terrain map was generated using laser and ultrasonic rangefinder measurements. A generated map of obstacles from the measurements was then used to define an obstacle-free, detector path which was verified by experiments on a prototype mine-detector robot. For example, Wells and Deguire [121] described TALON, a mobile manipulator originally developed under Defense Advanced Research Project Agency's (DARPA's) Tactical Mobile Robotics (TMR) Program to extend "the reach and capabilities of the war fighter" for explosive ordinance disposal and to counter improvised explosive devices.

In 2006, Yang and Brock [122] stated that the "autonomous execution of manipulation tasks in unstructured, dynamic environments requires the consideration of various motion constraints. Any motion performed during the manipulation task has to satisfy constraints imposed by the task itself, but also has to consider kinematic and dynamic limitations of the manipulator, avoid unpredictably moving obstacles, and observe constraints imposed by the global connectivity of the workspace. Furthermore, the unpredictability of unstructured environments requires the continuous incorporation of feedback to reliably satisfy these constraints." They presented a novel, feedback motion planning approach, called "elastic roadmap framework," which satisfied all motion constraints in autonomous mobile manipulation, when tested via simulation, as well as their respective feedback requirements.

2.3.8. Miscellaneous

Again, for thoroughness, this section includes several research efforts that define or improve the performance of mobile manipulators during load-carrying, navigation, etc. In 1988, Graettinger and Krogh [123] defined the acceleration radius, as opposed to the acceleration tangent, as a global index for quantifying the dynamic capabilities of manipulator-positioning systems over a continuous operating region. The authors developed a numerical algorithm to solve the unbounded acceleration issues and applied the solution to the acceleration radius concept. Manipulator design and workspace specification examples were illustrated. In 1998, Chung and Velinsky [124] presented mobile manipulator modeling and control where the equations of motion were derived using the Lagrange-d'Alembert formulation (i.e., considering applied forces) for a non-holonomic mobile manipulator model. The dynamic model, which considers slip of the platform's tires, was developed using the Newton-Euler method and incorporates Dugoff's tire friction model. In 2000,

Watanabe et al. [125] described analysis and control for a holonomic, omnidirectional mobile manipulator, in which their platform included three lateral, orthogonal wheel assemblies and a mounted manipulator with three rotational joints, located at the platform center-of-gravity. Simulated results showed that the mobile manipulator could be controlled to retain any end-effector pose, regardless of the external, applied-force direction. In 2005, Mbede et al. [126] applied a robust, adaptive, fuzzy, reactive motion-planning algorithm for mobile manipulator navigation. The system included an incomplete mathematical robot system model and sensor data uncertainties. For the vehicle platform, they combined the advantages of a probabilistic roadmap as a planner and fuzzy navigation to allow adaptability similar to an elastic band. Stabilization, mobilization, and manipulation are all considered. In 2004, Korayem et al. [127] developed the Iterative Linear Programming (ILP) method to determine dynamic load carrying capacity of mobile manipulators. The authors presented numerical method examples that included a PUMA robot mounted on a linear-tracked base and a wheeled, mobile manipulator.

2.4. Performance Measurements

This section surveys the performance measurement research for robots, mobile robots, and mobile manipulators. The literature search of robot performance measurement uncovered few published articles and mobile manipulation performance measurement, being a relatively new area of research, provided even fewer articles. None of the research articles include all aspects of this thesis case study. Calibration, standards, and artifacts to evaluate performance are surveyed in this section.

2.4.1. Calibration

Calibration greatly improves the correspondence between the real position of the robot end effector and the position calculated from the mathematical model of the robot. Elatta et al. [128] describe parametric robot manipulator calibration as using the kinematic parameters to define models of an industrial robot. Kinematic parameters describe the relative position and orientation of links and joints of the robot while the dynamic parameters describe arm and joint masses and internal friction.

Robot calibration and metrology systems vary widely in performance, but as a general rule, they are considered to be expensive systems that are normally beyond the budget of the average company. Hidalgo and Brunn [129] performed a market survey involving some of the leading systems available and revealed that the leading performers are characteristically easy to set-up and operate, and are more economical. Nevertheless, the price range of these systems is still too high for them to be in widespread, regular use. They suggest that development of systems that combine these characteristics, but at a low-cost, would fill an important void in the automated manufacturing industry.

Greenway [130] discussed robot accuracy and repeatability and the mechanical and control aspects of robots that lead to errors occurring in static positioning and dynamic path following. He described both “string pull” devices (two examples of which are described in [131], see Figure 6, and in [132]) with 1 mm accuracy and laser-based systems, that utilize laser light for both alignment and distance measurement. An example of one such laser-based system mounted a laser on a 2 axis tracking head that follows the movement of a target. For the thesis case, string pull devices severely limit the mobile manipulation work volume and, as described in section 1.2, laser-based systems measure a single point with high accuracy, although the laser beam is continuously

broken with mobile manipulator movement. Additionally, the tracking head is relatively large and heavy with respect to the mobile manipulator, especially as these systems get smaller (i.e., mobile robots as opposed to AGVs). However, laser trackers are ideally suited for tracking the tool center point of a robot arm alone to determine its accuracy and repeatability.

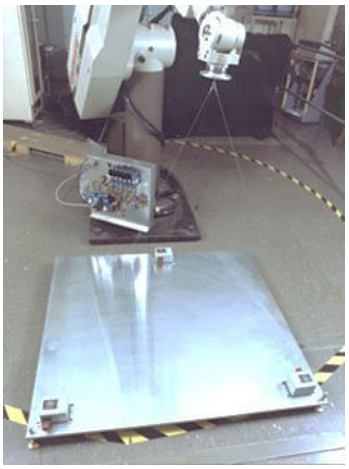

Figure 6. NIST Robot Calibrator.

Vision-based photogrammetry typically has accuracies at best of 2 mm in a plane and 15 mm depth and videogrammetry systems (i.e., optical target tracking as in the system proposed in section 1.2), which are vision systems with a minimum of two cameras, are stationary while a fixed pattern of light sources attached to the robot moves within the field-of-view of the cameras where the location and orientation of the light sources can be calculated from the camera images. OTS system calibration will be detailed in section 3.3.1.

Sensors must be calibrated both to the manipulators and to each other, since fused sensor data is often needed. Pradeep et al. [133] proposed an extendable framework that combined measurements from the robot's various sensors (proprioceptive and external) to calibrate the robot's joint offsets and external sensor locations. The framework was validated by implementing it on a commercial mobile manipulator robot, providing a significant improvement in the robot's calibration. A popular configuration widely used in a variety of robotic applications is to mount a camera on the robot manipulator hand. Before performing a measurement task using such a system, both the camera and the robot need to be calibrated. Zhuang et al. [134] discussed a procedure developed for simultaneous calibration of a robot and a monocular camera. Unlike conventional approaches based on first calibrating the camera and then calibrating the robot, the algorithm solved for the kinematic parameters of the robot and camera in one stage, thus eliminating error propagation and improving noise sensitivity. Preising and Hisa [135] demonstrated the use of a single camera 3D computer vision system as a position sensor to perform robot calibration instead of being calculated from the kinematic equations. The authors describe a vision feedback scheme they termed vision-guided robot control (VRC) which may improve the accuracy of a robot in an on-line, iterative manner. The degree of accuracy was determined by setting a tolerance level for each of the six DoF in Cartesian space. In general, a small tolerance level requires a large number of iterations in order to position the end effector, while a large tolerance level requires fewer iterations.

All of the calibration schemes previously described are interesting and may be useful for determining the manipulator calibration. However, when considering the thesis case, a test method

is not required to only calibrate the onboard manipulator of a mobile manipulator unless the manufacturer or user expect to fixture the mobile base to the assembly workstation. Again, this is not the thesis case of fixtureless mobile manipulator use and performance measurement. However, for thoroughness, as will be shown in sections 4.2 for the mobile base and 5.2 for the onboard manipulator, respectively, this thesis research addressed the calibration issues towards low-cost methods for calibrating these two components. The OTS provided a suitable measurement system for the manipulator calibration, as well as the mobile base, and the RMMA concept allowed a laser retroreflector to be aligned with the manipulator tool center point to ensure the thesis case application of assembly can be achieved with the mobile manipulator system as a whole.

2.4.2. Standards

The standards landscape is represented by both safety and performance standards. For industrial robots, safety is addressed in both international (ISO 10218 parts 1, 2 [136]) and national (American National Standards Institute (ANSI)/Robotics Industry of America, RIA, 15.06 [137]) standards. AGV safety is currently defined only in national standards (e.g., ANSI/Industrial Truck Standards Development Foundation (ITSDF) B56.5 [138], and European Standards (BS EN) 1525 [139]). Industrial robot performance is also defined at both the international (ISO 9283 [44]) and national (RIA 15.05 [140]) levels. AGV performance standards are currently being developed through ASTM International Committee F45 [141].

However, these standards are not combined for mobile manipulators, and leave gaps in both safety [142] and performance. RIA began a standards development working group for mobile manipulators in 2015. At the time of writing this thesis, there are no performance standards efforts or standard test methods for mobile manipulators to compare capabilities of various manufacturers systems as they evolve. Assuming mobile manipulator safety [143] will be solved and standardized in the near-term, performance standards must follow so that potential users can compare systems against tasks. ISO 9283 and the RIA 15.05 standards depict the performance criteria and related testing methods to determine performance characteristics of industrial robots. They define the important performance characteristics, describe how they shall be specified, and recommend how they should be tested. The ASTM F45 committee of performance standards for automatic guided industrial vehicles includes environmental effects, docking and navigation, communication and integration, object detection and protection, and terminology areas. F45 is expected to include performance test methods for mobile manipulators where “precision” docking of the system may be expected to provide, for example, two or more orders of magnitude smaller tolerance docking than are needed for pallet acquisition for assembly or other similar tasks.

2.4.3. Artifacts to Evaluate Performance

Performance evaluation artifacts for safety of robots and mobile robots/AGVs appear in their respective safety standards. However, industrial safety system performance artifact research is non-existent for robots: a literature search provided no results and minimal results for mobile robots/AGVs [170]. Similarly, a literature search for artifacts used to measure mobile manipulator performance, until recently at the U.S. National Institute of Standards and Technology (NIST) [170], is virtually non-existent. Mobile manipulator users could spend a relatively large amount of money having artifacts machined. However, advancements in additive manufacturing technologies enable rapid prototyping capabilities that significantly reduce the cost and effort necessary to produce such artifacts. Figure 7 (a) shows a graphical depiction of an artifact developed for this thesis research to be used for measuring performance of mobile manipulators.

The artifact allows a machined surface (flat as in Figure 7 (a) or convex/concave as in Figure 7 (b)) with patterned holes to position reflectors and to be tilted horizontally, vertically, or at any angle beside or above the mobile manipulator. Each reflector can be positioned perpendicular to the surface or at any pitch and/or yaw angle. A laser retro-reflector is wielded by the manipulator and positioned above and in-line with each reflector to measure manipulator position accuracy (within the laser and reflector tolerance), repeatability, detection, time for detection, efficiency of motion, dexterity, and autonomy. Many of these parameters can be determined by measurement from one mobile base position. Additionally, travel distance coupled with dexterity and autonomy can also be measured using the apparatus by indexing or continuously moving the mobile base along or around the apparatus. Alternatively, the robot could wield a reflector while the apparatus houses laser retro-reflectors, resulting in a much simpler robot interface, but with greater cost from additional lasers.

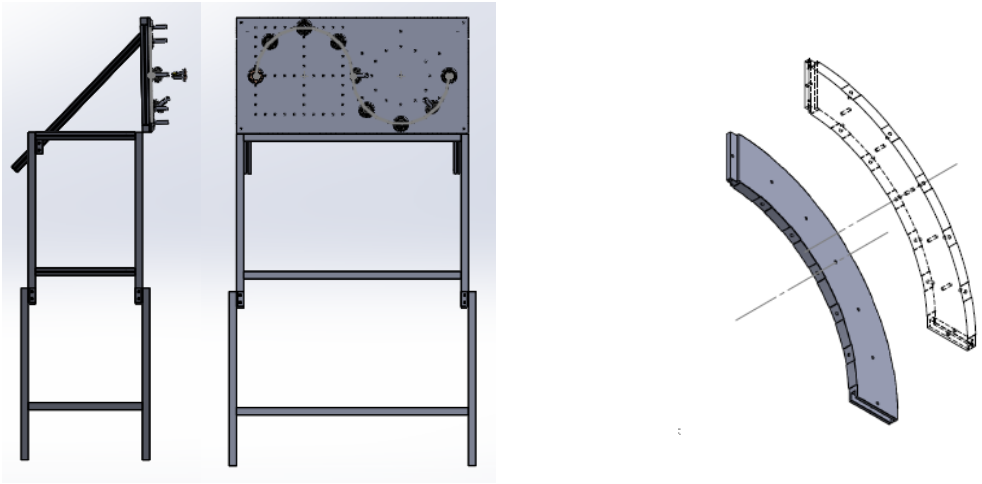

a b

Figure 7. Graphic of the NIST mobile manipulator artifact showing (a) adjustable height table with multiple geometric patterns of tapped holes and (b) flat (top/bottom), concave (inside edge), convex (outside edge) patterns of holes for mounting reflectors or laser retroreflectors and designed to mount into circular or sinusoidal shapes.

2.4.4. Robot Performance Measurement

It is important to include here the state-of-the-art for robot arm (manipulator) performance measurement where implementation of ideas may affect the thesis research case study. There have been very few published works pertaining to robot performance measurement research, especially for industrial robots. Most papers discuss the systems used to measure robot performance, instead of the test method developed, and are included in the Section 1.2. Included in this section is, instead, research describing mathematical tools, measurement of a teleoperated robot, and a software framework for robot performance measurement. With regards to the case study for this thesis, these have minimal bearing, although the research is included for thoroughness to mobile manipulator measurement.

Dynamic capability equations (DCE) are described by Bowling and Khatib [144] and provide a description of robot (non-redundant manipulators with as many actuators as DoF) acceleration and force capabilities, which they called a “new tool for analyzing manipulator performance.” Robot

acceleration and force capabilities refer to a manipulator's ability to accelerate its end-effector and to apply forces to the environment at the end-effector. The key features in the development of these equations were that they combined the analysis of end-effector accelerations, velocities, and forces, while addressing the difference in units between translational and rotational quantities. For mobile manipulators used for assembly, these equations may be useful to describe the assembly effects on the manipulator. Although this was not the intent of the thesis research, it is possible that the analysis posed here could affect the thesis case study to provide additional performance measurements results for acceleration, velocity and force (assuming contact) metrics.

Although teleoperated, Hannaford et al. [20] measured performance of the flight telerobotic servicer robot in a series of generic and application-driven tasks with and without force feedback, and with control shared between teleoperation and local sensor referenced control. Measurements defining task performance included 100 Hz recording of six-axis force-torque information, task completion time, and visual observation of predefined task errors. Park et al. [145] evaluated methods of measuring motion characteristics (i.e., payload, repeatability, maximum speed, and position accuracy) of pose and path for a dual-arm robot and provided results. These researchers provided measurements for human-controlled manipulators that could also be applied to automatic manipulators onboard mobile bases where the metrics are similar.

Although not aimed at industrial robot performance measurement research, a software framework was developed in 2006 by Balakirsky et al. [146] that allowed for the realistic modeling of robots, sensors, and actuators, as well as complex, unstructured, dynamic environments. Because it was a simulation framework for these performance measurements, it could therefore be adapted to industrial applications as well. Multiple heterogeneous agents could be concurrently placed in the simulation environment thus allowing for team or group evaluations. Perhaps additionally, mobile manipulators could be included.

2.4.5. Mobile Robot Performance Measurement

As with manipulators, it is important to include here the state-of-the-art for mobile robot performance measurement where implementation of ideas may affect the thesis research case study. Mobile robot motion performance evaluation methods and systems remain a challenge, although substantial progress has been made in recent years. Off-line evaluation techniques are non-existent yet, evaluation is "deeply influenced by the task, the environment, and the specific representation chosen for it." Calisi and Nardi [147] concentrated on tasks that require the mobile robot to move from one configuration to another, for example navigating to an assembly workstation. They describe that the task can either be an independent sub-task of a more complex plan or represent a goal by itself. After characterizing the goals and the tasks, the authors described the commonly-used problem decomposition and different kinds of modeling that could be used, from accurate metric maps to minimalistic representations.

In 2000, Baltes [148] described a benchmark suite for mobile robots that provided quantitative measurements of a mobile robot's ability to perform specific tasks. The benchmarks tested the path- and trajectory-tracking control and accuracy, the static path planning, and the dynamic path planning ability of a mobile robot. A set of metrics that provide important information about a mobile robot's performance are also presented. Baltes states that, "benchmarks could also be used as simple games which would lead to an increased opportunity for researchers to evaluate their

work without having to buy expensive or special purpose equipment." This research directly mimicks the thesis case study for navigating to assembly workstations. The metrics listed in section 1.2 include and go beyond metrics described in [148] with inclusion of autonomy, efficiency, stability, and explosration of unknown environments and even more with addition of the manipulator dexterity, stability, etc. In 2014, Ceballos et al. [149] developed a mobile robot simulator for research and education that was implemented in Matlab. It modeled the robot's differential kinematics and proximity sensors. It allowed the performance assessment of navigation algorithms through various quality metrics that are useful for comparing and analyzing simulated navigation algorithms of mobile robots.

Commercially available AGV's could provide the mobility for onboard manipulators for agile manufacturing applications. To ensure that all AGV's performance characteristics are expressed in the same manner, Bostelman et al. [2] measured the performance of an AGV towards development of standard performance test methods. Measurements of the AGV navigating standard geometrically shaped paths (e.g., circle, square, etc.) and in various steering modes and velocities were compared to a multiple camera tracking system used as ground truth. More details of these tests will be described in section 4.3.

In 1998, Duckett and Nehmzow [150] researched self-localization in autonomous mobile robot navigation, including a general performance metric and a standard experimental procedure. The concept allows disparate localization systems to be compared on the same robot in the same environment. To demonstrate the utility of the approach taken, they tested the evidence-based localization system in six different environments, comparing its performance to that of localization using dead reckoning or currently observable landmarks. This may become useful for addition to the thesis case study as more autonomous mobile robot bases are used as components of mobile manipulators.

A survey of the mobile robot competitions that fostered quite a lot of mobile robot research progress is found in [151]. A recent competition, not included in [151], is RoCKIn [152] which fostered benchmarking of mobile robots for home and work. The survey led to the formation of the ASTM International F45 driverless automatic guided industrial vehicle performance standards committee. For example, one competition in the survey included the US Defense Advanced Research Project Agency's Learning Applied to Ground Robots (LAGR) program, which ran from 2004 until 2008. LAGR had the goal of accelerating progress in autonomous, perception-based, off-road navigation in robotic unmanned ground vehicles (UGVs) using one mobile robot. In the LAGR program, mobile robot performance was measured, against other robots, by completion of a task over three consecutive attempts, learning during each run to decrease travel time to the goal. After LAGR and other surveyed competitions in [151], the Multi-Autonomous Ground Robotics International Challenge (MAGIC) 2010 [153] occurred. MAGIC invited competing teams to field squads of unmanned vehicle prototypes that autonomously coordinated, planned, and executed a series of timed tasks including classifying and responding to simulated threats and exploring/mapping diverse terrains.

2.4.6. Mobile Manipulator Performance Measurement

Of the few references uncovered, the most generic physical measure used to develop controls for mobile manipulators appears in 1992 in Hootsmans et al. [119]. They emulated the performance

of the mobile manipulator system by mounting a robot arm onboard a six DoF Stewart platform, parallel-link manipulator. Unfortunately, this research doesn't directly address the case study for this thesis having a rolling base, although it provides some performance measurement basis as perhaps a physical simulator for mobile manipulators performing assembly. The authors experimentally investigated the behavior of a manipulator mounted on a compliant or moving base. The system could emulate a wide variety of linear and non-linear compliant vehicles. Dynamic interaction measurements were made using a six DoF force and torque sensor mounted on top of the platform and underneath the robot arm. Using an inverse kinematic model of the platform, the required vehicle motions were translated into Stewart mechanism commands.

Simulations of stability performance measurement were conducted by Yamamoto and Yun [154] in 1994 to evaluate the performance of dynamic interactions by using a mobile manipulator model for three different trajectories: straight line with a constant velocity along a 145° direction with respect to the initial heading angle, circular trajectory, and straight line with constant velocity while the arm followed an oscillatory motion along the X-axis. If actually implemented, this concept may add well to the metrics posed for mobile manipulator performance measurement for the thesis case study. In 2007, Zadarnowska and Tchon [155] proposed a control theoretic methodology for defining mobile manipulator dynamic performance measures, including compliance and admittance measures. They introduced both local and global performance characteristics, including: the agility ellipsoid, the agility and mobility, the condition number, and the distortion. The authors demonstrated the measures on a mobile robot to only determine optimal motion patterns. The motion patterns could perhaps be implemented on mobile manipulators used in assembly operations and measured using the performance test methods described in section 4.

And in 2010, performance measurements, although not for industrial use, were performed by Advait and Kemp [76] to evaluate completion of specific tasks for a mobile manipulator. The robot approached and grasped objects from 25 object categories that were ranked most important for robotic retrieval by motor-impaired patients. Perhaps a similar list of items could be considered for task specific, performance measurements of mobile manipulators to be used in assembly applications.

2.5. Conclusions

This chapter provided an extensive literature review for mobile manipulators, including robot arm and mobile robot research since they are the main components and form the basis of mobile manipulators. Beginning with a brief discussion of what types of mobile manipulators have been studied, experimental applications research is then surveyed as they have driven research in other areas. Experimental applications have been considered and will drive their rapid use in industrial settings (e.g., assembly, inspection, opening doors, material handling, etc.). After considering the vast number of mobile manipulator applications, development of planning and control methods has been at the forefront of mobile manipulator research. Most of the planning and control research areas for mobile manipulators have included: unified motion; trajectory planning; configuration optimization; multiple tasks; stability; obstacle avoidance; outdoor use. However, specific to this thesis and continually compared to the state-of-the-art is the case study which narrows the performance measurement of mobile manipulator focus to an area that has barely been considered. To reiterate, the case study for this thesis is as follows and was compared to the current state-of-

the-art demonstrating the lack of performance measurements and replicable performance measurement test methods for mobile manipulators:

1. Complete (demonstrate) the commanded (assembly) task, including navigation to the task area,
2. Fixtureless mobile manipulator,
3. Non-contact measurement,
4. Rapid measurement,
5. Relatively inexpensive measurement system.

Perhaps the two closest research to this thesis effort are first in [68] and [69] although they too lack the rapid calibration and non-contact nature of mobile manipulator performance measurement desired in this thesis research. The second is in [70] although they utilized an expensive measurement system opposing the thesis focus for a relatively low-cost solution.

The lack of metrics and quantifiable measures of performance have been considered major barriers in the development of other intelligent systems. Benchmarks are important for mobile manipulators and may even guide developments in the correct directions. Benchmarks are the framework to standards where the metrics listed in section 1.2 should be considered for mobile manipulators.

The tools that are used to measure the performance of systems, whether machine tool or robots, were surveyed where the machine tool and part measurement systems and their methods may prove useful in, or at least contrast, measuring performance of mobile manipulators. However, motion tracking systems are the focus of the majority of literature reviewed since mobile manipulators are dynamic in nature. The review considered various motion tracking technologies, such as: camera, multi-camera, laser, and rotating laser systems.

Lastly, performance measurement research, specific to robots, mobile robots, and mobile manipulators are surveyed, beginning with calibration. In this area, contact and non-contact calibration systems are surveyed, including string-pull, laser, vision, light emitting diode with cameras, etc. and the fused sensor algorithms. Performance, as well as safety, standards are then listed for robot and mobile robot/AGV systems where ASTM F45 will be an ideal venue for mobile manipulator performance test methods. One area that shows promise for performance measurement, including calibration, of mobile manipulators is with standard artifacts. Metrology bars or other calibrated artifacts can provide a simple, reproducible, cost-effective measurement system with known accuracy and repeatability for measuring mobile manipulator performance. NIST has been developing such a system that promises a virtually unlimited number of measurement configurations for mobile manipulators.

Perhaps the least published area of mobile manipulator research is in performance measurements, including artifacts. Minimal performance measurement of robots, mobile robots, and mobile manipulators literature was uncovered. A few research works were published discussing software frameworks, teleoperated systems measurements, benchmarks, and localization. A survey of research that includes military competitions leading to the ASTM F45 performance standard was also included. Mobile manipulator performance measurement research was suggested as not being

explored systematically. Expectedly, robot and mobile robot performance measurement research is more prevalent than for mobile manipulators since this area is relatively new, and even less prevalent in the thesis case study of assembly applications. However, robot and mobile robot measurement provides excellent basis for mobile manipulator measurement methods and is included in the survey. The survey is useful to practitioners as a sound basis for mobile manipulator implementation for planning, control, stability, indoor and outdoor use, etc. followed by a comparison of technologies and research results that support mobile manipulator application. Since artifacts provide such a simple, yet useful method for measuring mobile manipulator performance, it is in this area of mobile manipulator performance measurement and test method development that are suggestions or challenges to the research community.

As mentioned throughout this section, following sections will demonstrate areas cited in the state-of-the-art research with regards to the case study. The performance measures will be demonstrated for the mobile robot, manipulator and mobile manipulator in sections 4, 5, and 6, respectively.

3. SYSTEM MODELING AND MEASUREMENT

The mobile manipulator must be aligned to tasks, in this case assembly, with the appropriate reach, speed, dexterity or manipulability, and other parameters. Additionally, mobile manipulator control must be known so that users can rapidly and cost-effectively program the system to perform as expected. As any quick search on the internet can provide, there are many programming languages available today and used to control robots, including: LISP, Assembly, MATLAB, C#/.NET, Java, Python, and C/C++ to name a few. For example, just within this thesis research, the AGV used NDC code, the manipulator used C++ code, the OTS used Motive code, the laser tracker used Automated Precision control code, etc. Just as there is a need for a standard performance measurement test method for measuring mobile manipulators, there should also be a standard robot modeling and control language for use within the test method, especially if the models can also provide control code.

An additional aspect to modeling the mobile manipulator and its control is to model the performance measurement system for measuring the mobile manipulator. The combined model of a mobile manipulator and its measurement system has not been found in prior research. However, the models described in this thesis section include two competing measurement methods followed by their actual details.

3.1. System Modeling

Modeling can use many forms to conceptualize and construct systems in business and industry. Business models for process workflow (e.g., Gantt and Pert charts) and architectural models for structures are frequently used for the administrative needs of organizations and the building industry, respectively. Pertinent to this thesis, however, is classic modeling using functional flow block diagrams (e.g., flow charts), for example systems architectures, which are easily decomposed into sub-component models and can even be linked to system requirements. However, these classic modeling tools only capture basic principles of system interconnections, and software flow with calls in sequence/parallel to other hardware components and/or software modules. They do not support the system description, design, analysis, and system constraints through machine-readable models.

Over, perhaps, the past twenty years or so, well-published model based approaches to systems engineering for complex systems began describing huge space and earth-based systems due to the complexity of software. The concept of reusable software modules that could be simply shown as boxes, which incorporate complex software with associated parameters and function calls, simplified system development over the years. The additional benefit is the potential for this industry-adopted system development method to become a standard method applied to, not only the mobile manipulator, but also their performance measurement.

Model Based Systems Engineering (MBSE) provides a simplified representation of a system. Specifically, Systems Modeling Language (SysML) is a graphical modeling language that supports

the "specification, analysis, design, verification, and validation of systems that include hardware, software, data, personnel, procedures and facilities." [156] SysML provides four essential tools, also called pillars: Structure (with definition and use), Behavior (with interaction state machines, and activity/function), Requirements, and Parametrics (with equations and units). Very large projects with multi-user access may suggest a different modeling language, such as Teamcenter System Engineering (TCSE). [157] However, the case at hand for modeling the performance measurement of mobile manipulators is ideally suited for SysML. Rahman, et al. [158] make a similar case for using SysML in the design of mobile robots. In this work "the software for a mobile robot is developed using the model-based system engineering (MBSE) approach. The claim is that using MBSE (with SysML as the specific implementation) can enable the creation of reusable software modules for programming the robot to allow platform independent design and reduce development time. While this work demonstrates that SysML can be applied to some robotic systems with varying degrees of success, they do not describe how it might be applicable to other robot application domains." Additionally, Rahman, et al also suggest that SysML is uniquely suited for both accurately modeling increasingly complex and physical robotics systems, as well as the standardization of such an approach useful across many different industries. They state: "Instead of modeling the hardware or software of the system, we are instead considering a generalized system in a given domain, and modeling the capabilities of the generalized system for the application domain. This helps illustrate the flexibility of SysML in being able to model a wide variety of robotic systems from a number of different perspectives."

This thesis, therefore, applies SysML modeling to the performance measurement of mobile manipulators where all of the models described therein are referenced in [159][160]. The SysML models are verified through their post-development upon reviewing the pre-built systems, their components, and the knowledge of their control methods, including the mobile base (AGV), manipulator (robot arm), mobile manipulator, and measurement systems. For example, more detailed information is described through models: the interconnected mobile manipulator system and subsystems, methods of performance measurement (search and bisect) and overall sequential timing of the experimental control programs, and the use cases of the performance measurement experiments and potential real-world implementation. The experiments described within this thesis verify the mobile manipulator performance measurement concepts modeled. SysML models describing uncertainty propagation are also provided and demonstrate a theoretical basis inherent in performance measurement of any mobile manipulator. Hence, the intent of describing the performance measurement of mobile manipulators and the associated systems through SysML models is to explain to the reader:

- the interconnections, dependencies, and functionality of mobile manipulator systems and components;
- the interconnections, dependencies, and functionality of performance measurement systems and components;
- the interrelations between the mobile manipulator and the performance measurement systems.

The models designed in this thesis are intended to provide standard mobile manipulator design, analysis, and implementation of performance measures to the mobile manipulator community. Beyond the scope of this thesis and using the models designed herein, it is possible to further demonstrate control implementation through SysML C++ and other compilers that are available.

Each of the following chapters include SysML models to describe the systems, uncertainties, and/or use-cases of mobile manipulator performance measurement. Initially, two measurement systems used to measure performance are modeled and described. Following chapters show and describe models for the mobile base, the manipulator, the combined mobile manipulator and the performance measurement of the mobile manipulator through block definition and internal block diagrams which show their interconnections. Additionally, parametric diagrams that model the uncertainty propagation describe how the systematic performance is affected during measurements. Lastly, is a discussion of a use case diagram that model the measurement process and how the process could be included in a production facility.

3.2. Measurement Systems

This sub-section provides information and SysML models [159][160] of two methods chosen, based on the findings from section 1.2 when applied to the case study of this thesis, for measuring performance of mobile manipulators, namely optical tracking measurement systems and artifacts. Both methods are useful and provide benefits. Due to the complex motion of the dual system (AGV and robot arm), the optical tracking system was chosen as a ground truth measurement system because of having multiple cameras with a large, combined field-of-view and provides the measurement accuracy required for the thesis case. Also, the OTS could be used as, not only ground truth but as the measurement method should the mobile manipulator manufacturer and/or user have such a system. An alternative to the OTS is an artifact that was designed and developed and could prove to be, by comparison to OTSs, cost effective while providing the desired uncertainty for mobile manipulator performance measurement.

3.2.1. Optical Tracking Measurement System Model

Optical tracking systems (OTS) measure the three-dimensional, static and dynamic pose of multiple markers attached to objects within a measurement space. OTSs are used in a wide range of fields including: neuroscience [161], biomechanics [162], robotics [163], and automotive assembly [164]. The market for optical tracking systems has dramatically increased over the past several years to $1.2 B revenue in 2014 with annual growth of nearly 53% from 2009 to 2014. [165][166][167]

Figure 1 (a) shows a SysML package diagram and Figure 8 shows a SysML internal block diagram of the OTS structure. The OTS controller, as with the AGV and manipulator controllers, was also time-synchronized at 1 µs with global positioning system (GPS) through an antenna. This OTS included 12, 4 MP (megapixel) cameras attached to the controller via Ethernet through two hubs (EthHub1 and EthHub2) and through an Ethernet switch (e_switch), all with 1000 MB maximum data flow capacity. An external timesync shown in the figure is also available and was not used for these experiments. Experimentation has demonstrated that the OTS used for measuring performance of the mobile manipulator described in this thesis has a static measurement

uncertainty of 0.022 mm and 0.046° and dynamic measurement uncertainty of 0.26 mm and 0.20°. [168] The measurement concept developed for evaluating the OTS used is detailed in section 3.3.1.2.

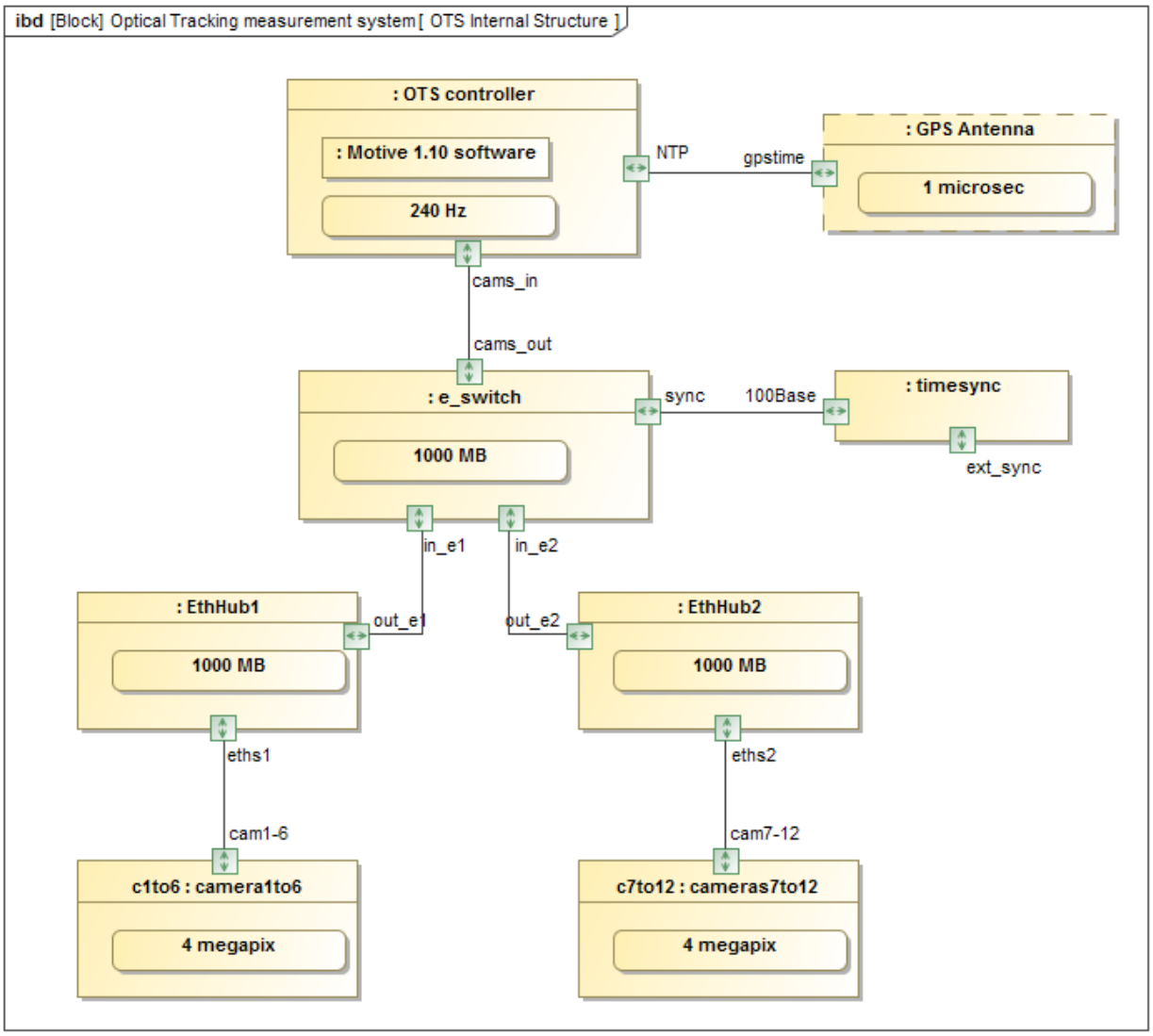

Figure 8. SysML internal block diagram showing the optical tracking measurement system structure.

3.2.2. Reconfigurable Mobile Manipulator Artifact Concept and Model

An alternative to the measurement system discussed in Section 3.2.1 is the use of artifacts as modeled in the package diagram shown in Figure 1 (a). Bostelman, et al describe in [168] the use of a novel artifact [169] standardized in ASTM E3064-16 and used in the test method for measuring OTS performance. Similarly, the author conceptualized, designed, and developed an artifact, called the reconfigurable mobile manipulator artifact (RMMA), to measure the performance of static manipulators and mobile manipulators. The RMMA [170][171][172] is a test fixture developed at NIST to emulate the environment that would be encountered by a mobile manipulator, especially for the thesis case. As will be shown in section 7.2.4, additional uses for artifacts, such as the RMMA are also possible.

The concept includes positioning a mobile manipulator next to an artifact as well as positioning and orienting the end of arm tool (EOAT) attached to the manipulator at specific locations above an artifact to digitally detect fiducials with known uncertainty. The performance evaluation criteria can include the:

- Time to register the mobile manipulator to the artifact
- Time to move from the registration points to the assembly points
- Repeatability after registration
- Number of search steps equating to the initial distance from registration/assembly points
- Detection of reflectors with varying diameters

The RMMA was designed primarily to emulate the positioning requirements of an assembly task, specifically the peg-in-hole insertion task. It does this by providing a set of precisely positioned mount points for reflective targets. The targets are detected using a non-contact, laser retroreflector sensor designed to detect the presence of retro-reflective targets in line with the laser beam. The sensor is mounted as the EOAT. A camera, with a light source, could instead be used as the detection sensor, especially with a larger diameter reflector or other spot. For the laser retroreflector concept, no camera software algorithm was required as the laser retroreflector connected directly into one of the manipulator digital inputs. The reflectors can have specific diameters depending upon the required uncertainty for their location. The targets are designed to determine if the manipulator position is accurate enough for successful peg-in-hole insertion. The RMMA provides a way to test and verify the performance of mobile manipulator systems without the use of expensive 3D tracking systems [168].

The target fiducials are constructed using a piece of reflective material fixed behind a circular aperture. In some of the targets a fixed radius aperture is used, in others a variable aperture is used. The laser retro-reflector sensor is used to detect the alignment of the manipulator with the fiducial. A signal is returned by the sensor when the laser beam is reflected back by the fiducial. The EOAT position accuracy can be adjusted by varying the size of the aperture or fixed radius used to expose the reflector.

In addition, a tubular collimator is added to the reflector to restrict the detection angle of the reflector. The position of a reflector on the RMMA determines the mobile manipulator position relative to that reflector. Using more than one reflector, pose of the mobile manipulator can be calculated.

By comparison, it is estimated that the use of the RMMA could be 20 times lower cost than the OTS described in 3.2.1. In this case, the RMMA is a 13 mm thick aluminum plate with reflector mount points at precise locations. The RMMA, shown in Figure 1 beside the mobile manipulator, could also be made using additive manufacturing and is estimated to further reduce the artifact cost by another order of magnitude (or approximately 200 times less cost than the OTS described).

Non-contact performance measurements ensure no risk of damage to the mobile manipulator. It cannot be expected to perform mobile manipulator calibration by contacting hard surfaces during assembly operations as the contact may also affect the system performance or worse, cause mobile manipulator damage. Therefore, reflective fiducials are to be detected using a single laser

retroreflector sensor that emits a laser and also detects the emitted light. These devices are approximately US$100.

A 305 mm (12 in) diameter circle pattern and a 457 mm (18 in) square pattern of reflectors are machined into the RMMA. These two patterns were modeled and used for experiments in this thesis, although circle, square, triangle, straight and curved lines, sinusoids, etc. patterns of tapped holes are also drilled into the RMMA as shown in Figure 9. Other components are also part of the RMMA where all components are modeled in a SysML internal block diagram shown in Figure 9.

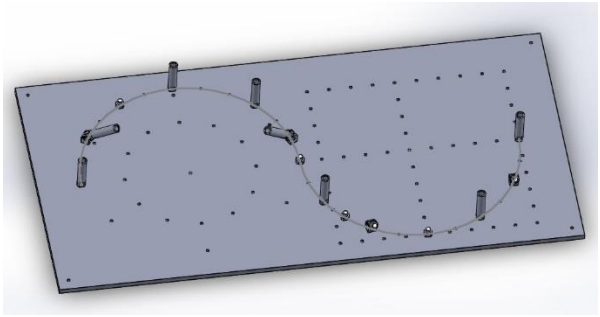

Figure 9. RMMA CAD drawing showing fiducials mounted in a double-curved pattern, as well as showing circle, multiple squares, and triangular patterns.

The RMMA can be configured to be in horizontal, vertical, overhead, (as shown in Figure 10) or at any angle between these configurations and at relatively short-to-tall heights as would be typical of assembly operations in, for example, automobile or aircraft manufacturing facilities. The RMMA legs can be changed to be shorter or taller. Due to the infinite number of configurations that the RMMA can provide, the horizontal configuration with vertical fiducials and collimators were used for this thesis research to demonstrate proof of concept and it was setup to be nearly the same height as the base of the manipulator onboard the AGV.

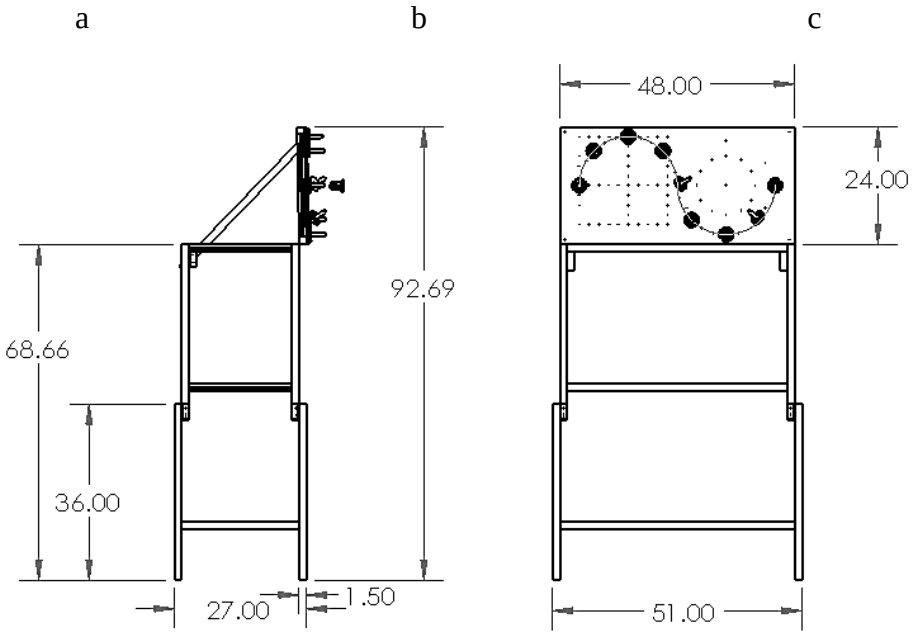

Figure 10. (a) Mobile manipulator beside the horizontal RMMA configuration and CAD models of (b) vertical (c) and overhead RMMA configurations. (d) Dimensioned drawing of RMMA.

Reflector angle mechanisms were also designed and fabricated and can provide even more complex performance measurement capabilities. The reflector and collimator can be perpendicular to the flat surface, as used throughout this thesis, or rotated to pitch angles between ± 90° and yaw angles between 0° and 360° using angled "surface connectors" as shown in Figure 11 (a and b). Adjustable fiducials were also designed and used in this thesis research and are shown in Figure 11 (c and d).

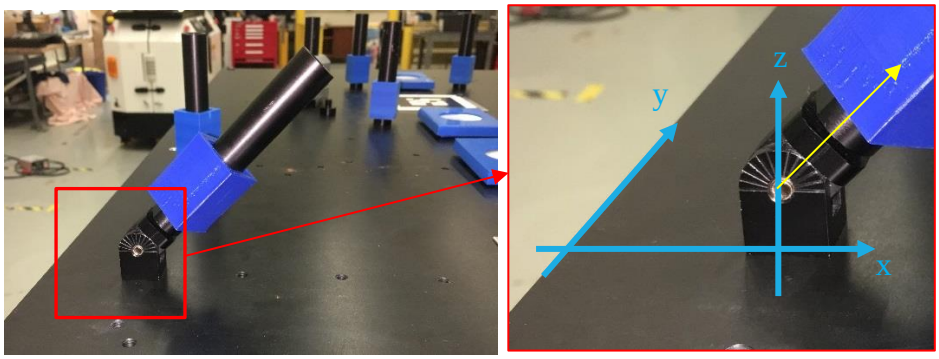

a b

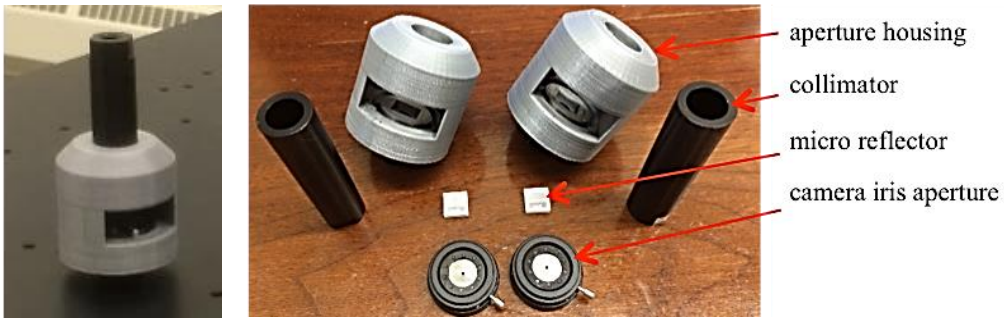

c d

Figure 11. (a) Angled "surface connectors" for "fid-refl-reducer-fixed" (left-foreground) showing 15^0 incremental markings attached to the RMMA. (b) Inset of (a) showing relative axes with respect to the RMMA edge to the square-base of the angled fiducial adapter. Other vertically-mounted "fid-refl-reducer-fixed" are shown in the background. (c) "fid-refl-reducer" attached to the RMMA and (d) "fid-refl-reducer" components.

Without the collimator, the reflector can be detected by the laser retroreflector (see Figure 12 (a)) at approximately ± 20° to the vertical axis as per the manufacturer specifications. For the collimators used, the reflector can be detected: 1) at a maximum 3.2 mm radius from the reflector center; 2) at approximately ± 7° to the vertical axis (see Figure 12 (b)); 3) with the laser retroreflector at 10.2 cm or farther from the reflector; and 4) when using a 12.7 mm inside-diameter collimator. Collimators could be made with even smaller inside-diameters to force more perpendicular manipulator tool point axis pose to the reflector. The laser retroreflector used was specified to detect a minimum 4 mm diameter reflector repeatedly at a distance of 10 cm.

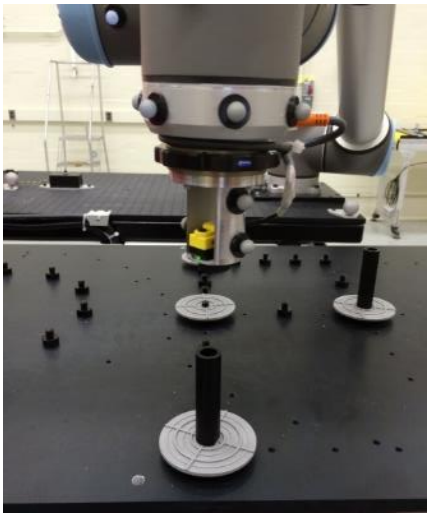

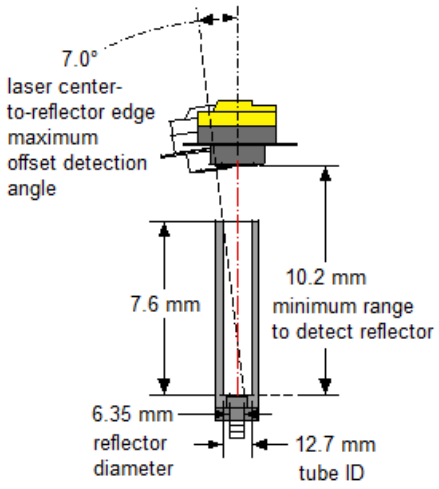

a b

Figure 12. Laser retroreflector sensor (yellow and black) and sensor assembly attached to a robot adapter. Spherical OTS markers are also shown attached to the laser retroreflector, robot, tool-mount, and the AGV (background). (b) Collimator dimensions and laser retroreflector measurement distances and offsets.

For this thesis research, detector-to-reflector distance parallel to the laser axis was approximately 127 mm where the manufacturers specified minimum and maximum detection

distances are 100 mm and 10 m, respectively. The distance researched would be representative of a programmed manipulator waypoint above and in-line with the next manipulator task point aligned to grip or insert a part or perform another task. The desired uncertainty may be, for example, a part insertion alignment tolerance required for a manufacturing assembly process. Moving along this grip/insertion line, parallel to the laser, at the aligned pose to the task point, also provides some knowledge of insertion performance (i.e., if the task point is continuously detected along the grip/insertion line).

A generic SysML model was developed to show the various RMMA components and their relation to one another. The model is important as nomenclature described in the model is used throughout this thesis, as would be the case in a system setup and use in industry. Beginning at the laser retroreflector (Figure 13, bottom-left), a positioning constraint is applied to the EOAT provided by the robot manipulator manufacturers specification. Moving up the left of the model, the collimator has a 13 mm inside diameter limiting the EOAT angle relative to the RMMA where fiducial detection can occur. The collimator is attached to two different types of fiducial reducers ('fid-refl-reducer-fixed' with a fixed reflector diameter 2 mm or greater, depending on the EOAT uncertainty chosen, and a 'fid-refl-reducer' with a variable reflector diameter of approximately 0.5 mm or greater that uses an optical aperture to minimize diameter to the center of the reflector). Both of the fiducial reducers are above 10 mm square 'fiducial-reflectors' and attached to the RMMA through surface connectors into circle and square patterns embedded in the machined surface of the RMMA. However, the 10 mm square fiducial-reflectors will be further discussed in section 3.3.2.2. The fiducial and the collimator inside can be any diameter, dependent upon the sensor specification and the desired measurement uncertainty.

Since the mobile manipulator may or may not already be registered to the RMMA, a means is needed to allow this registration. The Figure 13-left modeled parts can be used for mobile manipulator registration with the RMMA using search methods where the fiducial locations are previously taught using a manual operation. A second set of parts is also modeled (Figure 13-center) showing the laser retroreflector being used to detect 42 mm diameter reflectors (bisect-refl-reducer) for an alternative mobile manipulator-to-RMMA registration method. Off-the-shelf 50 mm x 80 mm rectangular reflectors (bisect-reflectors) were covered by the bisect-refl-reducer and mounted to the RMMA using surface connectors at initially taught manipulator locations (registration-laser) on the machined surface. The 42 mm diameter was chosen so that the EOAT would always detect these reflectors using a control method called bisect and described in Chapter 6.2.3.3.

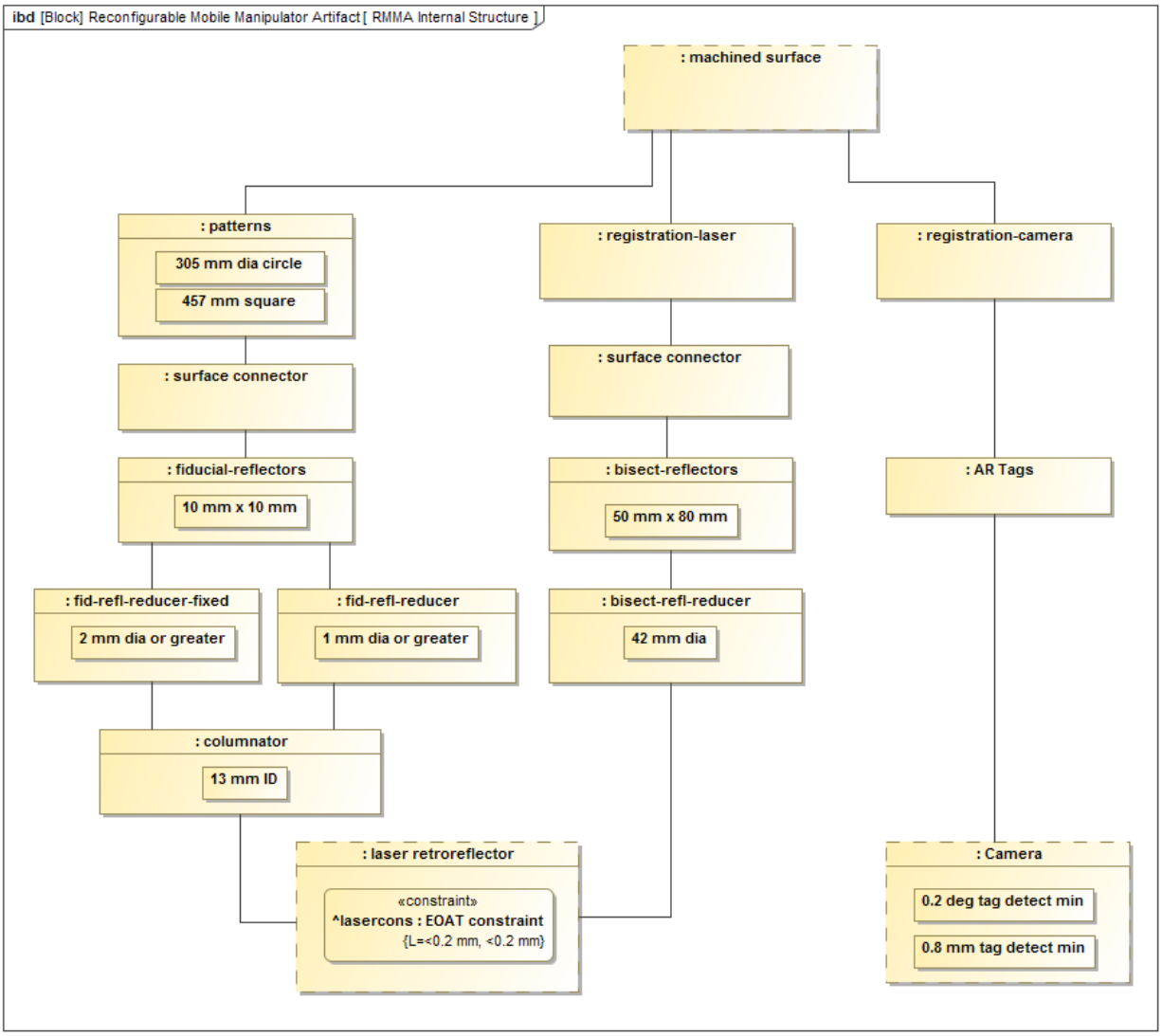

Figure 13. SysML internal block diagram showing the reconfigurable mobile manipulator artifact (RMMA) structure.

A third, parallel RMMA structure was modeled (Figure 13-right) showing a camera that detects augmented reality tags (AR Tags) with 0.2° and 0.8 mm tag detection capability using the AR Toolkit software and calibration as described in [7]. The registration-camera method provides an alternative to the two laser retroreflector registration methods previously described. Although to the date of this thesis, this third method has not been verified for uncertainty as a useful registration method for performance measurement of mobile manipulators and is therefore, left for future research.

3.3. Measurement Systems Uncertainty

3.3.1. Optical Tracking System

The OTS used is called Optitrack and is made by NaturalPoint, [173] although several manufacturers produce similar systems. OTS calibration is required prior to using the system to measure static and dynamic reflective markers instantaneous positions. The manufacturers method is briefed and an extension to the calibration process is explained in the following sub-section as the manufacturers calibration alone did not provide necessary uncertainty information needed for the OTS to be used as a ground truth measurement system (i.e., a system that provides factual data that is at least an order of magnitude better than the system under test). Other OTS uncertainty in camera movement and in OTS data collection can also cause measurement system uncertainty. The following subsections also describe these areas.

3.3.1.1. OTS manufacturer calibration process

Calibration includes a manufacturers procedure to first cover all reflective surfaces as shown in Figure 14 (a). As shown, several areas were covered including the floor, the AGV which has markers attached, the AGV reflectors used for AGV navigation, and any other reflective surfaces that may appear and can be covered.

Once reflections are eliminated as much as possible, a masking occurs that removes reflections detected by cameras so that they are not mistaken as markers. However, this also eliminates camera rays from the camera to the reflection which may cause OTS tracking issues if there are many or large reflective areas masked. After masking, coverings are removed and a floor reference frame, shown in Figure 14 (b), is position on the floor and selected in the OTS control panel to be the floor plane. This step locates all cameras one to another and to the floor. Potential uncertainties therefore can be caused by missing camera rays and the use of only a two-dimensional reference frame for system calibration. Measured uncertainty can therefore depend on the type and camera setup, number of cameras, number of markers used within the space, and several other factors.

3.3.1.2. Measuring the OTS

Although a calibrated OTS provides the best possible system performance, potential OTS users still have difficulty knowing system performance because of the lack of standard performance metrics and test methods. The user must therefore rely on vendor claims regarding the system's performance, capabilities, and suitability for a particular application. An OTS measurement concept was therefore suggested to ASTM, who develop three-dimensional imaging system standards. The ASTM International Committee E57 on 3D Imaging Systems' subcommittee on test methods addressed the static performance measurement of optical tracking systems [48]. A new standard test method was developed called "ASTM E3064 Standard Test Method for Evaluating the Performance of Optical Tracking Systems that Measure Six Degrees of Freedom (6 DoF) Pose" [174]. E3064 presents metrics and procedures for measuring, analyzing, and reporting the errors and deviations of dynamic optical tracking systems.

a

b

Figure 14. OTS calibration method used to calibrate the OTS: (a) coverings for all reflective surfaces and objects, (b) reference frame located on the floor.

An artifact, developed by the author and his colleagues in [168] and shown in the inset of Figure 15, was first used to measure a multi-camera system and then expanded by the ASTM E57.02 task group to apply to all types of optical tracking systems. Development of the artifact and measurement test method is further detailed in [169] which also shows and describes an artifact that can be used for systems that use geometric features as markers. The artifact description in the standard allows for a variety of markers to fit the optical tracking system's measurement method. The end markers are measured relative to one another in each right and left cluster on the bar and

combined through mathematical analysis to output the resulting bar length throughout the measurement space. A photo of the laboratory with artifact to measure the OTS static performance (and later, the mobile manipulator performance) is shown in Figure 15.

The GT system measured the distance between each bar ends of markers. [170] Analysis of data provides bar length measurement uncertainty when positioned at various locations within the space. Uncertainty is based on the [175] describing standard deviation (σ) as 68 % confidence. Measurement σ of the static uncertainty was 0.022 mm and static angle was 0.023°.

OTS dynamic measurements were then performed. Figure 16 shows the paths that were walked with the artifact and later agreed upon by the standards committee to be included in E3064. Three different orientations of the artifact are walked along the paths as shown in Figure 17. A sample data plot of the X and Y tracked paths is shown in Figure 18. The plot is of data collected from walking with the artifact in the vertical orientation (Figure 17 b) during the second trial. Results are shown in Table 3 for the two trials including analyzed data from both the artifact bar length and angle between artifact end-markers. The root mean square deviation (RMSD) shows approximately 0.5 mm length difference from the actual 300 mm length and approximately 0.34° difference from 0° actual angle. The maximum error, 50th percentile, 95th percentile, and 99.7th percentile length and angle results are also shown.

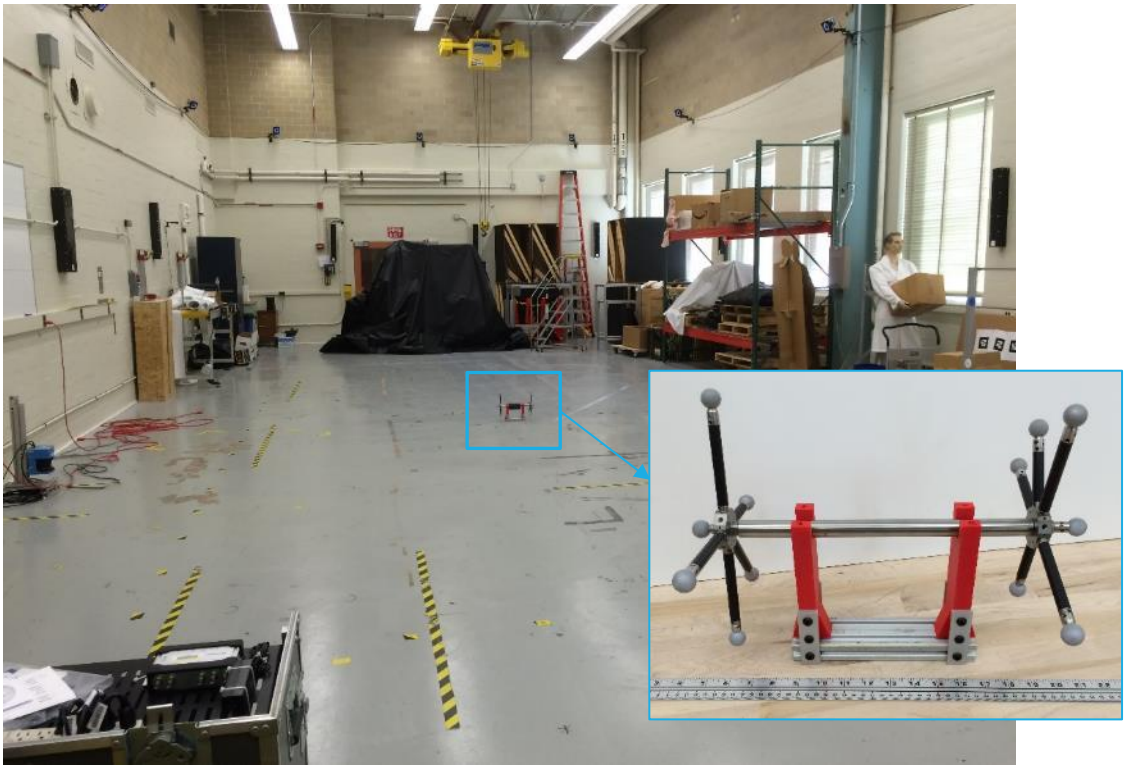

Figure 15. OTS calibration artifact (see inset) and placed on the floor for static measurement.

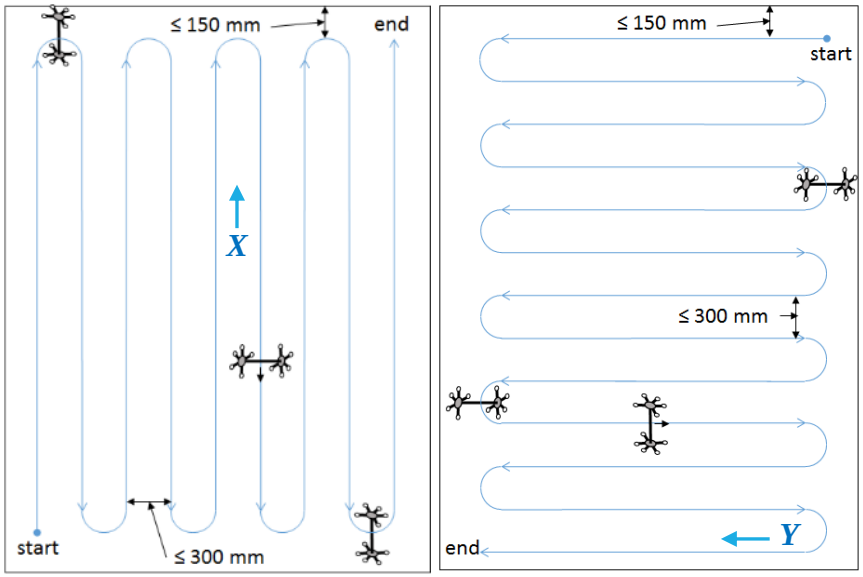

Figure 16. (a) Forward-back (aligned with the X axis) and (b) side-to-side (aligned with the Y axis) paths and dimensions for moving the artifact in a test space.

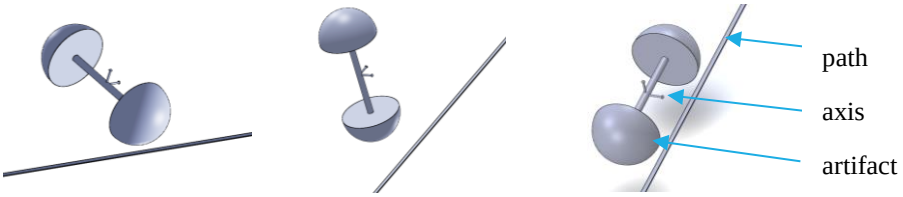

Figure 17. The artifact (shown with axes on the bar centroid) orientations with respect to the path: (a) perpendicular to the path segments in the plane of motion, (b) perpendicular to the path segments and normal to the plane of motion, and (c) in-line with the path segments in the plane of motion.

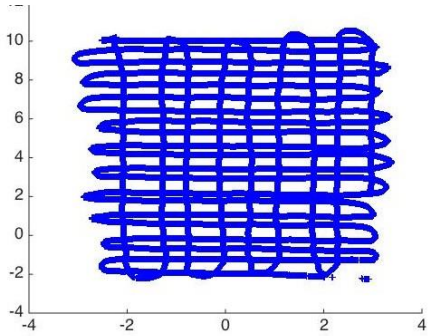

Figure 18. Sample data plot of the X and Y tracked paths of the artifact center.

Table 3. Experimental results for two trials to test the OTS dynamic uncertainty.

LENGTH						
test	number of samples	RMSD , mm	Max, mm	50 percentile, mm	95 percentile, mm	99.7 percentile, mm
Length 1	86617	0.532	31.804	0.15	0.606	2.068
Length 2	84892	0.499	30.933	0.136	0.633	2.152
ANGLE						
test	number of samples	RMSD , deg.	Max, deg.	50 percentile, deg.	95 percentile, deg.	99.7 percentile, deg.
Angle 1	86311	0.349	28.545	0.262	0.565	1.305
Angle 2	84751	0.334	44.819	0.159	0.569	1.415

Note: The author includes the following test method to be thorough and which was also included in [169]. Although the author developed much of the artifact, measurement concept, and made the measurements described above, he did not individually develop the analytics described to the end of this sub-section.

ASTM E3064 provides statistically-based performance metrics and a test procedure to evaluate the dynamic performance of optical tracking systems. Measurements from optical tracking systems include inherent positional and orientation angle errors relative to fixed optical measurement components. Metrics are therefore the static and dynamic position and orientation of tracked objects. Beyond the scope of this paper are metrics that are currently being researched which include system latency and maximum dynamic measurement capability.

The test procedure outlined in E3064 measures the relative pose between two sets of markers that are rigidly attached to the ends of a metrology bar as shown in Figure 15. The relative pose is then decomposed into positional and angular components and measurement errors are calculated by comparing results to a known metrology bar length of the artifact.

The artifact includes a 300 mm long metrology bar with markers rigidly attached to each end. The bar is called a 'metrology bar' since it has stiffness and thermal expansion characteristics to allow deflection of less than or equal to 0.01 mm. Example metrology bars are made of carbon fiber or titanium that meet the mandatory minimal deflection characteristic. One form of artifact includes two clusters of passive, reflective, spherical (see Figure 15) or active, light-emitting diode (LED) markers located at the ends of the metrology bar. Another form uses reduced pose ambiguity cuboctahedron markers. Both types of markers must be contained within hemispherical volumes of 100 mm maximum radius from the ends of the bar.

The basic procedure for determining the pose measurement error of an optical tracking system first includes rough (hand-held) alignment of the X and Y axes (Figure 17) and Z axis (aligned with the vertical axis) within the test volume to be measured. The options for the test volume are: (1) 3000 mm long x 2000 mm wide x 2000 mm high, (2) 6000 mm long x 4000 mm wide x 2000 mm high, and (3) 12000 mm long x 8000 mm wide x 2000 mm high.

The optical tracking system tracks the metrology bar as it is moved throughout the test volume along the two patterns shown in Figure 16 a and Figure 16 b for three trials. The metrology bar in each trial corresponds to one of the three orientations shown in Figure 17. The centroid of the metrology bar is to remain at approximately 1 m above the test volume floor and should be moved at approximately the walking speed of 1.2 m/s ± 0.7 m/s. The metrology bar length is used as a guideline for determining both the distance between the boundary lines and the limits of the test volume. The data from these three trials are then combined into one data set.

The data gathered from the OTS consist of the six DoF pose of the left and right ends of the artifact at time *t* represented as the homogeneous matrices

$$ {}_{OTS}\hat{H}_{Left}(t) = \begin{bmatrix} \hat{R}_{Left}(t) & \hat{T}_{Left}(t) \\ 0 & 1 \end{bmatrix} \text{ and } {}_{OTS}\hat{H}_{Right}(t) = \begin{bmatrix} \hat{R}_{Right}(t) & \hat{T}_{Right}(t) \\ 0 & 1 \end{bmatrix} $$

Then the relative pose between the left and right markers is defined as

$$ {}_{Left}\hat{H}_{Right}(t) = {}_{OTS}\hat{H}^{-1}_{Left}\,{}_{OTS}\hat{H}_{Right} = \begin{bmatrix} \hat{R}_{Left}(t) & \hat{T}_{Left}(t) \\ 0 & 1 \end{bmatrix}^{-1} \begin{bmatrix} \hat{R}_{Right}(t) & \hat{T}_{Right}(t) \\ 0 & 1 \end{bmatrix} = \begin{bmatrix} \hat{R}(t) & \hat{T}(t) \\ 0 & 1 \end{bmatrix} $$

where $\hat{R}(t)$ is the 3x3 rotation matrix describing the relative orientation between the left and right markers and $\hat{T}(t)$ is the 3x1 vector describing the relative translation between the left and right markers. The angle of rotation can then be described as

$$\hat{\theta}(t) = 2 * \text{ asin}(\sqrt{\hat{q}_x^2(t) + \hat{q}_y^2(t) + \hat{q}_z^2(t)}\ ),$$

where $\left(\hat{q}_w(t), \hat{q}_x(t), \hat{q}_y(t), \hat{q}_z(t)\right)^T$ is the unit quaternion representation of $\hat{R}(t)$ and $\hat{q}_w(t)$is the scalar component of the quaternion.

If the relative pose between the left and right markers has been measured by a reference system and represented as

$$ {}_{Left}H_{Right} = \begin{bmatrix} R & T \\ 0 & 1 \end{bmatrix} = \begin{bmatrix} I & T \\ 0 & 1 \end{bmatrix} $$

then the position error at time t can be defined as

$$e_{p(t)} = \left\|\hat{T}(t)\right\| - \|T\|,$$

and the orientation error at time *t* can be defined as

$$e_{o(t)} = \hat{\theta}(t) - 0 = \hat{\theta}(t).$$

Statistics on these errors include:

Root Mean Square	RMS	$\sqrt{\frac{1}{N}\sum_{t=1}^{N} e_t^2}$
Maximum Error	e_{max}	$\max(\lvert e_1\rvert, \lvert e_2\rvert, \ldots, \lvert e_N\rvert)$
Percentile Error	$E(p)$	$\begin{cases} E_k + d(E_{k+1} - E_k), & 0 < k < N \\ E_1, & k = 0 \\ E_N & k \geq N \end{cases}$

Here, e_t denotes either the positional error $e_{p(t)}$ or the orientation error $e_{o(t)}$. In addition, the percentile error *E(p)* on the ordered set $\{E_1, E_2, \ldots, E_N\}$ is constructed from rearranging the set of errors $\{|e_1|, |e_2|, \ldots, |e_N|\}$ by increasing value. Moreover,

$$\frac{p}{100}(N+1) = k + d,$$

where *k* is an integer and $0 \leq d < 1$. The specific percentile errors reported are *E(99.7)*, *E(95)*, and *E(50)*.

The percentile error for the OTS calibration experiment described is listed in the ASTM E3064 standard, as opposed to the standard deviation, since the data distribution may not be Gaussian. Histogram plots of the 99.7th percentile distribution are shown in Figure 19. As shown, the length data is relatively evenly distributed whereas the angle data is shifted positive.

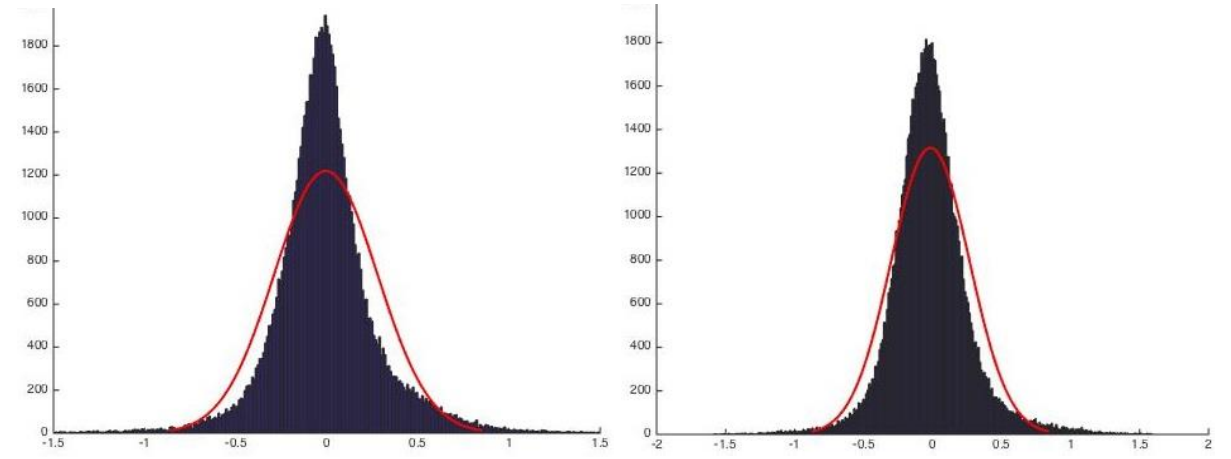

a b

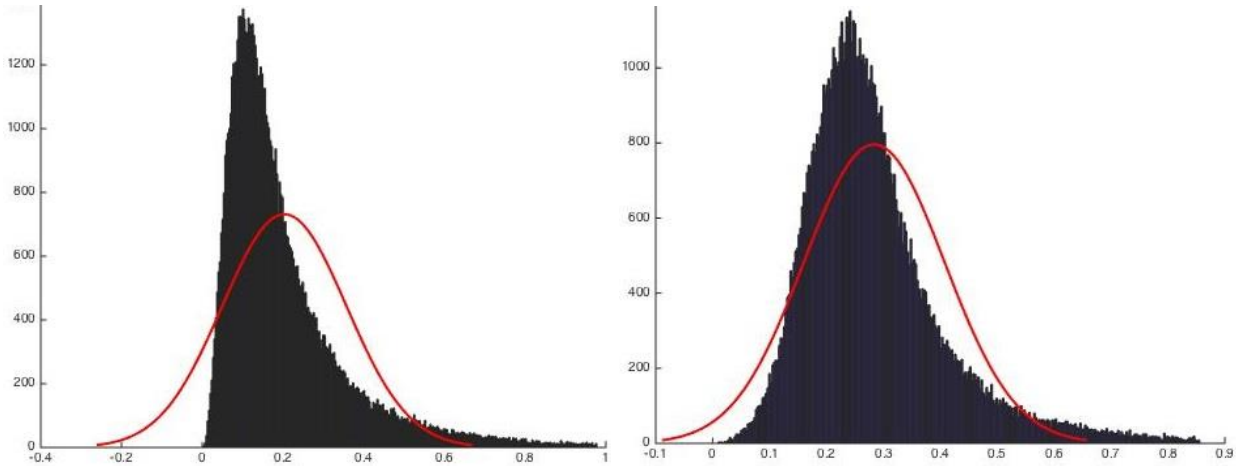

c d

Figure 19. Histogram plots of the 99.7th percentile data shown in Table 1 for (a) Length from Trial 1, (b) Length from Trial 2, (c) Angle from Trial 1 and (d) Angle from Trial 2. The Gaussian distribution (red) is shown for comparison.

3.3.1.3. Wall movement

An experiment was performed to test the motion of OTS camera mounts. OTS camera mounting is critical to providing the best system calibration possible. If there is camera motion, the system measurement can provide high uncertainty. Hence, a measurement of camera motion is useful to determine how much motion the reference frame provides including all cameras. Motion of two cameras mounted in worst-case locations was measured to further understand this concept.

In the experiment, two optical tracking system camera mounts were tracked for 24 hours each using a laser tracker with an uncertainty of approximately 10 µm [176]. Magnetic retroreflector mounts were glued to the two camera mounts located near the center of the longest walls of the rectangular laboratory. The laboratory, shown in Figure 20, has 12 optical tracking system cameras mounted at a height of 4.3 m on 6.7 m high perimeter walls. The laser tracker was programmed to take a data point each second for a total of 86,400 data points. The inside laboratory environment remained at a relatively constant room temperature and humidity. However, during the outside wall motion measurement, the outside temperature changed by approximately 30° F between day and night according to local weather reports for the measurement period. The day was rainy, cloudy with no sun, and a high of approximately 55° F. OTS calibration and experiments were not, however, performed during the same day when measuring each wall since the laser tracker beam would have been obstructed during calibration and the experiment.

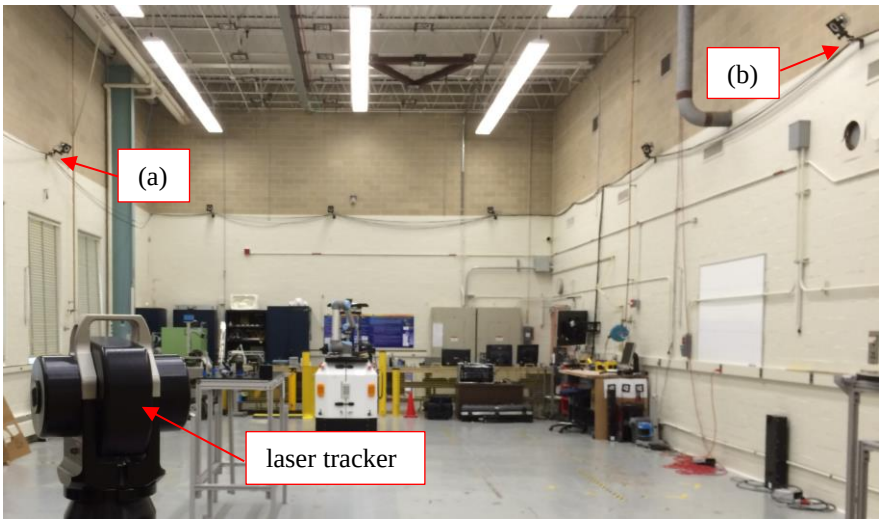

Figure 20. Laser tracker measuring a laboratory, outside-wall, mount (a) that supports an optical tracking system camera. On the right is the (b) inside-wall mount that was measured.

The laser tracker provided results as expected where the inside wall moved much less than the outside wall. The data is shown in Figure 21 for both wall measurements.

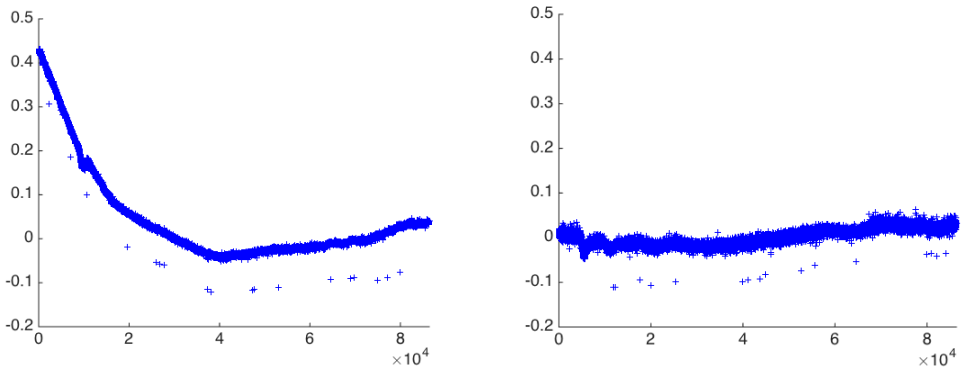

Figure 21. Laser tracker data from measurement of two camera mounts supporting optical tracking system cameras inside the laboratory on (a) an outside block wall and (b) an inside block wall. The horizontal axis is in sample points and the vertical axis is in mm.

For example, disregarding outliers, wall motion data spanned between approximately + 0.04 mm and - 0.05 mm for the inside wall and between approximately + 0.43 mm and - 0.05 mm maximum for the outside wall. Outside wall measurement began at 2 PM. Most motion of the outside wall was between 2 PM and 2 AM as shown in the left half of Figure 21 (a). Measurements of the mobile manipulator will be across a short time period relative to the 24 hour wall movement test and therefore, should not be affected by the camera motion.

3.3.1.4. Missing data

During data review and analysis, it was noted that there were several locations where data in log files was missing. Although not all data entries during experiments were blank, portions of data at various instances in time spanning several seconds was missing. This was caused by OTS cameras being mounted to walls where some or all markers on, for example, the EOAT were not within three or more OTS camera fields-of-view or were occluded by the manipulator. It is unclear as to the extent that missing data caused uncertainty. Where the data stopped recording and started again was not out of the ordinary. However, it is possible that some phenomena could have occurred during the instance when data was missing. Uncertainty of this random measurement phenomena cannot be readily included in uncertainty propagation equations and therefore, this cause of measurement system uncertainty is not included further in discussion.

3.3.2. RMMA

The RMMA concept also has measurement uncertainties to consider when using it to measure performance of mobile manipulators. The measurement uncertainties considered for developing the RMMA concept were to initially consider the mobile manipulator use-case, i.e., assembly. The RMMA was therefore designed and manufactured with machining tolerances typical of assembly of gears, screw insertions, and metal or plastic pegs inserted into assemblies (i.e., in automotive body assemblies). These assembly uncertainties led to machining tolerances of the RMMA surface and parts, the reflector type, the registration orientation uncertainty, and the RMMA movement.

As such, a representative model of a generic industrial assembly is designed into the RMMA that was included in this thesis research. It should also be noted that the RMMA concept could be expanded to relatively high tolerance assembly areas, such as piston insertion into engine blocks or even subatomic particle assemblies. These assembly applications would require a micro-scale RMMA tolerance and measurement scheme. However, this thesis research introduces the generic concept only and addresses the assembly scale described above. These uncertainties will be further detailed in the following subsections.

3.3.2.1. Machining tolerances

The RMMA base plate was designed and machined using the drawing shown in Figure 22. Tolerances were provided on the drawing to two decimal places and in imperial units. In this case, machinists used a +/- 0.01 in tolerance equal to +/- 0.254 mm. Hole positions can therefore have an uncertainty in position equal to +/- 0.254 mm.

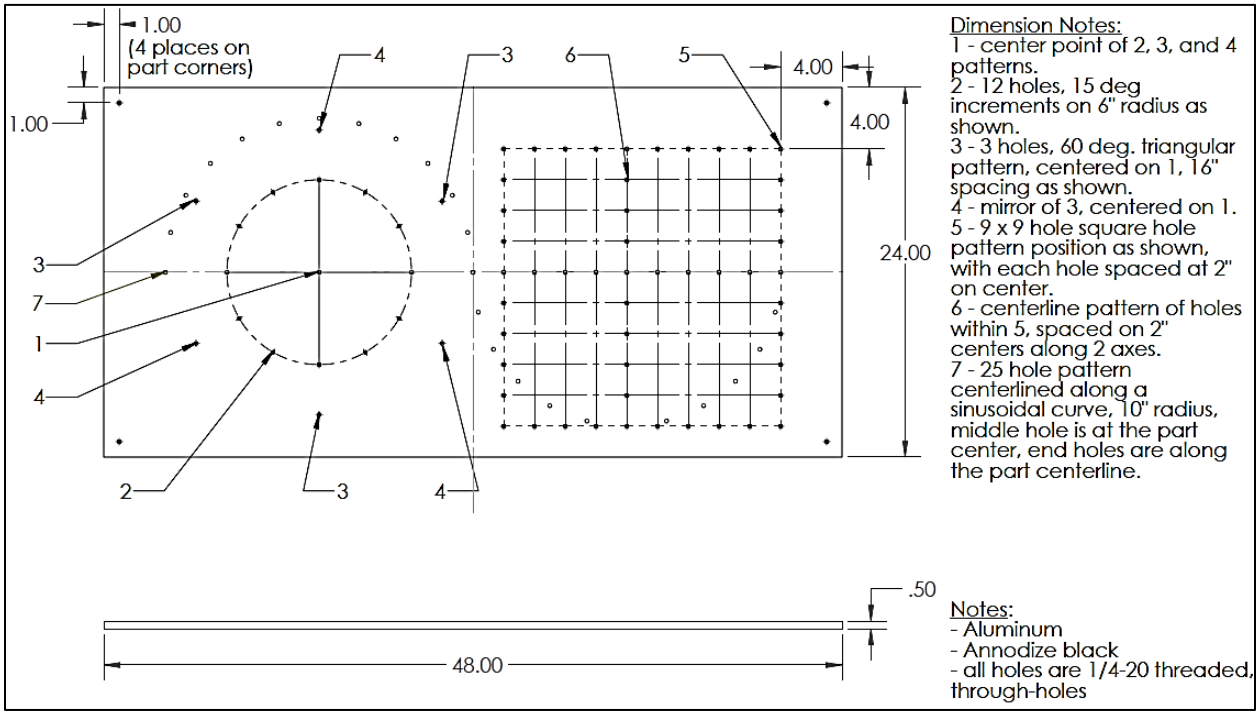

Figure 22. RMMA computer aided design drawing provided to a machinist to make the part. Dimensions are shown in inches.

3.3.2.2. Reflector types

A seemingly simple, yet critical part of the RMMA concept are the reflectors used to provide non-contact feedback to the mobile manipulator during performance measurement. The reflective device was required to provide the most precise fiducial dependent upon the desired mobile manipulator performance. The fiducial must also be detected within the tolerance of the laser retroreflector combined with the ideal reflective surface. It was initially determined that a passive reflector would be an ideal fiducial since no power- or signal-carrying tether to the RMMA was

required so that it can be accessed from any vehicle pose and a battery powered RMMA would require additional power maintenance. Choosing the correct reflector type was determined to be a critical performance measurement uncertainty. Therefore, multiple reflector types were tested, as shown in Figure 23, beginning with honeycomb reflective tape which is used for the AGV navigation reflectors.

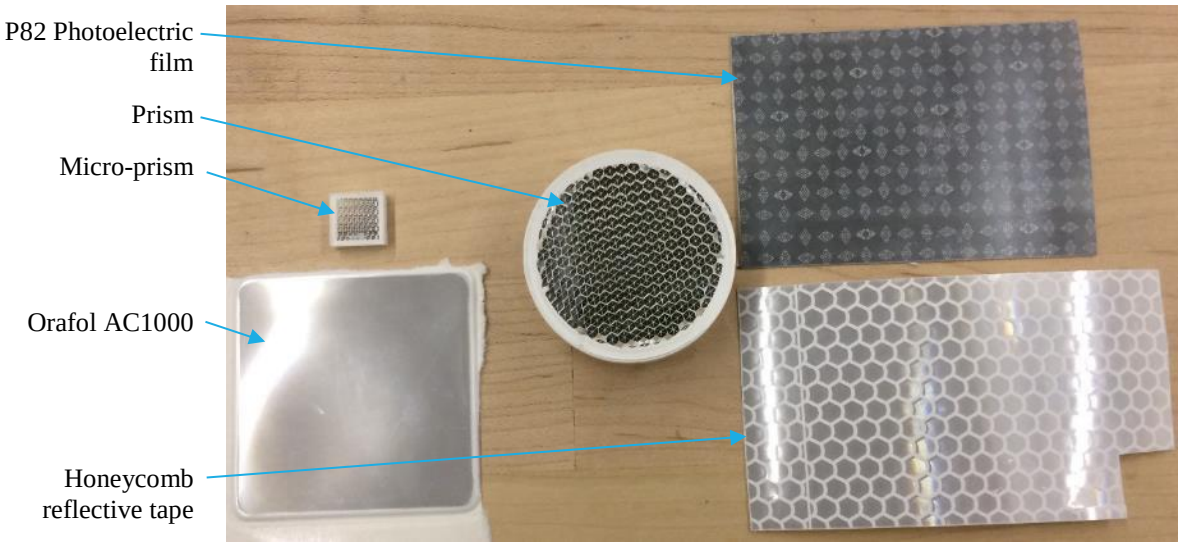

a

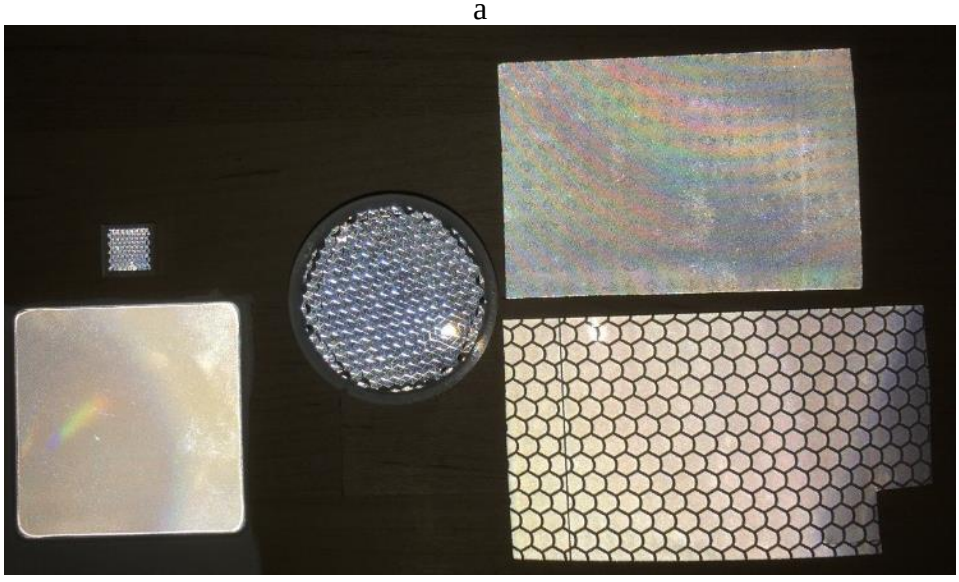

b

Figure 23. Photos showing various reflectors, (a) not illuminated and (b) illuminated with flash, that were tested with the laser retroreflector.

Data voids potentially caused by the honeycomb pattern lines were experienced as measured using a precision, manual, micrometer-driven, X-Y stage as shown in Figure 24 (a) with the laser retroreflector mounted to it. Figure 24 (b) shows the laser retroreflector shining directly on an example reflector being tested. The green light indicates only power to the laser, although the light should be yellow when the reflector is detected. Figure 24 (c) shows the non-illuminated, 6 mm

diameter, honeycomb reflective tape being tested and clearly shows that the honeycomb lines that cause disruption in detection of the relatively small laser beam. The test included setting the laser retroreflector height just above the reflector and scanning horizontally left to right (L-R), then right to left (R-L) along the same vertical position, and then incrementing down using the micrometer stages and repeating until no detection occurred. Figure 24 (d) shows the plotted data for this example. After each horizontal scan, the height was lowered 0.1 mm. When scanning horizontally, the micrometer position was logged just as the laser detected the reflector. As shown in the figure, a large void occurred in the center and no further detection occurred from just below the halfway line to the bottom of the reflector. Other honeycomb pattern reflectors were also tested and provided similar results. The P82 Photoelectric film was therefore deemed as not useful since it also had a pattern that may cause data voids or other anomalies.

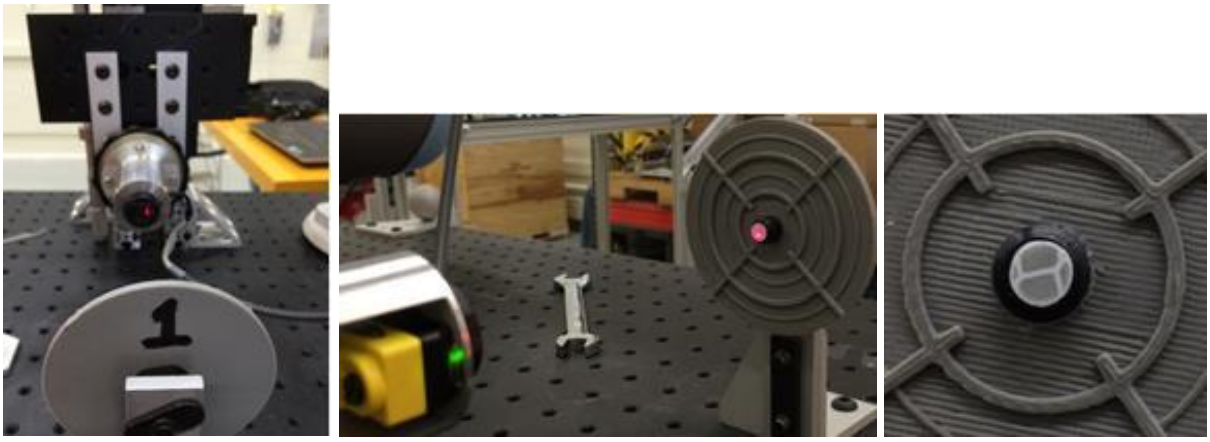

a b c

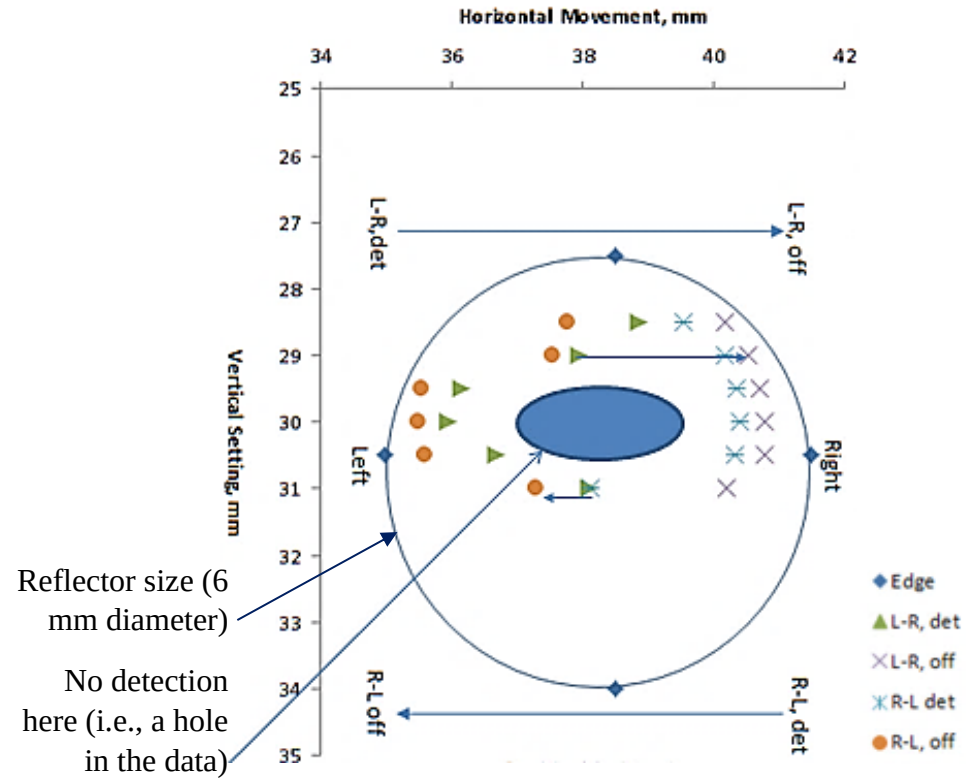

d

Figure 24. (a) Micrometer-driven, X-Y stage with laser retroreflector mounted horizontally. (b) Laser retroreflector shining on an example reflector being tested. (c) Non-illuminated, 6 mm diameter, honeycomb reflective tape being tested. (d) Plotted data from a raster scan of the reflector using the X-Y stage.

The legend is as follows: "Edge" = 6 mm diameter ground truth edge; "L-R, det" = left to right stage movement when the laser first detects the reflector; "L-R, off" = left to right stage movement when the laser stops detecting the reflector; "R-L, det" = right to left stage movement when the laser first detects the reflector; "R-L, off" = right to left stage movement when the laser stops detecting the reflector.

Prism reflectors of various sizes were tested with coverings to allow only a 6 mm or smaller opening for detection by the laser. The relatively large diameter prism reflectors were tested to be used as registration reflectors for a bisect method that will be explained in Chapter 7. The micro-prism was determined to be an interim candidate reflective material for tests that included fiducial sizes of 2 mm and larger. Because it had a prism above the reflector, although relatively small as compared to typical off-the-shelf reflectors of larger diameter, fiducial sizes smaller than 3 mm caused intermittent performance measurements dependent upon their exposure to the laser. Figure 25 shows the setup and plotted results of testing the micro-prism reflector through a 6.4 mm diameter opening. The results were relatively good providing some scatter beneath the 3D printed reflector cover with hole even though it was printed with a boss to touch the plastic prism cover. Therefore, it can be summarized that the plastic reflector cover allows some light scatter beneath the 3D printed part caused by the prism although nearly always it provided a uniform detection pattern.

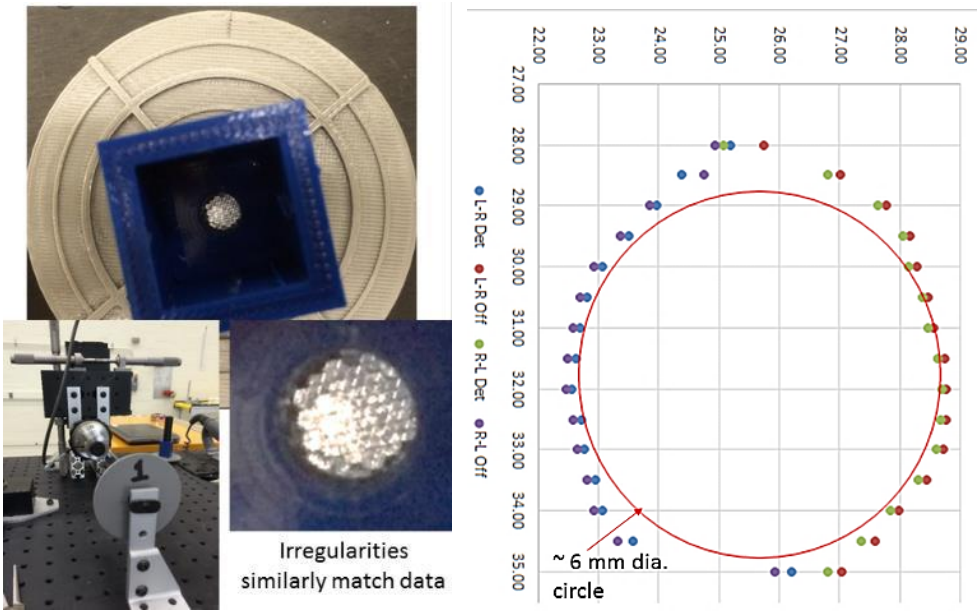

a b

Figure 25. (a) Setup (lower left), reflector within the 3D printed reflector cover (top), close-up of the reflector, and (b) results of testing a micro-reflector with the micrometer X-Y stage where the graph in (b) was rotated attempting to match the rotation of the close-up reflector photo.

The most uniform reflective material with no prism was found to be the Orafol AC1000 reflective patches which were cut into 12 mm square pieces equal to the size of the micro-prism reflectors since fiducial parts were 3D printed to accommodate the micro-prism reflectors. The patches are not designed to be cut although cutting and inserting them into each RMMA fiducial provided excellent laser detection results. Various sized holes in 3D printed reflector covers were then used to cover the reflector to test how small a hole diameter the laser retroreflector could be used and still detect the reflector with the laser.

Table 4 shows the data and Figure 26 shows the plotted results of laser retroreflector scanning at 0.5 mm vertical increments (providing a sufficient pattern of results) of a 3 mm diameter, Orafol AC1000 reflector inserted into a fiducial apparatus. As shown, the laser detects approximately 82% of the reflector with a standard deviation of 0.10. Interestingly, the initial detect is approximately 0.29 mm on average with uncertainty of 0.1 inside the edge of the reflector (note the start locations of arrows shown in Figure 26). Therefore, it could be shown that when attempting to detect a 3 mm diameter fiducial, a hole size of 3.29 mm should potentially be calibrated and used. This consideration was then expanded to even smaller fiducials to compare results and to determine the minimum size reflector that could be detected with the laser retroreflector.

Table 4. Data from the laser retroreflector scanning a 3 mm diameter Orafol AC1000 reflector.

					Difference		Detection %	
Vertical	L-R Det	L-R Off	R-L Det	R-L Off	L-R (Det - Off)	R-L (Det - Off)	L-R	R-L
40.00	37.13	39.18	39.36	36.65	2.05	2.71	0.68	0.90
40.50	36.74	39.35	39.13	36.50	2.61	2.63	0.87	0.88
41.00	36.67	39.41	39.17	36.45	2.74	2.72	0.91	0.91
41.50	36.77	39.31	39.05	36.50	2.54	2.55	0.85	0.85
42.00	37.11	39.12	38.68	36.75	2.01	1.93	0.67	0.64
							0.80	0.84
						Total Mean	82%	
						Std Dev	0.10	

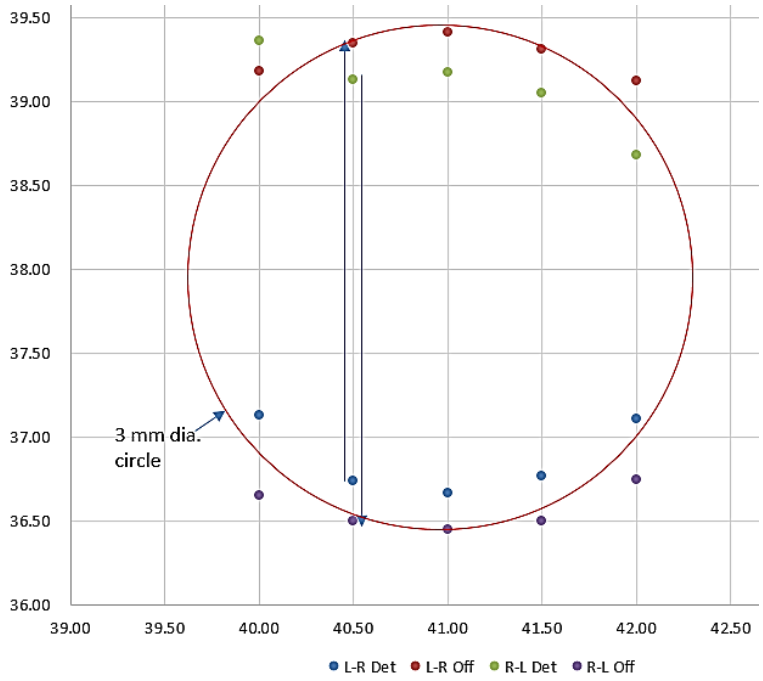

Figure 26. Plotted data from the laser retroreflector mounted to a micrometer X-Y stage used to scan a 3 mm diameter Orafol AC1000 reflector.

A photography aperture was procured and incorporated into reflector tests. The aperture was inserted over the Orafol AC1000 reflector and tested with the X-Y stage at various aperture openings. Since the opening was relatively small as compared to previous tests, 0.1 mm vertical increments were again used during scans. Figure 27 shows the experimental setup noting that Figure 27 (d) shows an oval shape to the aperture opening. Table 5 shows the data and Figure 28 shows the data plotted for a 1.07 mm diameter aperture opening above the Orafol AC1000 reflector. The diameter for the aperture openings was set by inserting a micrometer-tested #60 drill bit to be 1.07 mm diameter, closing the aperture to the bit, and then removing it once the aperture was set. The plot also shows a somewhat oval shape to the data, i.e., extending data points beyond the circle. Results show the same offset-edge phenomena that was experienced with the 3 mm opening (note the start locations of arrows shown in Figure 28). The outer edge was not detected until the laser scanned across from either direction to, in this case, again 0.29 on average from the reflector edge with uncertainty in this case being 0.03. Hence, a desired performance measurement uncertainty of 1 mm would therefore use a reflector sized to 1.29 mm diameter. Again, a laser-to-reflector calibration would be required prior to measuring mobile manipulator performance.

Table 5. Data from the laser retroreflector scanning a 1.07 mm diameter Orafol AC1000 reflector.

						Difference, mm		Detection %	
	Vertical	L-R Det	L-R Off	R-L Det	R-L Off	L-R (Det - Off)	R-L (Det - Off)	L-R	R-L
1	40.20	38.64	39.17	38.87	38.35	0.53	0.52	0.50	0.49
2	40.30	38.58	39.24	38.95	38.33	0.66	0.62	0.62	0.58
3	40.40	38.62	39.24	38.94	38.30	0.62	0.64	0.58	0.60
4	40.50	38.60	39.25	38.96	38.30	0.65	0.66	0.61	0.62
5	40.60	38.60	39.24	38.96	38.34	0.64	0.62	0.60	0.58
6	40.70	38.63	39.27	39.00	38.35	0.64	0.65	0.60	0.61
7	40.80	38.62	39.26	38.96	38.32	0.64	0.64	0.60	0.60
8	40.90	38.60	39.27	38.96	38.33	0.67	0.63	0.63	0.59
9	41.00	38.52	39.25	38.98	38.28	0.73	0.70	0.68	0.65
10	41.10	38.55	39.26	38.97	38.28	0.71	0.69	0.66	0.64
11	41.20	38.59	39.24	38.94	38.32	0.65	0.62	0.61	0.58
12	41.30	38.73	39.20	38.94	38.35	0.47	0.59	0.44	0.55
						0.63	0.63	0.59	0.59
							Total Mean	59%	
							Std Dev	0.05	

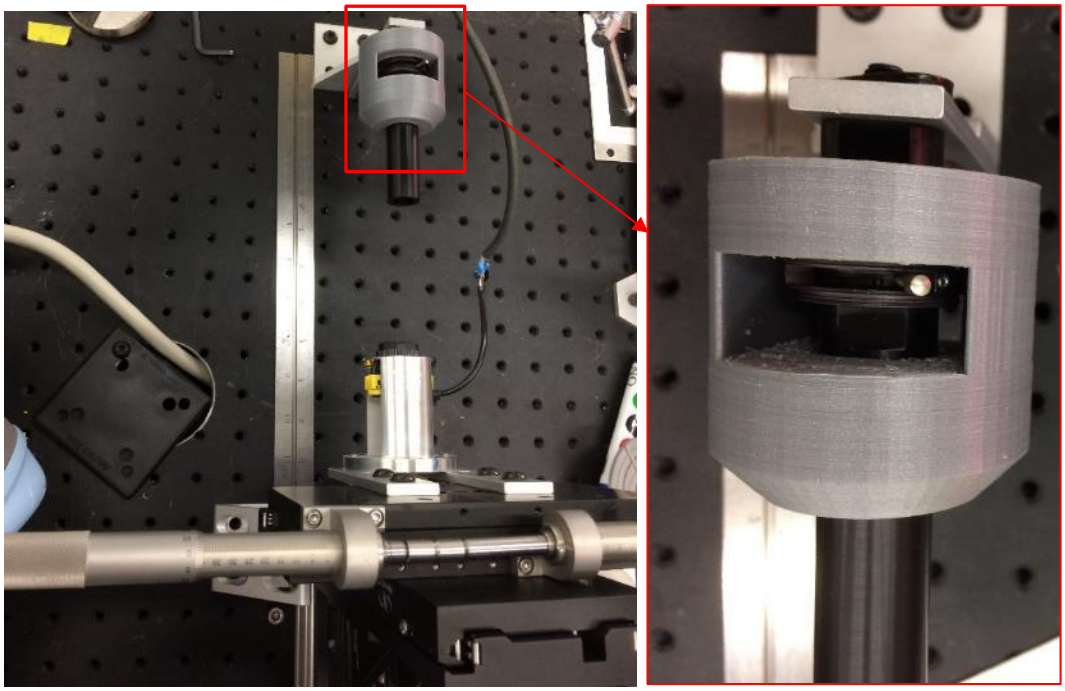

a b

c d

Figure 27. (a) Experimental setup of the laser retroreflector mounted to a micrometer X-Y stage and the aperture within a 3D printed (gray) housing. (b) Close-up of the aperture and housing. (c) The aperture removed from the housing and beneath a scale and 1.07 mm drill bit. (d) Close-up of the aperture showing an oval shape.

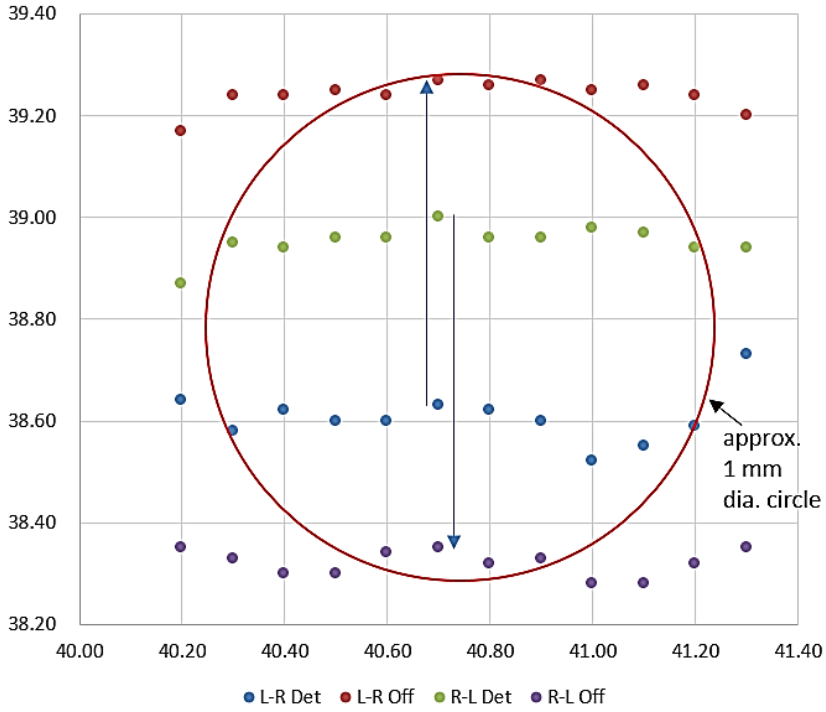

Figure 28. Plotted data from the laser retroreflector mounted to a micrometer X-Y stage used to scan a 1.07 mm diameter Orafol AC1000 reflector.

One last step was to determine the smallest diameter reflector that could be detected using the chosen laser retroreflector. A similar method was used with the aperture and varying drill bits of smaller and smaller sizes. Table 6 shows the results with 0.8 mm being the smallest detected opening of the aperture above the Orafol AC1000 reflector. As these were the only drill bit sizes

available, it is possible that between 0.8 mm and 0.65 mm detection could occur. Applying the phenomena of edge-offset detection, as described previously, it may be considered that a 0.8 mm diameter reflector would cause an uncertainty measurement of 0.51 mm diameter as the smallest detectable area.

Table 6. Aperture openings above the Orafol AC1000 reflector showing the laser retroreflector detection or no detection.

Aperture opening, mm	Detected?	Applying 0.29 mm edge-offset detection)
0.95	yes	0.66
0.90	yes	0.61
0.80	yes	0.51
0.65	no	-
0.50	no	-

3.3.2.3. Registration orientation uncertainty

Orientation uncertainty of registration using a circular search method on relatively large (e.g., 6 mm diameter) reflectors initially did not consider raster scanning the reflector to find it's center. As a result, for the early experiments performed (described in chapter 6.2.1) when developing the RMMA concept, it was determined that using relatively large fiducial reflectors may cause the error shown in Figure 29. The laser detection points may be at the upper and lower edges of two reflectors used for registration to the RMMA which would then cause a large rotation error and potentially failed attempts on following reflector detections.

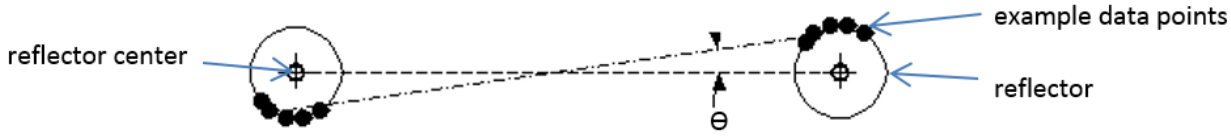

Figure 29. Graphic of possible orientation uncertainty when the reflector center is not detected.

3.3.2.4. RMMA movement

An experiment was performed [50][170] to test if there was RMMA motion that may add to the uncertainty of fiducial detection by the mobile manipulator. The static RMMA was nearly centered in the vehicle-use area of the laboratory which was located on the ground level and with a concrete floor. Six markers were placed on the RMMA, one at each of the four corners and two in the center. A rigid body was formed from the markers and recorded for approximately 12 minutes while the AGV was docked next the RMMA. Also during the experiment, the manipulator onboard the AGV was programmed using the teach pendant to continuously move without contact from one reflector location to another of the four reflectors in a square pattern.

It might be expected that the relatively heavy AGV (approximately 1137 kg), with respect to the onboard lightweight manipulator (29 kg), does not move. In addition, the one story, 7 m high lab is located on a ground level with concrete floor, yet there is ground truth-measured building movement that may affect precision assembly performance of a mobile manipulator. The lab is perhaps even more ideal than typical factory settings where many more machines and processes

could cause even larger measurement-disturbing vibrations than the experiments uncovered. Figure 30 shows a ground truth point cloud of the RMMA movement. Table 7 lists the mean (μ) and standard deviation (σ) of position (in mm) uncertainty with respect to the ground truth origin for each of the three runs for the RMMA. The mean RMMA movement spans from approximately 0.5 mm in X and 0.6 mm in Y.

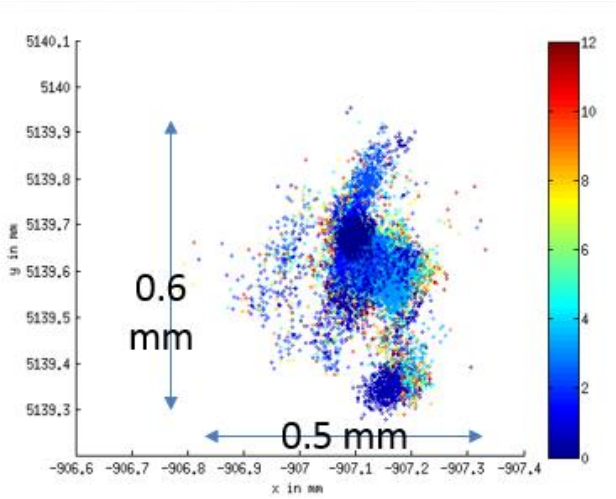

Figure 30. GT data points relative to the GT system origin (in mm) of the RMMA movement over time (in minutes), shown by the varying colors, while the manipulator moves.

Table 7. GT measured distances, with respect to the GT origin, of the RMMA movement

	Run1		Run2		Run3	
Axis	*μ*	*σ*	*μ*	*σ*	*μ*	*σ*
X	-907.13	0.040	-907.13	0.043	-907.13	0.041
Y	5139.67	0.15	5139.59	0.099	5139.61	0.085

3.4. Conclusions

Two measurement systems were modeled using SysML showing their interconnected components. The internal block diagram for the OTS provides internal measurement speeds Ethernet rates, and camera pixel count for the system used in this thesis. The generic model provides a simple computer science method that could easily be modified to show any OTS system used for mobile manipulator performance measurement. Similarly, the alternative concept of using an artifact was modeled using SysML showing three measurement options – search, bisect with search and augmented reality. The three methods were generically modeled in the internal block diagram showing tolerances, patterns of fiducials, and other pertinent information useful for the performance measurement test method to be implemented.

OTSs measure the three-dimensional, static and dynamic pose of multiple markers attached to objects within a measurement space. OTSs are used in a wide range of fields and have dramatically grown in market share over the past several years. Performance of a 12 unit, 4 MP camera OTS was verified using a new concept that used an artifact with markers on each end of a known-length metrology bar. The bar was measured using the OTS as it was statically positioned and was moved throughout the space in a raster-scan motion within the measurement space. This test method was

recently standardized as ASTM E3064 due to its usefulness across OTS manufacturers and users. Experimentation demonstrated that the OTS used for measuring performance of the mobile manipulator and described in this thesis has a static measurement uncertainty of 0.022 mm and 0.046° and dynamic measurement uncertainty of 0.26 mm and 0.20°.

Uncertainties of the OTS are caused by only using the current manufacturers methods to measure OTS performance, from wall movement, and from missing data due to markers occluded or outside OTS cameras field-of-views. Potential uncertainties in calibration can be caused by missing camera rays and the use of only a two-dimensional reference frame for system calibration. Measured uncertainty can therefore depend on the type and camera setup, number of cameras, number of markers used within the space, and several other factors. Missing data was discovered during data review and analysis and noted that there were several locations where data in log files was missing. It is possible that some phenomena could have occurred during the instance when data was missing. However, without the data, the cause and therefore, the uncertainty of a measurement phenomena cannot be readily included in uncertainty propagation equations. Lastly, worst case (i.e., inside and outside wall) OTS cameras were measured using a high-accuracy laser tracker throughout a 24 hr period. Throughout the period, camera mounts only slightly moved (i.e., approximately 0.02 mm for the inside wall and 0.04 for the outside wall), although could cause increased uncertainty. However, measurements of the mobile manipulator will be across a short time period relative to the 24 hour wall movement test and therefore, should not be affected by the camera motion.

An alternative to the measurement system to the OTS was conceptualized, designed, fabricated and provided as a new method for measuring both static and mobile manipulator performance. The concept, called the Reconfigurable Mobile Manipulator Apparatus (RMMA), includes posing a mobile manipulator next to an artifact as well as posing the EOAT attached to the manipulator at specific locations above the RMMA to digitally detect reflective fiducials with known uncertainty. The performance evaluation criteria can include the:

- Time to register the mobile manipulator to the artifact
- Time to move from the registration points to the assembly points
- Repeatability after registration
- Number of search steps equating to the initial distance from registration/assembly points
- Detection of reflectors with varying diameters

Uncertainties of the RMMA are machining tolerance, the various reflector types, the registration orientation uncertainty and the RMMA movement. Machining tolerance on the RMMA for drilled holes can have an uncertainty in position of +/- 0.254 mm. There are a variety of reflectors that were measured and the large prismatic types and honeycomb pattern types caused the most uncertainty. Micro-prism reflectors and uniform Orafol AC1000 tape provided the most certainty in performance as measured by scanning across reflectors with the laser retroreflector. Registration orientation uncertainty was initially discovered and was soon remedied by using an optical aperture over a reflector to detect its center. Through experimentation, it was determined

that RMMA movement occurred when the mobile manipulator will move during mobile manipulator measurements approximately 0.5 mm in X and 0.6 mm in Y. Delaying or slowing measurement is a method that could minimize the RMMA movement uncertainty.

4. MOBILE BASE

Mobile base navigation includes sensing the world, computing the next motion, and actuating the base. A vast amount of research has occurred in this area and a brief summary of navigation methods are listed in [177]. Those methods include potential field methods that addressed the first sensor-based motions [178][179], vector field histograms as the first alternative to doing obstacle avoidance with high-uncertainty sensors like ultrasounds [180], elastic bands as the first technique combining planning and reaction schemas in a unified framework [181], the dynamic window as the first technique to address kinematics and dynamics to carry out motion at high speeds [182], the curvature-velocity method as a similar method developed [183], and nearness diagram navigation as the first technique to address motion in troublesome scenarios [184], among many other techniques discussed in [185]. Navigation-error reduction has been researched, uncovering a variety of successful and unsuccessful methods [186]. An example of the latter is dead reckoning, which can increase navigation position error. An example of the former is vision-based navigation combined with non-linear filtering techniques. Those techniques include Extended Kalman or Unscented Kalman Filters, which use a series of measurements observed over time; Gaussian Sum Filtering, which tracks filtering and predictive distributions encountered in dynamic, state-space models; and Particle Filtering, which implements a recursive Bayesian filter using Monte Carlo simulation.

Automatic Guided Vehicles (AGVs), have been used for industrial material handling since the 1950's, without much change to design since then, and typically include much less onboard sensing of the world than the autonomous mobile robots. Figure 31 shows the NIST-owned 1.7 m W x 2.9 m L x 3.1 m H AGV and 0.6 W x 0.6 m L x 1.2 m H mobile robot. AGVs use, for example, position-calibrated fiducials, mounted to walls or superstructures, detected by laser azimuth and range sensing to triangulate vehicle pose. AGVs also use minimal computation to choose the next motion and they are commanded when to actuate by, typically, a central, off-board controller. As AGVs begin to navigate through unstructured environments or precisely position tools for manufacturing [187], they too may utilize some of the previously discussed mobile robot navigation techniques. Equipment manufacturers provide specifications for how accurately the vehicle must perform; for example, the AGV navigation laser sensor has a manufacturer specified range measurement resolution of 3.9 mm and angular resolution of 0.125° with statistical error distance of ±10 mm. [188] This specification is only for the navigation sensor without adding all other vehicle components, such as wheels, amplifiers, controls, motors, etc. and parameters such as weight and size. However, the manufacturer typically does not provide the overall mobile robot or AGV accuracy and repeatability specifications for all navigation and positioning situations. Moreover, navigation performance measurement methods for mobile robots and AGVs have been minimally defined in the literature.

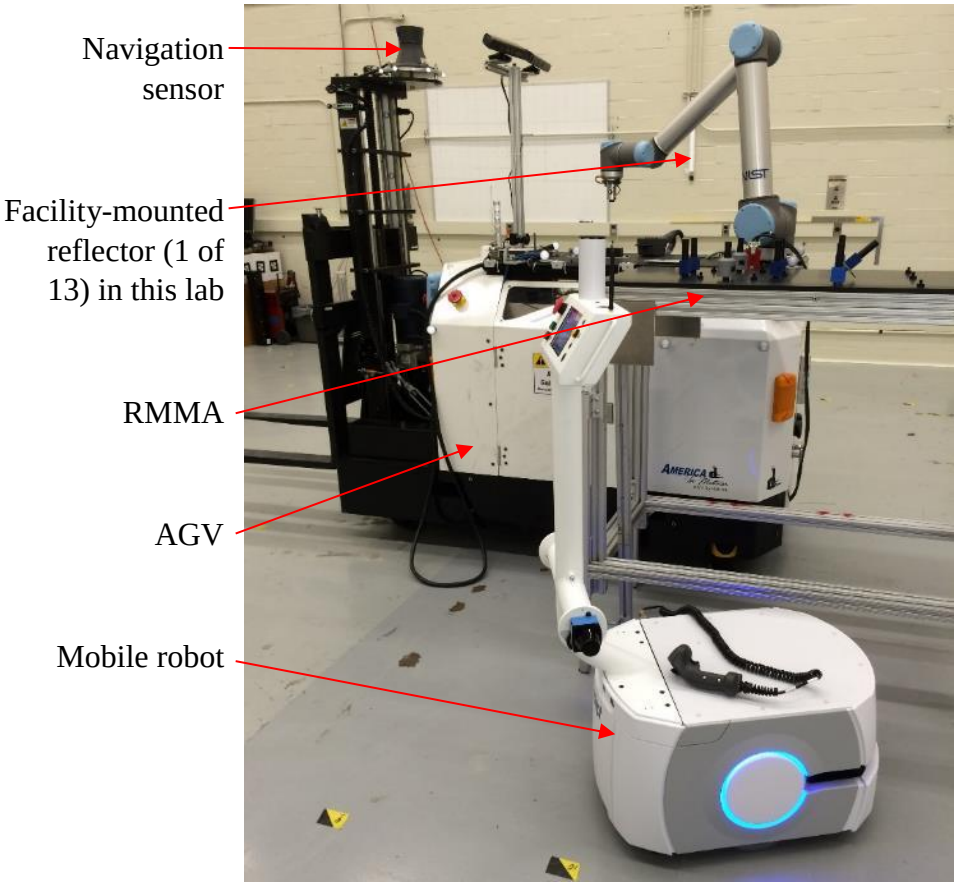

Figure 31. AGV with onboard manipulator behind an autonomous mobile robot (foreground) and the RMMA between the vehicles.

To achieve navigation-performance measurement for mobile robots or AGVs, a set of metrics must first be defined. Use of quantitative metrics for AGV navigation is limited to measuring the length of the path or the time needed by the vehicle to complete the task. [177] Deviation from the path could also be used since the AGV may be required to navigate within a small tolerance in proximity to some infrastructure – sometimes called localization accuracy. More autonomous mobile bases also add path planning and obstacle avoidance as metrics. In most autonomous mobile bases, they too can be made to perform path planning like AGVs where a preferred path is used to constrain the base during navigation and even docking. Obstacle avoidance is, however, not typical of AGVs and is included in section 4.5.3 in tests performed in this thesis research for stability and the effects on docking performance prior to docking. As stated in [189], "the lack of consensus on how to define or measure these systems impedes rigor and prevents evaluation of progress in this field and compare its different capabilities." One proposed method [190] for evaluating the localization accuracy of an indoor navigation system in arbitrarily large environments is to use onboard, mobile, robot vision and facility landmarks consisting of distinct patterns. This is instead of using externally mounted sensors, as required by most ground-truth systems. For this method, the combined mean position error was 15.2 mm and mean orientation error was 0.4° with maximum errors of 52.9 mm and 2.8°. For the thesis case, this is a relatively large uncertainty that would

require the manipulator to compensate for the mobile base pose error causing additional registration time and maneuvers.

U.S. [138] and European [139] AGV safety standards have evolved to protect nearby workers. These standards have minimal test methods to describe how manufacturers and users are to perform AGV safety measurements, resulting in potential measurement differences across the industry. Initial performance standard developments began with a review of other research and standards efforts for mobile robots as applied to emergency response and military applications [191]. This reference also discusses research challenges, test and evaluations, and intelligent systems development programs that can support advancement of industrial AGVs towards attaining greater levels of intelligence. These other efforts also provide useful standards development criteria for AGV performance test methods. Experiences and results in advanced mobility and intelligence for robotics will be essential for AGV manufacturers and users to fully understand capabilities and specific applications of their automatic through autonomous vehicle systems.

Performance test methods for autonomous industrial vehicle navigation and obstacle detection, a practice for recording environmental effects, and a terminology standard have recently been published, based on past research [192][193], under the new ASTM Committee F45 on Driverless Automatic Guided Industrial Vehicles performance standards. Of particular concern are test methods that potentially do not require purchasing relatively expensive ground-truth measurement equipment with accuracy that is at least 10 times better than the system under test. However, development of standard test methods do require accurate ground-truth measurement systems as suggested in section 3.2.2. Additionally, docking and communication interruption standard work items have been initiated and are F45 committee work items that have not been published as of the date of this thesis.

Terminology is often developed using slang or other pseudo-standard terms causing potential misunderstandings of manufactured products. For example, an automatic guided vehicle has been termed an AGV, SGV (self-guided vehicle), LGV (laser guided vehicle), mobile robots, etc. The recent ASTM F3200-17 Terminology Standard terms industrial vehicles with the capability to be driverless as A-UGV's (automatic/automated/autonomous-unmanned ground vehicles) providing a generic term where the "A" describes the different levels of autonomy incorporated into the single term as needed for test method development. This is critical during vehicle testing since the various autonomy levels cause the range of vehicles to perform differently as will be discussed further in this chapter. This thesis will mainly focus on and use the most prevalent industry term "AGV" (which has the autonomy level "Automatic") with some discussion on future vehicles having "Autonomous" capabilities, as with mobile robots.

This chapter will discuss the mobile base model that uses the AGV as the example industrial vehicle with some information about advanced mobile bases or mobile robots. Following is a discussion on calibration of the AGV infrastructure and vehicle where navigation performance evaluation is then discussed through experiments analysis and a recommended test method. Beyond navigation is the performance evaluation of AGV docking and an extension of the concept

to more advanced mobile base docking. AGV and advanced mobile base stability is then described where stability plays a critical role in obstacle detection and avoidance.

4.1. Mobile Base Models

4.1.1. Mobile Base

The SysML internal block diagram, shown in Figure 32, models the internal components of the mobile base, in this case focused on the AGV. [160] The diagram also displays the types of signals that are passed between components. The diagram also shows signal flow direction stemming from ports attached to various components. Much of the same components for an AGV (referenced and shown in SysML as a dashed box) are the same for a mobile robot or advanced mobile base, including wheel encoders, drive and steering motors and amplifiers, an onboard controller (e.g., AGVBrain), wheels, safety sensors, and navigation sensor (Nav sensor). As explained in the previous section, the Nav sensor is a spinning laser sensor for triangulating vehicle position to the referenced facility reflectors. The dashed arrows toward the wheels and to the referenced AGV show their reliance on the internal block diagram components that make up the mobile base.

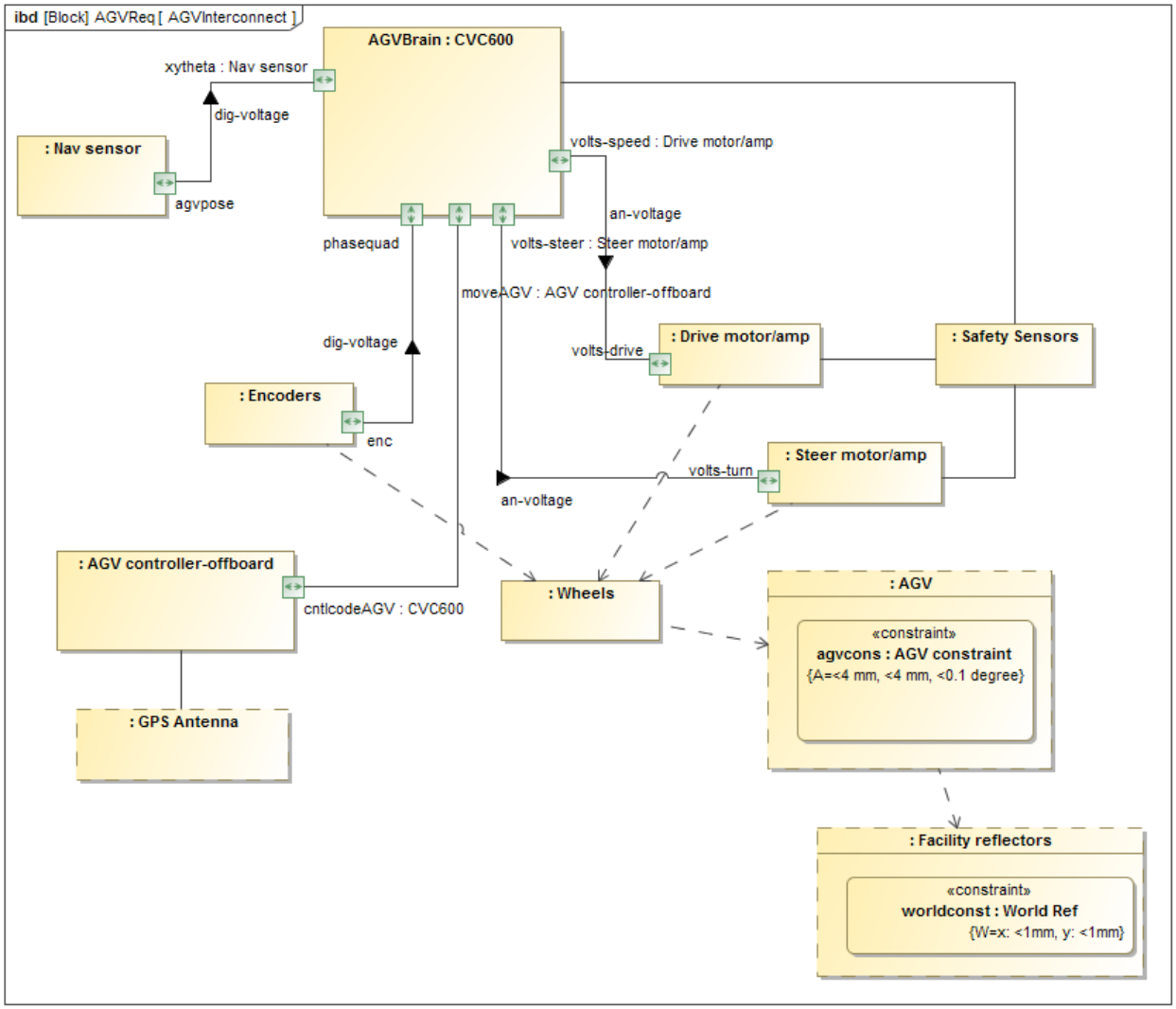

Figure 32. SysML internal block diagram of the mobile base (AGV) and subcomponents.

Many of the components shown in the model are further described in this thesis since calibration, navigation, docking, etc. all rely heavily on the individual or combination of one or all of these components. A GPS Antenna is also referenced by the AGV controller-offboard so that analysis can be tracked across all test computers (e.g., Mobile Base controller, Manipulator controller, and OTS computer). AGVs will remain the major mobile base focus of this thesis, although a comparison to mobile robots provides a more thorough understanding of how a model will differ when mobile robots become more prevalent.

Mobile robots typically use natural landmarks, such as obstacles sensed by an onboard laser scanner, cameras, acoustic sensors, and/or other sensors where each has characteristics that fit the mobile robot application and environment. Additionally, the sensors may be used for more than one function, such as navigation and safety. The obstacles are then stored in a map onboard the vehicle control computer and can typically be monitored by an offboard vehicle computer.

In the AGV case, a map of paths (segments) and stop locations and orientations (points) are created using software applications that function on the AGV controller-offboard. The applications [194] used to control the AGV are shown in Figure 33 using a high-level diagram. NDC8 is the AGV control program suite: Layout Designer includes the segments and points; Systems Manager Run includes the control interface for the user to step through the vehicle command and response; CWay allows execution and simulation of the transport structure (control program) written in the Systems Application Designer; and Vehicle Application Designer includes the AGV parameters to adjust, for example, the navigation sensor orientation, AGV reference point, the base pose, and the drive and steering setup, such as all wheel steer (AWS) capability. Programs written and used for this thesis using NDC applications are shown in Figure 74 (a) and Figure 75 in section 6.2.1.2. The programs will be described in section 6.

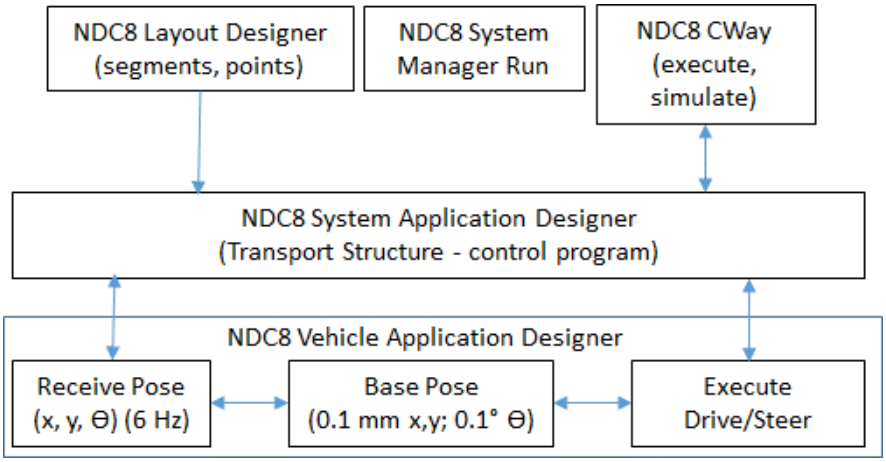

Figure 33. High-level diagram of the AGV control and monitoring applications used in this thesis.

4.1.2. Tests

Mobile manipulator high performance is highly dependent upon performance of the independent mobile base and onboard manipulator. The ideal requirement for the mobile base is to be positioned exactly at the commanded location. In the real world, of course, this cannot occur due

to, for example, sensing tolerances, uncalibrated mobile base, and other uncertainties causing the user to settle for some uncertainty. An example requirement for mobile manipulator performance is to achieve the RMMA fiducial uncertainty of 1 mm, as in section 3.3.2.2 where the requirement will mostly be compensated for by the manipulator which has much less uncertainty. However, the most achievable AGV performance should also allow improved mobile manipulator performance. As such, validation (i.e., assurance that the AGV meets the requirement – e.g., striving for the 4 mm Nav sensor specification) of the best performance through verification (i.e., evaluation of compliance) is needed. The AGV propagation of uncertainty therefore, stems from the facility reflector positions, the calibration of the AGV itself (e.g., wheel alignment and proper measurement, e.g., encoder settings), the navigation capability to follow a path and then to dock at the commanded location, and stability of the vehicle, especially when supporting the manipulator.

Figure 34 shows a SysML block definition diagram of the many tests that were performed on the AGV, as well as some that were performed on the mobile robot to also validate the model for a more autonomous vehicle. However, expected requirements of the mobile base remain unknown, except for verifying improvements to vehicle performance upon making adjustments to sub-components, shown in Figure 32, and/or the software modules that drive/read the sub-components. The following sections detail each of the tests shown in the model of mobile manipulator tests that depend on performance of the mobile base.

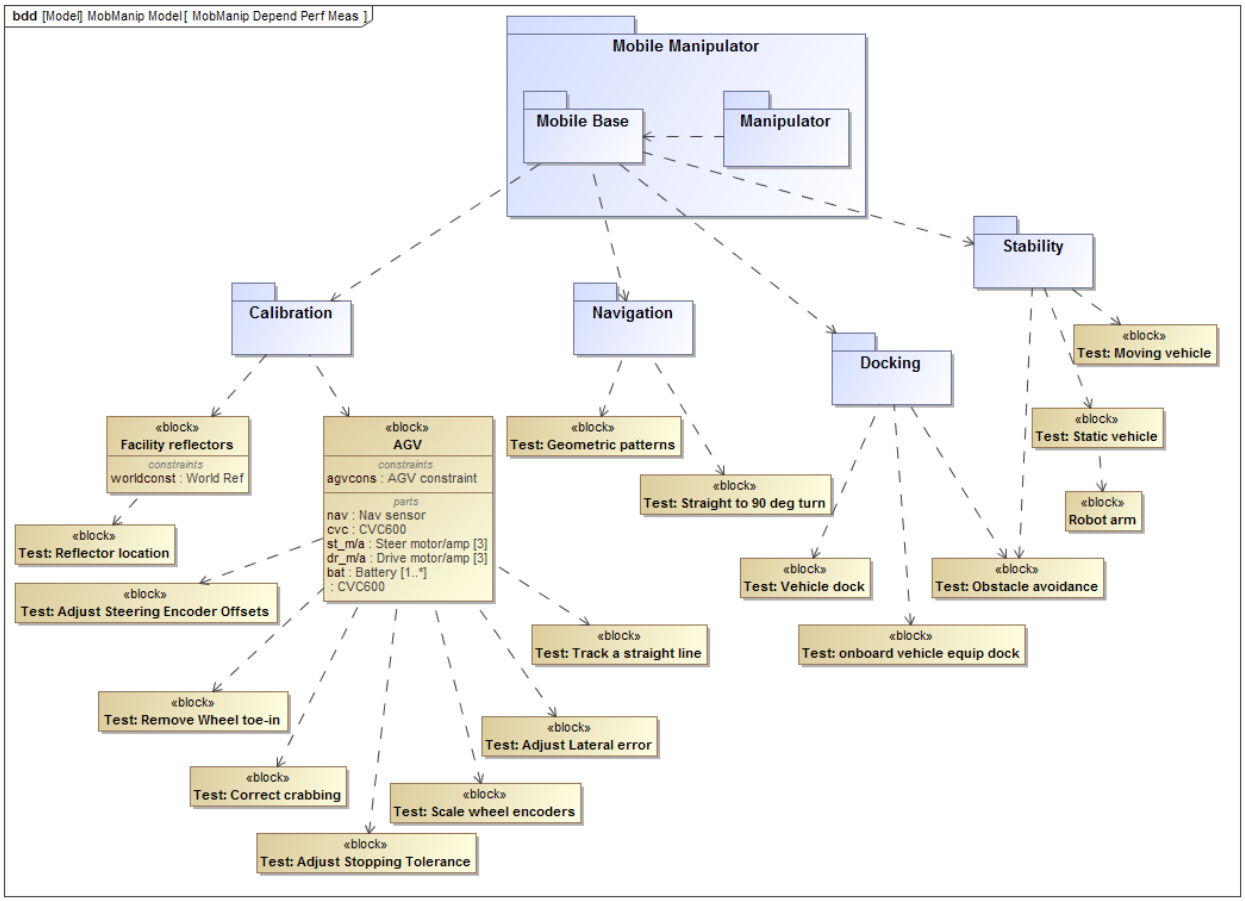

Figure 34. SysML block definition diagram of mobile manipulator tests that depend on performance of the mobile base.

4.2. Mobile Base Calibration

Early manufactured AGV's typically detected embedded wires in the floor. More recently, AGV's detect tape or chemical lines on the floor while most AGVs use laser guidance detecting facility reflectors mounted to the walls or other superstructures using a one-dimensional, spinning laser Nav sensor that detects range and azimuth to the vehicle. Less typical of AGVs and most typical of autonomous mobile robots is the use of "natural navigation" which is the detection of obstacles, such as walls, racks, etc.) typically using a scanning laser or vision. Laser detection of obstacles occurs, mainly in two dimensions while vision detects obstacles in three-dimensions, both called simultaneous localization and mapping (SLAM). Laser guidance used by AGVs will be the focus of this thesis since the majority of AGVs use this navigation method. However, SLAM using laser scanning will be briefly discussed to compare mobile robot navigation and docking to AGVs that use laser guidance.

4.2.1. Facility-Reflector Calibration

The AGV described in this thesis uses laser guidance for navigation and stopping or docking at a programmed point. Facility reflectors were mounted to the walls of the laboratory upon AGV purchase approximately 6 years ago and prior to this thesis research. Facility reflectors are typically calibrated in position only once at installation assuming they don't move throughout the time AGVs use the reflectors.

At the time of purchase and installation, a typical metrology method was used by the manufacturer to determine the 13 facility reflector locations in the laboratory with total laboratory space measuring approximately 9 m wide x 22 m long where facility reflectors are mounted. The method used a Total Station metrology system [195] (e.g., costing approximately $3K) to measure the approximate centroid of the reflector. This is the manufacturers cost effective method for ensuring that the facility reflectors are mounted with 'enough' certainty to complete the intended tasks, i.e., material handling of pallets and tray drop-off/acquisition to/from tray stations. However, given the thesis case of assembly, the use of an even less uncertain measurement system is required.

Later, a high-performance laser tracker was used to measure the reflector locations determining that maximum X and Y facility reflector location error was approximately 5 mm or more. The laser tracker detected a retroreflector that was manually moved about the circular reflector and analysis used a circle fit to the data to calculate the reflector centroid. The new laser tracker numbers were instead used and AGV navigation and docking performance improved. Since laser trackers can cost approximately $100K or more, they may not be feasible for AGV manufacturers or installers to use where for example, the Total Station is approximately a least one order of magnitude less than laser trackers.

Given these dramatic differences in capability and cost, the author developed a new method using the OTS. First viewing cost, a minimal OTS (i.e., 2 cameras and controls) can be at a midpoint cost between the laser tracker and Total Station, dependent upon camera cost which is tied to

camera performance. A high-end three camera OTS can be approximately $20K with a stereo OTS being approximately $3K. Since the high-end system resulted in low uncertainty as compared to the mobile base and manipulator, the OTS system appears ideal for facility reflector calibration too.

The OTS views the reflector as a large white spot as shown in Figure 35 (a). Hence, a cover was designed using a cardboard tube with a slot cut out the size of the reflector. Also, 3D printed parts were designed and printed to allow a marker to be mounted on top and bottom of the reflector and held to one another with a long spring as shown in Figure 35 (b). A method to expand and contract the spring using an attached string allows for marker installation to the reflector and for removal of the apparatus. Figure 35 (c) shows the assembled apparatus and one additional marker mounted to the wall near the reflector since the OTS requires at least three markers to track within a rigid body. A short, 10 s of data was collected and used to analyze reflector position.

There was no improved reflector position as compared to using a laser tracker. However, a pro for using the OTS are that it is approximately half the cost of a laser tracker. Another pro is that, if the OTS was used as a reference system for all activities within the facility that includes AGVs, the AGV can be referenced to the OTS with the same reference origin simplifying calculations. A con for using the OTS is that it would require three or more cameras to be focused on the AGV reflectors for testing causing the OTS to be recalibrated each time the cameras are moved. In the case used for this thesis research, cameras would be required to move three times for three calibrations requiring approximately three total hours of calibration.

a b c

Figure 35. a) AGV reflector illuminated by flash, b) novel AGV reflector cover (left) and repeatable marker pose apparatus (RMPA) parts (right), and c) AGV reflector with cover and RMPA attached. A third, randomly placed marker is mounted to the wall (right) since a minimum of 3 markers are required

for OTS measurement of the reflector. The OTS markers could be replaced by laser tracker retroreflectors or other measurement system markers.

4.2.2. AGV Calibration

Proper AGV functioning relies on its navigation and docking accuracy and repeatability used to move materials and equipment around the workspace. A key to obtaining the desired accuracy is proper calibration of the AGV. [196] AGVs may eventually become uncalibrated through regular use. An uncalibrated vehicle does not follow a commanded path or stop/dock at a commanded point with minimal relative uncertainty (standard deviation of measured vs. ground truth) as does a calibrated vehicle. To correct this, vehicle manufacturers have calibration procedures for their vehicles, although these procedures can be tedious, time-consuming, and may not be appropriate for all vehicles. For example, calibration of Ackerman steered vs. AWS steered vehicles have different procedures. It is not always clear what will happen when a vehicle is uncalibrated nor when the vehicle becomes uncalibrated, except that as experienced within the AGV industry and this thesis researcher, vehicle path and docking offsets exist. The effects of calibration on vehicle control and uncertainty are typically not specified by the manufacturer either. There is also typically no specification describing how far from the commanded path a vehicle navigates. This may be important to users who have tight tolerance AGV paths (e.g., paths between infrastructure) that must be followed.

A variety of approaches to AGV navigation are discussed in the literature. [197][198] Navigation approaches can be separated into two broad categories, those that perform dead reckoning and those that rely on external positioning references. Dead reckoning relies in a large part on accurate estimation of the distance and direction the AGV travels. Poor calibration of an AGV can lead to large positioning errors. Small errors in the commanded steering and the measured distance accumulate to produce large positioning errors [199][200]. For AGVs that rely on external navigation resources, the ability to accurately servo to a desired location can be affected by the quality of the vehicle's calibration, as well as the quality of the external positioning reference (see the previous section 4.2.1).

However, current AGV steering calibration mainly includes locking the two rear steer wheels together at 0°, allowing only the front wheel 0° steering rotation to be adjusted, and then testing that the AGV moves along a straight line. Figure 36 shows this technique where the AGV has an onboard laser pointing along the travel direction and shining on a piece of paper taped to the wall. The laser was aligned to a plate (see Figure 36 (a)) mounted to the breadboard mounted on top of the vehicle. It is possible that the breadboard was mounted at a slight angle to the vehicle travel. However, this may be the best possible method for this type of test as used by AGV manufacturers. An initial laser spot position is marked on the paper. The vehicle is then moved approximately 10 m or more along a straight line and the laser spot position is again marked. Ideally, the laser spot does not move laterally when the vehicle moves demonstrating that the steer wheel is aligned with the fixed wheels. Up and down spot motions are due to floor undulations and are not relevant to the test. The test, unfortunately, does not include calibration of the rear steer wheels.

a b c

Figure 36. Current AGV calibration method showing (a) an onboard laser, (b) an initial laser spot position, and (c) a moved-AGV laser spot position on a piece of paper taped to the wall. The difference in lateral motion is shown in (c).

This document discusses the specific procedures used to calibrate the NIST AGV having AWS and is considered an industry advancement. The method for updating the parameters will be different on every vehicle, but the calibration procedures should have a wide applicability to different vehicles. These procedures cover several steering, drive, and navigation sensor calibrations issues. The possible uncertainties associated with these tests with remedies described in the following sub-sections are:

1. Laser alignment to the vehicle path – uncertain if the vehicle structure is aligned with the path and may cause calibrated parameters to be changed to uncalibrated;
2. Uncalibrated path following - when the laser is aligned with the path, the vehicle path calibration may be uncalibrated;
3. Crabbing – if coupled with 1, could cause the laser to provide a false-positive test outcome;
4. Only one wheel steers the AGV - misaligned non-steered wheels may cause vehicle pull to the side;
   a. Single wheel steer, even for AWS vehicles
   b. Locked wheels (i.e., other than steered wheel) could drag if they are toed in or out
5. Slower or faster wheel velocity on each wheel – may cause off-path navigation and/or wheel drag;
6. Wheel misalignment to the path – as with 5, may cause off-path navigation and/or wheel drag;
7. Tolerances of stop positions – may cause over- or under-shoot of docking poses

Although not a focus of this thesis, a useful test method would be to estimate the best value that is possible for each of the uncertainties and the links between them, if any, from the above list and then match a best measurement method to each. However, there is coupling between the uncertainties and the best practice is then to isolate the uncertainties to a single parameter change, (e.g., rotated wheel, navigation sensor pose with respect to the mobile base reference, etc.) to reduce the measurement complexity. Static and dynamic mobile base measurements fall within the capabilities and measurement tolerance of an OTS and could have been performed for all AGV measurements. However, manual measurement methods, described below, were chosen to provide appropriate calibration parameters for the AGV used in experimentation and provide a cost effective test method for adoption by the industry when they have no OTS. Similar methods are expected to also be used on other mobile bases. In the following Calibration Procedures sub-section, the tools are listed with their tolerances and an example is provided as to why these

methods were chosen. Following, each calibration procedure performed is described. The theoretical chain of uncertainties for mobile manipulators is then provided in section 6.3 which forms the generality that includes, not only the mobile base, but also the manipulator, tool, and RMMA measurement apparatus applied to the thesis case.

A number of observations led to the conclusion that the NIST AGV was out of calibration. High repeatability can often be achieved by always approaching a commanded stop location along the same path segment and from the same direction. Alignment of the AGV and the workstation can be achieved by moving the workstation to match the stop location of the AGV. In this situation, small errors in the vehicle tracking may go unnoticed, as long as they are repeatable. For mobile manipulator research, the AGV needed to be able to accurately stop at the commanded position, regardless of the approach direction or angle. Noted was a large deviation between the commanded stop point and the actual stop point, as reported by the vehicle's own navigation system. The AGV was consistently pulling to the left of the direction of travel and stopping short of the desired point by several centimeters. Errors as great as approximately ± 25 mm were measured between stopping points when the AGV was driven to the same coordinates from opposite directions. This is not reasonable when the specified navigation system repeatedly can provide position resolution down to 4 mm.

There are several papers describing methods for calibration of AGVs [201][202][203][204][205]. Reference [201] used manual calibration methods (e.g., a dummy front wheel to calibrate the rear wheels and axel length, pens marked on the floor for AGV radius, etc.). The concepts of [201] are similar to the methods described herein although this thesis does not use dummy wheels and methods described in the following sub-sections are on a commercial 1360 kg AGV that go well beyond [201]. The remaining references perform automated calibration methods.

Reference [202] used a self-calibration technique on a three-wheel, one-wheel steer vehicle using a gyro and without external absolute position sensing. Reference [203] used an augmented Kalman filter with vision measurements of floor markings to improve the odometric model. The camera was required to be carefully calibrated to support the measurements. Reference [204] used odometric pose estimation and a 2D laser scanning sensor fused to correct the vehicle path. As with [202], [204] described loops driven by the AGV that were corrected after a number of iterations. Reference [205] also used a gyro as in [202] to correct for odometric pose estimations. All of these automated calibration methods intended to calibrate the vehicle to the path during operation. Whereas the manual method used in [201] and in this thesis, intended to correct component or vehicle parameter errors that caused the AGV to be uncalibrated. Hence, the correction not only provides for optimal AGV performance but corrects other issues that industry is concerned with, for example: minimized wheel wear, unseen issues such as wheel toe in/out, and vehicle crabbing. In addition to the manual method, the automated calibration methods described in the literature could also be used to provide even more improved vehicle performance, although at the cost of additional sensors and controls. However, an ideal future research topic may be to include prognostics so that mobile base performance measurement issues can be anticipated and either corrected automatically or can alert a vehicle supervisor to correct them.

Calibration Procedures

The following calibration procedures were performed on the NIST AGV in order to improve its ability to repeatedly move to a commanded point from different directions. The calibrations also improved the ability of the AGV to accurately track a commanded path. A number of parameters will need to be read from the AGV controller, and some will have to be modified, in order to perform the calibrations described in this document. The specifics of reading and modifying the AGV parameters will be vehicle specific, and the operator will need to refer to the AGVs technical documentation for the specific names of the parameters and the methods required to access them.

The tools used to make the calibration measurements included mm increment rulers and mm printed grids, as well as a 10 m or longer tape measures pulled taught to create a relatively long straight line. Also, as with toe-in/out measurement, a 3 m long ruler was used to amplify the wheel diameter to exaggerate wheel rotation errors. Modifications to software parameters could only be set in mm's and tenths of a degree as set by the AGV manufacturer. Therefore, a system that measured smaller uncertainties below a tenth of a mm or 100^{th} of a degree provided no improved calibration. For example, measuring a 250 mm diameter wheel with toe-in of 0.1° and extended 3 m from the wheel caused a 5 mm offset at 3 m which was easily measured with a mm incremented ruler.

Steering Encoder Offsets

The NIST AGV has three drive wheels, each of which can be independently steered. Each wheel has a steering encoder offset that defines where 0° turn is located. If the wheels are not properly aligned, the vehicle will tend to turn left or right when commanded to drive straight ahead. This affects the vehicle's ability to servo to the commanded path. Typically steering is controlled using a PID (position, integral, differential) controller. The error is measured as deviation from the desired path. When driving along a straight path, the steering error will increase until the proportional correction offsets the steering offset error, causing the vehicle to track off to the side of the desired path by some amount. The wheels on the NIST AGV are arranged in a tricycle pattern, with two wheels in the rear and a single wheel at the front; however, these procedures apply to four wheeled vehicles as well.

Wheel toe-in

Toe-in is the alignment of paired wheels. On the NIST AGV, since it has a tricycle arrangement of wheels, this only applies to the rear wheels. On a vehicle with four wheels, the toe-in of the front and rear pairs of wheels needs to be adjusted. Ideally the wheels should be parallel to each other, a toe-in of 0°. Toe-in on the rear wheels was corrected by physically measuring their alignment. This was done by laying a ruler along the sides of the wheels as shown in Figure 37, drawing the lines on a piece of paper, and then measuring the divergence/convergence of the lines. The total angle was computed, and half that angle was added/subtracted from the right/left wheel rotation parameter. The absolute alignment of the wheels with the AGV chassis is dealt with in a later calibration step. The angle needs to be scaled into encoder counts and added or subtracted from the appropriate steering encoder offset. The relationship between encoder ticks and steering

angle is determined by the gearing ratio and the number of encoder ticks per revolution of the steering mechanism. This information should be available in the AGVs technical documentation.

Figure 37. Marking out toe-in angle on a sheet of paper.

The toe-in angle can be computed as,

$$\theta = \tan^{-1}\frac{(d_2 - d_1)}{L}, \qquad (1)$$

where d_1 and d_2 are perpendicular distances from one line to the other, and L is the distance between the perpendiculars.

Tracking a straight line

The next step in calibrating the steering encoder offsets is to get the vehicle to track straight. The current straight-line steer measurement technique is discussed in the Introduction and is expanded here. If the front wheel(s) are not parallel with the rear wheels, the AGV will drive along an arc when commanded to drive straight. In order to perform this test, all AGV wheels are set to their 0° position and the vehicle is rolled forward and back between two positions on the floor. The technical documentation for the AGV should be referred to for determining how to perform this operation. The front wheel encoder offset is then adjusted until the AGV tracks a straight line with the rear wheels locked. If the AGV is turning to the right, the encoder offset value should be increased. A discussion on the calibration of a three-wheeled mobile robot is given in [201].

The curvature of the vehicle path was observed with respect to a straight line while manually moving the vehicle forward and backward with the steering locked at 0°. First the AGV is moved

forward and back to establish the endpoints of the path. A straight line visual reference is created by stretching a flexible tape measure taut on the ground between the start and end points of the path. The deviation from the straight path is observed visually. The tape is shown stretched across the floor with the AGV at one end of the path in Figure 38 (a). In Figure 38 (b), the AGV is shown at the mid-point of the path and has deviated from the straight line. The steering offsets can be adjusted incrementally until the AGV drives straight, or the steering correction can be calculated from the length and deviation of the path. In either case, the correction should be applied to both the front and rear wheels, simultaneously. Half of the correction is added to the front steering offset and half is subtracted from the rear wheel steering offsets.

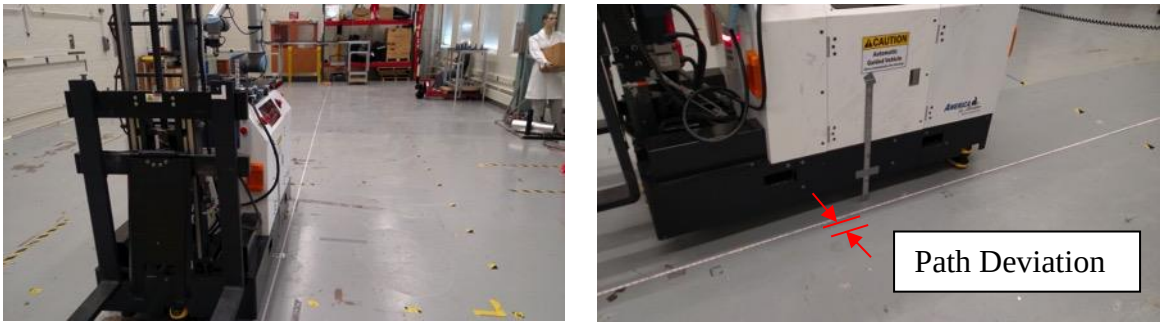

(a) (b)

Figure 38. Path deviation is measured relative to a tape measure stretched between start and end points marked on the floor (a) AGV at start point (b) AGV at mid-point showing deviation from straight path.

Using the intersecting chords theorem, the radius of curvature of the vehicle path can be computed as,

$$R = \frac{4d^2+L^2}{8d}, \qquad (2)$$

where d is the offset from the straight line path, and L is the length of the straight line path. Then the steering offset can be computed as,

$$\theta \approx \tan^{-1}\frac{w}{R}, \qquad (3)$$

where w is the distance between the front and rear wheels. The value of R needs to be adjusted up or down based on how far the reference point (tape measure) is from the centerline of the vehicle.

Correct crabbing

Crabbing describes the AGV body orientation remaining constant while the AGV steers, for example, keeping the body straight while moving diagonally rather than straight ahead. The undesirable crabbing is corrected by moving the AGV back and forth past a fixed reference point (the corner of the RMMA was used) and measuring the clearance distance as the front then the back pass this fixed point. This is done in manual mode with the wheels locked at their 0° position. The difference in the measurements and the base line are used to compute an angle correction. The angle correction is then added to all three wheels. The corrections are done in unison to

preserve the steering alignment done in the previous step. At this point, the AGV should be driving straight, with no crabbing.

Figure 39 shows the measurements being made from a stationary reference point (i.e., the corner of the RMMA) to the vehicle as it is driven past along a straight line. The measurements are made to a feature on the vehicle that is parallel with the centerline of the AGV. In this case, it is the edge of a mounting plate on the top of the vehicle. In Figure 39 (a), the distance is measured as the front of the AGV moves past the corner. In Figure 39 (b), the distance is measured at the trailing end of the plate.

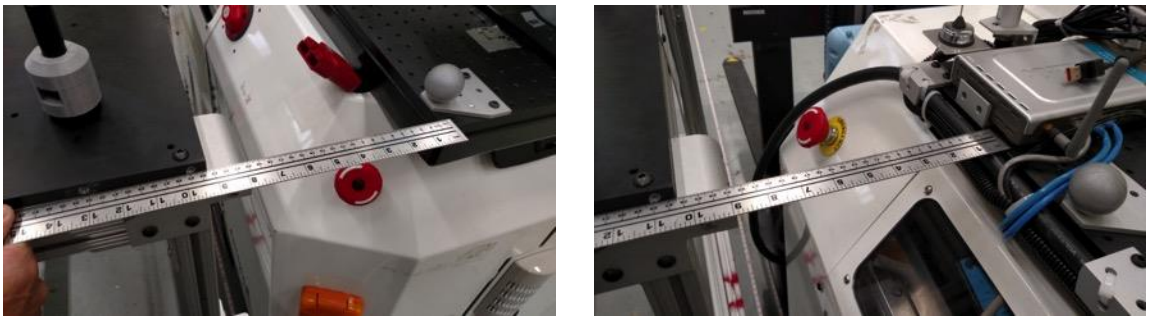

(a) (b)

Figure 39. Crabbing is measured as the AGV moves past a fixed reference point (a) measuring from front of vehicle to corner of table (b) measuring from back of vehicle to table corner.

The offset angle can be computed as,

$$\theta = \tan^{-1}\frac{(d_2 - d_1)}{L}, \qquad (4)$$

where d_1 and d_2 are the distances between the stationary reference point and the vehicle, and L is the distance between the points along the length of the vehicle.

Adjusting lateral error

When stopping at a commanded point, it was observed that the vehicle was stopping consistently to one side of the point relative to the direction of travel. Since the vehicle was tracking straight with the wheels locked at their 0° position in manual mode, it was deduced that the problem lay in the alignment of the navigation sensor with what the AGV considered straight ahead. Under servo control this misalignment would cause a consistent pull to one side or the other until the PID controller built up enough position error to compensate for the misalignment.

The sensor position on the NIST AGV relative to the vehicle coordinate frame origin is given by four controller configuration parameters:

- ScannerX – The distance of the sensor mount point from the vehicle origin along the lateral axis of the vehicle.
- ScannerY – The distance of the sensor mount point from the vehicle origin to the left of the lateral axis.

- ScannerZ – The vertical distance of the sensor mount point above the vehicle origin.
- ScannerAngle – The angle between the vehicle axis and the sensor axis in degrees.

Of these, the ScannerAngle is the only one we are concerned with. It compensates for the mounting alignment of the sensor relative to the vehicle centerline. The navigation sensor used on the NIST AGV derives the position of the vehicle by measuring the distance and angle to a collection of fixed reflective markers placed about the vehicle workspace. This data is processed and filtered to produce the two-dimensional (2D) position and orientation of the vehicle in real time. The navigation sensor mounting angle, ScannerAngle, was adjusted until the lateral error at the path points was reduced to an acceptable value. The technical documentation from the manufacturer should be referred to for the vehicle being calibrated to determine how to adjust the offset for the scanner mounting angle.

This procedure corrected the lateral error that was occurring during autonomous motions by more than an order of magnitude. At this point, the AGV had a much reduced lateral positioning error when driving a straight line.

Wheel Encoder Scale

Each of the wheels has an independent distance encoder scale parameter that is used to translate revolutions of the wheel to distance traveled. Over time, the diameter of the wheel will change slightly with wear, and even when new, the diameter of the wheel is not known with a great degree of precision. Changes in the diameter of the wheel will cause the AGV to travel different distances per revolution of the wheel. Precision control of the vehicle stopping relies on an accurate mapping between wheel motion and distance traveled.

To adjust the wheel encoder scale, the AGV is driven along a straight line and the distance traveled is measured. The distance traveled, as reported by the control system for each wheel, is compared to the actual distance traveled. The current wheel encoder scale setting is observed, and a correction is computed. The equation for computing the new scale is:

$$S_1 = \frac{D_e\, S_0}{D_a}, \qquad (5)$$

where S_1 is the new encoder scale, S_0 is the initial encoder scale, D_e is the encoder distance, and D_a is the actual measured distance. The value of the encoder scale is typically expressed in distance traveled per encoder tick. The reported encoder distance D_e needs to be read from the AGV controller. There will typically be an individual encoder scale parameter and drive encoder distance value for each of the wheels. The encoder distance D_e is determined by noting the drive encoder distance at the start and end of the move and taking their difference.

In our case, the measurements were taken by commanding the AGV to move between two positions located along a straight path using the AGVs control system. The drive encoder distance was recorded at the start and end points to compute D_e. The actual distance was measured by marking the start and end positions on the floor and measuring with a measuring tape as shown in Figure 40. To provide an accurate mark for the start and end positions, a ruler was taped to the side of the AGV to allow that point on the vehicle to be accurately transferred to the ground plane.

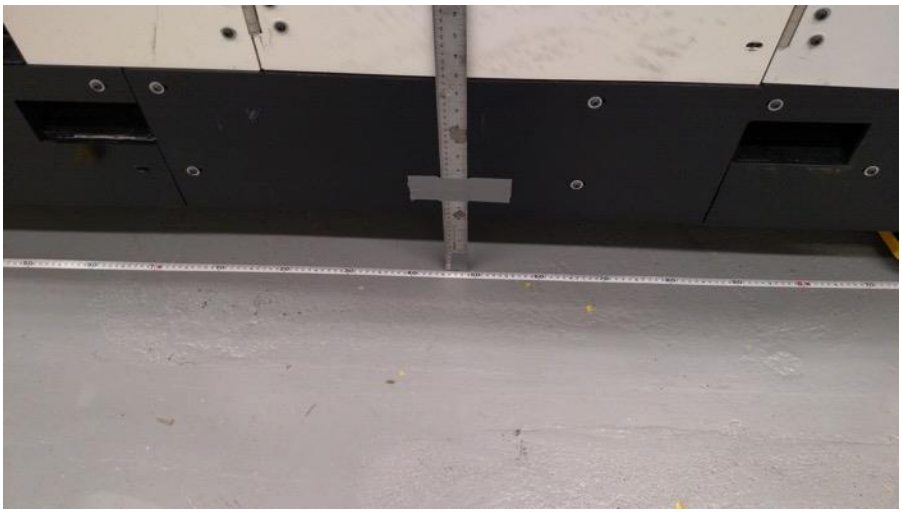

Figure 40. Actual distance traveled is measured using a tape measure on the floor with ruler used as a reference point on the vehicle.

Stopping Tolerance

At this point the AGV was still stopping short of the commanded point by a distance that was significantly larger than the corrected side-to-side positioning error. The AGV technical documentation described the parameters that affect how the AGV decelerates and stops when it approaches a commanded stop. From this description, it was determined that the parameter that needed to be adjusted to correct the stopping error was the StopTolerance. This parameter specifies the distance from the goal where the final deceleration to the stop point begins. The deceleration starts from a fixed 'creep' velocity used during the final approach to the goal point. The distance traveled during the deceleration interval will be nominally constant but unknown. The stop tolerance is adjusted to match this deceleration distance.

A three-point path was configured along a straight line. The vehicle was programmed to stop at the center point coming from both directions. The locations where the AGV stopped were marked on the floor. The distance between the marks was measured, and half of this distance was added to the StopTolerance, since the AGV was stopping short of its goal. If the AGV overshot the goal, half the distance would be subtracted from the StopTolerance instead. This correction improved the NIST AGV's stopping accuracy by more than an order of magnitude.

Observations

Calibration of the AGV's control parameters is critical to optimal performance of the vehicle. For vehicles that rely on dead reckoning to determine their position, small errors in steering and odometry can accumulate quickly over time and adversely affect the navigation of the AGV. For AGVs that make use of external navigational aids, proper calibration of the vehicle is needed for accurate servoing to meet navigation goals. When applying mobile base calibration to the mobile manipulator, the manipulator can compensate for small base errors. However, if the errors are too large, even the manipulator cannot properly compensate. Additionally, less time to dock the manipulator EOAT will occur when the AGV is calibrated as EOAT search time will be reduced.

Automated calibration is an interesting research topic, and can be a great labor saver when a large number of identical vehicles need to be calibrated. However, automated calibration systems rely on the availability of specific sensing systems on or off the AGV. For the small manufacturing system, reliance on specific, and often expensive, sensor systems for calibration of the AGV is not always practical. Therefore, a minimalistic manual approach to adjusting the necessary AGV parameters is suggested.

The order of the calibration steps listed reflects the order in which is recommended for adjustments to be made. The order in which calibration steps were actually performed was slightly different than the order presented. The order in which the calibration steps were performed was the result of systematically trying to eliminate various flaws in the motion of the vehicle, and was not specifically planned-out ahead of time.

In this ordering, alignments relying on strictly physical measurements are done first, followed by alignments done while moving the AGV in manual mode with the wheel position locked, followed by tests where the vehicle is being moved between points under servo control. The wheel alignment steps were also reordered to reduce possible inaccuracies in the later calibration steps.

The specific calibration procedures described here were tailored to the NIST AGV needs. However, most of the procedures described apply to a large class of similar AGVs being used in industry. The calibration of the NIST AGV resulted in a significant improvement in the vehicle's performance.

4.3. Navigation Performance Evaluation

The most basic functions of AGVs and mobile robots are navigation to and docking with equipment in the workspace. However, the description of how well the vehicle navigates (i.e., commanded vs. actual AGV path-following deviation) has certain ambiguities. For example, navigation implies that the vehicle measures its current position, plans a route to another location, and moves from the current location to the planned location upon command. Most vehicle manufacturers don't provide specifications for how uncertain the navigation performance is (i.e., the error bounds on position or velocity), other than perhaps radius of vehicle turns, maximum velocity, and maximum acceleration. The vehicle velocity sets limits on the allowable turn radius for particular vehicles. Some controllers [7], if not all, will not allow high velocities on relatively small radii to prevent unsafe vehicle conditions. These limitations are not typically specified by AGV manufactures, causing AGV users difficulty in planning how many vehicles they may require for moving their products within the facility to maintain a desired throughput.

Two types of navigation experiments were performed: ground truth measurement system (OTS) as compared to a metrology bar and AGV as compared to ground truth. [2] It is essential that the ground truth is fully understood prior to comparison to the system under test. In this case, the metrology artifact, shown and described in section 3.3.2, was used to measure the uncertainty [175] of the 9 m W x 22 m L AGV lab so that measurement uncertainty of the ground truth system could be established. The bar was moved throughout the space using the, now standard, method of traversing the space where the AGV was to be used.

4.3.1. Navigation Experiments

Experiments were then performed using the AGV programmed to navigate simple geometric shapes, including lines (i.e., point-to-point), circles, and squares, and using All-Wheel Steering (AWS); i.e., the vehicle body rotates when wheels are steered, although at different angular rates. As described previously, AGV position information was achieved via spinning laser triangulation, time-of-flight measurement from the Nav sensor at 6 Hz to facility mounted reflectors that were previously calibrated to known locations using a laser-tracking, position-measurement system. Computer aided design models of the AGV paths (5 m long path between two points and 3.0 m squares and circles – see Figure 41) were pre-programmed using the AGV controller-offboard and sent wirelessly to the AGV to be traversed. The AGV command software cannot draw a complete circle and instead draws quarter arcs from each of the four points as shown. The AGV command software also forced AWS traversed squares to include rounded corners with 0.8 m radii whenever the non-stop velocity was 0.25 m/s or less. The controller can also track the vehicle position during navigation at 60 Hz.

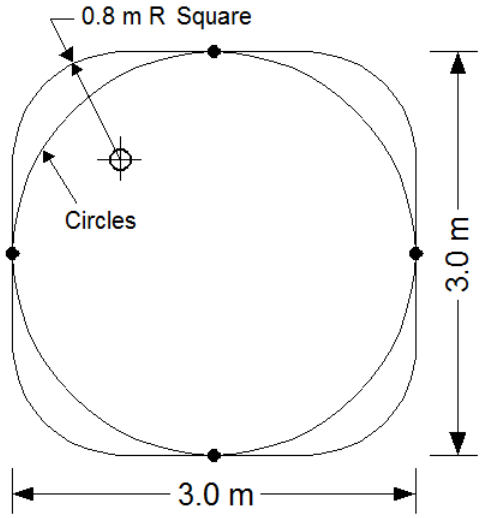

Figure 41. (a) NIST metrology bar used to measure ground truth system uncertainty. (b) Commanded AGV paths.

The AGV navigates using an approximately central vehicle point (minus the forks) that follows the programmed path. The navigation center point is located at floor level, at the center of the vehicle width, and halfway between the front and rear wheels. The navigation center point, used as reference by all AGV navigation and docking control programs, is very difficult to access; and, therefore, it may not be correctly input into the controller as navigation reference. For these tests, the point was approximated at floor level and transferred to the vehicle top using squares, tape measures, and straight edge instruments. Ideally, a standard AGV calibration exposes this point for measurement reference in vehicle control software to minimize path-following uncertainty. The vehicle parameters were instead including the origin and the orientation of the AGV, and used a mathematical solver as described in the following section 4.3.2 on collected data to solve for the parameters.

4.3.2. Performance Analysis and Results

The AGV was outfitted with several OTS markers that were combined into an OTS rigid body for the AGV as shown in Figure 42. A set of performance measurements was developed for evaluating the navigation performance of an AGV. First, it is important to discuss the data obtained from the experiments and registration between the data from the OTS and the AGV.

Input data: The data obtained from the experiments forms the inputs to the analysis. There are two types of input files expected. All of the files are in comma-separated-variable (CSV) format. The OTS and AGV data files contain a timestamp and six DoF information which includes x, y, z, and orientation (rotation about the vertical axis).

Sensor Registration: The OTS and AGV typically produce data in different coordinate systems. Several registration techniques were investigated and evaluated. There are two approaches to evaluate the AGV. The first approach is to determine the transformation between the AGV data to the OTS coordinates. This approach is required to register the AGV data and OTS data. Several algorithms were investigated which include closed-form solutions [2][206] and the Ceres Solver [207] - an open source C++ library for modeling and solving large, complicated, optimization problems. The Ceres Solver was selected to automatically register between the OTS system and the AGV using timestamp, through the GPS antenna, and 6 DoF data.

Several types of performance evaluation metrics are presented for an AGV programmed to navigate simple geometric shapes, including straight lines, circles and squares, and using AWS. The performance metrics used included mean, maximum, and standard deviation of the errors (i.e., uncertainty) for x, y, z distance and angle between the OTS and the AGV.

Initially, a measure of the performance of the OTS was made throughout the laboratory where the AGV was tested. This resulted in submillimeter uncertainty in the test area. Measurement standard deviation (σ) (uncertainty) of the distance is 0.26 mm and σ of the angle is 0.10°. Figure 43 shows graphed data of the distance uncertainty throughout an approximate 5.5 m W x 13 m L area of the laboratory where the AGV can be used. The data graphed for angle uncertainty appeared similar.

Extending from section 4.2.2 is the experimentation demonstration of the AGV when it was uncalibrated and when calibrated. A test can be developed to uncover the effects of uncalibrated vs. calibrated vehicle navigation performance when commanded to move along a path, as shown as a dashed line in the example in Figure 44. Should objects be near the vehicle path, such as walls or obstacles (depicted in Figure 44 as bordering lines along the path), the vehicle may stop, slow, or worse, collide with the boundary object. A user would then be required to provide additional and perhaps unnecessary space for one manufacturer's vehicle and not for another. How the vehicle handles (slow, stop, etc.) the event is also ambiguous. For example, some, but not all vehicles are equipped with obstacle detection based on non-contacting sensors that provide detection beyond the physical vehicle footprint.

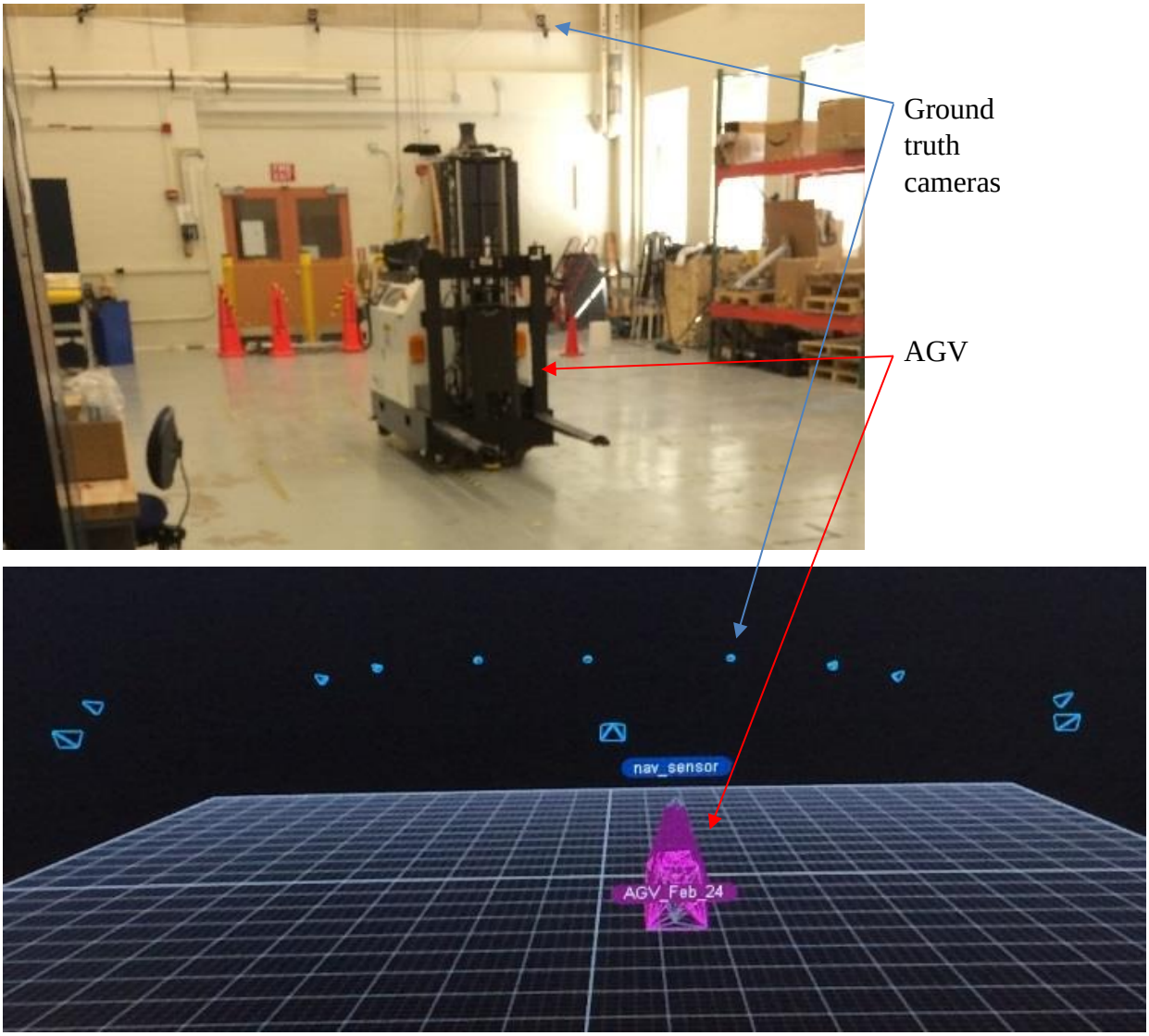

Figure 42. (top) Test setup showing the AGV traversing a path and cameras mounted to walls and (bottom) virtual multi-camera system display of the cameras, AGV, and relative workspace.

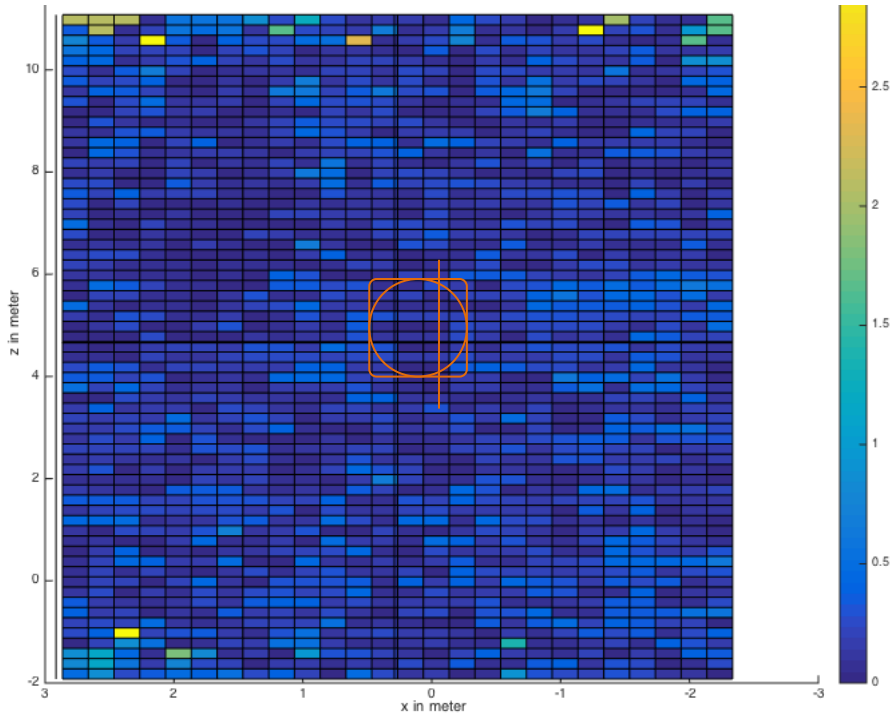

Figure 43. Graphed data of the distance uncertainty for the AGV lab. The orange straight line, circle, and rounded square depict the approximate size and location for AGV tests.

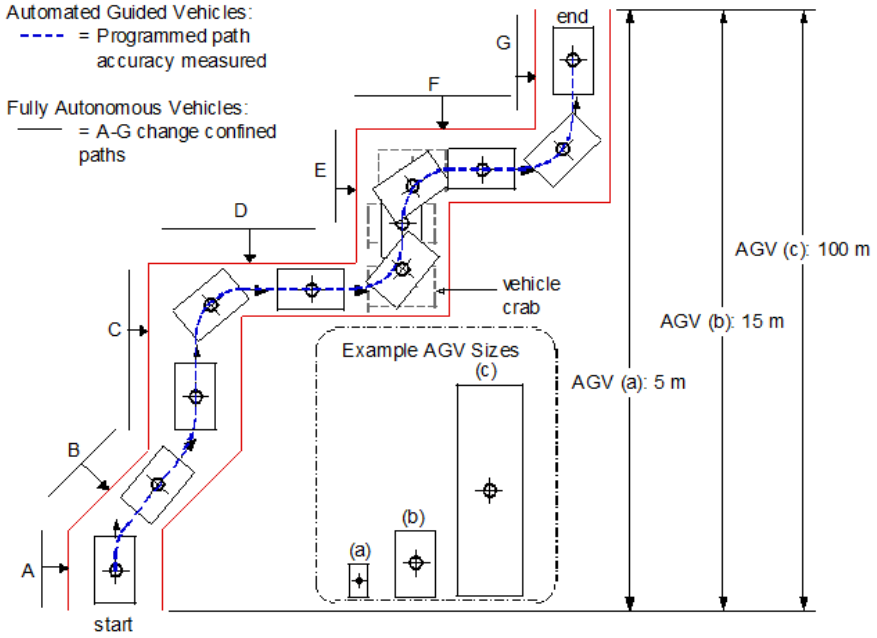

Figure 44. Example reconfigurable apparatus for navigation tests for various AGV sizes.

To address AGV navigation uncertainty, tests were executed, both with an AGV prior to and after being calibrated. The uncalibrated AGV test is similar to typical industry methods since not all

AGVs can be frequently calibrated. An uncalibrated AGV was commanded to navigate each path (straight, circular, and square) ten times where circle and square paths were traversed with AWS and all experiments were repeated three times resulting in a total of nine data sets. All OTS and AGV data were then analyzed and the metrics described previously were computed.

The first AGV experiment was a "straight line path test" with the AGV navigating at 0.25 m/s maximum. The results are shown in Figure 45 where X and Y axes scales are in meters, although X is expanded 100 times to clearly show the AGV performance as compared to the OTS. Maximum OTS and AGV deviation from the commanded path, represented by the blue line, was approximately ± 25 mm.

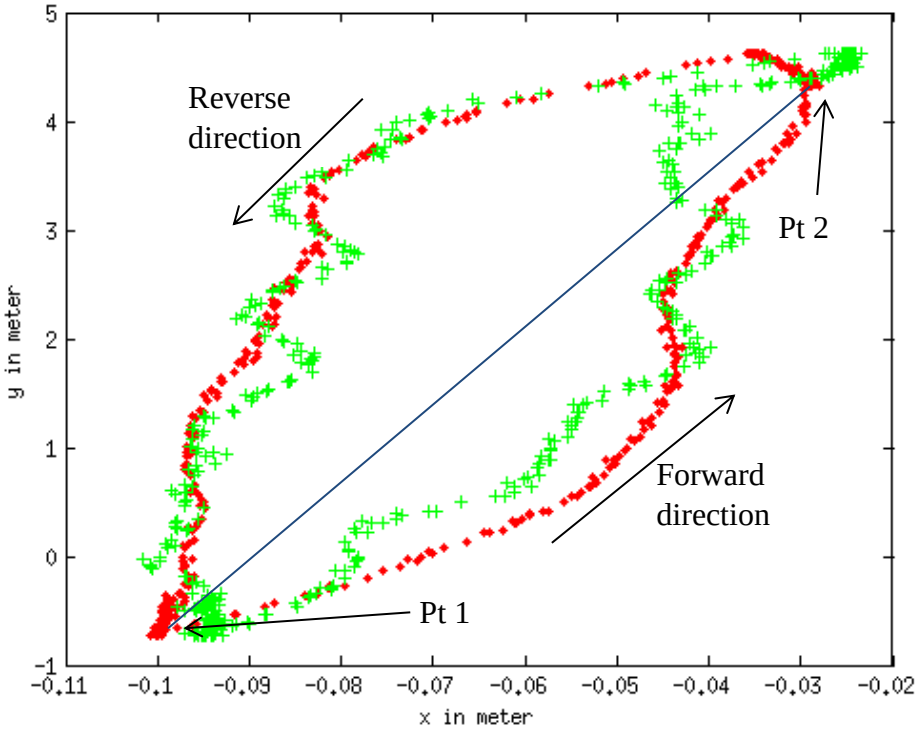

Figure 45. Ground Truth (red) and AGV (green) data of the straight-line path tests. Scales for X and Y axes are in meters where the X axis has been expanded to clearly show the AGV performance as compared to OTS measurement. The blue line represents the commanded path from pt 1 to pt 2 and back moving in the forward and reverse directions as shown.

The second AGV experiment was a "circle path test". The results are shown in Figure 46 and in Table 8 and Table 9 for the AWS tests. The raw data and fitted ellipses are shown in Figure 42. Table 8 and Table 9 show the uncertainty (mean and maximum errors and σ) for the AGV using the OTS. Each table entry shows the results of navigating the circle 10 times and for each of three different tests. Table 8 shows uncertainty results without adjusting and Table 9 shows the results after adjusting for the potential AGV origin and rotation offsets. Table 9 shows a clear need to adjust for these offsets. Ideally, the offsets are then reprogrammed into the AGV.

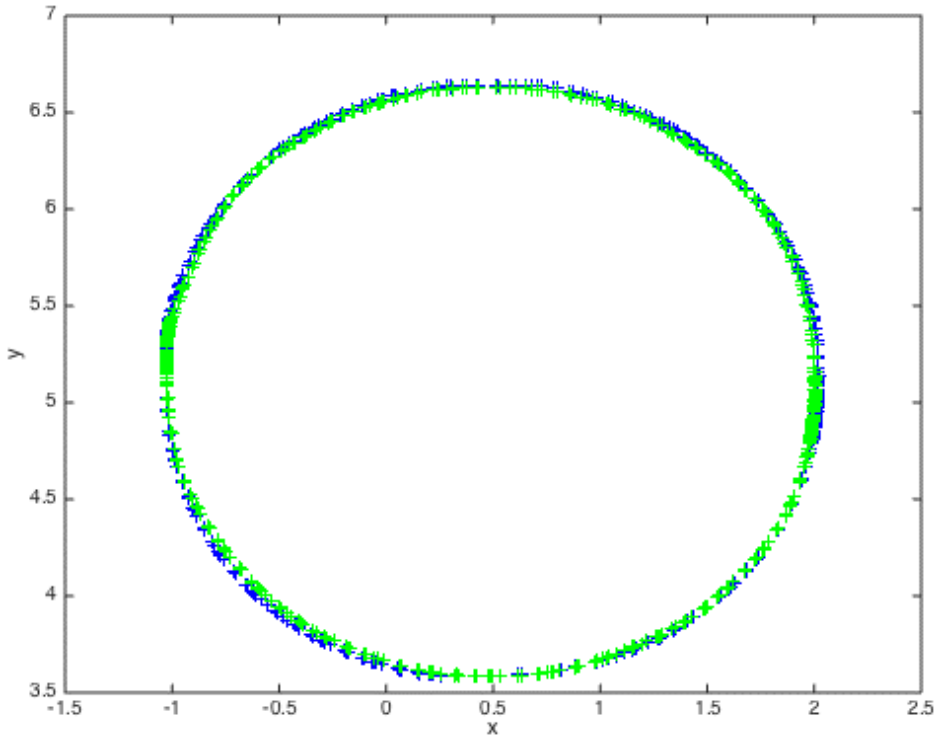

Figure 46. OTS (blue) and AGV (green) data of the 3 m diameter circle path tests for AWS steering.

Table 8. Statistical uncertainty (in mm) of the AGV navigating circle paths without adjusting the AGV's origin or rotation.

Circle A,B,C	*X*	*Y*	*Distance*
Mean Error	-0.04; -0.01; -0.027	0.01; 0.015; 0.019	10.8; 11.0 10.9
σ	9.7; 9.9; 9.8	8.5; 8.6; 8.6	7.0; 7.1; 7.1
Max Error	21.3	17.3; 17.7; 17.1	31.3; 32.2; 32.9

Table 9. Statistical uncertainty (in mm) of the AGV navigating circle paths after adjusting the AGV's origin and rotation.

Circle A,B,C	*X*	*Y*	*Distance*

Mean Error	-0.010; -0.018; -0.008	0.02; 0.002; 0.019	5.00; 5.06; 4.98
σ	4.5; 4.5; 4.4	5.1; 4.4; 5.1	4.6; 4.5; 4.6
Max Error	23.8; 23.0; 8.9	8.9; 22.1; 22.1	23.85; 22.2; 22.2

The third AGV experiment was a "square path test". The results are shown in Table 10 for the AWS tests. The overlapped data between the ground truth and the AGV are shown in Figure 47.

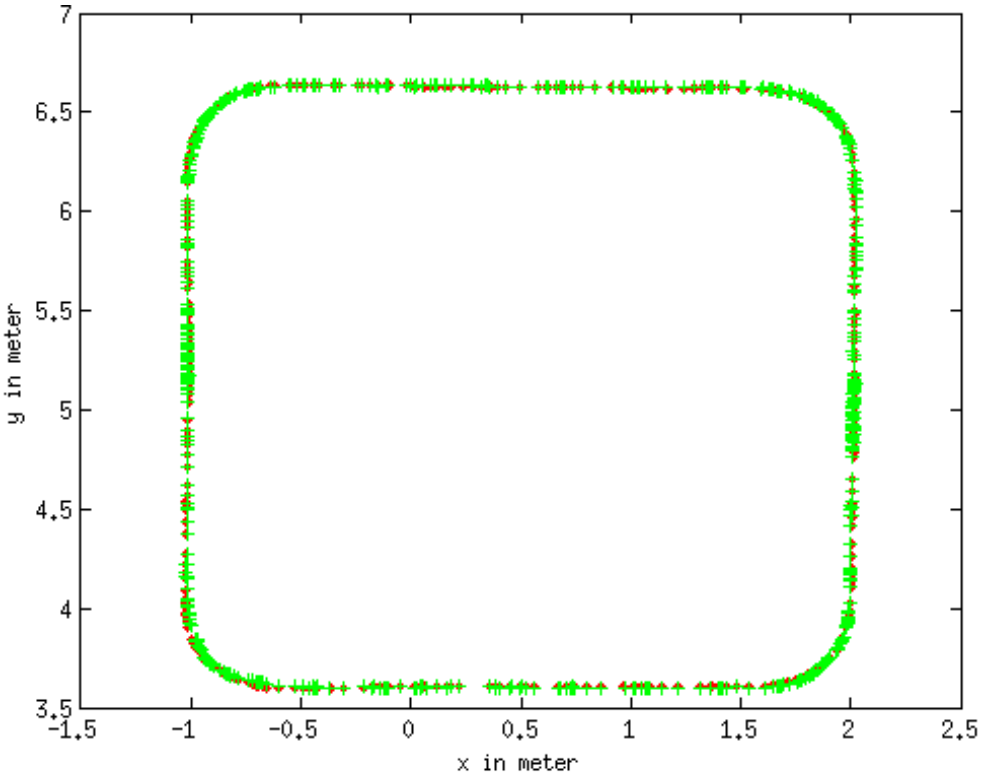

Figure 47. OTS (blue) and AGV (green) data of the 3 m square path tests for AWS steering.

Table 10. Statistical uncertainty (in mm) of the AGV navigating square paths after adjusting the AGV's origin and rotation.

Square A,B,C	*X*	*Y*	*Distance*
Mean Error	-0.023; 0.002; -0.004	0.029; -0.039; -0.001	5.2; 5.0; 5.1

σ	4.5; 4.3; 4.4	4.4; 4.3; 4.4	3.6; 3.5; 3.6
Max Error	10.4; 8.8; 9.9	12.4; 12.0; 14.1	10.4; 18.3; 18.6

As shown above, path deviation was approximately 20 cm maximum. By comparison to the uncalibrated tests described above, the AGV was then calibrated using the manufacturer's and authors methods described in section 4.2.

Another test setup was tried, with an eye towards a relatively less expensive test method that will allow all AGV systems to be measured, ideally, with an independent measurement method that doesn't use AGV controller tracking, yet captures the full AGV configuration (i.e., including safety sensing). The AGV was commanded to drive back and forth between temporary barriers, along a straight line defined by commanded points spaced approximately 10 m apart. The goal of the experiment was to measure the AGV deviation from the commanded path. A critical AGV navigation performance area is also deviation from the commanded path after turns. So, a 90° turn was added to the end of the straight path beyond the barriers to measure the vehicle navigation uncertainty when moving from/to a straight path to/from a turn. Figure 48 shows the test setup and Figure 49 shows a B56.5 test piece being used to define the safety laser stop field edges (a), the barriers and lines to which barriers are moved between trials (b), and the AGV emergency-stopped upon detection of the barriers (c). The safety laser, stop field edges were marked on the floor, as a ground truth, zero-tolerance spacing that the vehicle can navigate, when the vehicle was at position 1 and again at position 3, shown in Figure 48, for both left and right vehicle sides. The barrier position lines were measured from the edge line using a ruler and marked at 2 cm increments from the edge up to 10 cm away from the edge line. Smaller spacing between lines (e.g., 1 cm) could also be used for finer uncertainty measurement. For each test trial, the barriers were moved towards the AGV to the next line beginning at 10 cm for trial 1, 8 cm for trial 2, and so forth until the navigating vehicle detected a barrier and emergency-stopped the AGV, thus completing the test run.

A series of eight trials were completed with nearly all trials including three or more runs each to demonstrate the navigation test method concept. The OTS was used to measure the barrier and vehicle position during experiments to further understand the test method and vehicle performance. The barriers and AGV were marked with spherical reflectors, shown in Figure 49 (a, b, and c), detectable by the OTS. Figure 50 presents OTS data plotted for navigation tests showing ground truth data of: (a) test 8 vehicle path and emergency stopped vehicle (red circle) when a wall was detected, (b) test 1 path, and (c) test 1 path data from (b) zoomed in to show data points of three runs.

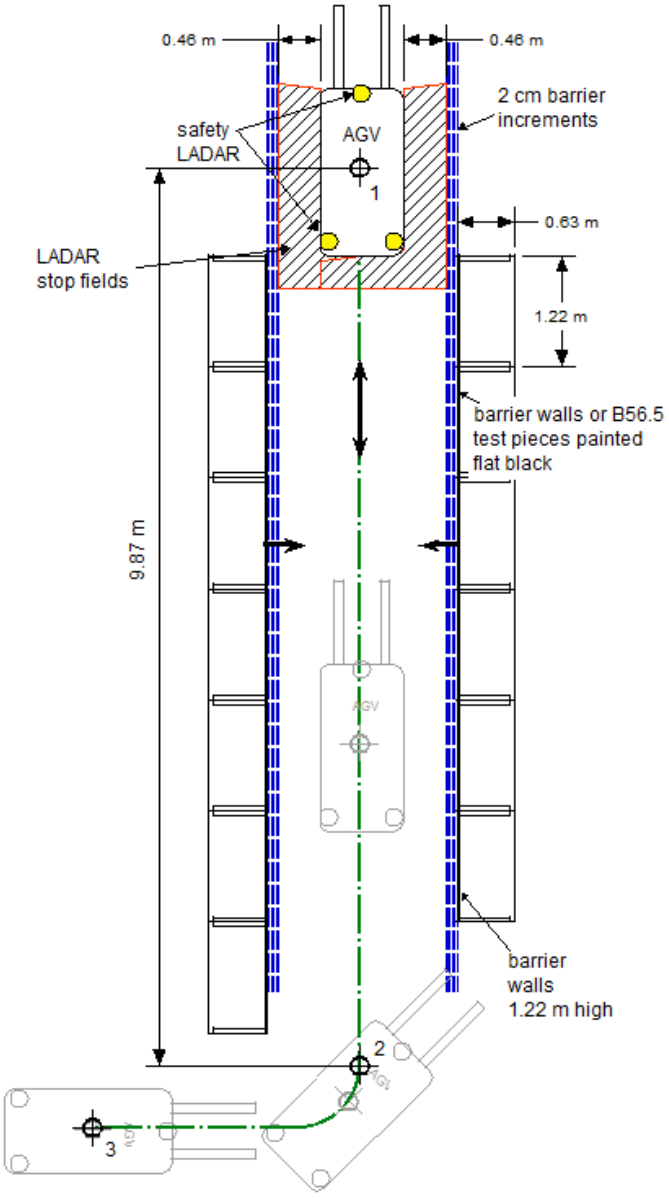

Figure 48. AGV navigation test setup.

a b c

Figure 49. (a) B56.5 test piece (black cylinder) used to define safety laser edge (note red emergency stop light (within the red circles) is on), (b) barrier (black) painted wood panel, blue lines spaced at 2 cm, and spherical reflector for ground truth system, (c) AGV emergency stopped, as noted by the red/yellow light, upon detection of barriers during a test.

Experimental results indicated a maximum path uncertainty of between 6 cm and 8 cm when the vehicle detected the boundaries at nearly the center of the straight-line path and when moving at either 0.25 m/s or 0.50 m/s. The navigation test method using barriers is simple and cost-effective for manufacturers and users to implement, as compared to the higher accuracy, but more expensive ground truth visual tracking system used for test method development. Although a simple straight line with one turn was tested, more complex test configurations, such as shown in Figure 44, could be set up using B56.5 test pieces instead of larger, physical barriers as were used in this research.

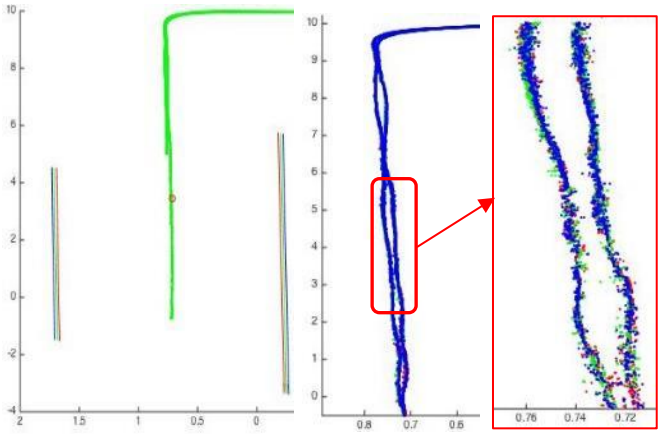

a b c

Figure 50. Example graphical results of navigation tests showing ground truth data of: (a) test 8 vehicle path and emergency stopped vehicle (red circle) when a wall was detected, (b) test 1 path, and (c) test 1 path data from (b) zoomed in to show (red, green, and blue) data points from three runs.

4.3.3. Recommended Test Method

A test method, based on the measurements and analysis from these experiments, was recommended in [2][208] as an initial working document to ASTM F45.02 Docking and Navigation subcommittee. The recommended test method included: Apparatus, Calibration and Standardization, Procedure, and Reporting. The navigation test method included two types: Undefined Space and Defined Space. Unconfined space is appropriate when virtual, pre-defined paths are used, i.e., the current technique used for AGVs and the experiments described above. Defined space is suggested for mobile robots and some AGVs with simultaneous localization and mapping (SLAM) capabilities to navigate using walls or other landmarks. The sub-committee agreed through consensus to develop and standardize the defined space test method. [209]

4.4. Docking Performance Evaluation

4.4.1. AGV Docking

Vehicle docking is another common application of AGVs and mobile robots. Unit load (tray, pallet, or cabinet carrying), tugger (cart pulling), and fork/clamp (pallet or box load/unloading) are typical industrial style vehicles that require different docking uncertainties. For example, a unit load vehicle that places/retrieves platters during wafer manufacturing would no doubt require a lower docking uncertainty than a fork style vehicle that places/retrieves pallets. Two types of docking are therefore required: 1) Vehicle docking (e.g., those just mentioned) and 2) Vehicle with Onboard Equipment docking (e.g., mobile manipulators). As robotics advances, current and potential users are requesting mobile manipulators to perform tasks such as unloading trucks or carrying and loading/unloading wafer pods into machines. Eventually, it is expected that mobile manipulators will be used for smart manufacturing assembly applications [68][170].

As with navigation, there are no performance measurement test methods that define how manufacturers and users characterize their vehicle's docking capabilities. Figure 51 (a) shows an example method for docking for any style vehicle. A vehicle approaches and makes contact with docking points 'a' and/or 'b' depending upon the vehicle type. Relative displacement from each of the points would be measured to determine vehicle docking uncertainty. A fork-type AGV is shown docked with a test apparatus in Figure 51 (b). The fork tips are marked with yellow points.

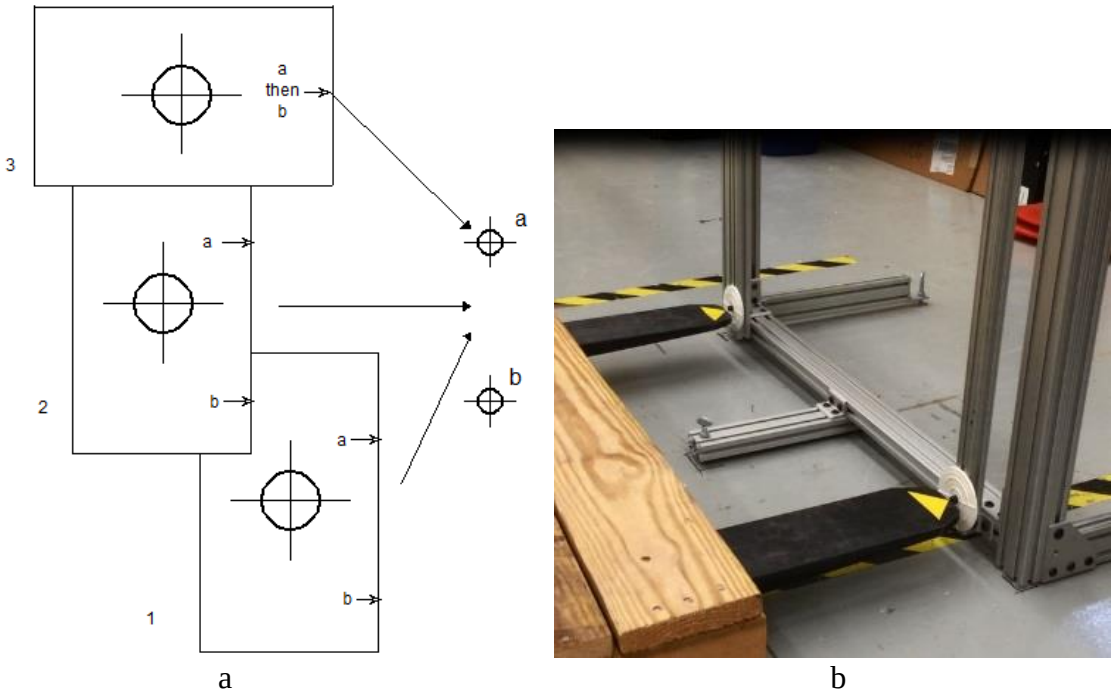

Figure 51. (a) Example docking test method using various AGVs (e.g., 1 and 2 for AGV unit load tray table docking, 3 for fork and tugger AGV docking). "a" and "b" are fixed points in space (e.g., contact or non-contact sensor locations in space). Approach vectors and sensor point spacing and locations are variable. (b) Fork-type AGV docking with a docking apparatus.

Two experiments were simultaneously performed: AGV docking relative to known facility locations and ground truth use for measuring AGV docking. For this early experiment, two different ground truth measurement systems were used to measure AGV performance: a laser tracking ground truth (laser tracker) with an uncertainty of approximately 10 µm [13] and OTS with standard deviation (uncertainty) of 0.02 mm (i.e., 20 µm) in position uncertainty and 0.13° in angle uncertainty as measured at NIST. The two systems are not so significant in their performance when measuring a mobile base. However, their measurement methods are quite different. For example, the laser tracker tracks the position of a single point, whereas the OTS can track multiple point markers and can compute orientation from them. Both ground truth systems can measure relatively high-precision displacement between two points, as compared to an AGV docking with an apparatus.

An experiment using an uncalibrated AGV that was programmed to stop at various points yielded an uncertainty range of approximately 1 mm to 50 mm. Figure 52 (a) shows the vehicle paths and Figure 52 (b) shows average errors for five runs at stop or dock points. The vehicle position was measured using a laser tracking ground truth system to achieve high-precision measurement of AGV stop points [12]. However, in several experiments, laser tracker positioning was impractical as the laser beam was continuously interrupted by onboard AGV hardware. This prompted a switch to using the OTS for ground truth measurements.

Docking was measured again after the AGV was calibrated using the manufacturer's procedures described in the previous section. The AGV approached similar dock locations and after AGV calibration, provided consistent 5 mm uncertainty.

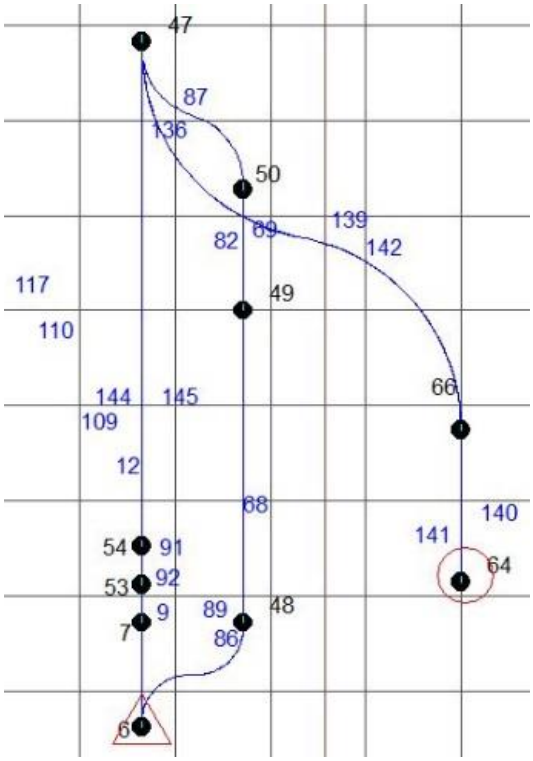

a

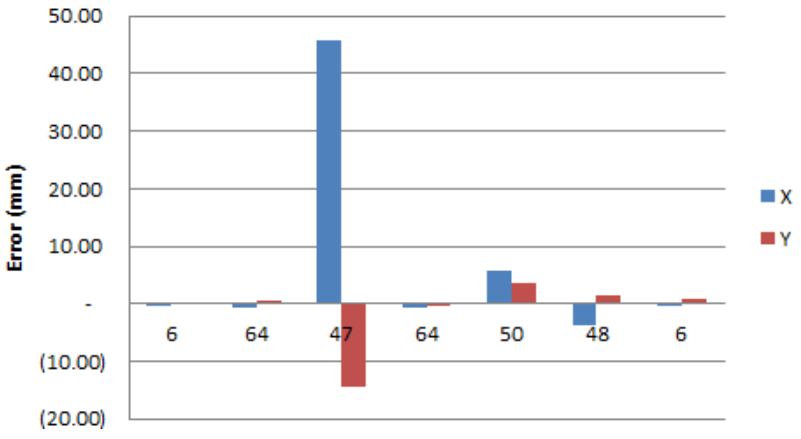

b

Figure 52. (a) Map of commanded segments and stop points and (b) stop point uncertainty of a single AGV point for each location in (a) averaged over 5 runs.

Additional AGV equipment docking experiments were also performed using a mobile manipulator and the RMMA and will be described in detail in Chapter 7. The mobile manipulator, with

uncalibrated AGV, repeatedly moved next to the artifact from a starting point. The uncalibrated AGV provided relative repeatability of more than 10 mm from the commanded docking points. As will be shown in the following sections, 5 and 6, the mobile base provides the highest uncertainty of the mobile manipulator system.

4.4.2. Mobile Robot Docking

Most recently, additional vehicle experiments were performed, as in section 4.4.1 AGV Docking, using a mobile robot where its pose was compared to ground truth near the RMMA. The test setup is shown in Figure 53 and Figure 54. An Adept Lynx mobile robot [210] was used for this experiment. A Universal Robot UR5 manipulator was mounted on a structure designed and integrated onboard the mobile robot. The mobile robot was programmed to stop at ten poses near the RMMA where six of the poses were RMMA-access poses and the remaining four poses were at the corners of the RMMA. The four goals were sub-goals at the RMMA corners to ensure that the mobile robot would not plan a path to the next point through the RMMA. For this experiment, the manipulator was only used to ensure that it could reach at least half of each circle or square RMMA pattern at each of the six poses and then the manipulator remained stowed for the duration of the experiment.

Cardboard, concave, triangular walls were placed within the base of the RMMA, and grids, as shown in Figure 53, and double, 100 mm x 100 mm with 1 mm square spacing grids were taped to the floor as shown. The cardboard walls were used to improve navigation performance using local, unique landmarks as opposed to surrounding lab walls with closest distance of approximately 3 m or more. The grids were used as relative ground truth. This simple test method is similar to the AGV docking experiment which also compared a chosen AGV point to a grid location taped to the floor. Figure 54 shows an apparatus designed with two docking test points spaced at 163 mm apart, positioned near the floor, and attached to the mobile robot. A camera, shown in Figure 54 (c), was also fixtured to the vehicle and used to remotely view the docking test points above the grids. The mobile robot docking poses were chosen to so that the manipulator base was nearly in-line with the RMMA square and circle pattern centers. The mobile robot was commanded to autonomously navigate and stop at each of the six docking poses while the two docking test point locations were aligned with grid locations and their grid locations were recorded.

Maximum displacement results of the three test runs accessing the six RMMA locations are given by the equation below equal to 8.2 mm and with maximum uncertainty equal to 2.2 mm. Table 11, shows the commanded X, Y, and theta (TH) minus the displayed X, Y, and theta in the last three columns where the maximum deviation is 18 mm in X, 65 mm in Y, and 1.8° in theta. Therefore, although the measured offset may show performance within perhaps an acceptable tolerance (i.e., 8.2 mm in this case), the mobile base controller would pass the commanded versus manipulator controller displayed value difference to the onboard manipulator controller where the commanded versus displayed uncertainties would cause a misleading mobile manipulator performance uncertainty.

$$\text{Max } (A = \sqrt{Ax^2 + Ay^2} \quad \text{or} \quad B = \sqrt{Bx^2 + By^2})$$

Table 11. Docking performance results for a mobile robot base showing commanded versus manipulator controller displayed uncertainties. X and Y are in mm and Theta is in degrees.

	Xcom-Xdisplayed	Ycom-Ydisplayed	THcom-Thdisplayed
Run 1	3.62	(5.80)	(0.11)
Run 2	1.07	(5.83)	0.49
Run 3	0.52	(5.24)	0.10
max:	17.95	64.99	1.78

This inexpensive docking method is now being considered by ASTM Committee F45 as a simple method for measuring mobile base docking performance. An example grid result for location 6 is shown in Figure 55.

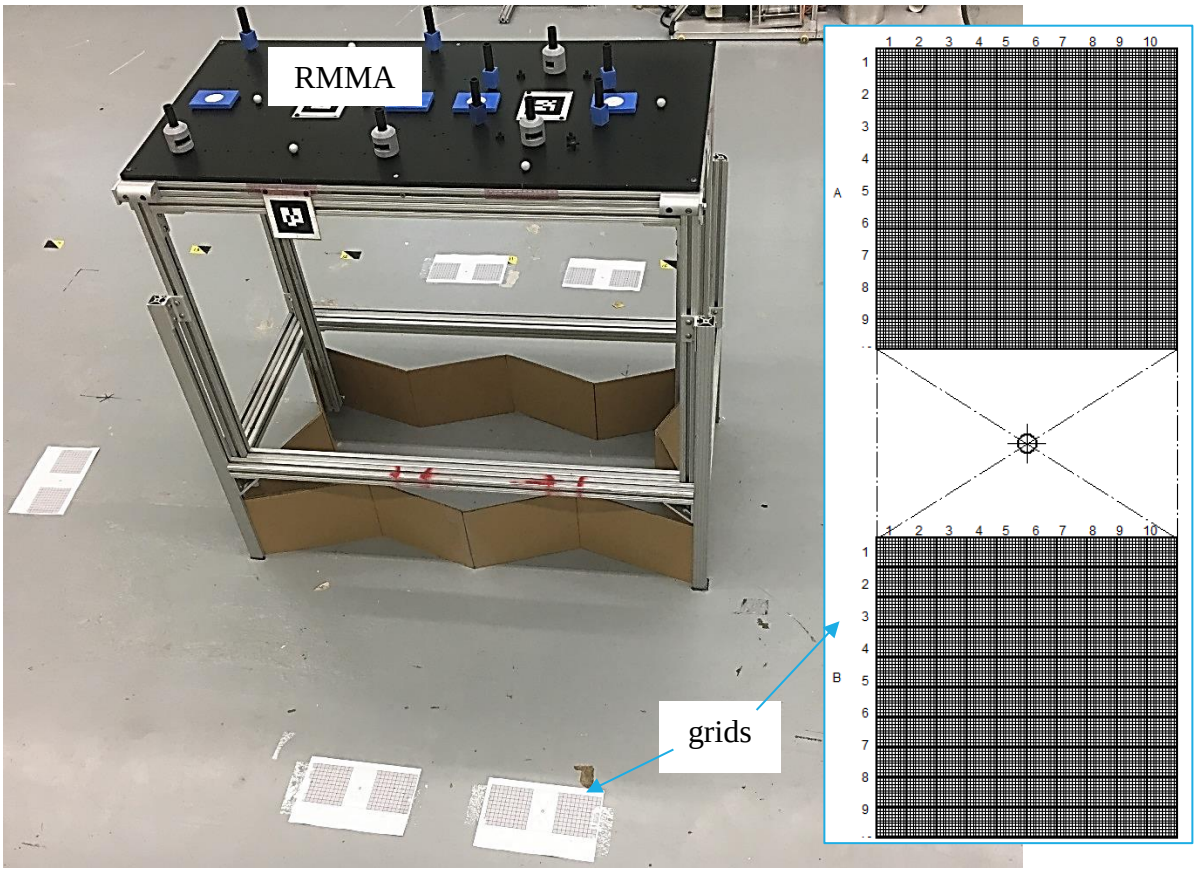

Figure 53. Experimental mobile robot docking setup showing grids (see close-up taped to the floor next to the RMMA and at each of six docking positions (one is beneath the inset).

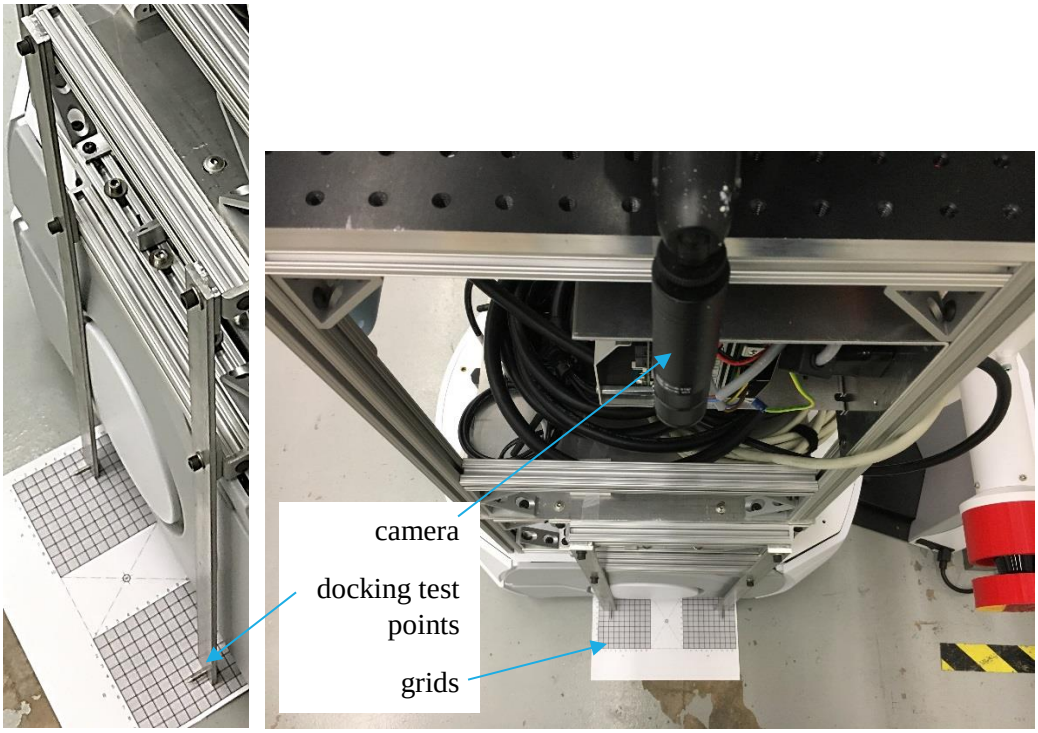

a b

Figure 54. (a) Screenshot of an example vehicle pose taken during the docking experiment showing the floor grid and docking test point apparatus. (b) Top view of the camera, docking test points, and grids.

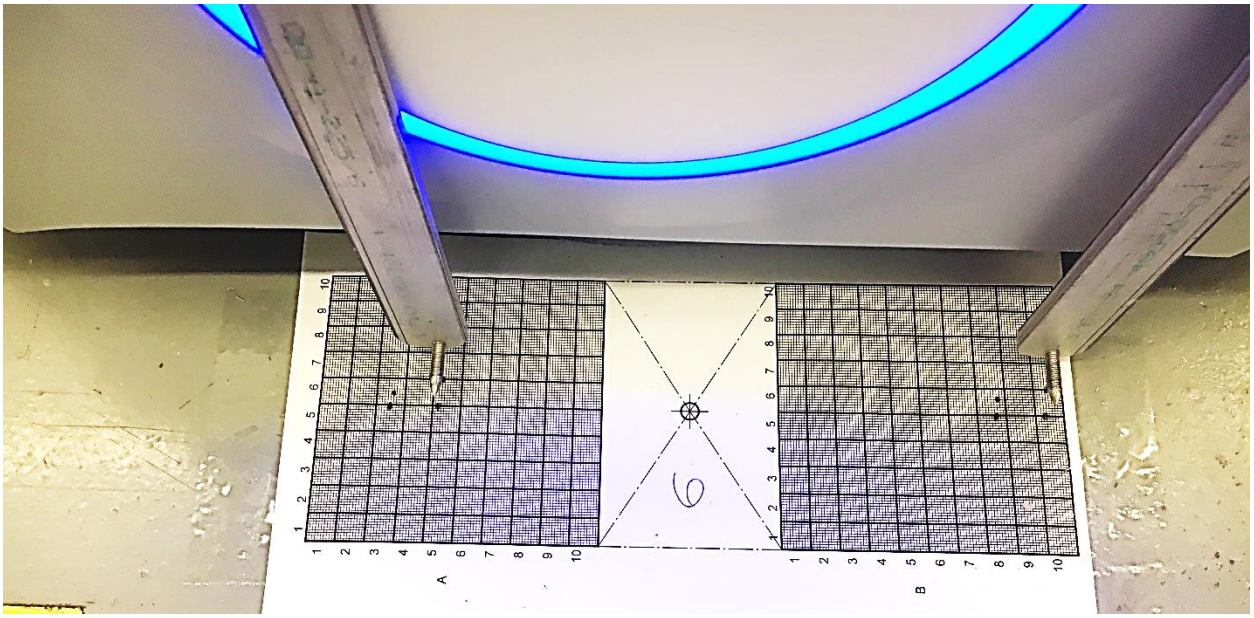

Figure 55. Example showing location 6 grid results of the mobile base docking experiment. Note the points marked on the grid indicating the varying repeatability at this location.

4.5. Mobile Base Stability

The last three metrics listed in section 1.2 (stability, obstacle detection and avoidance, and exploration of unknown environments) are important as manufacturing methods advance. Stability and obstacle detection and avoidance are further explored in the following subsections. Perhaps the most advanced manufacturing facilities will apply the third of these three metrics (i.e., exploration of unknown environments) although, for the research described in this thesis, this metric is not considered. Manufacturing environments typically have assembly stations or other infrastructure so the mobile manipulator will navigate planned paths, as with AGVs, or preferred paths as with more autonomous mobile robots, where the start and end goal points are known. Therefore, the exploration of unknown environments metric is not considered further in this thesis.

4.5.1. AGV Stability

Moving AGV stability was not tested since the vehicle is extremely stable in the navigation velocity tested for approaching an assembly area (i.e., 0.25 m/s or less). However, stationary vehicle stability could affect the mobile manipulator used for assembly. Typical methods to stabilize mobile manipulators may be to use fixturing, [211] although as stated previously, this is a relatively expensive method. Ideally, the vehicle is free to access the assembly area without fixtures for assembly access at multiple poses and for rapid manipulator deployment. The AGV is typically a relatively heavy, low center-of-gravity machine. As such, the AGV may be expected to be stable even with a moving, lightweight manipulator mounted onboard the AGV. For example, the system used for experimentation includes a 1364 kg (3000 lbs) forklift style AGV able to lift and carry a 455 kg (1000 lbs) load at the vehicle rear. A 23 kg (50 lbs) manipulator, nearly 40 times less than the AGV, was mounted on the front of the AGV and maneuvered through an assembly process to be detailed in section 6. An experiment was performed [50][170] that measured the uncertainty of the static AGV when the manipulator uses noncontact positioning above the RMMA points. Uncertainty results are shown in Figure 56. Table 12 lists the mean (μ) and standard deviation (σ) of position (in mm) uncertainty with respect to the ground truth origin for each of the three runs for the AGV. Although the mean is relatively small for the AGV, the movement spans from approximately 0.15 mm in X and 0.25 mm in Y. The experiment proved that the AGV had motion even while the AGV was stopped and during manipulator motion. Tests were conducted on the ground level of a building with concrete flooring. Results show that position uncertainty spans from approximately 0.15 mm in X and 0.25 mm in Y for the AGV. When the uncertainty of the RMMA (see chapter 4.2.2.5 RMMA Movement) and the AGV are combined, maximum uncertainties can be (X = 0.52, Y = 0.65). Dependent upon the assembly tolerance desired, this instability could induce enough position offset of the manipulator to affect the results of manufacturing operations, such as a relatively high tolerance assembly operation. However, most of the vehicle motion occurred while the manipulator was moving between RMMA pattern assembly points which, during a typical assembly task, this may only affect both assembly time and EOAT positional accuracy.

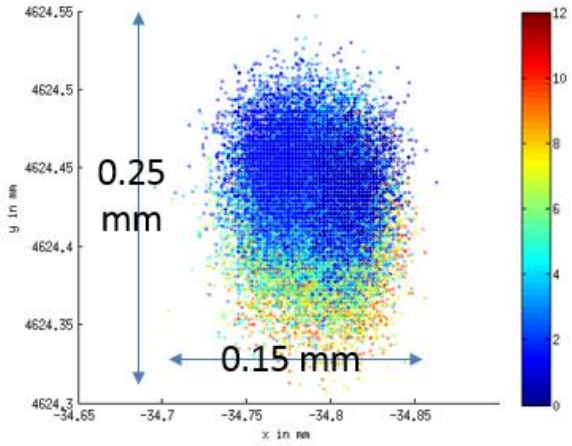

Figure 56. Ground truth data points relative to the ground truth system origin (in mm) of the stationary AGV movement over time (in minutes), shown by the varying colors, while the manipulator moves.

Table 12. Ground truth measured distances, with respect to the ground truth origin, showing the AGV movement when stopped beside the RMMA and while the laser retroreflector attempts to detect RMMA reflectors.

	Run1		Run2		Run3	
Axis	μ	σ	μ	σ	μ	σ
X	-34.79	0.021	-34.67	0.028	-34.13	0.027
Y	4624.43	0.032	4626.50	0.032	4626.0	0.042

4.5.2. Mobile Robot Stability

Advanced mobile base stability was recently considered for navigation in [213]. In this case, a cantilevered load was attached to the top of the mobile robot as a mockup of the onboard manipulator overhanging the vehicle while navigating. The mobile robot with onboard manipulator and structured weighed approximately 136 kg (300 lbs). For safety, the manipulator remained stowed and a bar with added weights was attached to simulate the cantilevered manipulator beyond the mobile robot footprint. Results showed that with only 5 kg (10 lbs) extended approximately 0.5 m beyond the edge of the mobile base, instability can occur. A critical use-case, therefore, for mobile manipulator users is to ensure that instability is considered during autonomous mobile manipulator navigation.

As a comparison to the AGV experiment described in section 5.5.1, the mobile base was statically positioned while the onboard manipulator was in motion. The OTS was used to measure the mobile robot motion as the manipulator repeatedly moved to three poses. Figure 55 shows photos and OTS screenshots of the three poses. Figure 57 shows a plot of the mobile robot centroid (i.e., manipulator base) movement versus time. The onboard manipulator moved at 50 % velocity from stow to a near point to the vehicle and then to an extended reach point (~ 0.5 m) repeating six times. The mobile robot moved approximately 2.5 mm in X and 2.8 mm in Z (optical tracking system axes) with standard deviation of x = 0.004 mm in X, 0.07 mm in Z. The mobile robot motion versus the AGV motion is as expected where the relatively lighter weight, smaller frame

mobile robot moves more than the AGV noting that the manipulator was the smaller model manipulator than the larger manipulator mounted on and used for AGV motion tests.

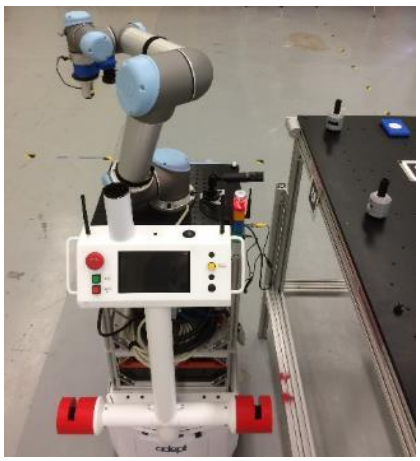

a

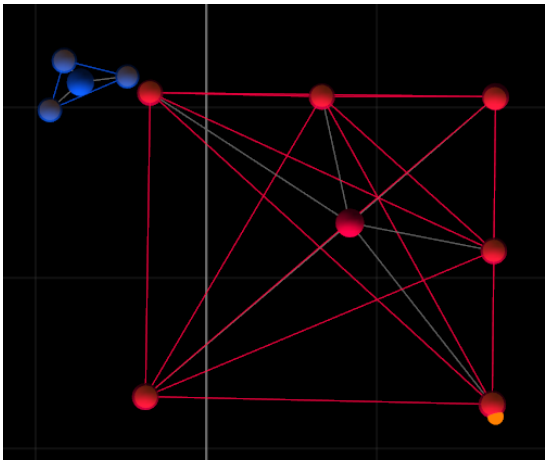

b

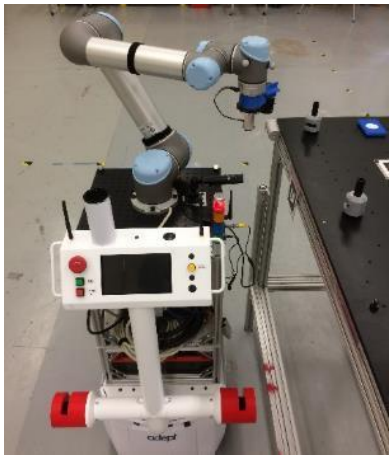

c

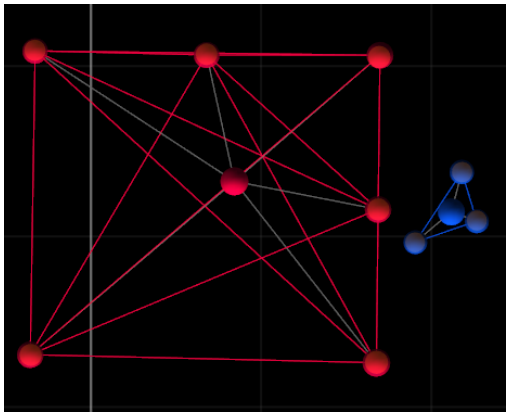

d

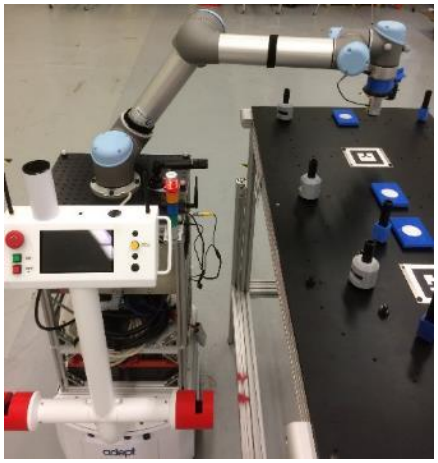

e

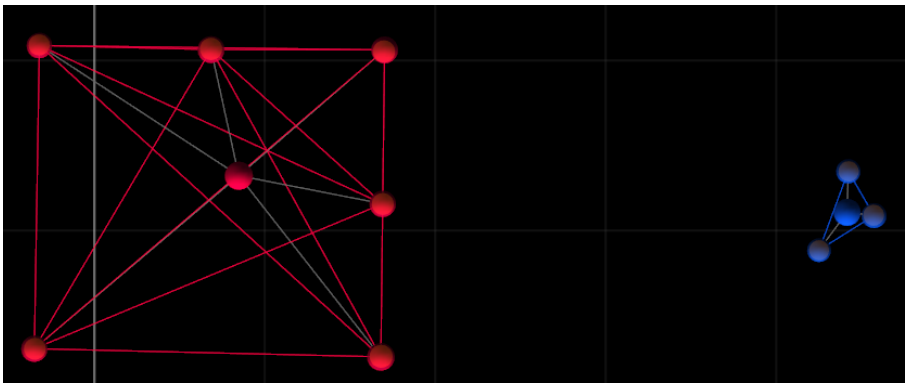

f

Figure 57. Photos (a, c, e) and OTS screenshots (b, d, f) of the three manipulator poses during the mobile robot static movement.

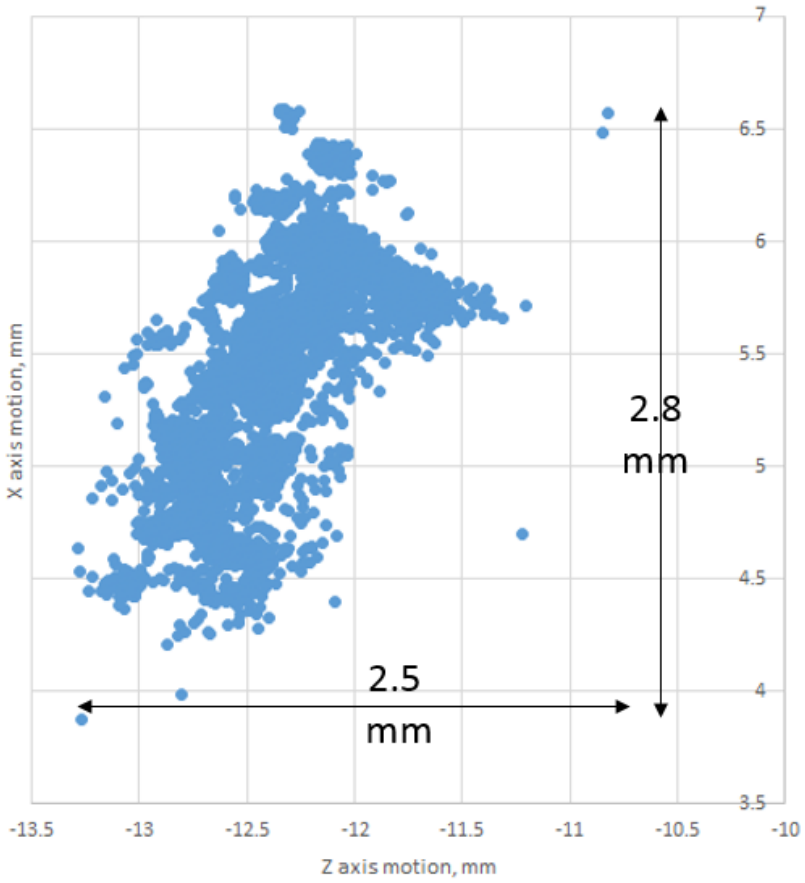

Figure 58. Plot of Lynx movement vs time when the mobile robot is stationary and the onboard manipulator moves from stow to a near point to the vehicle and then to an extended reach point.

4.5.3. Obstacle Detection and Avoidance

Described in section 4, ITSDF B56.5:2012 provides language to generically handle a situation when an object suddenly appears within the AGV stop region. (The stop region is the area surrounding the AGV in which the non-contact safety sensor detects obstacles and stops the

vehicle.) AGVs will typically stop when an obstacle appears in the vehicle path and then proceed to the goal once the obstacle is removed. This concept is straightforward and deemed as not affecting the mobile manipulator performance.

Mobile robots, however, may use obstacle detection and avoidance (e.g., plan and drive around obstacles) for navigating a relatively long distance (e.g., more than 3 m) to the assembly area. If the mobile manipulator is too close to the assembly area (e.g., within 1 m), the vehicle will typically stop and abort the mission to proceed noting that the goal cannot be reached. Once removed the vehicle would proceed similar to the AGV. An experiment was performed to consider the effects of obstacle detection and avoidance on the mobile manipulator base positioning at the assembly area when an obstacle was inserted into the vehicle path at approximately 3 m from the RMMA. A baseline experiment first considered the mobile robot when approaching the assembly area with no obstacle in the vehicle path. A second experiment considered when an obstacle was in the vehicle path and then was avoided by the mobile robot and proceeded to the assembly area goal point. Results were indecisive between the two tests as determined by the grid method used in 4.4.2, slightly modified with different grids and alignment lines relative to the RMMA (note the lines drawn on the floor). See Figure 59 which shows a close-up of a grid showing the randomness of points for nine trials – 1 - 4 with no obstacle and 5 - 9 with an obstacle in the path, and one trial (7) that was aborted in trial 7 due to the mobile robot colliding with the RMMA. When avoiding the obstacle, no vehicle instability occurred.

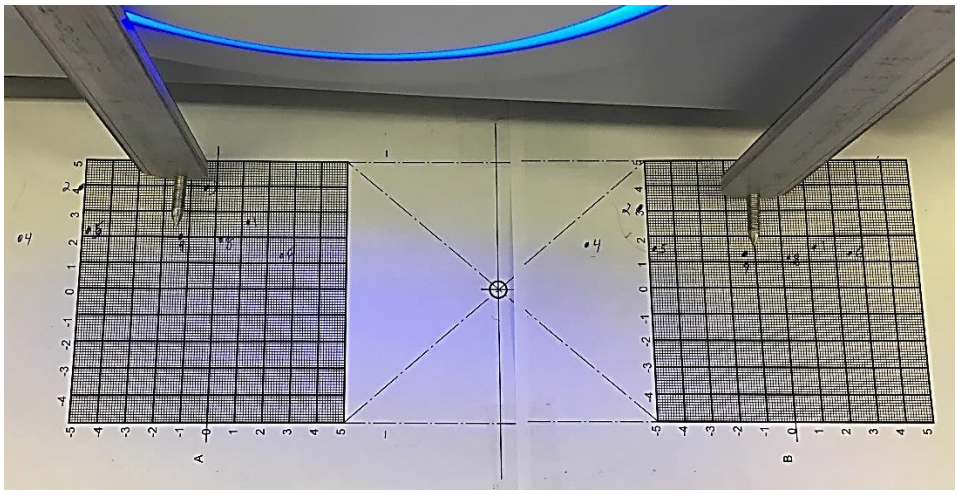

Figure 59. Obstacle avoidance test resulting pose points marked on a floor grid.

The mobile robot corrects for obstacles and continues to use natural feature navigation to reach the goal. However, the laser used to detect natural features provides relatively low mobile robot positioning uncertainty of approximately 100 mm maximum deviation between the 4th and 6th trials. Much more in depth obstacle detection and avoidance scenarios could be experimented to determine the crossover from no visible effects as was experienced to more noticeable effects, such as never reaching the goal. However, this is not the focus of this thesis as it is assumed that the mobile manipulator is not prevented from reaching the RMMA for mobile manipulator performance measurement.

4.6. Conclusions

The mobile base, whether an AGV or mobile robot, is relatively complex in components that make up the mobile base, as well as its performance. The mobile base SysML internal block diagram model described in this chapter shows the interconnect of the AGV components as a generic model describing passing signals, reference to system constraints (e.g. AGV and Facility reflectors) and the vehicle itself, and the internal controller (AGVBrain) that inputs and outputs the signals for expected vehicle performance. The same model for the AGV can be readily extended to the mobile robot or any other autonomous industrial vehicle since the components are similar. Differing among systems are the referenced, designated by the dashed boxes, AGV and Facility reflectors constraints that can be changed to match the mobile base being modeled.

Following on from the model are the combination of components that make up the mobile base capabilities, although their complexity in combination requires much deeper consideration, such as: calibration; navigation, docking, and stability performance; and obstacle avoidance.

Initial calibration of the facility reflectors was determined to be critical to the AGV performance and a new method using the OTS was developed and tested to not improve the method using the laser tracker, as expected. However, the reference frame remains the same for the OTS measuring the facility reflectors as it does for measuring the AGV performance. Proper calibration of the steering and drive parameters of an AGV is critical for accurate dead-reckoning navigation, and improves the performance of an AGV servoing based on navigational information. Calibration of the navigation system alignment is also important for proper control of the AGV. Calibration of the distance encoder, the steering offsets, and the sensor mounting angle on the AGV were addressed. Manual methods for performing the AGV calibration were found to be ideal as they require a minimum of specialized equipment.

AGV navigation performance measurements experiments were conducted and the OTS was first measured and then used for AGV navigation evaluation towards standard test method development. Simple, geometrical, path-navigation experiments were then conducted with an AGV. Results show path deviation from commanded paths. Analysis of the AGV tracked data as compared to ground truth system data shows that the AGV could track to within approximately 3 mm and 5 mm uncertainty, for both the circle and square tests, while moving at 0.25 m/s. However, AGV calibration, tolerance, or other parameter adjustments in the vehicle controller may allow improvements to navigation performance. For example, adjustment to the translational and rotational offsets provided better navigation performance.

AGV docking experiments were also performed and again demonstrated the differing uncalibrated vs. calibrated AGV results. Uncertainty ranged from approximately 1 mm to 50 mm for the uncalibrated tests and improved by an order of magnitude, or 5 mm uncertainty, for the calibrated AGV tests. Minimal deviation from the dock point was demonstrated run-to-run for an uncalibrated AGV when approaching the same point from the same direction. However, the eventual goal of mobile bases, such as AGVs, should be to improve performance and capability by approaching docking points from any trajectory where the docking uncertainty will be most evident as results proved.

Stability of the mobile base, AGV or advanced mobile base (i.e., mobile robot), is affected by onboard manipulator motion, even when the manipulator does not make contact with another object. Even with an AGV that is 40 times heavier than the onboard manipulator, AGV motion was measured to be approximately 0.15 mm in X and 0.25 mm in Y. Hence, the AGV had motion even while the AGV was stopped and during manipulator motion. Similarly, stability of the stationary mobile robot weighing approximately 10 times more than the manipulator was affected by the moving manipulator to approximately 2.5 mm in X and 2.8 mm in Y. Further, a stability experiment was performed on the mobile robot demonstrating that just 2.2 kg of load cantilevered from the mobile robot can cause instability of the mobile base when in motion. These measurements provide critical performance criteria that will factor into the mobile manipulator system.

5. MANIPULATOR

5.1. Models

SysML models were created for the manipulator, to generalize the hardware interconnections, as well as a model describing the manipulator tests performed. Fewer tests were performed for the manipulator versus the mobile base since the uncertainty is much lower than for the mobile base. Also, there are no parameter adjustments that can be made to the robot. However, tests were also performed to measure a critical manipulator-to-mobile base pose determination. Because of its reliance upon the mobile base control, the manipulator software algorithm model will describe the basic control in section 6.2.1.2 within the mobile manipulator performance measurement discussion.

5.1.1. Manipulator Model

The manipulator internal block diagram [160] shown in Figure 60 (a) includes an end-of-arm-tool which adds a constraint of tool positioning along with the base mounting constraint (Manipulator Base constraint) referenced to the AGV. This part constraint describes the mounting uncertainty that can occur when the manipulator is mounted to the mobile base. And, although the AGV is linked to the Robot arm part due to the onboard manipulator mount, the AGV includes its additional constraint of pose uncertainty. These will be further detailed in section 6.

The OTS can be used to measure the manipulator performance to uncertainties as described in section 3.3. The OTS may be especially useful for measuring the performance of redundant open-chain manipulators where manipulator configuration may be important (e.g., manipulating around an object to perform an assembly). However, the RMMA was instead used for measurement towards a more cost-effective solution for mobile manipulator uncertainty measurement. In the redundant open-chain manipulation case cited, the RMMA could be used to compare the redundancies by testing all possible solutions for completing the assembly. To test the positioning accuracy and repeatability of the mobile manipulator, a laser retro-reflector sensor was mounted as the end-of-arm-tool (EOAT) of the manipulator. A digital signal is output from the sensor when the laser is emitted and reflected to the sensor. The signal is then read by the manipulator controller. Less intense reflections from other objects in the workstation are ignored. The laser is used to interact with the Reconfigurable Mobile Manipulator Apparatus (RMMA) described in section 3.3.2.

The manipulator performs intermediate motions to two poses that cause the manipulator to approach the Bisect Control and Search Control registration points on the RMMA the same way. This ensures that the manipulator will not attempt to pass the end-of-arm-tool through the base of the robot or other self-destructive motion at different AGV poses next to the RMMA. Dependent upon the operator selection of performance measurement type, either the bisect or search methods are performed. Step sizes for the Bisect Control are variable allowing the operator to choose the time for the manipulator to bisect to find the large reflector center and/or the accuracy of the center. For example, a 0.25 mm step size will take much longer to find the reflector center verses a 2 mm step size which also includes much higher uncertainty. Similarly, when using only the Search Control for registration to the RMMA, a very small step size provides relatively higher accuracy. However, a step size of half the diameter of fiducial reflector was determined an ideal step size.

For example, when 1 mm fiducial diameters were used, the 0.5 mm step size was used. Based on the AGV location, one of two patterns are then traversed. Stowing the manipulator was programmed to occur when the pattern was completed or when performing Bisect Control or Search Control that did not produce appropriate results within a chosen time period. For example, if the Bisect Control did not initially result in a reflector detect or if the Search Control took more than 200 steps, the manipulator Stow function was executed and the AGV System Manager Run program was alerted that the AGV could move.

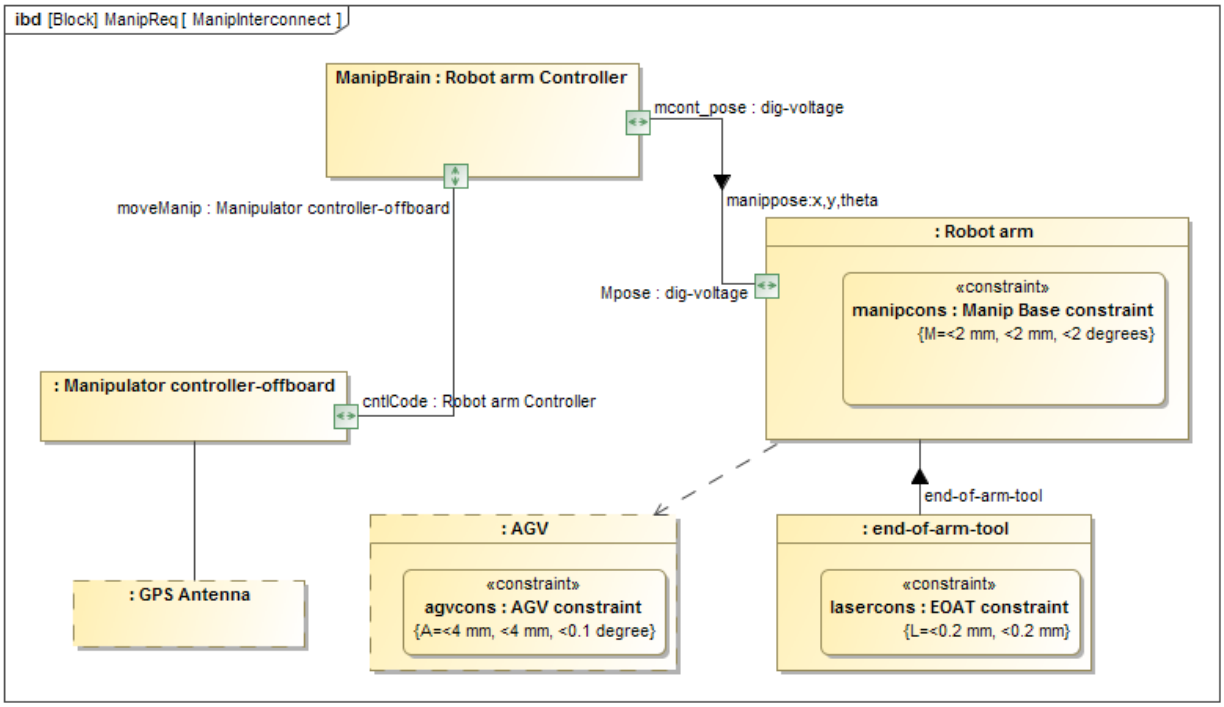

Figure 60. SysML internal block diagrams of the physical manipulator (Robot arm) subcomponents.

5.1.2. Tests

As with measurements of the mobile base described in section 4, performance measurements are required of the onboard manipulator to understand and potentially gain the highest level of mobile manipulator performance. Through experimentation, it was determined that the manipulator is much less uncertain than the mobile base (e.g., 4 mm or greater specified for the AGV tested) for accuracy and repeatability (e.g., ± 0.1 mm specified for the robot arm tested) of acquiring goal points independent of the mobile base. Isolation of the manipulator was achieved by using a machined breadboard, with similar hole spacing and tolerance to the RMMA, onboard the AGV and on which the manipulator base was mounted. The measurement concept was initially coarsely tested for feasibility followed by data collection with ground truth. These tests aligned with the performance measurement standard that is available for robot arms and are described in the next sub-section 5.2.

The next critical manipulator performance area is to determine the manipulator base pose with respect to the AGV reference. Figure 61 shows a SysML block definition diagram of the manipulator tests performed, including the manipulator to mobile base tests. Again, as with the mobile base, an example requirement for mobile manipulator performance is to achieve the RMMA fiducial uncertainty of 1 mm, as in section 3.3.2.2 where the requirement will mostly be

compensated for by the manipulator. Validation of the best manipulator performance of specified ± 0.1 mm through verification is needed. The manipulator propagation of uncertainty therefore, stems from the robot base mounting position, to the position certainty of the EOAT, to the laser aligned with the tool center point, and then to the RMMA fiducial detection. With these uncertainties, the model shown in Figure 60 shows the Robot arm uncertainty which includes the mounting onboard the AGV as being < 2 mm in translation and < 2° in rotation. Therefore, verification is needed here.

The following sections detail each of the tests shown in the model beginning with the Test paths. The modeled tests were reversed so that dependency lines were not crossed when maintaining the original mobile manipulator package diagram from Figure 1 (a).

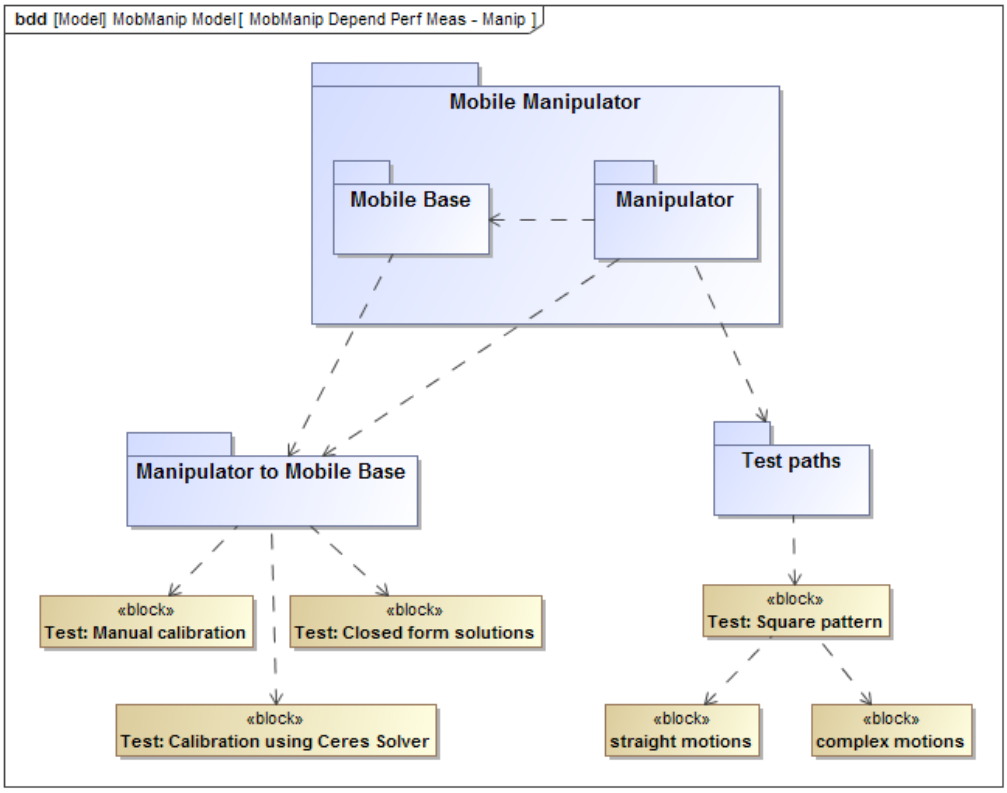

Figure 61. SysML block definition diagram of mobile manipulator tests that depend on performance of the manipulator.

5.2. Manipulator Performance

In ISO 9283, 6.6 “Load to the mechanical interface” section, [44] an example test end effector is shown (see Figure 62) with a tool center point (TCP) in line with the EOAT and also with the TCP offset from the EOAT centroid. Similarly, the test method described in this thesis uses a laser retroreflector that is in line with the EOAT centroid. ISO 9283 6.8.6.2 “Shapes and sizes of the test paths” also describes a cube working space (see Figure 63) used to measure robot performance with the two criteria that the cube is located where the robot is mainly used and that the cube has a maximum volume with the edges parallel to the base coordinate system. The performance tests in this thesis are mainly focused on the thesis case, assembly application, and therefore only the

endpoints of the straight paths within the cube are important. Hence, the endpoints of a square are embedded in the RMMA as one such test. The development of a test method for measuring mobile manipulator performance may include assembly at various angles as shown in Figure 63. However, this point is considered duplicated for the tests described here by simply using the Base coordinate system X/Y plane parallel to the robot base as shown in Figure 63 "Plane 3". The paths and points that were measured are shown in red.

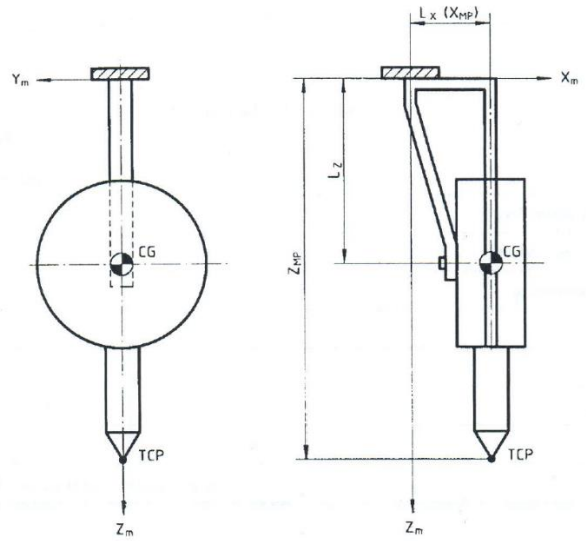

Figure 62. Example test end effector from ISO 9283.

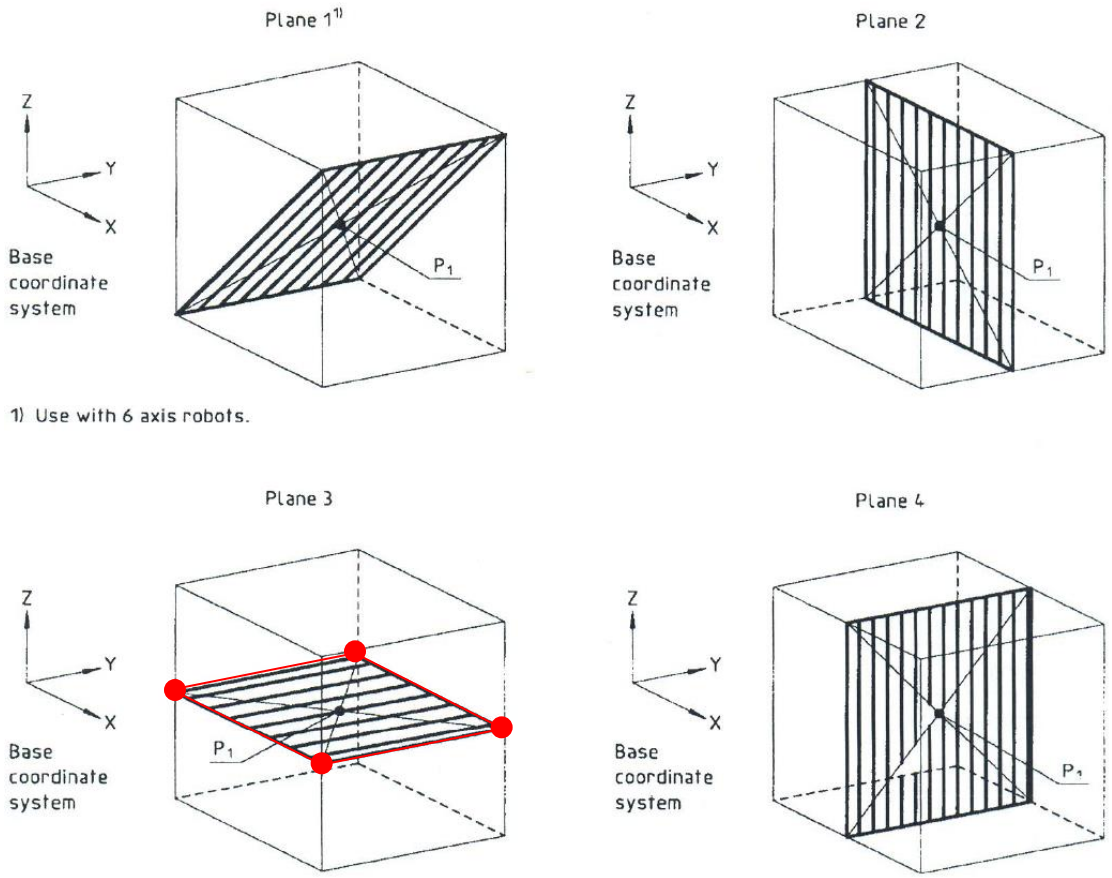

Figure 63. Example test cube and paths within the cube from ISO 9283. Tests performed in this thesis use the lower left Plane 3 configuration and test to the outer perimeter and points shown in red.

The specifications for the Universal Robot UR10 [214] used for experiments within this thesis are shown in Table 13. Repeatability is shown as ± 0.1 mm although accuracy is not listed.

Table 13. Universal Robot UR10 Specifications

Weight	28.9 kg / 63.7 lb
Payload	10 kg / 22 lbs
Reach:	1300 mm / 51.2 in
Joint ranges:	+/- 360° on all joints
Speed: Joint:	Max 120/180°/sec. Tool: Approx. 1 m/sec. / Approx. 39.4 in/sec.
Repeatability:	± 0.1 mm / ± 0.0039 in (4 mil)
Footprint:	Ø190 mm / 7.5 in
Degrees of freedom:	6 rotating joints
Control box size (WxHxD):	475 mm x 423 mm x 268 mm / 18.7 x 16.7 x 10.6 in
I/O ports:	10 digital in, 10 digital out, 4 analogue in, 2 analogue out
I/O power supply:	24 V 1200 mA in control box and 12 V/24 V 600 mA in tool
Communication:	TCP/IP 100 Mbit: IEEE 802.3u, 100BASE-TX
	Ethernet socket & Modbus TCP
Programming:	Polyscope graphical user interface on
12 inch touchscreen with mounting	
Noise:	Comparatively noiseless
IP classification:	IP54
Power consumption:	Approx. 350 watts using a typical program
Collaboration operation:	Tested in accordance with sections 5.10.1 and 5.10.5 of EN ISO 10218-1:2006
Materials:	Aluminium, ABS plastic
Temperature:	The robot can work in a temperature range of 0-50°C
Power supply:	100-240 VAC, 50-60 Hz
Calculated Operating Life:	35,000 Hours
6 metre / 236 in cable between robot and control box	
4,5 metre / 177 in cable between touchscreen and control box	

A preliminary repeatability experiment (1) was designed to coarsely measure the performance of only the manipulator, i.e., not including the AGV. A 457.2 mm square pattern of 2 mm diameter fiducial reflectors were positioned on a breadboard, mounted to the top of the AGV, that includes a 50.8 mm square pattern of mounting holes. The breadboard is also the mounting surface for the manipulator base. The manipulator was programmed to move the EOAT (laser retroreflector) above and in-line with the fiducial to detect the fiducial reflector 30 times. The experiment was performed twice with the manipulator moving straight from one reflector to the next. Upon all 60 stop points, the laser detected the fiducial reflector without any errors. This starting point provided a quick test to isolate the manipulator from the AGV while using a similar test that will be used to test the mobile manipulator and described in section 6.

Deeper into the manipulator performance measurement, a second experiment (2) was performed that also followed the ISO 9283 standard described above. The manipulator was again programmed to traverse a 457.2 mm square pattern on the AGV, isolating it from AGV mobility, although, for experiment 2, no RMMA fiducials were used. Instead, only the OTS was used, as shown in Figure 64, to measure the manipulator repeatability with respect to ground truth. To provide a more complex motion, as opposed to a straight line, the manipulator was programmed to move off plane along curved trajectories from markers 2 to 3 and markers 4 to 1 as shown in Figure 64 (d).

Approximately 5 s or more of data was collected at each of the 60 points resulting in approximately 600 or more data captures per manipulator pose. The data captures were then averaged and a standard deviation for each of the 60 poses in both X and Z angles were all calculated to be at 0.00002 mm or better.

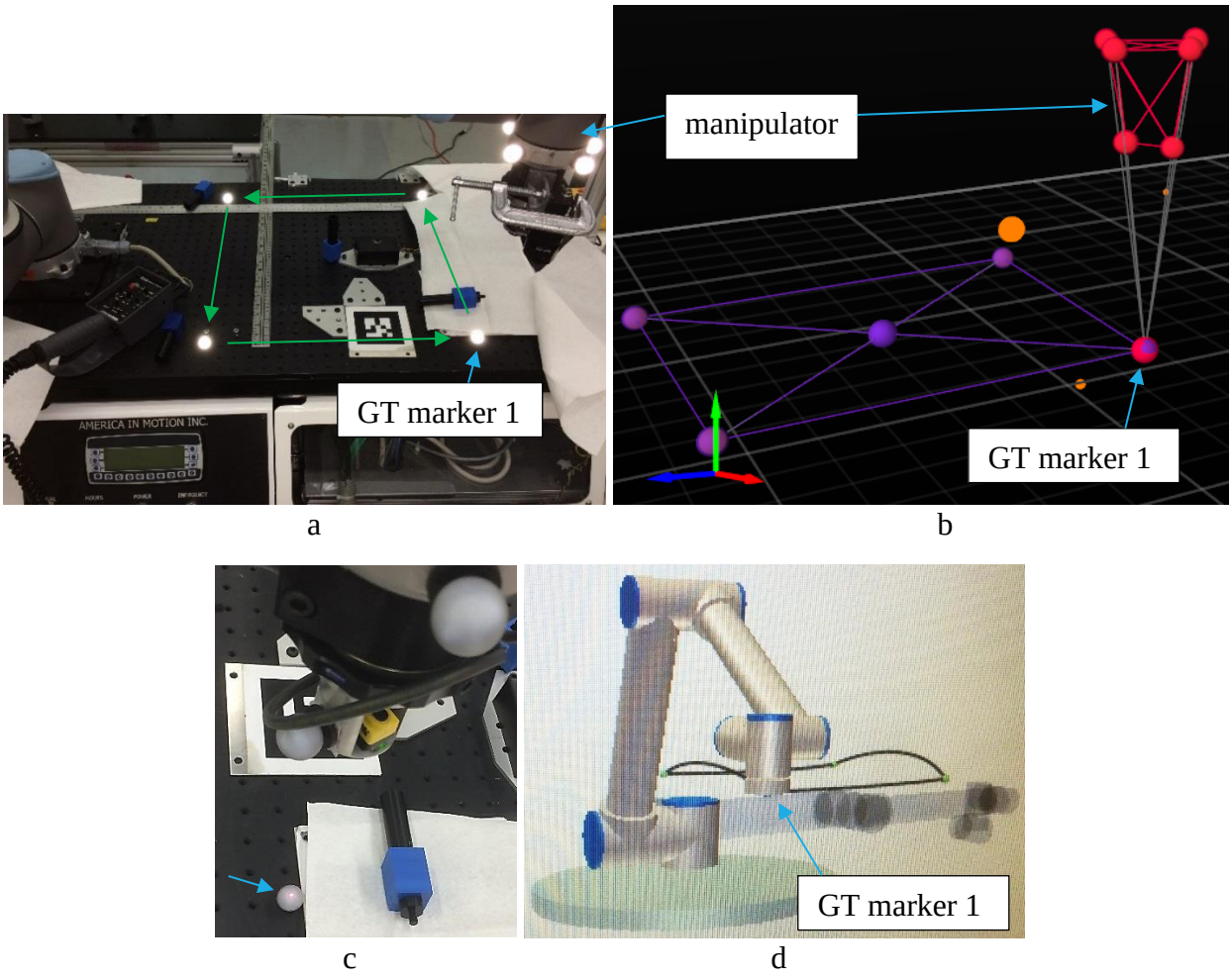

Figure 64. (a) Illuminated markers from camera flash (green lines show manipulator motion pattern) and (b) OTS screenshot of the manipulator and ground truth square pattern of markers. (b) The EOAT rigid body centroid was snapped to marker 1 after (c) the laser retroreflector was aligned (red dot on marker) to marker 1 of the ground truth square pattern of markers. (d) Manipulator motion trajectories (black lines) between the four, square pattern stop points.

The OTS data was analyzed for the 60 points recorded in experiment 2 with 15 points at each corner of the square pattern. Experiment 2 results are shown in the plots in Figure 65 and Figure 66. Figure 65 shows plots of OTS data from 15 repeatability measurements at each corner of the square pattern for manipulator. The Figure 65 plots show a drift that occurred for each of the manipulator poses, where poses 1 and 2 showed the most drift. Approximate maximum drift plots for the 60 measurements are shown in Table 14 with the largest drift being shown for pose 3 along

the OTS X axis and for pose 2 along the OTS Z axis. All points are within the manufacturers specified ± 1 mm repeatability, including the drift.

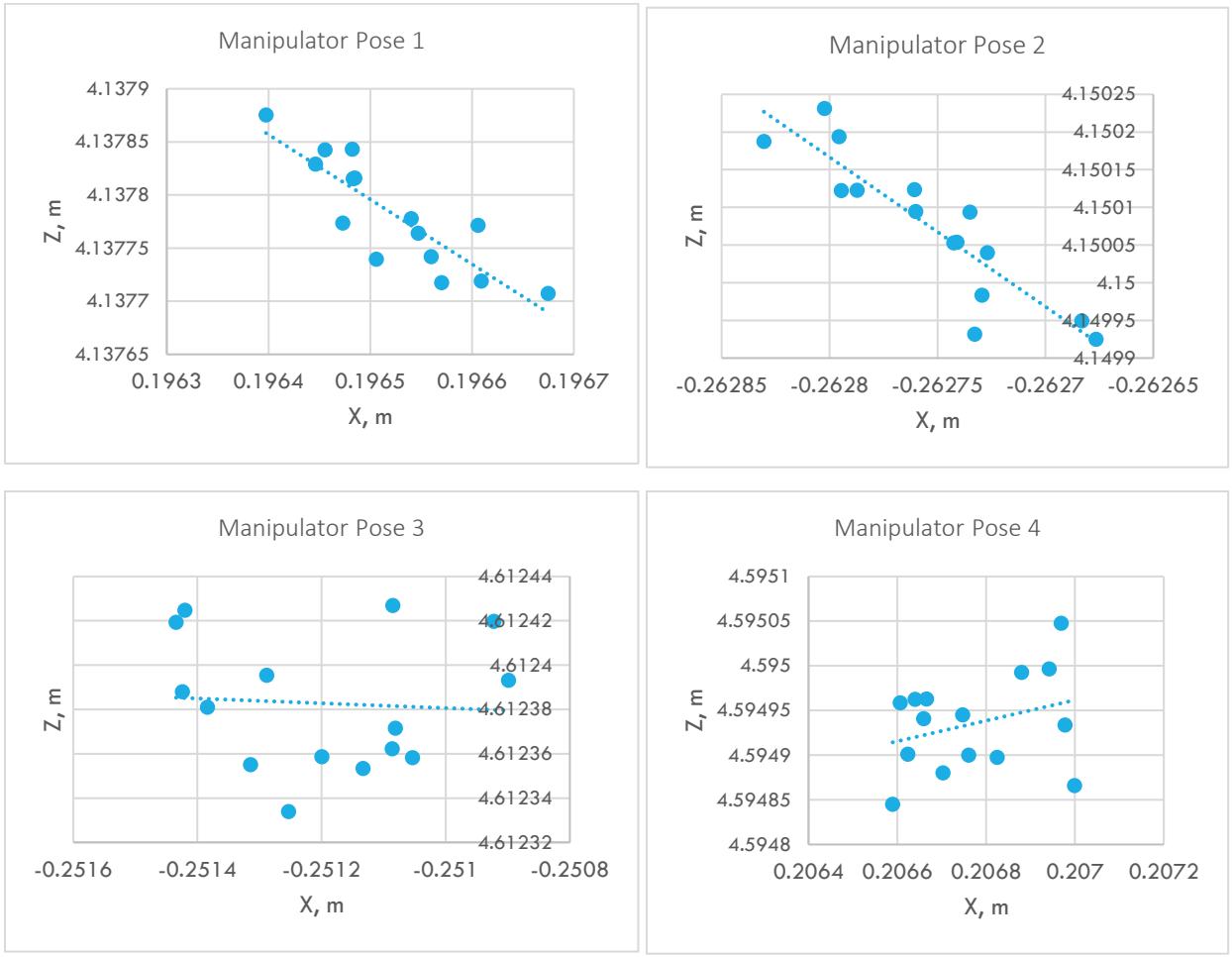

Figure 65. Plots of OTS data results from 15 repeatability measurements at each corner of the square pattern for manipulator (a) pose 1, (b) pose 2, (c) pose 3, and (d) pose 4.

Table 14. Approximate maximum drift in mm for the 60 measurements shown in Figure 65.

Manipulator Pose	X	Z
1	0.25	0.2
2	0.2	0.35
3	0.8	0.1
4	0.4	0.2

Figure 66 also shows plotted OTS data from the 60 measurements of the square pattern, 15 at each corner. The figure shows the angled offset from misalignment of the manipulator base to the AGV, as well as the performance uncertainty of the manipulator since all angles are not the same (i.e., over 40% worst case difference).

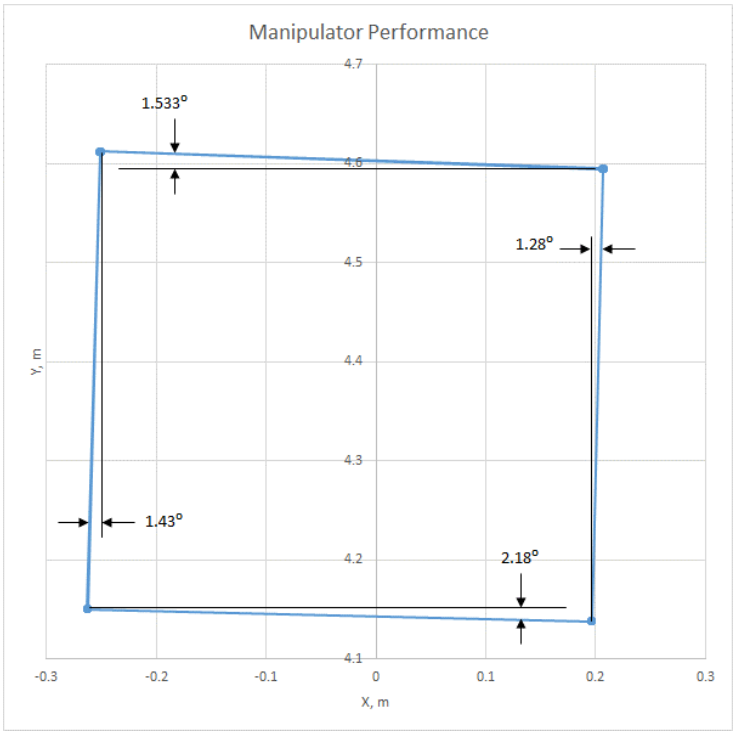

a

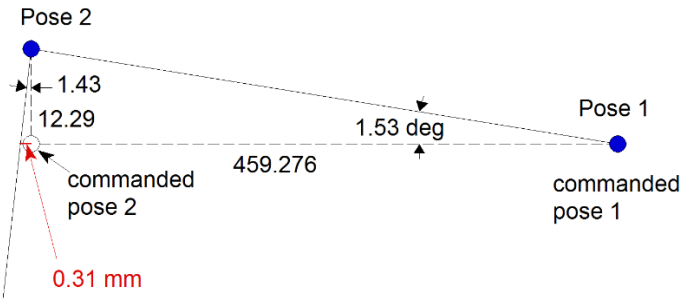

b

Figure 66. (a) Plotted OTS data from 60 measurements, 15 at each corner of a square pattern. The angled offset shows the misalignment of the manipulator base to the AGV, as well as the performance uncertainty of the manipulator since all angles are not the same. (b) Example offset for pose 1 to pose 2 trajectory that is subtracted from the offset measurement as in Table 15 "Arctangent of offset".

Table 15 shows the manipulator repeatability uncertainty for Experiment 2. The offset angle was compared to the next, adjacent manipulator stop pose on the square (e.g., pose 1 moved to pose 2, etc.) which was as high as 2.2°, although with uncertainty (standard deviation) of 1.63°. The mean pose to ground truth difference does not consider the angular offset and was included to show the AGV to OTS coordinate frame rotation offset, which was not used for further calculations. When the associated pose offset angles are applied to the translational measurements, offset error from the 457.2 mm square was between 0.32 and 4.67 mm. This is significant and is similar to the

minimum offset of the AGV pose when docking with the RMMA or other assembly workstation that may be used in industry.

Table 15. Results of repeatability uncertainty for the square pattern of manipulator stop points performed onboard the AGV.

	Robot pt 1		Robot pt 2		Robot pt 3		Robot pt 4	
	X	Z	X	Z	X	Z	X	Z
Mean manipulator pose	0.19652	4.13778	(0.26275)	4.15007	(0.25120)	4.61238	0.20677	4.59494
Standard deviation	0.00007	0.00005	0.00004	0.00009	0.00017	0.00003	0.00014	0.00005
Ground Truth	0.19713	4.14560	(0.26075)	4.15049	(0.25557)	4.59301	0.20244	4.58727
Mean pose to GT difference	0.604	7.813	2.004	0.419	(4.371)	(19.378)	(4.335)	(7.661)
Diff. in adjacent X poses, mm	459.2755659		-11.5546485		-457.9710424		10.25012494	
Diff. in adjacent Z poses, mm		12.29		462.31		(17.45)		(457.15)
Offset angle to adjacent pose, rad		0.027		(0.025)		0.038		(0.022)
Offset angle to adjacent pose, deg		1.533		(1.432)		2.182		(1.284)
Offset angle Std dev								1.625
difference in GT to offset point, mm		2.076		5.109		(0.771)		0.047
ArcTangent of offset		(0.31)		(0.44)		0.39		0.27
Manipulator mean offset from programmed 457.2 mm square pattern, mm		1.77		4.67		(0.38)		0.32

Table 15 shows that the uncertainty in manipulation is on average, 1.59 mm with a high uncertainty of 1.94 mm. The generic SysML internal block diagram model shown in Figure 60 (a) shows an approximated Robot arm, Manipulator Base constraint of < 2 mm in both X and Y and < 2° in rotation that has been verified by repeatability experiments. The model can vary dependent upon the manipulator and its attachment to the mobile base. A remaining unknown is that there is no certainty in the alignment between the surface on which the manipulator base is mounted and the AGV reference point. Therefore, it is necessary to further develop a method to measure the manipulator base pose, extended to the manipulator EOAT, to the AGV reference point. The following section describes this method.

5.3. Manipulator-to-Mobile Base Measurement

The goal is to be able to use the AGV to move the manipulator to a workstation and be able to accurately assemble items in that workspace [170]. To perform this task, it is necessary to accurately determine the location of the manipulator relative to the workspace. Two crucial components of this are determining: (1) the actual (not just the commanded) position of the AGV and (2) the position of the manipulator relative to the AGV. For component one, we need to be able to get the position of the AGV from the navigation system in near real time. All prior research to this point has involved off-line, AGV position data processing from log files. As such, the position information must pass directly to the offboard computer system that is controlling the manipulator. The second requirement is to establish the offset between the AGV and the base of the manipulator. This will allow the AGV's position to be used to determine the global location of the manipulator when the AGV stops at a particular work station.

The initial focus on manipulator-to-mobile base measurement is on indirect methods for determining the mounting offset of a manipulator to a mobile base reference point. The following discusses the need to calibrate the offset between the manipulator base and the AGVs coordinate system, as well as the equipment and methods used to collect the data and evaluate the results of the mounting offset calibration. Two methods of computing the mounting offset are described: 1) using measurements taken at selected positions around a test artifact, and 2) a method of computing the offset using Ceres Solver on a selection of measurements from a random set of poses around the test artifact. The effectiveness and accuracy of the two calibration methods are discussed along with the relative merits of using Ceres Solver for solving this type of calibration problem and the effects of measurement noise on the procedure.

The use of intelligent sensing systems such as computer vision or light detection and ranging (LADAR) sensors [68] can be used to measure a workpiece pose relative to the manipulator. To effectively act on sensor information, the systems need to know precisely where those sensors are located with respect to the other elements of the system. The calibration of a new sensor involves the determination of the sensor pose relative to other sensors and manipulators. These parameters are difficult, or even impossible, to directly measure. Sometimes the only way of determining these unobservable system parameters is through the mathematical analysis of the sensor's own data. The calculation of arm-mounted camera offsets using images from the camera has been widely discussed in the literature [215][216][217][218][219][220][221][222][223][224][225]. In most of these methods, a key feature is the simultaneous solution of two sets of independent transformations. These transformations are typically the desired offset of the sensor and the pose of a calibration target. The solution of the calibration target pose is typically incidental to the solution of the desired offset. Similar methods can be applied to determining other system offsets.

5.3.1. Manual calibration method

An experiment using a manual calibration method was performed to determine the manipulator mounting offset to the AGV using a number of simple measurements. The concept was to select pairs of calibration data measurements that would lead to the simple calculation of a single value of the manipulator mounting offset. This was done by selecting pairs of positions around the RMMA where the other parameters of the manipulator mounting offset would effectively cancel each other out.

The AGV positions were chosen to cancel out the effects of the other base offset parameters, or to minimize their effect on the computation. In testing, these values were good enough to come up with rough values of the offset, but not good enough for precise positioning of the manipulator. There were some interactions between the calibration variables that could not be completely eliminated using this method. However, the method works well as a sanity check for the other computation methods.

The equations below describe the manipulator offset calibration in a 2D plane. The value being determined is the 2D translational offset and rotation offset of the manipulator relative to the AGV. The reason for doing the calculations in 2D is that the method for taking the measurements using the laser sensor only constrains the position in 2D, and the AGV navigation solution is only 2D.

Figure 67 (a) illustrates a pair of mobile manipulator locations that isolates the x offset of the manipulator base.

$$A_{x1} + O_x - P_{x1} = A_{x2} - O_x + P_{x2}, \quad (1)$$
$$O_x = \tfrac{1}{2} (A_{x2} - A_{x1} + P_{x1} + P_{x2}), \quad (2)$$

where:

P is point in manipulator coordinates (P_x, P_y)
A is AGV coordinate (A_x, A_y, A_a=angle)
O is the manipulator mounting offset (O_x, O_y, O_a=angle)

Figure 67 (b) illustrates a pair of mobile manipulator locations that isolates the y offset of the manipulator base.

$$A_{y1} + O_y - P_{y1} = A_{y2} - O_y + P_{y2}, \quad (3)$$
$$O_y = \tfrac{1}{2} (A_{y2} - A_{y1} + P_{y1} + P_{y2}) , \quad (4)$$

Figure 67 (c) illustrates a pair of mobile manipulator locations that isolates the angular offset of the manipulator base.

$$A_{x1} + O_x - P_{x1} + R_1 \sin O_a = A_{x2} + O_x - P_{x2} + R_2 \sin O_a, \quad (5)$$

where

$$R_n = (P_{xn}^2 + P_{yn}^2)^{1/2} \quad (6)$$

and

$$O_a = \sin^{-1}((A_{x1} - A_{x2} - P_{x1} + P_{x2}) / (R_2 - R_1)) . \quad (7)$$

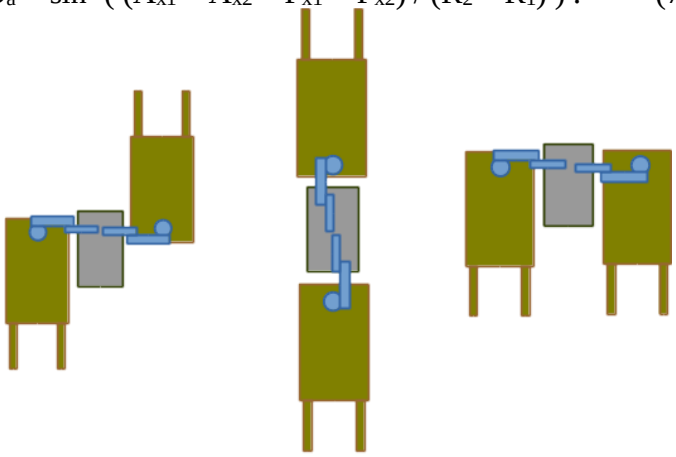

a b c

Figure 67. Mobile manipulator (green) positions relative to the RMMA (gray) selected for manual calibration of manipulator (blue) mounting offset.

These formulas assume the manipulator is mounted on the AGV with its positive y-axis pointing toward the rear (fork-end) of the AGV (in the direction of the AGVs negative x-axis).

There are issues that limit the effectiveness of this approach for determining the manipulator base location. One issue is that despite the best efforts to position the AGV as described, there will be some errors in alignment. The result is that the other offset terms will not cancel out exactly, and there will be some interaction between the parameters that will affect the results of the calibration.

Another issue with this method is that it does not deal well with measurement error. Each parameter is calculated using a single pair of AGV positions. So, any errors in the measurements are reflected directly in the calculated mounting parameters. The effects of measurement noise can be compensated for by averaging together several measurements at a given location.

The initial set of calibration data was collected manually. The AGV was moved manually to various locations around the RMMA and its position was recorded. Then the manipulator was moved manually (using the teach pendent) to the positions of the first and second reflectors of the square target. The manipulator was moved until the retro-reflector sensor detected the reflectors. Then the position of the manipulator was manually recorded.

The reflectors used to collect the calibration data had a 3.2 mm (1/8 in) aperture. The positions of the AGV relative to the RMMA for the manual data collection are shown in Figure 67. A subset of these measurements, shown in Figure 67, was used to perform the manual calibration described above. The orientation of the EOAT was maintained constant relative to the manipulator base so that any lateral offset of the sensor from the tool center could be ignored. Any offset at the tool becomes part of the base offset for the purposes of this calibration.

5.3.2. Calibration using Ceres Solver

A better way to solve for the manipulator base offset is to express it in terms of a non-linear minimization problem. This allows all the interactions between the base offset parameters and the calibration measurements to be explicitly modeled. After the interactions between the calibration parameters and the calibration data have been modeled, the calibration parameters can be solved using iterative methods. The tool used to compute the iterative solution was the Ceres Solver library [207].

The calibration data consists of paired AGV and manipulator position data taken at various locations around the RMMA. The only constraint on the data is that it needs to be collected at different AGV poses so that the solver converges properly. Data from multiple EOAT target points can also be used, as long as the association is maintained in the data model.

The mobile manipulator system model is formulated as:

$$wp(k) = agvPose(t) * robotPose * rp(k,t), \quad (8)$$

where:

wp(k) is the estimated position of the k^{th} target point in world coordinates;

agvPose(t) is the measured pose of the AGV in world coordinates at time t;

robotPose is the estimated pose of the manipulator in AGV vehicle coordinates;

rp(k,t) is the measured location of the kth target point in manipulator coordinates at time t.

The agvPose(t) and robotPose are 2D transformations consisting of a translation and a rotation. The points wp and rp are 2D points. Individual calibration targets are enumerated by k, and

individual calibration measurements are enumerated by t. The program adjusts the values of wp(k) and robotPose to minimize the residual between the estimated world coordinates of the target points and the position value computed in (8) using the calibration data. The estimate of the manipulator mounting offset is calculated using the data collected for the manual calibration augmented with additional samples not used in the manual calibration.

The relationship between the calibration data and the free variables is established in Ceres Solver by the creation of residual blocks. The residual is defined as the difference between the estimated value of wp and the value of wp calculated by (8). The Ceres Solver then iteratively solves for the values of wp and robotPose that minimize the sum of the squares of all the residuals defined by the residual blocks. Ceres can also make use of a loss function, which can be used to minimize the effect of outliers. When the loss function is $\rho(x) = x$, Ceres minimizes the mean squared error of the residuals. The encapsulation of the residual computation in the residual blocks also allows Ceres to automatically compute the partial derivatives of the modeling equations. This eliminates a potential source of user error.

This problem bears a close similarity to the three-dimensional (3D) simultaneous, robot-world, hand-eye calibration discussed in [170][215][226]. The camera calibration problem is typically expressed as AX = ZB, where X is the 3D pose representing the camera offset and Z is the 3D pose representing the location of the calibration target. It is easy to see that (8) can be manipulated into this form. Both X and Z are unknowns that must be solved simultaneously. Closed-form solutions [226][227] have been proposed to solve for these values and one recent version will be discussed in section 6.2.3. The principle difference between the different solutions is how they resolve the weighting between the positional and rotational components [7] of the residual that defines the 'best' solution to the problem. Given the 2D nature of the current problem, it is probable that a closed-form solution to the problem can be formulated. However, since the calibration parameters do not need to be computed in real time, the iterative solution implemented with Ceres Solver is sufficient. The iterative solution method is also easily adapted to solve for other calibration constants, some of which may not be solvable with a closed-form solution.

More data is generally better data. Unlike the manual calibration approach, the iterative minimization approach can use additional data to minimize the effects of measurement noise. However, care must be taken to provide a suitably rich set of input data. For example, if all the samples were taken at different positions around the workspace, but with the same orientation, it is not possible to determine the orientation offset of the manipulator base. The iterative solution would either not converge, or would converge to an unstable value.

Care must also be taken in the construction of the system model used for iterative minimization. If two or more of the free variables are correlated, the model will be under constrained, and may not be able to converge to an answer. A high degree of correlation between variables can also lead to a high degree of sensitivity to the input data.

A subsequent calibration of the base offset, using all of the collected data, was performed using Ceres Solver. Testing of the manipulator base calibration was performed using an automated test program and the RMMA. A program was set up to drive the AGV to ten different positions around

the RMMA as shown in Figure 69. At each docking location, the position of the AGV, the world coordinate of the reflector, and the manipulator base offset were used to compute the robot coordinates of the reflectors using (8). After positioning the sensor, a search was performed to determine how far off the position calculation was.

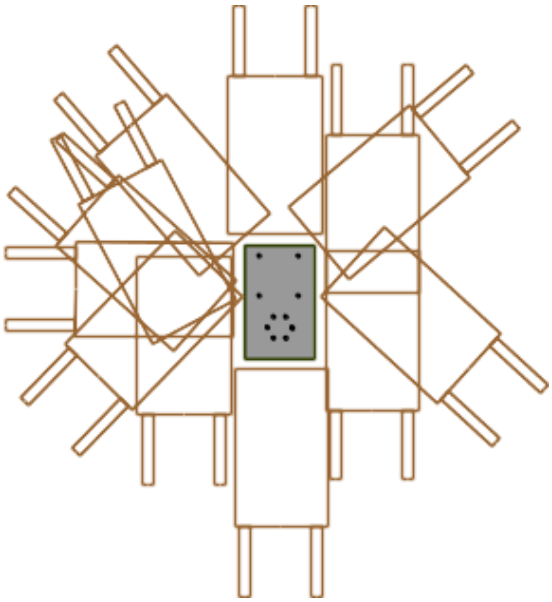

Figure 68. Position and orientation of AGV relative to the RMMA from manually collected calibration data.

Ideally, it should be possible to move the manipulator directly to the reflector based on the position of the AGV. Unfortunately, noise and systematic errors in the AGV position data prevent this. Figure 70 shows a plot of consecutive samples of the AGV's *x*-axis position as the AGV sits motionless. The graph also shows a plot of the average value of samples 1 through n. This shows roughly how many samples need to average together to produce a reasonably stable position value. The *y* position and the orientation angle exhibit similar noise. The AGV position data is available at about 16 Hz, so it requires about 6.25 seconds to collect 100 samples. In this 2D case a simple average of the orientation angles is sufficient. In the general case of 3D orientations, greater care needs to be observed in averaging the orientation [228][229]. In addition to the random noise, tests also indicate that there are some systematic biases in the AGV position data depending on the location of the AGV.

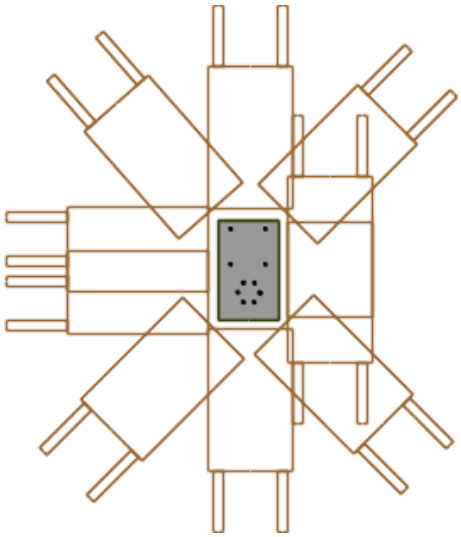

Figure 69. Docking locations used for automated data collection and system evaluation.

The goal is to be able to align the manipulator with the workspace in the minimum amount of time. The ideal situation is to be able to perform the insertion task immediately on arrival at the workstation. However, in this case it is necessary to compensate for the unavoidable measurement errors. It becomes a tradeoff between time spent averaging the position data to produce a stable value vs. time spent searching for registration points in the workspace.

The manual calibration method generated a base offset of (x = 831.5, y = - 7.5) mm and a rotation of 90.6°, yielding a mean square error of 1.25 mm and a maximum residual of 6.3 mm. The Ceres Solver came up with an offset of (x =833.6, y = -8.2) mm and a rotation of 90.53°, yielding a mean square error of 1.19 mm and a maximum residual (cost function) of 10.7 mm. The Ceres Solver was seeded with a variety of initial conditions, including setting all the variable parameters to 0, and had no problems with convergence. The resulting offset positions agreed with each other within 0.1 mm.

The main issues that were observed are that the model cannot be either over or under constrained if Ceres Solver is to converge properly. Using Ceres Solver, the base offset was computed for the manipulator mounted on a mobile base despite the fact that the location of the vehicle origin was not directly measurable. Using the computed offset and the location of the AGV, we were able to position the manipulator end effector within a few millimeters of the target regardless of the position and orientation of the AGV. While perfect initial positioning was not possible, the search time required to achieve the desired alignment accuracy was greatly reduced by improving the initial positioning of the manipulator.

The limiting factors in being able to accurately position the end effector are the noise and systematic errors in the AGV navigation sensor. This affects both the final position calculation and the accuracy of the manipulator base transform. The AGV position errors in the measurement used to compute the base offset affect the quality of the solution derived. The quality of the solution can be assessed by examining the residuals left after the model has converged to a solution for the free

parameters. Large residuals indicate corresponding errors in the calibration data, either random or systematic.

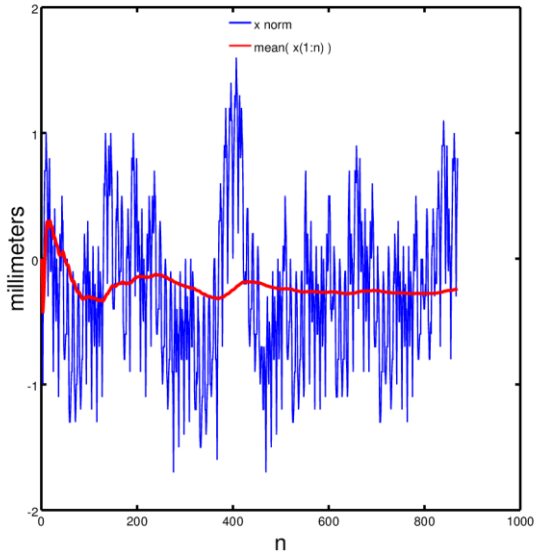

Figure 70. (blue) AGV position along x-axis, normalized to the first sample, x(1); (red) the mean of the normalized x value from x(1) to x(n).

5.3.3. Closed-Form Solutions

Shah, et al. describe in [230] closed form solutions for the offset between the manipulator base and the AGV by constructing a robot-world/hand-eye calibration problem AX = YB. This thesis author worked with Shah in [230] and provided performance measurements and data to support the development of the calibration solutions by Shah. The developments in this section provide preliminary theoretical basis to section 6.3 Propagation of Uncertainty for mobile manipulators. The approaches presented in the paper were novel since the data provided was missing certain orientational data and the problem was reduced to just two dimensions. The methods were applied to data collected in a laboratory setting and compared to iterative solutions.

Mobile manipulators often use intelligent sensing systems that measure the pose of a given object. These measurements are calculated with respect to the system's own coordinate frame. Therefore, techniques are needed to transform the measurements into a common world coordinate frame.

To gain an understanding of the problem, consider the mobile manipulator setup shown in Figure 1 b. A navigation system computes the 2D pose of the AGV in world coordinates with a Nav sensor that detects the locations of reflectors strategically placed throughout a given work area. Then the AGV pose is calculated based on the angle and range of the Nav sensor to each of the reflectors within its field-of-view, since the positions of the reflectors are known a priori. In addition, the 2D position of a target can be calculated with respect to the manipulator's own coordinate system. However, since the manipulator is placed on top of the AGV, its coordinate frame moves as the AGV moves. As a result, it would be beneficial to know the target location with respect to a

stationary world coordinate frame. In order to compute this location, the transformation from the AGV to the robotic manipulator must be found which was the goal for [230].

These types of problems are often represented as a robot-world/hand-eye calibration problem and are mathematically formulated as $A_iX = YB_i$ where A_i and B_i are known homogeneous matrices calculated at time-step $i = 1; 2; \ldots ; n$, while X and Y are the unknown homogeneous matrices. For this work

Ai = inverse of the AGV pose in world coordinates

Bi = target pose in robotic manipulator coordinates

X = target pose in world coordinates

Y = transformation from AGV to robotic manipulator.

Here homogeneous matrices are of the form $\begin{pmatrix} R & t \\ 0 & 1 \end{pmatrix}$ where orientation is represented by the rotation matrix R and position is represented as the vector t. Using this representation, the robot-world/hand-eye calibration problem can be posed as

$$\begin{pmatrix} R_{A_i} & t_{A_i} \\ 0 & 1 \end{pmatrix} \begin{pmatrix} R_X & t_X \\ 0 & 1 \end{pmatrix} = \begin{pmatrix} R_Y & t_Y \\ 0 & 1 \end{pmatrix} \begin{pmatrix} R_{B_i} & t_{B_i} \\ 0 & 1 \end{pmatrix}, \quad (9)$$

which can be split into its orientational component

$$R_{Ai}R_X = R_YR_{Bi} \quad (10)$$

and positional component

$$R_{Ai}t_X + t_{Ai} = R_Yt_{Bi} + t_Y. \quad (11)$$

Closed form solutions in [230] describe separable solutions which first solve for the orientational component and use that information to solve for the positional component [227][231]. Therefore, [230] focused on the latter separable solution form. However, due to the single point laser retroreflector that was used, the orientational information R_{Bi} are not computed, $R_{Ai} = \begin{pmatrix} \cos\theta_i & \sin\theta_i \\ -\sin\theta_i & \cos\theta_i \end{pmatrix}$ consist of only the heading angles θ_i, and the positional information t_{Ai}, t_{Bi} are only in two-dimensions. Therefore, current closed form solutions are not applicable and force the novel closed form solution as in [230] where only the target locations in world coordinates (t_X) and the sensor calibration (R_Y; t_Y) are needed.

The algorithms were applied to data gathered in a laboratory setting where the AGV was moved to ten stops as described in section 6.2.3.3 through 6.2.3.7. However, in this case, the manipulator tried to only reach the four bisect-reflectors. The 2D position of each of the bisect-reflectors reached by the manipulator was recorded, as well as the 2D pose of the AGV. From this data, the location of each of the bisect-reflectors in the world coordinate system was calculated and compared with the iterative solution presented in [232]. The maximum uncertainties of distances

between successive targets was calculated to be 0.09 mm for the iterative solution and 0.04 mm for the closed form solution.

5.4. Conclusions

As with mobile bases, manipulators today are readily available with relatively low uncertainty with respect to mobile bases. Performance measurement for robot arms has been standardized in ISO 9283:1998 Manipulating industrial robots -- Performance criteria and related test methods [44]. A SysML internal block diagram was developed to include the robot arm controller, manipulator controller-offboard, as used for this thesis research, and robot arm. The model shows the interconnections and information that is passed between the components, as well as an approximated manipulator base constraint as compared to the mounting upon the mobile base. Additionally, an EOAT is modeled with constraint within the bounds of the manufacturers specification for the chosen manipulator. A dependency is therefore on the AGV constraint that is approximated at less than 4 mm in X and Y and a rotation constraint of less than 0.1°. These are, of course, approximated since the model is generic to apply to any manipulator. Tests were described in another SysML internal block diagram which further describes, not only the model for verifying the manipulator uncertainty on a fixed base, but also the manipulator-to-mobile base adjustment determination from the previous model.

Beginning with the manipulator performance measurement, first a rough measurement using relatively large fiducial reflectors (2 mm diameter) as compared to the manipulator demonstrated the basic test technique. As expected, the manipulator detected every fiducial. Since fiducial reflectors could only be measured down to 0.8 mm, a more precise measurement method using the OTS was then used to measure the manipulator moving through the same square pattern. Results showed point spreads of approximately 0.6 mm, i.e., within the manufacturer specified ± 1 mm repeatability. However, there was drift in measurements of between approximately 0.1 mm and 0.35 mm. Additionally, angular misalignment of the manipulator base as compared to the AGV was expected, although all angles were expected to be close in comparison to one another. The angular offset to the AGV varied from 1.28° to 2.18° over 15 measurements at each location. When the associated pose offset angles are applied to the translational measurements, offset error from the 457.2 mm square was between 0.32 and 4.67 mm.

Three indirect test methods were described for manipulator-to-mobile base adjustment determination, including a manual calibration method, a calibration method using Ceres Solver, and a closed-form vs. iterative solution method. The manual calibration method provided an approximation method to align the vehicle so that effects of the base offset parameters were cancelled out. With remaining interactions between calibration variables, the variables could not be eliminated. Alternatively, the Ceres Solver method proved to be a valuable tool in calibrating a variety of hard to measure constants. It provides an easy to use framework for solving difficult non-linear problems iteratively. The main issues that were observed are that the model cannot be either over or under constrained if Ceres Solver is to converge properly and that some alignment errors remained where offset terms did not completely cancel out. The manual calibration method generated a base offset of (x = 831.5, y = - 7.5) mm and a rotation of 90.6°, yielding a mean square

error of 1.25 mm and a maximum residual of 6.3 mm. The Ceres Solver came up with an offset of (x =833.637, y = -8.22) mm and a rotation of 90.53°, yielding a mean square error of 1.19 mm and a maximum residual (cost function) of 10.7 mm.

Lastly, Shah used data collected from this thesis research and developed closed-form solutions for the offset between the manipulator base and the AGV by constructing a robot-world/hand-eye calibration problem AX = YB. The research was described here to be thorough and the maximum uncertainties of distances between successive targets was calculated to be 0.09 mm for the iterative solution and 0.04 mm for the closed form solution.

6. MOBILE MANIPULATOR PERFORMANCE MEASUREMENT

Mobile manipulators (i.e., robot arms onboard mobile robotic bases) hold promise in industrial applications for flexible and reconfigurable automation and are now being marketed at industrial material handling exhibitions as useful tools [233][234]. "Mobile manipulators offer high mobility and manipulability. An ideal utilization of the motion redundancy in the mobile manipulator is to perform assembly tasks on a moving vehicle body while tracking." [5] Mobile base and onboard manipulator motion may or may not be known a priori for applications such as assembly or even welding. Other typical applications currently being considered for mobile manipulators are, for example: i) unloading trucks [12], ii) bagged-goods (e.g., dog food bags) handling, iii) conveyer loading/unloading, iv) picking canned and boxed goods from shelves in supermarkets, and v) delivering, placing, and manipulating semiconductor wafer pods within wafer fabrication facilities [210]. The first four applications have looser constraints on the mobile manipulator pose and do not require precise alignment with the workspace. Vision is integrated into these systems to position a vacuum gripper to pick up the box, bag, or metal can in the manipulator's workspace. However, the last application, wafer pod manipulation, and other assembly-type operations, (e.g., peg-in-hole), require a much less uncertain pose capability from the mobile manipulator.

Generalized measurement of mobile manipulators performing routine tasks (e.g., moving to different poses and generating motion profiles) has been relatively non-existent except for simply ensuring that the task is more or less completed. Prior to industrial acceptance for mobile manipulators, just as with their base components of industrial robot arms and AGVs, these new mobile manipulator systems require their manufacturers to have real, verifiable performance data so users can apply these technologies appropriately.

Measurement of the robot's Cartesian pose, which is combined with the mobile base's pose, is complex since the system can include nine or more degrees of freedom. To simplify measurement, the RMMA concept, as detailed in section 3.3.2, was designed to allow various geometric patterns to be traced by the robot wielding a non-contact, tool point sensor (laser retroreflector) to sense the dimensional points along the patterns.

6.1. Models

The mobile manipulator performance measurement concept was designed to use the RMMA metrology artifact as ground truth. The concept is compared to the OTS as modeled in Figure 1 (a). [160] In the figure, the Mobile Manipulator shows that the Manipulator is referenced to the Mobile Base using a dashed arrow pointing to the Mobile Base. Similarly, the Mobile Manipulator is referenced to the OTS, as well as the RMMA. Also, the RMMA is referenced to the OTS which shows that the initial measurements of the RMMA and Mobile Manipulator are both referenced to the OTS. A GPS Antenna is also shown to provide reference timestamp to the Mobile Manipulator computers during tests. Within the RMMA are two bisect-reflectors within the patterns and one or more fiducial-reflectors that make up patterns. Reflector types are detailed in section 3.3.2.2 and Figure 23.

Up to this point, the mobile manipulator system and the measurement systems have been modeled, mainly as individual components. Generic models are therefore needed to show how these systems are combined into the mobile manipulator and how the concept of using the RMMA fits into the performance measurement process of mobile manipulators. Two additional models beyond the mobile manipulator system are therefore, needed to explain the measurement concept: 1) an activity diagram that shows activity flow that occurs during performance measurement, and 2) a sequence diagram to show the sequence of events that occurs during the measurements. These serve as the generic control algorithm for the mobile base and onboard manipulator.

The SysML activity diagram shown in Figure 71 begins with the Start performance test in the upper left and flows through activities to the Stop performance test in the lower right. Upon Start, the base (AGV) is commanded to begin the performance measurement test. The base moves to the first pose at the artifact. If the move is incomplete, the base continues to move until it informs the manipulator that it has stopped at the RMMA. The manipulator then moves from stow to the initial registration position. Again, if the move is incomplete, the same manipulator moves until completed where the manipulator performs one of the registration types (search, bisect, or ARTag). Upon completion, the manipulator moves and aligns the laser retroreflector with assembly reflector (fiducial) until completion. The manipulator then stows and informs the base that it has stowed. If the AGV has not completed all ten poses (or any number the user prefers), it moves to the RMMA at the next pose and once again informs the manipulator the base has stopped at the RMMA. If the AGV has completed all ten poses, five each at circle and square patterns, the base returns to the home position and stops the test.

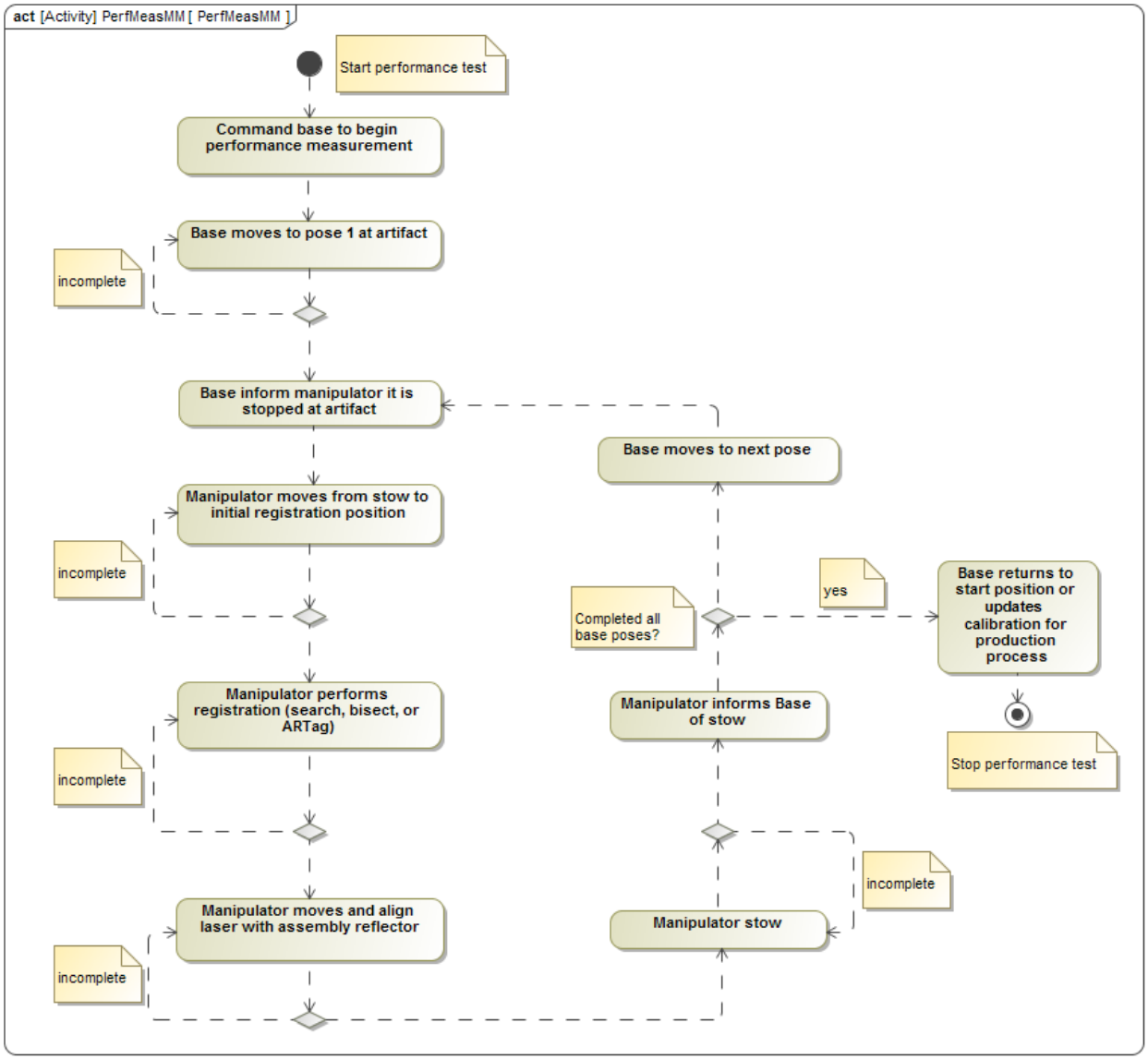

Figure 71. SysML activity diagram showing the flow of activities for mobile manipulator performance measurement.

The SysML sequence diagram of events shown in Figure 72 is read from top to bottom. The model shows eleven different sequential tasks beginning in the upper left by starting to measure using the optical tracking system. Next, the AGV offboard controller controls the AGV to begin movement towards the RMMA until it arrives and parks with a controlled pose at the artifact. Once parked, the AGV then informs the manipulator of the AGV arrival from the AGV onboard controller to the manipulator offboard controller. The manipulator is moved from the stow position and begins a registration process to the RMMA. Upon registration, the manipulator then traverses through the set of fiducials associated with the pattern closest to the AGV parked pose. After traversal, the manipulator returns to the stow position, informs the AGV of the stow and that it's safe for the AGV to again begin motion. The AGV transport structure (control program) is incremented to the

next pose and repeats until all ten poses have been completed. Upon completion, the optical tracking system stops tracking the mobile manipulator motion. The entire process combines both measurement systems as an experimental comparison of the two methods. Ideally, only one method would be used. For example, if only the OTS is used, the mobile manipulator may be programmed to move through a similar process as described although no registration to the artifact would be required. If only the artifact is used, no start and stop tracking of the OTS would be required.

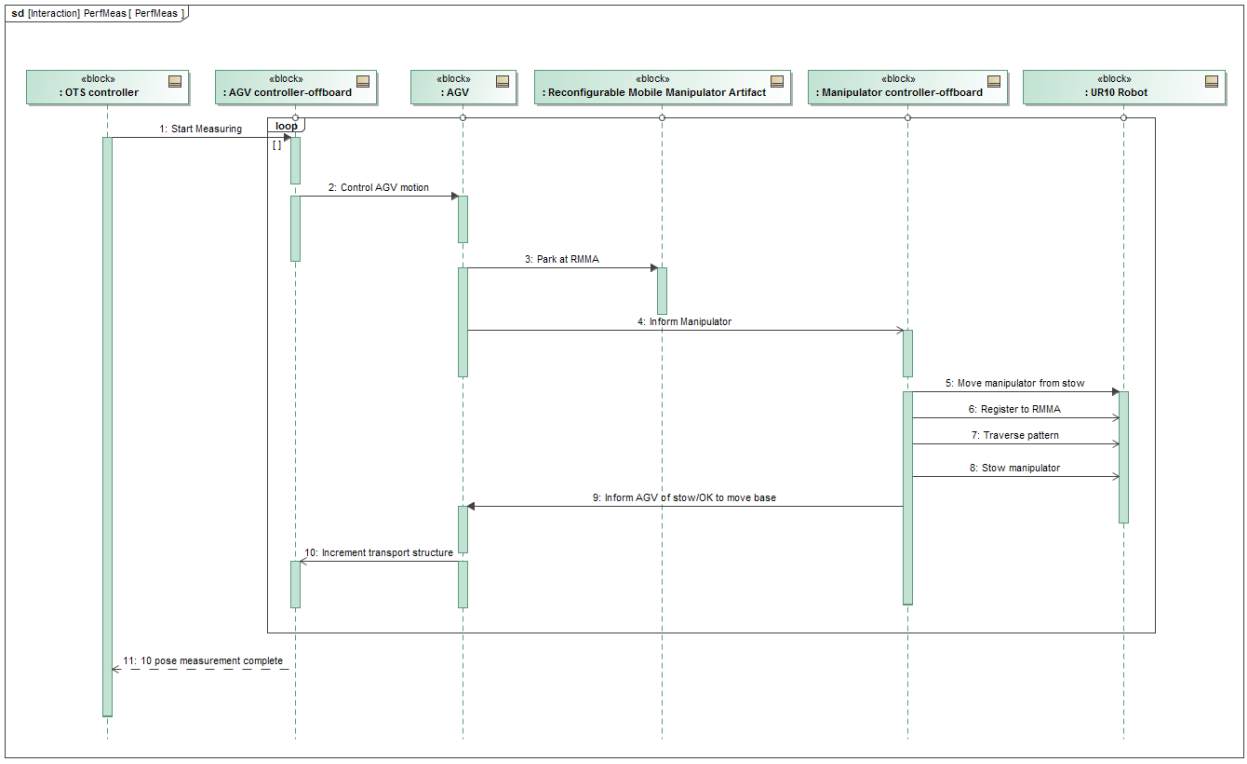

Figure 72. SysML sequence diagram of mobile manipulator performance measurement using the RMMA.

The concept includes positioning a mobile manipulator next to an artifact, as well as posing the EOAT attached to the manipulator at specific locations above an artifact to digitally detect fiducials with known uncertainty. The performance metrics leading to evaluation criteria include the:

- Time to register the mobile manipulator to the artifact
- Time to move from the registration points to the assembly points
- Repeatability after registration
- Detection of reflectors with varying diameters
- Number of search steps equating to the initial distance from registration/assembly points

6.2. Methods

Mobile manipulator system performance measurement must again first consider independent mobile base and manipulator criteria as will be described in the following sections. Section 6.2.1 describes three manipulator base positioning methods provided by the mobile base. Once the manipulator is positioned, it requires registration to the assembly area. Section 6.2.2 describes three mobile manipulator registration methods. Experiments to then measure system performance follows in section 6.2.3 and provide results for the AGV and onboard robot arm chosen.

6.2.1. Manipulator Base Positioning

This section considers manipulator base positioning by the mobile base using three methods: static, index, and dynamic. Manipulator positioning is based on the manufacturing requirements of the mobile manipulator and therefore, the mobile manipulator performance measurements follow the same consideration. For example, can the mobile manipulator reach the entire assembly from one docked location, or must it reposition to reach the entire assembly, or can it even continue moving while assembling? Here, "docking" refers to free-form or fixtureless posing in a commanded location near an apparatus to perform an assembly task. Static means that the mobile manipulator was programmed to move to the RMMA, park the base, move the manipulator throughout a measurement pattern on the RMMA, and then return to a home position. This is the case where the manipulator can reach all assembly points from a single location. A brief description of the AGV and manipulator control is described in section 6.2.1.1.

Index manipulator base positioning is when the manipulator cannot reach all assembly points, requiring the mobile base to move and park at one or more additional locations and poses. Static manipulator positioning allows mobile manipulator system uncertainty to occur at a single location where the mobile base is measured once. This would be similar to current AGV operations where most vehicle docking occurs at a location and when approached from the same direction. Indexed manipulator positioning is an extension of static, although complicates the mobile base and manipulator pose by approaching various docking locations from different directions. For this thesis research, static was initially researched followed by the more complex index method as static positioning was considered one aspect of indexing (i.e., one of many mobile base dock poses). A description of the AGV and manipulator control is described in section 6.2.1.2.

Dynamic manipulator base positioning is when both the mobile base and the manipulator simultaneously move to perform a task, such as assembly. Dynamic mobile manipulator performance may be useful on relatively long assembly or other tasks, such as in automotive assembly line tracking [1] or rivoting aircraft [235]. There are many fewer current applications for dynamic manipulator positioning as there are for static and index manipulator positioning as evidenced by the references in section 7. Nevertheless, consideration for the few applications is considered in this thesis in the form of artifact development and parallel grant efforts briefly described here and in section 7.2.2.

It is expected that future mobile manipulators and their applications will require dynamic manipulator base positioning. Hence, the author designed, had machined, and assembled an RMMA (numbered as RMMA-2) that will be used for measuring performance of dynamic mobile

manipulators used for assembly tasks. As this has been completed, it is described here. Additionally, as further briefed in section 7.2 Beyond This thesis and specifically in section 7.2.2, the author recommended providing a university grant to both, transfer this thesis effort and to develop in parallel the dynamic performance measurement methodology. Figure 73 (a and b) shows CAD models of the RMMA-2 in horizontal and vertical configurations. Figure 73 (c) shows the 3.7 m (145 in) long x 1 m (40 in) wide RMMA-2, tilted from horizontal using two pistons, near the RMMA-1. The same types of height and rotation are evident in the RMMA-2 as in RMMA-1. However, RMMA-2 is a modular artifact structure that also includes convex and concave fiducial measurement so that the manipulator is measured throughout even more complex configurations. The RMMA-2 could also be used for static and index mobile manipulator performance measurement.

a b

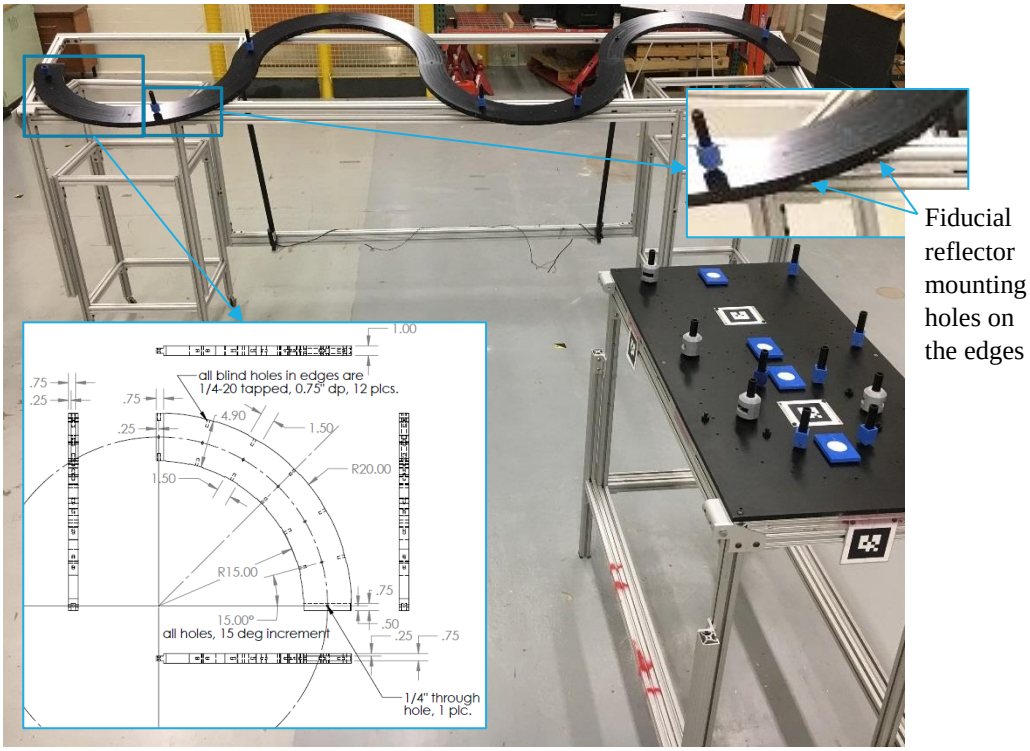

c

Figure 73. CAD models of the RMMA-2 shown in the (a) vertical and (b) horizontal configurations. (c) Manufactured RMMA-2 shown in an approximately 20^0 tilted configuration and near the RMMA-1 (foreground – right). The inset shows the CAD drawing of each module of the RMMA-2.

The following two subsections describe the static and index control methods. The concept utilized the RMMA, as modeled and shown in Figure 1, that can provide a desired measurement uncertainty as a comparison to ground truth (i.e., OTS). With the RMMA, manipulator pose is measured as a digital detect or no detect at a specified distance and angle from the task point. For our tests, detector distance above the reflector was approximately 127 mm. The distance would be representative of a programmed waypoint above and in-line with the next robot task point to grip or insert a part or perform another task. The desired uncertainty may be, for example, a part insertion alignment tolerance required for a manufacturing assembly process. Moving along this grip/insertion line, at the aligned pose to the task point, also provides some knowledge of insertion performance (i.e., if the task point is continuously detected along the grip/insertion line) although this measurement is for future research.

6.2.1.1. Static Control

For the static manipulator base positioning method, the AGV was programmed to move to the registration pose next to the RMMA square pattern of reflector fiducials from an initial "home" position, thus incurring some pose error at the registration point as described in section 4.4. As expected, results varied when testing the vehicle stop points before and after calibration. Once at the registration point, a beam break sensor attached to the AGV signaled the manipulator to initiate the manipulator control algorithm.

The manipulator moved to the first pose and began a spiral pattern. Once the reflector was detected, the position of the reflector was recorded and the manipulator moved to the second pose based on the pre-taught nominal distance offset and orientation. Again, a spiral search was initiated repeating the process. After all four reflectors were detected, the process repeated 32 more times recording uncertainty and repeatability measurements. The AGV then moved back to its home position, and the process repeated.

6.2.1.2. Index Control

The index manipulator base positioning method expands on the static method and was therefore used for all follow-on experiments. Communication between the AGV controller and the offboard manipulator controller allowed the removal of external vehicle position sensing that was initially used for the static method. The communication strategy allowed much more flexibility of mobile base poses whereas the laser line sensors required additional hardware (i.e., beam break sensor) and setup, as well as limited some AGV poses relative to the RMMA due to sensor positioning.

This section first describes the mobile base control and manipulator control algorithms. Experiments are then described that utilize both search registration methods: fine search and bisect with fine search. Following is a section that describes a published data set from the index/bisect with fine search methods.

Mobile Base Control

Computer aided design (CAD) was used for the AGV navigation paths and docking poses. The Kollmorgen NDC8 [194] Layout Designer Application Program was used to design the CAD model shown in Figure 74 (a). Figure 74 (b) shows a table of AGV stop locations corresponding to the CAD model, the point number corresponding to the transport structure point, and the vehicle orientation at each stop point (with reference frame shown above the table). A Transport Structure program, shown in Figure 75, was designed using the NDC8 Systems Application Designer Program and used to control the AGV to the 10 poses shown in Figure 76. The Transport Structure was designed to alternate between poses near the circle and the square patterns of fiducials. Poses 1 and 10 docked at the end of the RMMA, poses 2, 5, 7 and 8 docked at 45° to each of the RMMA corners, poses 3 and 4 docked perpendicular to the RMMA, and the remaining poses, 6 and 9, docked parallel to the RMMA. The AGV segments were programmed to allow the AGV to navigate to each of the docking poses at stop points through an elaborate network of paths designed to demonstrate a factory environment where AGVs can have long distances between each docking location. Stop points and segments are referenced to facility-mounted reflectors that correspond to a random X, Y reference point, in fact located just outside the lab and to the lower left corner of the CAD model drawing shown in Figure 74 (a).

The AGV logs data from the Vehicle Diagnostics Application with timestamping shown in Unix epoch format - 1488990089.9447 - (i.e., the number of seconds that have elapsed since 00:00:00 Coordinated Universal Time (UTC), January 1, 1970, not counting leap seconds in local time). A sample of the AGV logged data is shown here:

set 1488990089.9447 0 0.0285 0 0.0182 0 0.0182

which corresponds to the manipulator control data log shown in Figure 79. [247] This time is when the robot initially moves from the stow position to the first bisect reflector; i.e., marker -1. The remaining numbers show AGV pose at that time (i.e., X, Y, Θ). A correspondence to the timestamp will also be shown in section 6.2.3.9.

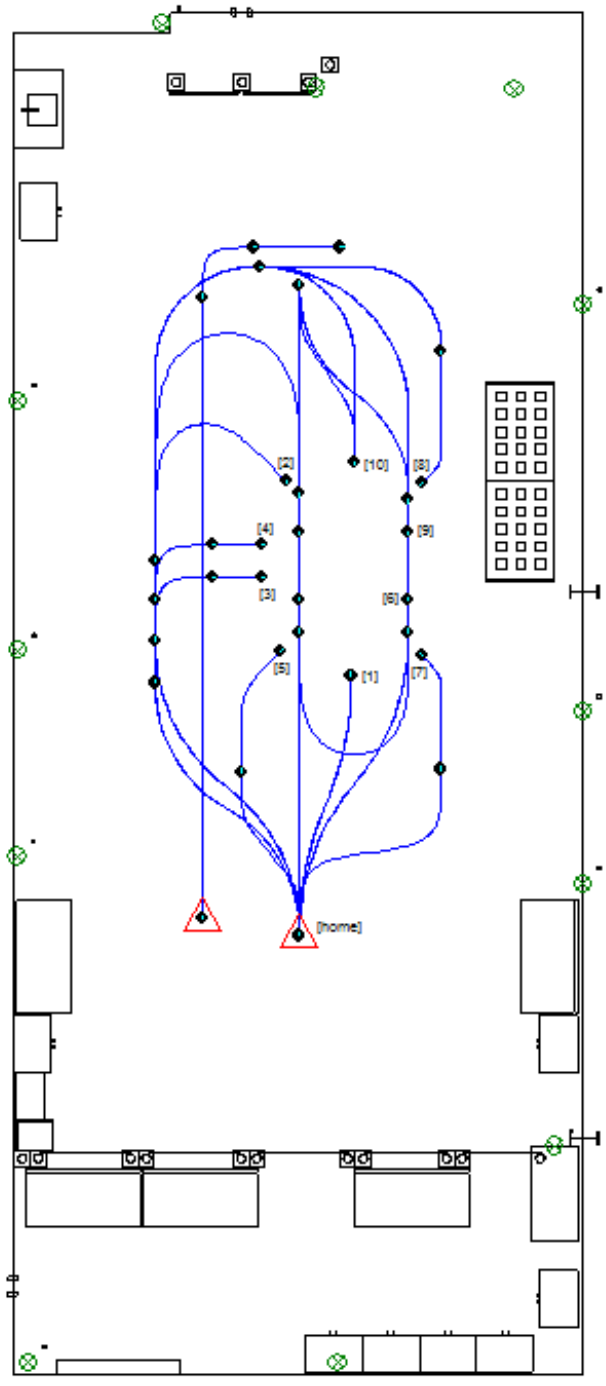

a

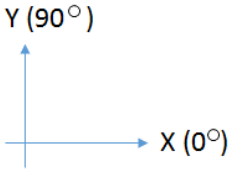

stop location	point #	vehicle orientation
home	320	90°
1	326	90°
2	346	315°
3	368	0°
4	333	0°
5	382	45°
6	328	90°
7	344	135°
8	390	225°
9	374	270°
10	370	270°
home	320	90°

b

Figure 74. (a) CAD model of the AGV segments (paths) (blue lines) and stop points (black dots on paths), and approximate locations of AGV wall-mounted reflectors (green circles with X's) used for navigation. (b) AGV stop locations corresponding to the CAD model, point numbers corresponding to the transport structure point, and vehicle orientations at each stop location (with reference frame above the table). The left straight-to-right turn path beginning at the unmarked home triangle was not used for these tests.

&Local Parameter	Value		Remark
&COUNT	0		
&TO	123		
&target	0		
320	0		home position
326	0		circle location
&target	2		signal that we have arrived at a target and have data
target	0		wait here till robot changes target to 0
346	0		square location
&target	1		signal that we have arrived at a target and have data
target	0		wait here till robot changes target to 0
368	0		circle location
&target	2		signal that we have arrived at a target and have data
target	0		wait here till robot changes target to 0
333	0		square location
&target	1		signal that we have arrived at a target and have data
target	0		wait here till robot changes target to 0
382	0		circle location
&target	2		signal that we have arrived at a target and have data
target	0		wait here till robot changes target to 0
328	0		square location
&target	1		signal that we have arrived at a target and have data
target	0		wait here till robot changes target to 0
344	0		circle location
&target	2		signal that we have arrived at a target and have data
target	0		wait here till robot changes target to 0
390	0		square location
&target	1		signal that we have arrived at a target and have data
target	0		wait here till robot changes target to 0
374	0		circle location
&target	2		signal that we have arrived at a target and have data
target	0		wait here till robot changes target to 0
370	0		square location
&target	1		signal that we have arrived at a target and have data
target	0		wait here till robot changes target to 0
320	0		home position
&COUNT	1		increment count and loop back to start
320	0		

Figure 75. Transport Structure program designed using NDC8 Systems Application Designer Program and used to control the AGV to the 10 poses shown in Figure 76 and along the segments and to stop points shown in Figure 74 (a).

1

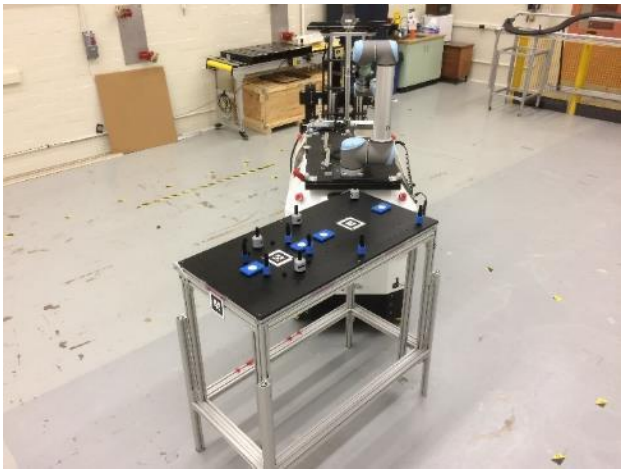

2

3

4

5

6

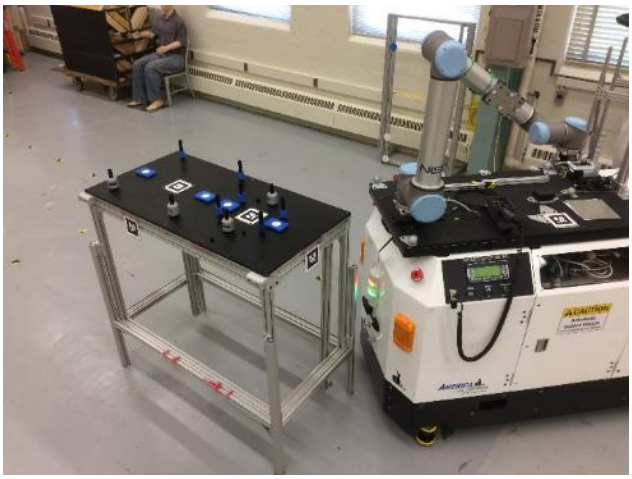

7

8

9

10

Figure 76. Ten different AGV poses for testing mobile manipulator performance.

Figure 77 shows a series of photos (shown left to right) of one example of the large motions that the AGV was programmed to perform prior to docking with the RMMA. In this example showing one of the ten navigation paths, the vehicle moved from the home position to pose #2. AGV motions in this example and other paths included: crab and Ackerman steering; relatively long distance, straight line; and in this case a turn of 135^0 where some turns were up to 180^0.

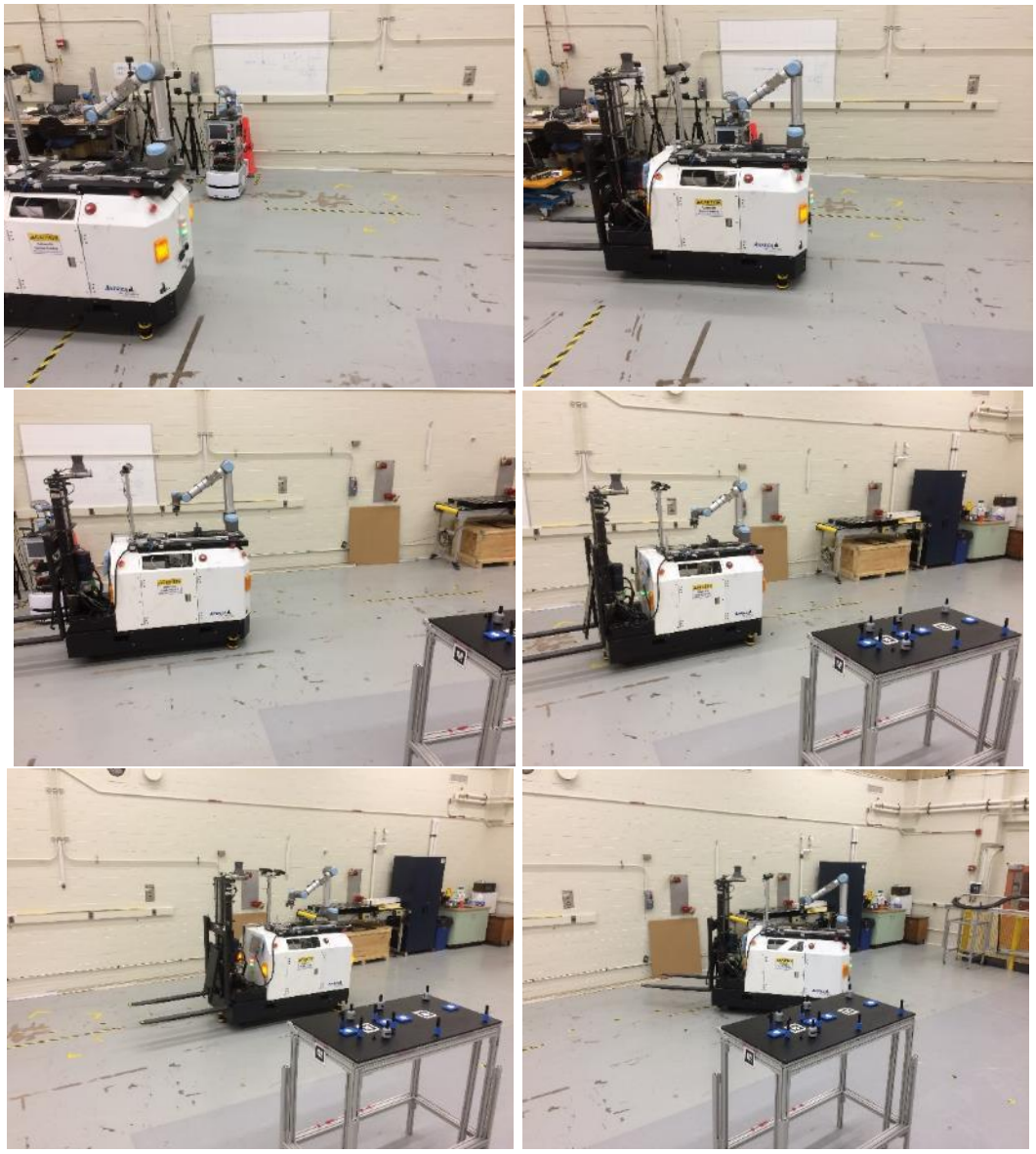

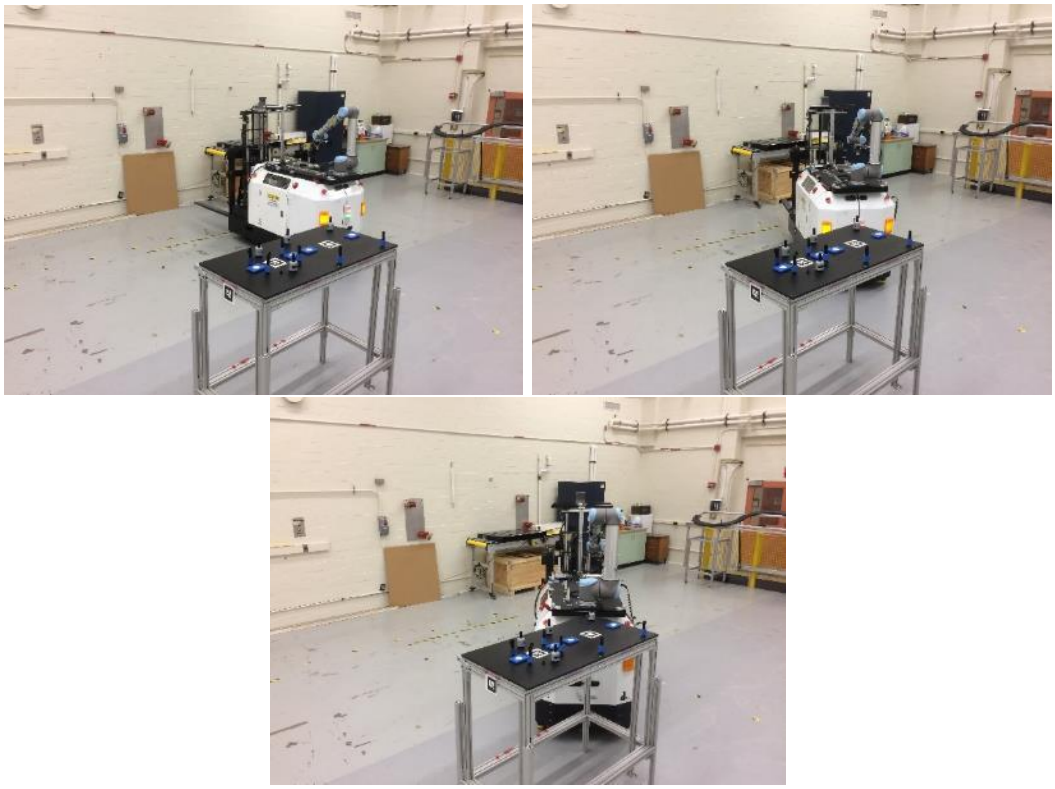

Figure 77. Example of the large motions that the AGV was programmed to perform (view left to right and top to bottom), in this case moving from the home position to docking with the RMMA at pose #2.

Manipulator Control

The Mobile Manipulator program, discussed in [171][172], controlled the manipulator during the tests. The author of this thesis teamed with a robot control expert and guided by the author to write a C++ program to control the manipulator. The program interfaced with the AGV directly to obtain the current AGV pose, and it interfaced with the AGV control program (Transport Structure) running on the Order Manager application to coordinate the motion of the arm with the motion of the AGV. The AGV control program signaled the Mobile Manipulator program when it arrived at one of the stop or test locations. The AGV control program also sent the identification number of the test location. The Mobile Manipulator program read the current AGV pose and used it to compute the initial search location of the two registration reflectors in the target pattern (circle or square). Additional patterns could also have been used in the Mobile Manipulator program.

Figure 78 shows an internal block diagram of the algorithms, shown through SysML model dependencies, that control the manipulator during mobile manipulator performance measurements. On the lower right are one hardware part (CVC600), where 'part' is a SysML term that equates here to 'component', and two software parts from the AGV (System Manager Run and CWay). However, for this early discussion, the manipulator is dependent upon the System Manager Run program informing the manipulator of the AGV pose when parked at the RMMA.

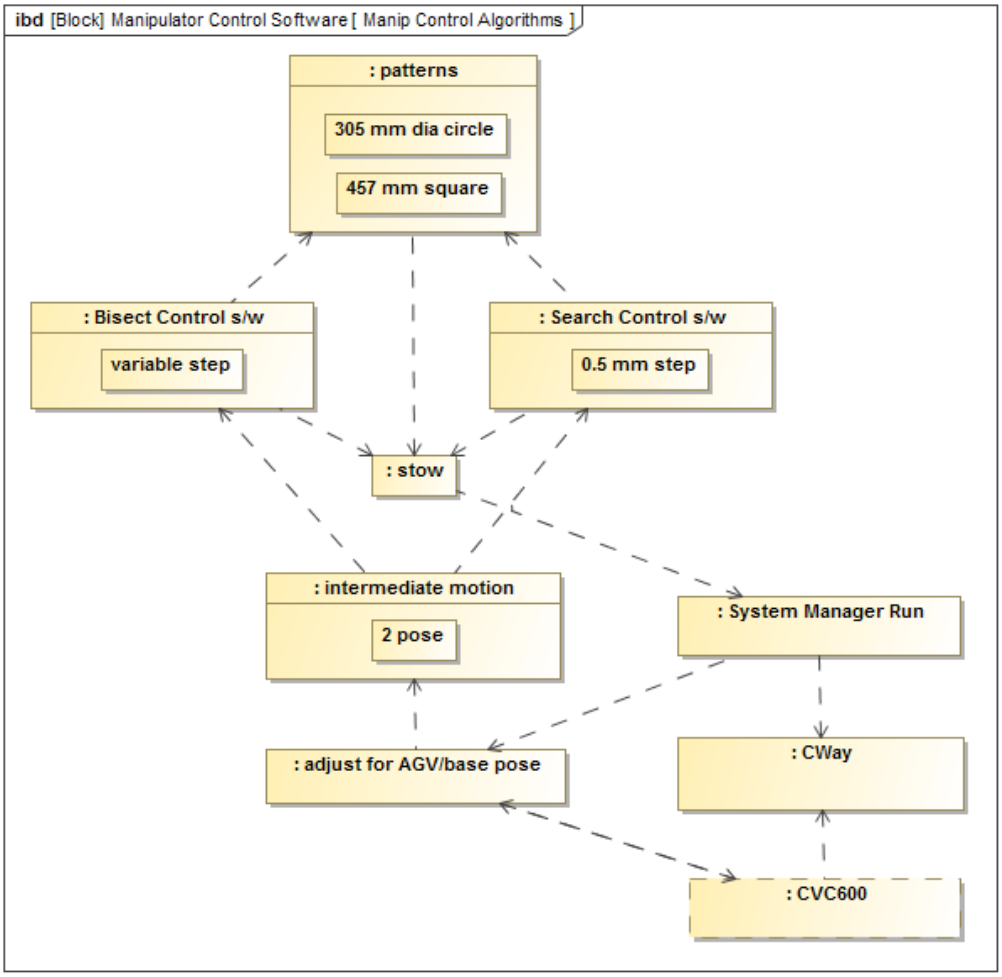

Figure 78. SysML internal block diagrams of the control software components.

The manipulator was first moved from a stowed location over the body of the AGV to a staging location directly in front of the AGV. The manipulator was then moved from the staging location to the first of the two registration reflectors. The staging location was chosen so that the manipulator could make a straight-line motion from the staging location to a registration reflector located in front of, or to either side of, the AGV without colliding with its shoulder joint. After moving to the first registration reflector, the manipulator performed a square spiral search to determine the exact location of the reflector. When it determined the location of the first registration reflector, the program repeated the process with the second registration reflector. When the locations of the two registration reflectors were determined, the program had sufficient information to compute the locations of the other fiducials in the square or circular patterns. For comparison to repeatability, the initial registration number of iterations count was logged and included in results.

A sample manipulator control log file is shown in Figure 79 and the corresponding OTS log file sample is shown in Figure 80. [247] When the AGV stops and the robot controller begins logging

data, the log file is produced and corresponds to the time when the manipulator begins moving from the stow position to the first bisect reflector (i.e., marker -1).

time	iter	marker	init_x	init_y	init_z	init_xrot	init_yrot	init_zrot	ok	time	steps	x	y	z	xrot	yrot	zrot	
8.959	0	-1	-6.85455	-768.837	328	180	0	90	1	27.8485	44	-17.681	-768.592	327.909	-179.999	-0.00476	89.996	
39.209	0	-2	-1.99696	-464.079	328	180	0	90	1	27.8012	44	-13.9864	-466.554	328.024	179.997	0.008815	89.9986	
67.972	0	0	-168.222	-615.709	328	180	0	90	78.187	1	8.80808	33	-167.274	-614.26	328.089	-180	0.012592	89.9948
78.19	0	1	137.503	-617.988	328.089	-180	0.012592	89.9948	113.058	1	33.2612	117	137.482	-620.425	327.953	-179.996	0.004393	89.9754
113.061	1	0	-167.265	-614.26	328.089	-180	0.012592	89.9948	114.665	1	0.000112	1	-167.318	-614.275	328.143	-179.999	0.021486	90.0102
114.667	1	1	-93.7501	-747.756	328.089	-180	0.012592	89.9948	119.067	1	3.20751	15	-93.1962	-746.887	328.142	179.999	0.026547	89.981
119.07	1	2	58.6187	-750.839	328.089	-180	0.012592	89.9948	120.269	1	0.000113	1	58.7203	-750.847	328.135	179.996	0.021242	89.9801
120.271	1	3	137.473	-620.425	328.089	-180	0.012592	89.9948	121.471	1	0.000101	1	137.48	-620.319	327.967	-179.991	-0.00579	89.9919
121.473	1	4	63.9577	-486.928	328.089	-180	0.012592	89.9948	122.674	1	0.000103	1	63.9949	-486.926	328.141	179.999	0.019586	89.9888
122.677	1	5	-88.4112	-483.846	328.089	-180	0.012592	89.9948	123.878	1	0.000203	1	-88.4738	-483.81	328.037	-180	-0.00159	90.0013

Figure 79. Example manipulator control log file and highlighted timestamped data line that corresponds with the AGV and OTS log files.

Within log file: "Take 2017-03-08 11.20.45 AM_truncated", see Figure 80, the timestamped data point: "44.95833" corresponds to the nearest timestamp to the manipulator control log data and AGV data.

5399	44.925	0.001055	-0.00147	0.001541	-1	-0.88665	1.95831	2.80056	0.000216	-1.02862	1.958421	2.746074
5400	44.93333	0.001059	-0.00145	0.001567	-1	-0.88664	1.958324	2.800544	0.000216	-1.0286	1.958442	2.746052
5401	44.94167	0.000861	-0.00143	0.001554	-1	-0.88659	1.958315	2.800521	0.000234	-1.02855	1.958451	2.746024
5402	44.95	0.00084	-0.00145	0.001587	-1	-0.88656	1.958323	2.800524	0.000238	-1.02852	1.95847	2.746034
5403	44.95833	0.000687	-0.0015	0.00159	-1	-0.88654	1.958299	2.800545	0.000247	-1.0285	1.958464	2.746066
5404	44.96667	0.000644	-0.00145	0.001613	-1	-0.88651	1.958284	2.800565	0.000252	-1.02847	1.958461	2.746073
5405	44.975	0.00144	-0.0016	0.001298	-1	-0.88637	1.958372	2.800542	0.00019	-1.02835	1.958372	2.746094
5406	44.98333	0.001533	-0.00163	0.001313	-1	-0.88633	1.958376	2.800533	0.000192	-1.02831	1.95837	2.746092

Take 2017-03-08 11.20.45 AM_Tru

Ready

Figure 80. Example OTS log file and highlighted timestamped data line that corresponds to the AGV and manipulator control log files.

Once the locations of all reflectors in the pattern were computed, the manipulator cycled through them a set number of times – randomly chosen to be 1 time for the circle and 2 times for square pattern. At each fiducial reflector, the laser retroreflector checked to see if the manipulator was aligned with the reflector. If the small reflector was not immediately detected, a search was performed. The distance between the initial position of the manipulator and the position at the end of the search were used to provide information on the accuracy of the mobile manipulator's position and the accuracy of the registration.

When the test was completed, the manipulator was moved to the staging location and then the stow location. When the manipulator was back in the stow location, the Mobile Manipulator program signaled to the AGV control program that it was clear to move.

The positions of the circle and square patterns of fiducials were recorded prior to performing the repeatability tests. The AGV was first moved to a location where it could reach both fiducial patterns. The current location and orientation of the AGV was recorded. The arm was repositioned manually until the sensor detected alignment with each of the "fid-refl-reducer" fiducials, and the manipulator position was recorded. This information, along with the manipulator base position

relative to the vehicle's coordinate system, allowed the correct manipulator coordinates for the index fiducials to be calculated for an arbitrary AGV location. This allowed the AGV to approach the target/work area from any direction and to compensate for variation in the AGV's stopping pose.

The calibration of the manipulator base location involved recording the position of one or more fiducials from a variety of locations. Both the AGV location and the manipulator coordinates of the fiducials were recorded. This data was processed using an iterative, non-linear model or Ceres Solver described in section 5.2.2 to find the best value of the base position and orientation. Experiments and experimental results are described in section 6.2.3.

6.2.2. Mobile Manipulator Registration

This section describes alternative methods for registering the mobile manipulator to the assembly area or workstation, or in this case the RMMA. Assembly is generally considered to be more complex when compared to other tasks such as machining or material handling. [236] Assembly operations performed by a mobile manipulator [237] require accurate registration to the workpiece. 'Registration' is viewed here as instrument (e.g., mobile manipulator) comparison to a workpiece (e.g., artifact), or sometimes called a workstation, and 'calibration' is viewed as instrument (e.g., camera) adjustment or output correlation of the instrument readings with its known accuracy. Calibration was described in section 5.2.2. These two terms are sometimes interchanged in the literature. Various registration methods have been researched, including:

- Quick Reference (QR) codes [258] combined with calibrated vision [1] - tracking error: under 20 mm, maximum errors: 45 mm at the largest camera-target distance.
- QR codes for mobile robot registration and end effector error [238] - maximum positional repeatability: 1.1 mm (one point) to 4.0 mm (multiple points).
- High-precision calibration - average errors based on the Tsai hand-eye calibration combined with a high-speed calibration - average errors: ± 0.1 mm and ± 0.1° - based on a combination of laser triangulation and image processing [68].
- Constrained manipulator endpoint to a single contact point while executing manipulator motion where manipulator joint angles are read to develop a calibration model [240].
- Touch probing using peg-in-hole and particle filter solutions [241][242].

This section describes three methods for registering mobile manipulators to a workpiece: two search methods and a method that builds upon [238] from Aalborg University where QR codes were used in combination with vision processing. Although the QR code method requires additional hardware and software, the method may be sufficient for registration and faster than searches alone. [243] As opposed to the methods listed above, the search methods are more closely related to the RMMA method to use a laser retroreflector as a non-contact alignment tool for performance measurement and can also be used for the registration process.

Beginning with the search methods and borrowed here from the assembly operation is that the robotic component mating process is achieved by means of search strategies. Additionally, assembly workcells most often consist of a robot performing a repetitive peg-in-hole insertion task,

although typically with positional uncertainties reduced by means of rigid fixturing. If the accuracy requirements of the task are low, then simple navigation of the base into the desired pose may be adequate for registering the mobile manipulator to the workpiece or work area. However, assuming the accuracy requirements are greater than the base accuracy, more information is required for a suitable transformation between the manipulator and workpiece coordinate systems. Robotic mating of components, i.e., peg-in-hole assembly, was summarized in [236] using three pertinent search methods: stochastic, spiral, and random. Examples from [236] of each method are shown in Figure 81.

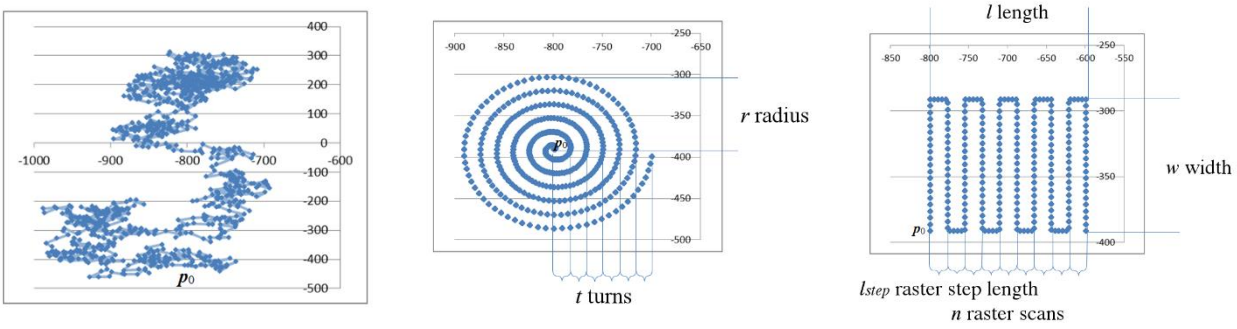

Figure 81. Generic, parameterized search strategies for peg-in-hole insertion include the walking stochastic search (A), the spiral search (B), and the raster search (C).

Stochastic search was summarized to add significant computational complexity, but results in generally good performance. Spiral searches are deterministic where they guarantee that the robot will find the peg insertion point provided that the hole lies within the search radius. This was also discovered during the static mobile manipulator experiment described in section 6.2.3.1. Random searches are typically used when the distance of the insertion point from the start search point is unknown and therefore, may explore a large region. As with the spiral search, raster searches are deterministic and guaranteed to succeed with the same criteria that the insertion point lies in the path of the raster or if the raster lines are too far apart. Based on this information, spiral searches (termed in this thesis as Fine Search Methods) were chosen as the best mobile manipulator method for registration using the laser retroreflector, considered as a non-contact alignment mechanism (e.g., a peg) to the insertion point (e.g., a hole).

Two types of Fine Search methods were also tested: circular and square searches. Circular spiral searches, like that shown in Figure 81 (b), are perhaps what is typically thought of when the term is mentioned. However, this type of search has limitations due to step size within the spiral. An alternative to the circular spiral method is a square spiral method that was implemented to solve the circular spiral issues. The square search, shown in Figure 82, perhaps combines the spiral and raster scan search methods by not only moving along straight, search lines but also stepping between the search lines. Figure 82 (a) shows the numbered steps of the search and Figure 82 (b) depicts the search steps, size and direction as used in this thesis experimentation to detect the fiducial reflectors attached to the RMMA.

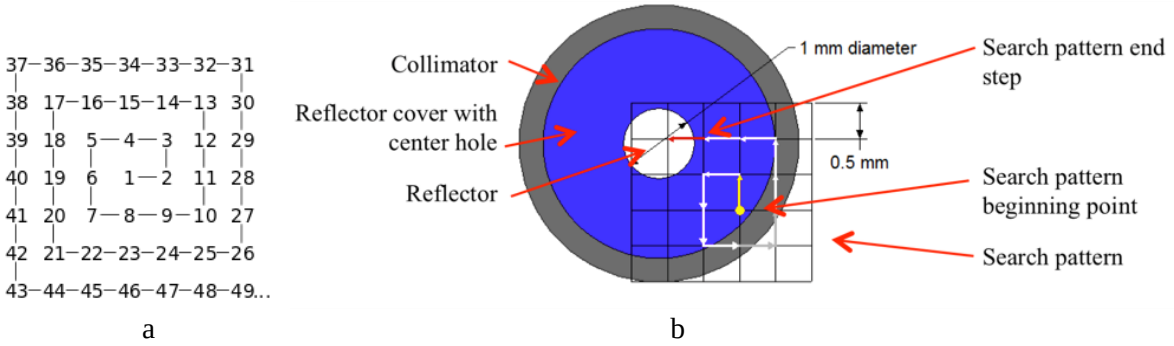

Figure 82. (a) Square spiral search with numbers at each step. [238] (a) Example square step search pattern drawing. The pattern begins with the yellow arrow dotted end and ends when the reflector is detected with the red arrow search step.

The square search begins away from the reflector at the chosen start point (yellow arrow dotted end) and each step moves along the small white or gray arrows until the laser retroreflector detected the fiducial reflector with the red arrow step. The circular and square search methods will be described in the next sections through experimentation.

An additional search registration method, called the Bisect with Fine Search Method, was developed and used during this thesis research. This registration method allows the same laser retroreflective laser to be used although also considers the mobile base pose uncertainty being larger than the manipulator uncertainty. Figure 83 shows a high-level, reference-frame drawing of the system components and the bisect search concept used in the Bisect with Fine Search registration method. The concept includes choosing and locating large reflectors on the RMMA. The reflector diameter was chosen to be larger than the largest system positioning uncertainty. In the case of the AGV and manipulator used for these experiments, the diameter was chosen to be 42 mm. Two reflectors were mounted along the square and circle patterns at their respective square spacing and circle diameter spacing. The manipulator was manually taught an initial position at the center of each of the large reflectors. This initial set of positions was programmed into the manipulator control program. As depicted in Figure 83, the initial offset of the laser retroreflector is not centered and therefore a crisscross or bisect manipulator control pattern must be implemented to find the reflector edges. Not knowing if the center is ever initially detected, the bisect manipulator control is initiated at each AGV pose. As described in section 3.3.2.2, it is again critical to choose the appropriate reflector so that the edges are detected.

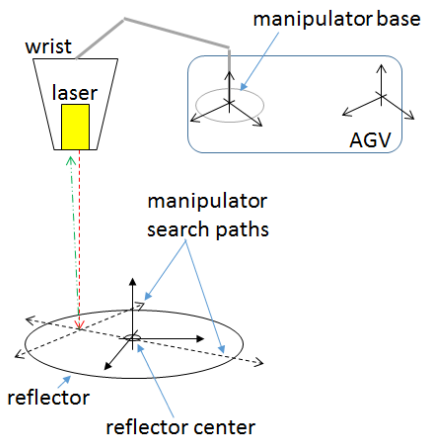

Figure 83. High level reference frame drawing showing the system components and bisect search concept.

The following subsections describe through experimentation the three non-contact methods for registering a mobile manipulator to a workpiece – i.e., two search methods: 1) Fine Search (circular and square search methods) and 2) Bisect with Fine Search using a laser retroreflector and reflective fiducials and 3) detection of QR codes using vision. A 'fine search' method was described in [170][171] as it evolved and later referenced in [243]. Research that also combines these registration methods using a laser spot detection method is described in [244] and [245] although was not experimented in this thesis.

6.2.3. Experiments and Results

Several experiments were performed combining the manipulator base positioning method and the mobile manipulator registration methods described in 6.2.1 and 6.2.2, respectively. The experiments and results are described in the following sections. Each of the experiments first lists the setup parameters for the experiment, including the fiducial pattern(s), size(s) of fiducials, search method and associated search details, and metrics.

6.2.3.1. Experiment 1 - Static + Fine Circular Search

Experiment 1 was used as a proof of concept for the use of the RMMA with laser retroreflector and circular search method.

- Square pattern of fiducials
- Four 6.3 mm fiducials
- Circular fiducial search
- 3.1 mm diameter x 15° increment step search for fine search
- Metric: registration, detect/non-detect, time, repeatability

In Experiment 1, described in [170], relatively simple AGV home-to-dock point, straight-line, 5 m paths were CAD modeled and used to statically pose the AGV near the RMMA for the manipulator to reach the square pattern of fiducials. This experiment also used the

The RMMA was originally setup as shown in Figure 63, including flat, background targets mounted perpendicular to each collimator and measuring 7.6 cm diameter with 6.4 mm incremental rings. The targets were used as simple visual cues for the test director to determine the approximate initial laser point position with respect to the fiducial. Figure 84 shows the experimental configuration and the 457.20 mm square pattern used for the static experiments.

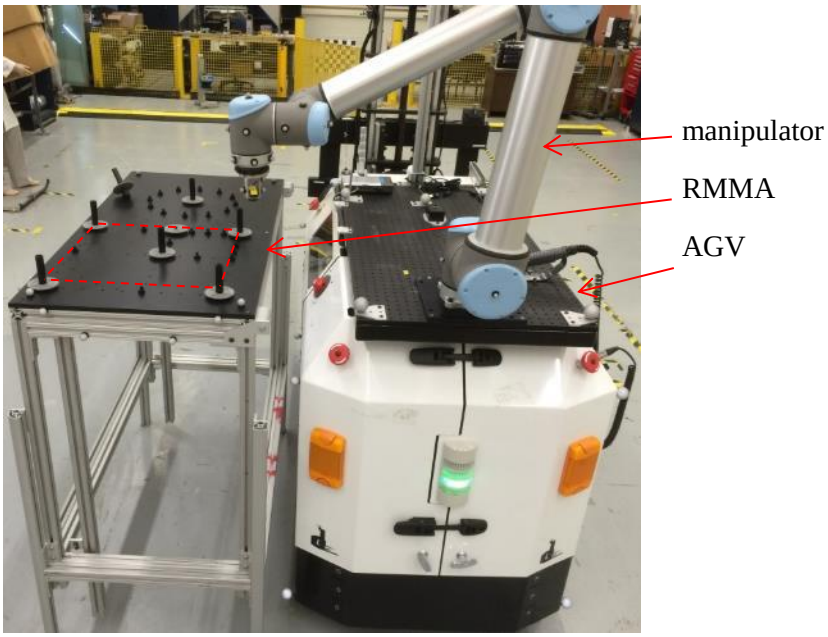

Figure 84. Static test configuration showing the mobile manipulator beginning the performance measurements. The manipulator test pattern is shown with red dashed lines between four vertices of a 457.20 mm square.

The performance measurement experiments used a laser retroreflector sensor that provided a relatively narrow beam consisting of both an emitting laser and a detector to detect 6.4 mm diameter reflectors (i.e., task points) positioned in known patterns (e.g., square, circle, triangle, sinusoids, etc.). [170] A camera, with a light source, could instead be used as the detection sensor, especially with a larger diameter reflector or other spot. The reflectors can have specific diameters depending upon the required uncertainty for their location. The laser retroreflector, shown in Figure 84, shows the sensor mounted in-line and perpendicular to the manipulator tool point.

Initial alignment to the reflector can occur using one of several methods briefed in [170]. The laser retroreflector was aligned using the manipulator jog mode from the teach pendant until the laser detected the two registration reflectors for both the circle and square reflector patterns. Therefore, the end-effector coordinates could be read directly from the teach pendant to return to during our experiment. The manipulator brakes were released and the manipulator was manually positioned so that the laser retroreflector detected all reflectors at the four locations. During the experiment, the manipulator began a spiral search pattern to detect the reflectors beginning with the manually taught positions. Each search pattern was parameterized to search in a growing, circular 15-spiral

pattern with a maximum radius of 50 mm; the trajectory took two minutes and would be interrupted when the reflector was detected. When a reflector was detected, the manipulator received a digital signal change from the laser retroreflector and the manipulator was commanded to move to the next taught reflector location and begin another spiral search, and so on. If no detector was detected, the spiral search pattern was executed. If there was still no detection within 2 min, the manipulator logged a "failed" and moved to the next reflector location. If detected, the manipulator logged a "success" and moves to the next location, and so on.

Figure 85 shows a screenshot of the OTS display for the static performance measurement experiment showing the cameras, AGV, manipulator, and the RMMA objects being tracked. The markers on each component are grouped together so that each component motion can be analyzed independent from one another. For example, the AGV markers are grouped separate from the manipulator markers, etc., as depicted by the different colors.

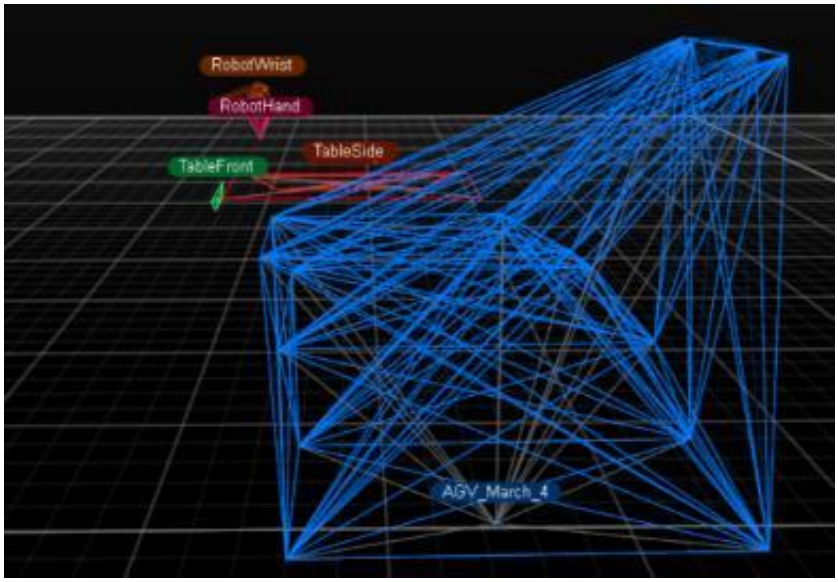

Figure 85. Screen capture from the OTS showing the AGV, manipulator, and the RMMA.

The static experiment included measuring the AGV position near the RMMA relative to the commanded AGV position. The first consideration was a non-ideal case, perhaps typical of industry, for the AGV calibration. The AGV was approximately two years old and had not been calibrated since purchase. The AGV was moved from a home position approximately 5 m to the RMMA location and back to home 10 times and was repeated three times. Table 16 shows uncertainty of AGV commanded versus AGV tracked data for a single stop point. The average offset is 29 mm in X and -9 mm in Y. Compensation for this offset was performed during test setup of the initial robot positioning over the first-accessed reflector location. Table 17 displays the uncertainty in the distance between the RMMA origin and the AGV origin in the RMMA surface plane. Table 17 shows that the expected AGV stop position near the RMMA has a fairly repeatable average offset.

Table 16. Difference (in mm) of the commanded AGV versus AGV tracked data for the AGV stop point beside the RMMA.

Axis	*Run1*	*Run2*	*Run3*
X	27	29	30
Y	-7	-10	-9

Table 17. Uncertainty (in mm) in the distance between the RMMA origin and the AGV origin in the RMMA plane.

	Run1	*Run2*	*Run3*
Distance	0.095	0.088	0.090

Another experiment included three runs to measure position uncertainty of the manipulator relative to the RMMA and to the OTS. Each trial consisted of 33 repetitions of a cyclic search for four reflectors with known characteristics. At each reflector, the manipulator initiated a spiral search to locate the reflector with the laser retroreflector. The first cycle allowed the manipulator to locate all reflectors followed by 32 cycles to measure repeatability.

The AGV was programmed to move from home to the RMMA as described in section 6.2.1.1. The manipulator moved to the pose where it expected to find the first registration point, p_1, and began the spiral pattern. Once the reflector was detected, the position of the reflector was recorded as p_1', and the manipulator moved to where it was expected to find the second registration point, $\tilde{p}_2$, based on the nominal distance offset and orientation expectations from p_1' defined prior to the trial. At $\tilde{p}_2$, the manipulator performed the spiral search again until the reflector was found, and then recorded the reflector's position, p_2'. The manipulator then updated its expectation of the artifact's position and orientation based on the Euler angle of incidence between p_1' and p_2', and moves to the new estimate for the location of the third registration point, $\tilde{p}_3$. The spiral search was again repeated until the reflector was located, the manipulator control program recorded its position as p_3', and the manipulator performed one last spiral search at the fourth registration point, $\tilde{p}_4$. This search process is illustrated in Figure 86.

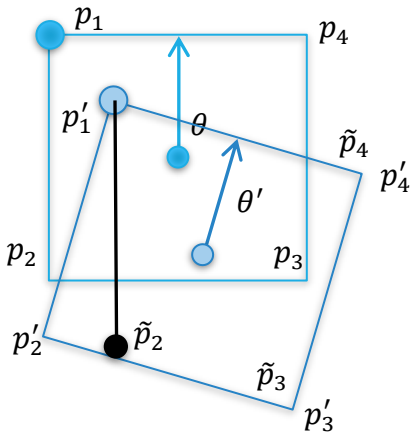

Figure 86. Comparison of the nominal (blue) and measured (red) poses of the registration artifact reflectors after the first search repetition. The expected positions for p_2 through p_4 are updated based on the measurements of the prior target locations.

At this point, all four registration points were updated with their actual poses, and the process was then repeated 32 more times using p_1' through p_4' as initial search locations to capture positional uncertainty and repeatability measurements. Once the 33rd iteration was complete, the manipulator signaled to the AGV that the manipulator had been registered with updated position (X-Y plane) and orientation (Z rotation) offsets. The AGV then moves back to its home position, and the process repeated. Figure 87 (a) shows the GT data at each of four locations and a close-up of location 1 data in Figure 87 (b) for Run 1 for 33 times over approximately 10 min as expressed by the color bar.

The close-up clearly shows data points plotted in curved lines from the first spiral search at location 1 at the beginning of Run 1. Then, no search was used detect location 1 for the remaining 32 times as depicted by the multi-colored data points in a much tighter data pattern which spans approximately 0.8 mm in X and 0.5 mm in Y. The plotted data is from only when the manipulator has a velocity of less than 0.1 mm/s. Note the larger data spots shown in Figure 87 (a) for locations 1 and 2 compared to locations 3 and 4 proving that the mobile manipulator has registered pose with the RMMA.

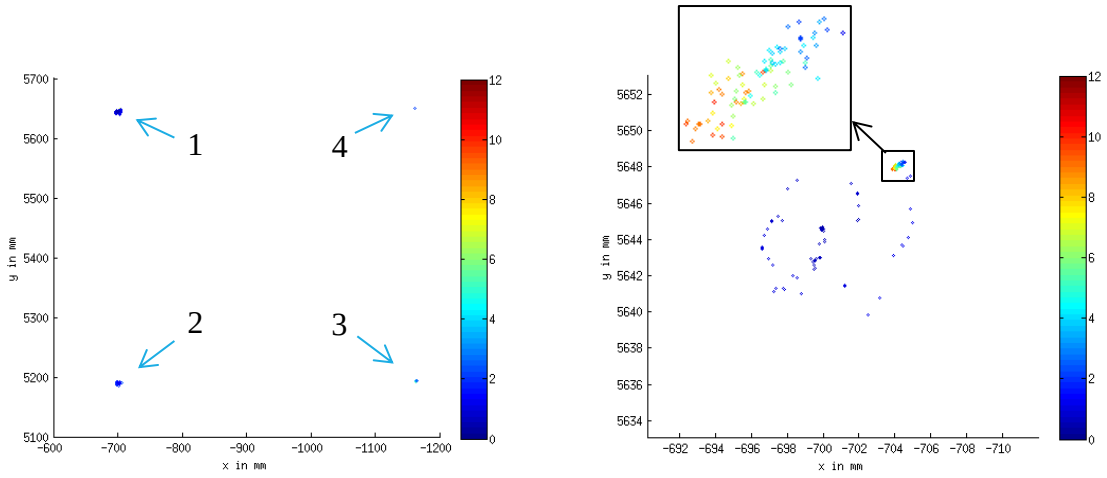

Figure 87. (a) GT data of time at each of four locations in Run 1 for 33 times over approximately 10 min as expressed by the color bar. (b) Close-up showing the first spiral search at location 1 beginning Run 1 and no search detect (inset) at location 1 for the remaining 32 times.

Table 18 shows the mean mobile manipulator position when the laser retroreflector detected the reflector for the remaining 32 time process, and for the number of thresholded points, as compared to each reflector center. Since the manipulator almost continuously moves, perhaps even when the reflector is detected (e.g., when the laser moves across the detector), displayed in the table is a mean uncertainty of the laser retroreflector position compared to the OTS reflector position center for all three runs.

Table 18. Actual reflector point locations and mean mobile manipulator positions when the laser retroreflector detected the reflector for the remaining 32 times as compared to each reflector center.

	Mean position (mm) relative to reflector center

	Run 1	*Run 2*	*Run 3*
# points	26	74	41
Location 1			
x (mm)	-2.61	-2.57	-2.35
y (mm)	1.09	0.05	0.83
Location 2			
x (mm)	-1.88	-1.74	1.46
y (mm)	0.50	0.28	-0.73
Location 3			
x (mm)	-1.20	-1.09	-0.74
y (mm)	1.29	0.94	0.69
Location 4			
x (mm)	-1.74	-1.81	-1.08
y (mm)	1.62	0.83	-0.09

After the third run, the data logs from the manipulator were also analyzed to estimate the positional and orientation accuracy and repeatability performances of the AGV as a function of the registration artifact's nominal position and orientation. The orientation error was calculated as the difference between the expected orientation of the artifact, θ, and the average calculated orientation, θ', as determined by the angle of incidence between the calculated centroid of the artifact's four measured registration points (p_1' through p_4'), and the mid-point between the measured registration points p_1' and p_4'. Two different methods were evaluated for calculating the position error. The first method simply compared the X and Y positional offsets of the centroid of the measured registration points with the centroid of the nominal registration point locations. The second method corrected for the orientation error about the centroid of the measured poses, and then compared the measured location of p_1' with the original nominal pose of p_1.

Two metrics were considered in the analysis: 1) *pass/fail* for initially detecting the reflector after the first search of all four reflectors and 2) the positional repeatability when the laser retroreflector detected the reflector. Table 19 shows results of the pass/fail test. Manipulator positioning was called a *fail* if after the first search trial and for the remaining 32 trials, the laser retroreflector did not detect a reflector immediately at each location requiring a search to begin.

Table 19. Pass/Fail and dwell time results for detecting the reflector without a search.

	Run1	*Run2*	*Run3*
Number Fails for each position (1,2,3,4)	1,1,0,0	15,1,0,0	1,1,5,1
Total search time (s) at each location (1,2,3,4)	41.5, 42.9, 0.0, 0.0	79.4, 40.2, 0.0, 0.0	41.6, 78.1, 38.6, 31.2

Fails, therefore, correspond to the total search time that was required at each location. This metric could correspond to the time the manipulator would require, for example, to perform an assembly operation. Assembly times varied according to position uncertainty, part tolerances, initial pose error, search parameters, etc.

Results of the second metric are expressed in Table 20 for all runs and with respect to the robot and to the OTS. The robot uncertainty spanned between 0.01 mm and 0.74 mm in X and between 0.11 mm and 0.42 mm in Y with orientation uncertainty between -0.6° and -0.8°. However, orientation uncertainty, for these initial experiments, does not consider the measured reflector center. Instead, as shown in Figure 29, laser retroreflector detection points may be at the upper and lower edges of location 1 and 2 reflectors, respectively, and cause large rotation error Θ and also failed attempts on following laser retroreflector detect attempts.

Table 20. Manipulator tool center point positional repeatability uncertainty, as logged by the manipulator and logged by the OTS, when the laser retroreflector detected the reflector for the remaining 32 times.

	Repeatability *uncertainty measured by the manipulator*		
	Run 1	*Run 2*	*Run 3*
Location 1			
x (mm)	0.15	0.74	0.11
y (mm)	0.11	0.42	0.11
Location 2			
x (mm)	0.01	0.09	0.07
y (mm)	0.27	0.18	0.28
Location 3			
x (mm)	0.21	0.01	0.35
y (mm)	0.12	0.28	0.16
Location 4			
x (mm)	0.03	0.022	0.05
y (mm)	0.27	0.28	0.27

As described in sections 3.3.2.4 and 4.5.1, the RMMA and AGV motions, when the AGV was stopped while the manipulator was moving (see data in Figures 26 and 50) causes maximum combined uncertainties of (X = 0.52 mm, Y = 0.65 mm). The motions could induce enough position offset to the reflector to cause the manipulator to begin a search at each location. However, the initial spiral search provided reflector detection by the laser retroreflector at the reflector edge and not at the center. Therefore, the spiral search is perhaps not the complete performance test method. Instead, an additional raster scan of the 6.35 mm diameter reflector should follow the spiral search and the average detect position should be at the center of the reflector.

By detecting the reflector center, it is expected that the specified manipulator repeatability of 0.1 mm combined with the AGV and RMMA movements would provide increased detects at each reflector location after the initial scan, potentially without the need for a spiral search again until the AGV moves and returns to the same location. As measured by the manipulator, the largest maximum positional repeatability uncertainty was (X = 0.74 mm, Y = 0.42 mm) where adding the maximum AGV and RMMA movements uncertainties could be as high as (X = 1.26 mm, Y = 1.07 mm). However, detection of the reflector edge potentially guarantees no better than 50% reflector detection since uncertainty could place the laser on or off the reflector. With respect to OTS, the maximum uncertainty when adding AGV and RMMA movement to mean reflector detect position, compared to the reflector center, was (X = 1.46 mm + 0.52 mm = 1.98 mm, Y = 1.62 mm + 0.65

mm = 2.27 mm) or 3.01 mm radius. Therefore, if the retroreflective laser sensor was initially positioned at the 6.4 mm diameter reflector center (i.e., 3.2 mm radius), the laser should always detect the reflector.

Additionally, the circular search began with a step increment chosen to be approximately half of the diameter of the fiducial being tested. For example, an initial step size of 3.1 mm was chosen for a 6.3 mm fiducial to be detected. However, after the initial circle of steps was completed, the step moved to the next larger 3.1 mm circle step radius (e.g., from 3.1 mm to 6.2 mm radius from the start location) and at the same step arc angle (e.g., 15°) causing much larger steps to occur as the circle pattern grew. Figure 88 (right) depicts this issue where a search diameter of 9.45 mm causes a 1.24 mm diameter arc step size while a search diameter of 12.60 mm causes the arc step size to increase 24% to 1.62 mm. With a fast-moving robot versus a slower to respond laser retroreflector, it was possible for the fiducial to not be detected. A worse condition would be for smaller diameter fiducials with the same step size as shown in Figure 88 (left)

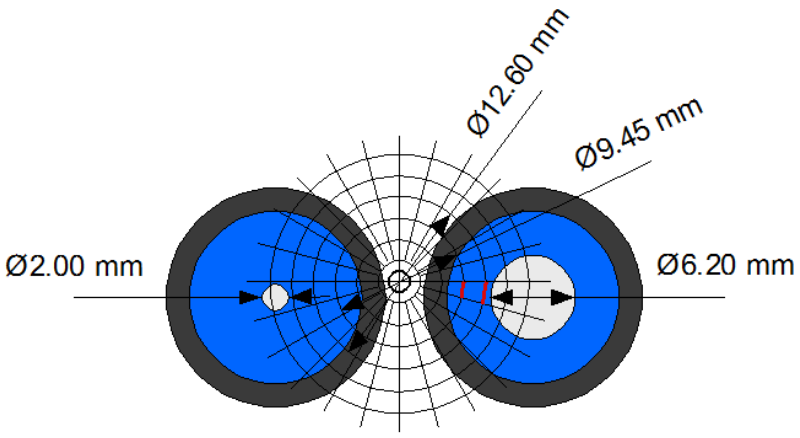

Figure 88. Circular search pattern over two different sized fiducials: (left) 2 mm diameter and (right) 6.2 mm diameter. The center gray represents the fiducial, the blue represents the fiducial cover with center hole, and the dark gray represents the collimator. Red lines are drawn at the two marked radii depicting arc step lengths.

6.2.3.2. Experiment 2 – Static + Fine Square Search

In Experiment 1, described in section 7.2.3.1, a proof of concept for the use of the RMMA with laser retroreflector. Here and follow-on experiments were meant to refine the concept. The main metrics for these tests were success rate and the number of steps required to detect the first and second points after registration. These metrics are similar to what manufacturers and users may consider when matching a mobile manipulator to assembly tasks.

- Square pattern of fiducials
- Two 1 mm fiducials
- 3 mm fiducials for two remaining square fiducials
- Square fiducial search

- 0.5 mm step search for fine search
- Metric: registration steps/time, detect/non-detect, repeatability

An experiment followed to change the circular spiral to a square spiral as shown in Figure 75. and to use 1 mm registration fiducials. Docking results after 10 trials using two 1 mm registration fiducials were that the success rate averaged 91 %, although an average of 794 steps in the square-spiral search were required to detect the first assembly point after registration followed by 12 steps to detect the second point.

Therefore, a re-registration concept, (bisect) was developed. Figure 76 includes a high-level reference frame drawing of the system components and crisscross search. The initial bisection search location was measured with the vehicle parked at one of the test locations near both the circle and the square RMMA patterns. The manipulator joystick was then used to jog the manipulator to detect a 1 mm fiducial at the center point where a large reflector was to be placed. The manipulator tool point location was recorded and the search was repeated for all four (two circles and two squares) registration point locations. The large reflectors were replaced at the recorded locations and the vehicle was programmed to move to 10 different poses near the RMMA as the manipulator performed the bisection registration. The bisection search used 3 mm steps to rapidly register the large reflector's center. Large step size on registration reflectors is perhaps one of the greatest uncertainties for this type of registration method, although lower tolerance steps provides much slower registration where a time/tolerance registration balance is a topic for future research.

6.2.3.3. Experiment 3 – Index + Bisect with Fine Square Search

- Square and circle pattern of fiducials
- Large bisect fiducials
- 3 mm step search for bisect
- Two 1 mm fiducials on each pattern
- 6 mm diameter fiducials for two remaining square pattern fiducials and 3 mm fiducials for all remaining circle fiducials
- Square fiducial search
- 0.5 mm step search for fine search
- Metrics: registration, detect/non-detect, repeatability

In Experiment 3, described in [172] and upon considering the outcome of the static measurements from 6.2.3.1 and 6.2.3.2, the AGV was programmed to move to ten different poses relative to the RMMA as described in section 6.2.1.2. The RMMA was setup as shown in Figure 89 and Figure 90 shows the AGV next to the RMMA and marks the circle and square patterns of fiducials for the mobile manipulator to index between.

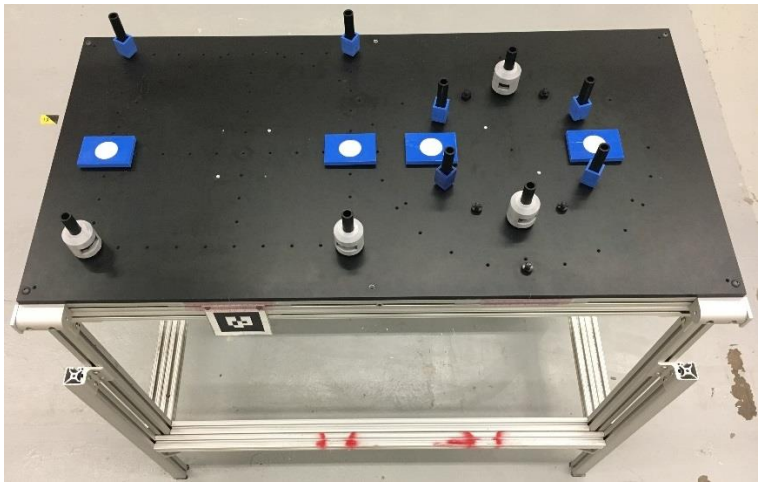

Figure 89. Experimental setup of the RMMA for the Bisect with Fine Search Method.

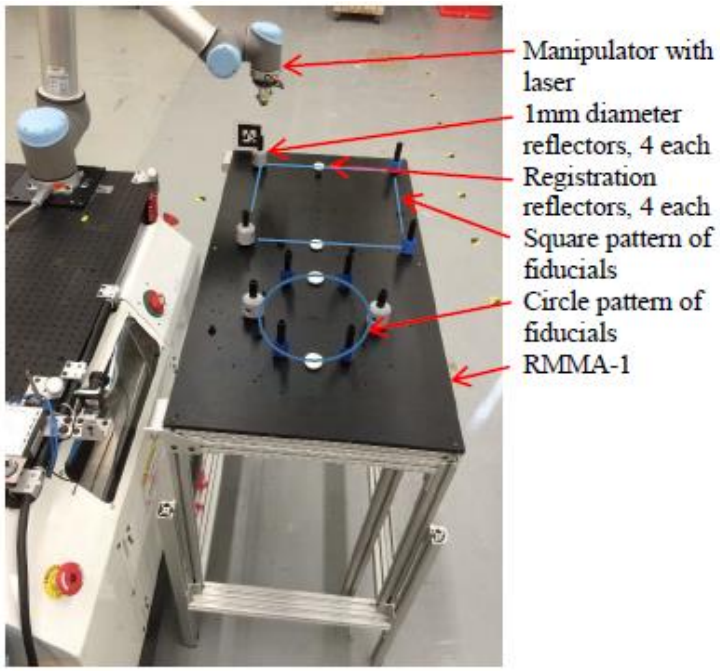

Figure 90. RMMA showing circle and square patterns of fiducials for the mobile manipulator to index between.

A modified registration method for registering the mobile manipulator to the RMMA was developed after the static experiments described in sections 6.2.3.1 and 6.2.3.2 that uses the "fid-refl-reducer" reflectors shown in Figure 13. The aperture allows the opening to the reflector to not only be any size, but to also center the opening on the reflector. This ensures that the two registration fiducials are centered on the reflector even when using a much larger reflector for all other fiducials. The smallest aperture opening used was 1 mm diameter while all other fiducials were 3.2 mm or 6.3 mm diameter. The laser retroreflector did not return a 'detect' at a smaller diameter than 1 mm diameter aperture setting.

The manipulator control program described in 6.2.1.2 was used for this experiment. The deviations from that section are described here:

- The initial search was not counted as a performance criteria since the mobile manipulator could use various types of registration techniques. However, for comparison to repeatability, the initial registration number of iterations count was logged and included in results.
- Once the locations of all reflectors in the pattern were computed, the manipulator cycled through them 32 times for each pattern in this experiment.
- The AGV was first moved to a location where it could reach both of the 1 mm diameter "fid-refl-reducer" fiducials.
- The arm was repositioned manually until the sensor detected alignment with each of the 1 mm diameter "fid-refl-reducer" fiducials, and the manipulator position was recorded.

The mobile manipulator performance measurement results using the RMMA included only the detection of reflectors for each pattern and after initial registration. By comparison, the initial number of search steps used to register the manipulator at the first reflector was recorded. Results are shown in Table 21. The repeatability performance measurement process began once the mobile manipulator was registered to the artifact after initial registration and moving through the square or circle pattern one time and with the AGV statically positioned at a pattern. Measurements of 'detect' or '1' were logged for each RMMA reflector location. If a search was required to find the fiducial after registration, the measurement at that reflector was counted as a 'no detect' and the number of search steps was recorded.

Table 21 shows: the consecutive position number and programmed AGV position, the AGV pose angle (heading), the circle or square pattern being detected, the total number of reflectors to detect for 32 pattern iterations after the registration pattern, the reflector diameters for each pattern (rounded to whole numbers), the number of reflectors detected and detection percentage, and the initial number of search steps needed to register to the first reflector after the AGV stopped. The AGV stop points programmed are shown in Figure 70. The lines leading to the stop points indicate the AGV orientation.

The table shows very high repeatability results at 97 % or above as shown in the "% detected" column of the table. The results demonstrate a good test procedure for determining repeatability of a mobile manipulator to register to and access assembly points within the reflector diameters chosen. Further tests are required to understand direct connections between mobile manipulator performance and system pose, for example, suggesting that AGV pose at 0° provides higher performance than at other angles. Results here do not show this since position 6 included the AGV being at 90° and yet, was repeatable to 100 %.

Table 21. Test results of the mobile manipulator accessing the RMMA from various Stop Points (see Figure 4) and various AGV poses. The gray rectangle in the center of the Stop Points map shows the approximate RMMA square and circle pattern locations.

position number	AGV position	pose angle, deg	pattern	number of reflectors to detect	reflector diameter sizes	number reflectors detected	% detected	initial number of search steps to register to fiducial #1
1	326	90	circle	192	1 mm, 6 mm	188	98%	561
2	346	315	square	128	3 mm	124	97%	613
3	368	0	circle	192	1 mm, 6 mm	192	100%	181
4	333	0	square	128	3 mm	128	100%	73
5	382	45	circle	192	1 mm, 6 mm	191	99%	377
6	328	90	square	128	3 mm	128	100%	1921

6.2.3.4. Experiment 4 – Index + Bisect with Fine Square Search

- Square and circle pattern of fiducials
- Large 30 mm diameter, large prism, bisect fiducials
- 3 mm step search for bisect
- Two 1 mm fiducials on each pattern
- 3 mm fiducials for all remaining square and circle fiducials
- Square fiducial search
- 0.5 mm step search for fine search
- Metric: registration steps/time, detect/non-detect

The fourth experiment, from [171], used the mobile manipulator to do bisect registration on two large reflectors for each circle and square pattern on the RMMA and then fine search to detect two 1 mm fiducials. After bisect registration, the manipulator was moved to detect the 1 mm fiducials and two more 3 mm fiducials on the square corners and four more on the circle. The experimental goal was to determine if the speed and success rate to detect the second registration were improved from experiment 3. The experiment 4 test results were that success rate was averaged over 10 trials at 92 %. However, the number of steps to detect the first and second 1 mm fiducials dropped to an average of approximately 11 steps and 4 steps, respectively. Two of the 10 trials included issues with detecting the large reflectors and were aborted and not included in the results. Future tests with the use of larger bisect reflectors and a smaller, for example 0.5 mm, step search will replace the current large reflectors and 3 mm step search to help remedy this situation. Additionally, improved vehicle pose and manipulator base references will be researched.

6.2.3.5. Experiment 5 – Index + Bisect with Fine Square Search

- Square and circle pattern of fiducials
- Large 42 mm diameter, micro-prism, bisect fiducials
- 1 mm step search for bisect
- Two 1 mm fiducials on each pattern
- 3 mm fiducials for all remaining square and circle fiducials

- Square fiducial search
- 0.5 mm step search for fine search
- Metrics: registration, detect/non-detect, repeatability

The fifth experiment, also from [171], included the bisect registration method followed by pattern registration to 1 mm fiducials and then performance measurement of repeatability. The square and the circle were repeated 32 times after registration where registration steps were not included in repeatability tallies. During repeated pattern detection, the success percentage averaged 98 %, detecting two 1 mm and two 3 mm fiducials on the square and two 1 mm fiducials and four 3 mm fiducials on the circle for a total of 1600 points. In all three experiments, the use of artifacts provided reproducible performance measurement methods verifying registration.

6.2.3.6. Experiment 6 – Index + Bisect with Fine Square Search

- Square and circle pattern of fiducials
- Large 42 mm diameter, micro-prism, bisect fiducials
- 1 mm step search for bisect
- Two 1 mm fiducials on each pattern
- 2 mm fiducials for all remaining square and circle fiducials
- Square fiducial search
- 0.5 mm step search for fine search
- Metrics: registration, detect/non-detect, repeatability

In experiment 6, described in [243] all reflectors were the same type micro-reflector, including the large “bisect-reflectors”. Additionally, two registration “fid-refl-reducer” type fiducials replaced the two “fid-refl-fixed” reflectors that were used for the Fine Search Method described in section 6.2.1. The RMMA was setup as shown in Figure 89. Once the bisect on the large registration reflectors were complete for a pattern, the manipulator began a fine square search method of the 2 mm fiducials that were used throughout the RMMA patterns.

The experiment was run for all 10 different mobile manipulator poses and was repeated five times for a total of 50 poses. The results shown in Table 22 include only the detection of the first 2 mm reflector for each pattern after bisect registration. The bottom of Table 22 shows a summary of all tests averaged over the 50 measurements and includes the average number of steps for the 2 mm reflectors and shows the RMSD from the mean.

Table 22. Mobile manipulator registering to the RMMA using the bisect search method.

AGV Position Number	Pose Angle	Pattern	Average num. of search steps to register	Total bisect + fine search time to register (s)
1	90°	circle	0	86
2	315°	square	6	89
3	0°	circle	0	86
4	0°	square	0	86
5	45°	circle	0	86
6	90°	square	0	86
7	135°	circle	0	86
8	225°	square	0	86
9	270°	circle	0	86
10	270°	square	12	92

Average Search Steps/Time (s)	1.8 / 0.8	RMSD Search Steps/Time (s)	3.8 / 1.8

When using the bisect method prior to the fine search, the total bisect plus fine search steps/time was a maximum of 184 steps/86 s or nearly 90 % less time than using only the fine search method. Larger bisect search steps, among many other improvements, could be used although would increase the number of registration search steps on the 1 mm or 2 mm fiducials to a potentially unknown amount.

6.2.3.7. Mobile Manipulator Performance Data

In all experiments described, the OTS was used to verify the mobile manipulator performance measurement concept that uses an artifact. It is expected that researchers that do not have these tools available to them may wish to utilize the 10 pose mobile manipulator performance measurement information and data for additional research and developments. Therefore, data was collected from the OTS, AGV, and manipulator controllers and published in [247]. A brief description of the test and data collection is described in this section.

Data collected from the AGV Vehicle Diagnostic Tool (VDT) and the robot control program include much information about their motion and measurement and are provided with the accompanying data set published in the NIST Management of Institutional Data Assets [248]. A reference publication [247] that describes the setup, procedure, files, etc. accompanies the data. The data set is available for researchers who wish to work with the data corresponding to two tests using the AGV, onboard manipulator, and RMMA. The data set also includes real world situations, such as emergency stops from detection of obstacles and from driving off the commanded path, and other information that were captured during the test and may be useful to the system designer, researcher, or user.

An OTS was used as ground truth to measure two, 10-pose, index tests described previously. Markers were mounted to the AGV and to the robot prior to the two tests as shown in Figure 91. Markers were attached to the appropriate RMMA hole locations (i.e., circle, square, and bisect reflector) after the two tests as shown in Figure 92. For ground truth of the RMMA, all fiducials and large bisect markers were removed from the RMMA. A 19 mm diameter marker was placed

on each screw hole where each fiducial and bisect marker is normally located. Rigid bodies were created for the bisect reflector markers, the circle pattern of markers, and the square pattern of markers. Three data sets of approximately 30 s each were collected using the OTS of only the static RMMA markers.

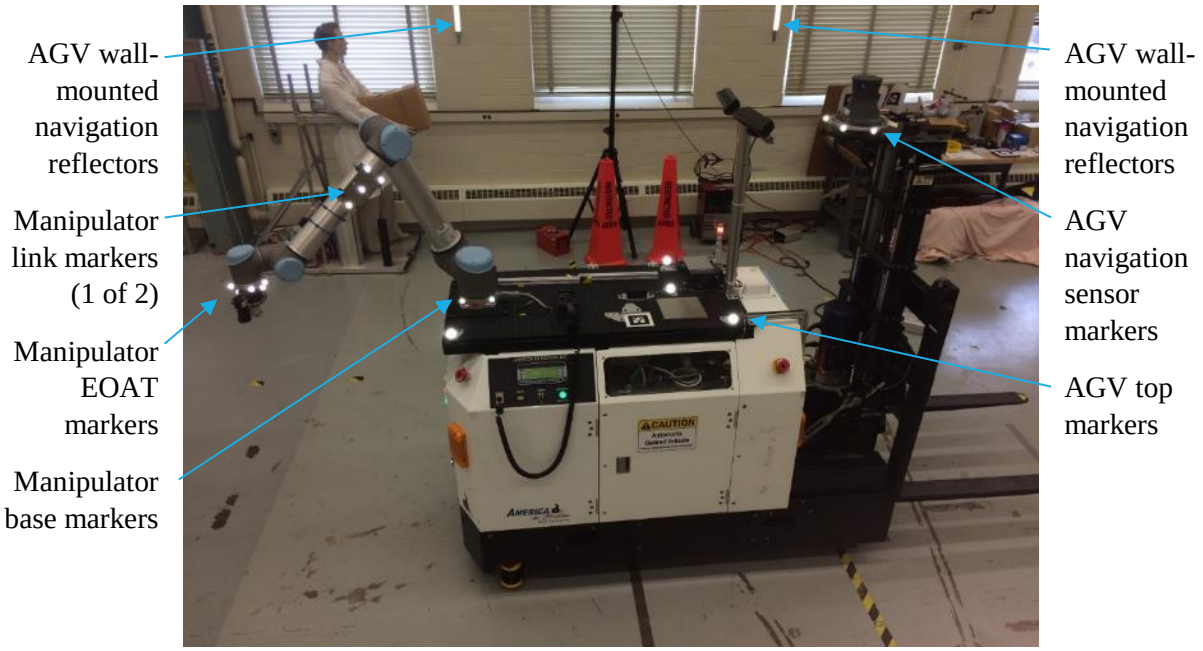

Figure 91. Highlighted (white) AGV- and robot-mounted markers and AGV wall-mounted reflectors. Two robot link markers were used, one is shown and one on the opposite side of the link (not shown). Robot base markers were not included in Tests 1 and 2.

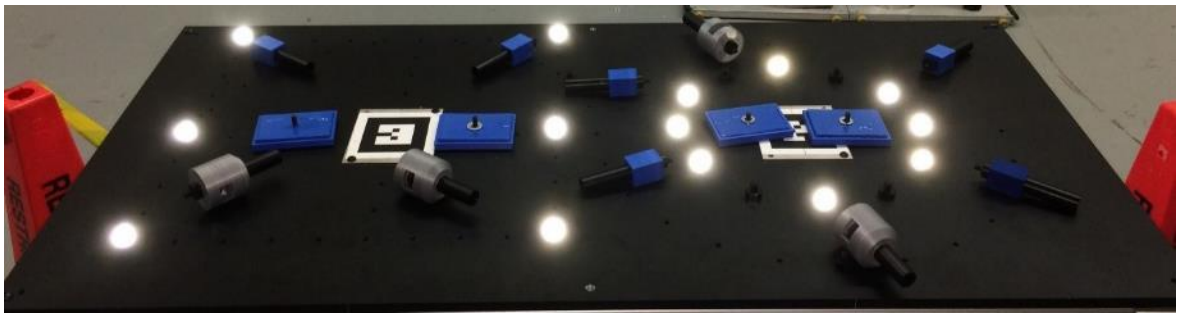

Figure 92. OTS markers located on the bisect reflector, circle pattern fiducial, and square pattern fiducial locations of the RMMA measured for use as ground truth. The associated bisect reflectors and fiducials and lying next to their respective mounting locations.

Critical to understanding the performance uncertainty of the mobile manipulator are the following (rigid body OTS names are in parentheses):

- wall-mounted reflectors – captured prior to the test as described in section 4.2.1
- AGV navigation sensor (NAV)
- AGV (AGV_TOP)

- Manipulator base (ROBOT BASE – added after the test)
- Manipulator end-of-arm-tool or joint 6 (EOAT)
- RMMA (RMMA_square, RMMA_circle, RMMA_bisect)

Since the AGV markers are fixed in relation to the ROBOT BASE, ground truth data was collected for the ROBOT BASE. Approximately 10 s of data was collected of the ROBOT BASE simultaneously with all other manipulator and AGV rigid bodies. Besides the ROBOT BASE and EOAT, two plates of markers were also attached to the manipulator forearm to capture it's pose during the tests in case this information is useful to other researchers. These plates are labeled as:

- Manipulator forearm (ROBOT_PLATE1, ROBOT_PLATE2).

Screenshots of the OTS rigid bodies developed for the AGV and manipulator and for the RMMA are shown in the screenshots in Figure 93 (a) and (b), respectively and correspond to Figure 91 and Figure 92, respectively.

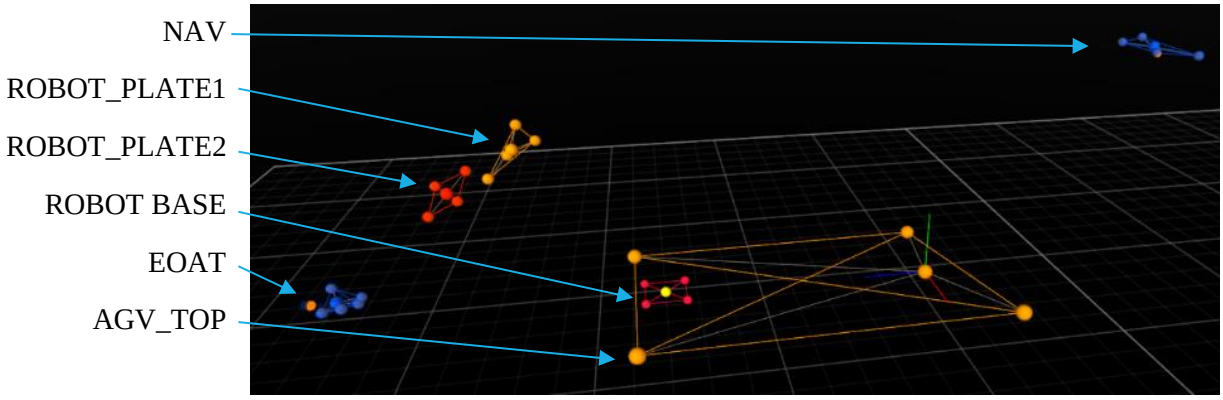

a

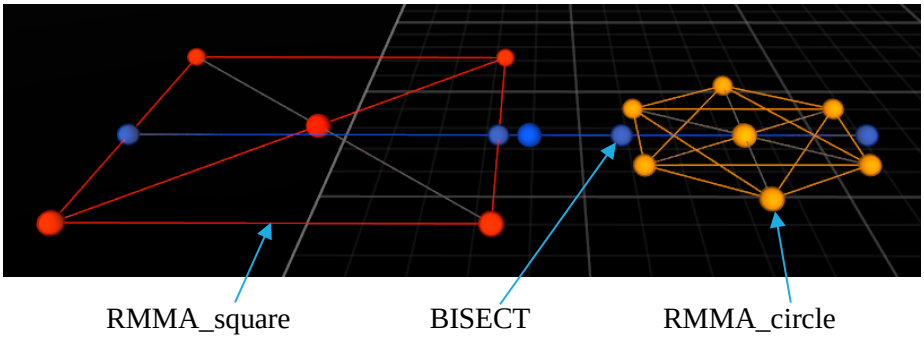

b

Figure 93. Screen shots of OTS rigid bodies developed for the (a) AGV and robot and (b) the RMMA.

6.2.3.8. Experiment 7 - Visual Method

In an effort to further improve on the bisect registration method, a camera snapshot of a target, calculation of registration of the camera to the target, and communication to the manipulator is expected to occur faster than the bisect registration method. There is added complexity and cost

to this method above the laser retroreflector with reflector method as an additional process of camera calibration, camera-to-fiducial calibration, additional camera control software, cost of a low uncertainty camera, etc. However, the question is, can this method produce similar or better uncertainty results at a much more rapid rate to justify the additional complexity and cost?

Visual fiducial systems allow for 6 degrees-of-freedom (6 DoF) positional tracking of fiducial targets, or tags. Since these systems are well-developed, and can be implemented with open source software, inexpensive cameras, and virtually free printed targets, they have a number of advantages for use in robotics research and testing procedures for industrial robot evaluation and validation.

As part of [243], fiducial systems commonly labeled as AR, or augmented reality, were reviewed. These systems include: ARTag, April tags, ARToolKit, and ALVAR [246]. The "A software Library for creating Virtual and Augmented Reality" or ALVAR version was used as a test case. Like the other systems, ALVAR uses rectangular black and white targets with a black outer square for location, and an internal matrix of squares that codes the identity of the target. To evaluate and validate the use of visual fiducial targets, two sets of experiments were conducted using the ALVAR implementation and a 17 mm machine vision camera with a resolution of 1296 pixels x 964 pixels and a fixed 4.5 mm focal length lens. Experimental results from the NIST study [243] determined the following:

- static repeatability of the ALVAR system when the 200 mm x 200 mm target was moved to static positions by a pan-tilt mechanism
- allowed to settle before static measurements
- camera – to - target separation distance 800 mm to 1000 mm
- moved to 26 positions of differing tilt and pan
- For each position, 306 measurements were taken over 30 s
- Repeatable measurements indicate systemic biases can be corrected by calibration
- Maximum difference from the mean in any one position in any dimension was 0.8 mm (along the Z-axis)
- Maximum angular error (in angle axis representation) was 0.18^{o}
- From initial results, we judge that the basic capabilities of ALVAR are adequate as a subsystem in workpiece registration.
- Expect that target detection (i.e., registration) can occur near camera polling speeds (e.g., 120 Hz = 1/120 s = 8 ms x # samples)

Experimental results reported for visual fiducials are consistent with the various registration methods from the literature. Under optimal conditions, estimated repeatability of a visual fiducial was under 1 mm and 0.2^{o} from a single image. Given other elements in the system, including calibration of camera-to-base, and base-to-arm, and the propagation of error, it is expected that the total error for the system would be higher.

An additional experiment was performed by the author to scan the 200 mm x 200 mm target at a camera to target separation distance of 147 mm as with the laser retroreflector experiments. The

experiment included moving in 10 mm increments along both X and Y axes. The following test parameters were noted:

- Point Grey Blackfly camera
- Manipulator used to move camera with change in manipulator position = ± 0.2 mm.
- Camera centered on marker origin.
- Marker was rotationally aligned with laser.
- Measurement range: ±100 mm along both X and Y
- Increments: 10 mm
- Samples: 100 per position

Results are plotted in Figure 94 for the camera error calibration experiment using a camera and ALVAR software. Based on the plot, should the camera be positioned directly over the Q-code target, the registration will be nearly ideal. However, should the camera not be positioned offset from the Q-code target center, the registration will nearly linearly fall to error at approximately 1 mm per 40 mm offset. Time to snap a camera image and for the camera control program to look-up in a table of calibration results is estimated to be within 1 sec (an order of magnitude better). Therefore, the method would be considered an ideal follow-on and comparative method to the laser retroreflector method, assuming there is justification for additional cost (approximately $1000) for a high-end camera and lens as was used for these tests.

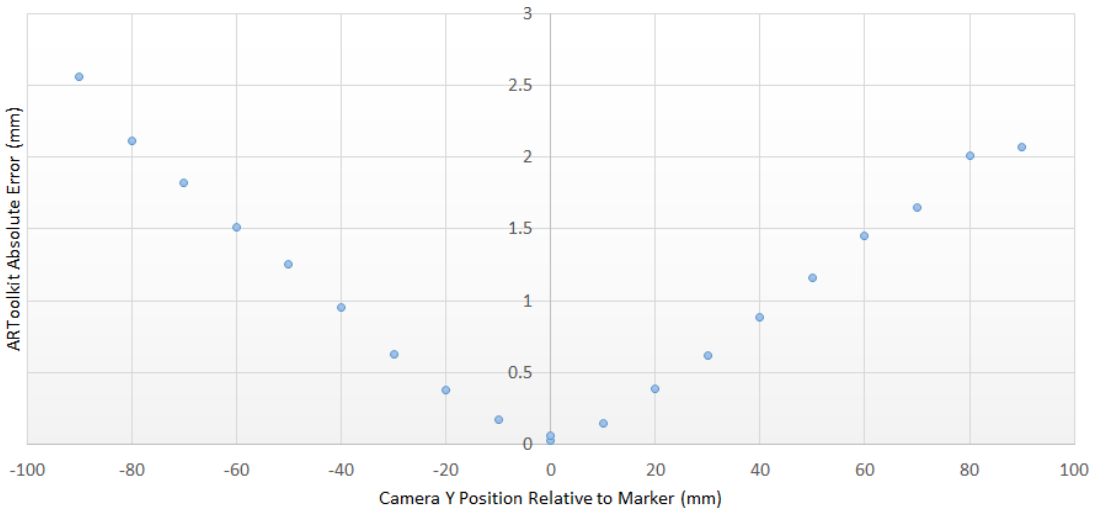

Figure 94. ARToolkit average absolute error versus perpendicular camera position with respect to the target.

6.2.3.9. Time Correspondence Between Systems

In order to facilitate the data correspondence between the AGV controller, remote manipulator control, and the OTS for data analysis of experiments 5 and 6 and for data publication, the system clocks must be synchronized to provide accurate time-stamping. [247] The author of this thesis teamed with a NIST timestamping expert to produce a time correspondence between systems. The system clocks of the three Windows computers running the OTS, manipulator control and AGV control were synchronized using a Network Time Protocol (NTP) time server with integrated

global positioning system, or GPS, antenna mounted inside in front of a lab window (see Figure 1). The Omicron time server software display showed that twelve satellites were detected and the time server clock was locked to GPS. The three off-board vehicle computers (OTS, offboard manipulator controller, and offboard AGV controller) were configured to synchronize to the time server via a power-over-Ethernet switch. Within 5 minutes prior to each test, a command was executed on all three computers to send a request to immediately resynchronize the system clock to the configured NTP time server. Baseline tests of system clock precision to NTP using a local time server can have a time offset on the order of tens of ms (see Figure 95).

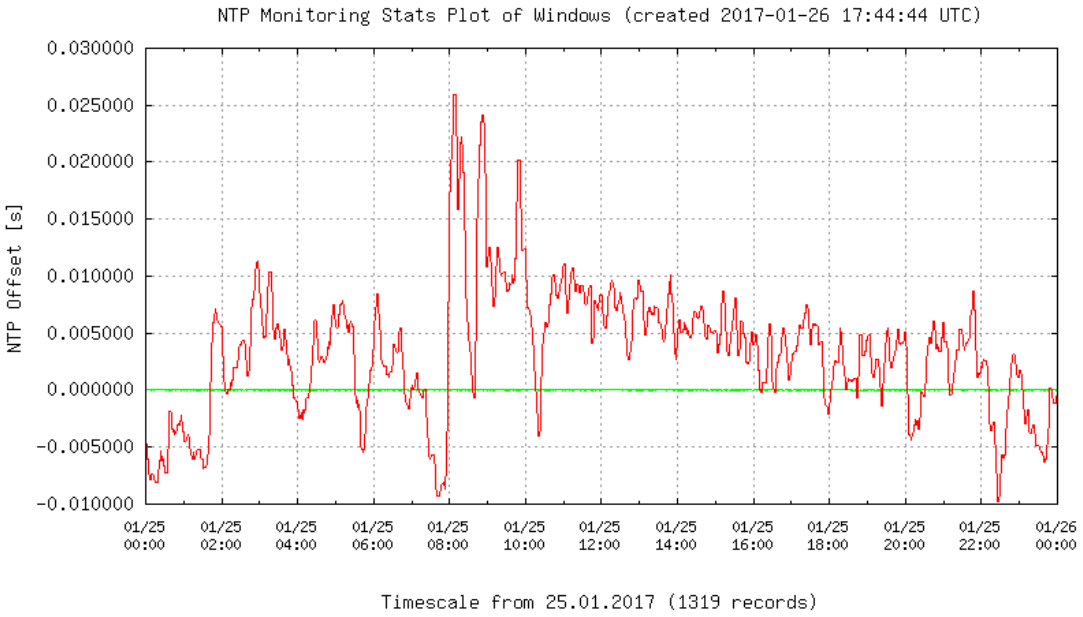

Figure 95. Screen shot of time offset between a local computer clock and a GPS-locked NTP time server over the course of 24 hours to establish a baseline approximation of the synchronization precision.

A Time Correspondence program was developed to correlate the time stamps when the robot, AGV, and OTS all logged data at approximately the same start-activity time, including the time when a file was produced and the time when a reflector was detected. An example of the program output is shown in Figure 96. The output includes data files from the Robot, AGV, and OTS and uses the three associated Unix timestamps when the laser retroreflector (i.e., EOAT) registers with the -1 marker (i.e., first bisect reflector). The program then shows the start time of the OTS program file and the time to generate the robot log file. It then provides an estimated offset time from the robot to the OTS files to provide a check to the data user on where to locate this data point and correlate times. The program translated the file's local timestamps from the OTS (OTS Time column) and robot (Robot Time column) into UTC and finally Unix timestamp epoch, which is the number of seconds since January 1, 1970.

Each measurement in the robot file has a relative offset from file creation; this offset was added to provide the values for the column "Robot Start Time" in Figure 96. The difference between the column Robot Start Time (s) and OTS Time is computed to provide a relative OTS Offset (s)

estimate. The estimate is then compared to the row in the OTS data with the closest time-stamp before the OTS estimated offset to determine the OTS data point corresponding to the robot and AGV measurements. Similarly, the corresponding robot time is shown for the AGV.

Robot Time (s)	Marker	OTS Time	Robot Start Time	OTS Offset (s)	AGV Set (s)
1488990081	-1	1488990045	1488990089.959	44.959	1488990089.9447

Figure 96. Example time correspondence across the robot, OTS, and AGV files output from the Time Correspondence program.

6.3. Propagation of Uncertainty

Up to this point, previous sections have discussed the mobile base and the manipulator as independent systems and the mobile manipulator as the combined system of mobile base and manipulator. It is these two points that mathematically create the concept of propagation of uncertainty. In [175], are the guidelines for evaluating and expressing uncertainty. Specifically, the reference describes the law of Propagation of Uncertainty which is defined as follows:

- "In many cases a measurand, Y, is not measured directly, but is determined from N other quantities X_1, X_2, ..., X_N through a functional relation f:

$$Y = f(X_1, X_2, \ldots, X_N) \tag{12}$$

- Included among the quantities Xi are corrections for other sources of variability, such as different observers, instruments, samples, laboratories, and measurement times, (i.e., …not simply a physical law, but a measurement process…)
- The combined standard uncertainty of the measurement result y, designated by $u_c(y)$ and taken to represent the estimated standard deviation of the result, is the positive square root of the estimated variance $u_c^2(y)$ obtained from

$$u_c^2(y) = \sum_{i=1}^{N} \left(\frac{\partial f}{\partial x_i}\right)^2 u^2(x_i) + 2\sum_{i=1}^{N-1} \sum_{j=i+1}^{N} \frac{\partial f}{\partial x_i} \frac{\partial f}{\partial x_j} u(x_i, x_j) \quad . \text{"} \tag{13}$$

- Equation 13 is based on a first-order Taylor series approximation of Equation 12 including sensitivity coefficients ($\partial f/\partial x_i$) and covariance ($u(x_i, x_j)$).

Applying the propagation of uncertainty to the mobile manipulator performance, each of the components that are included in the propagation of uncertainty must be considered. As a preliminary action, the world reference, within which is a mobile base, manipulator, etc. should be measured. In this case, the mobile base must initially be provided to the vehicle controller as reference since the vehicle pose will only be as accurate as its reference. Similarly, it has been shown in previous research [25] and described in section 4.4, that a mobile base approaching the same point from various directions is relatively inaccurate as compared to approaching the point

from the same direction. Therefore, mobile base calibration is essential to enable higher accuracy and repeatability (i.e., lower uncertainty) for the mobile manipulator which references the manipulator base pose to the mobile base. Figure 97 shows a drawing of the mobile manipulator, its reference to the world through facility reflectors, and the performance measurement concept of using a laser-retroreflector carried by the manipulator to register to reflectors. When compiling the three vectors: 1) from the world to the mobile base, 2) from the mobile base to the manipulator base, and 3) from the manipulator base to the laser, a propagation of uncertainty [26] equates to a vector that simply points from the world to the laser as shown in the figure.

A typical method of measuring reflector locations in the world is to use a metrology system, such as a surveyor's tool (i.e., approximately 1.5 mm uncertainty over 1.5 km [27]) or a laser tracker (i.e., approximately 18 µm uncertainty over 12 m [13]). The authors chose the laser tracker so that the AGV reference to the world would be relatively more accurate. An onboard, spinning, navigation laser range and azimuth sensor then provides pose information to the vehicle controller. One issue (i.e., first major uncertainty point (AGV)) with the AGV control is that it uses the measured pose with respect to the world (facility reflectors) and the AGV control reference location is at floor level, at the vehicle centroid (i.e., beneath the vehicle). As such, this location is very difficult to use as a measurement reference.

The robot arm is mounted on a machined breadboard with 50.8 mm spaced, threaded holes and the robot arm is mounted to the breadboard with a machined interface plate. There is some uncertainty as to how accurately the breadboard is mounted with respect to the AGV reference point and causing a second uncertainty point (Manipulator Base). The third uncertainty point is the relative accuracy of EOAT pose of the carried laser that the robot arm is capable of providing.

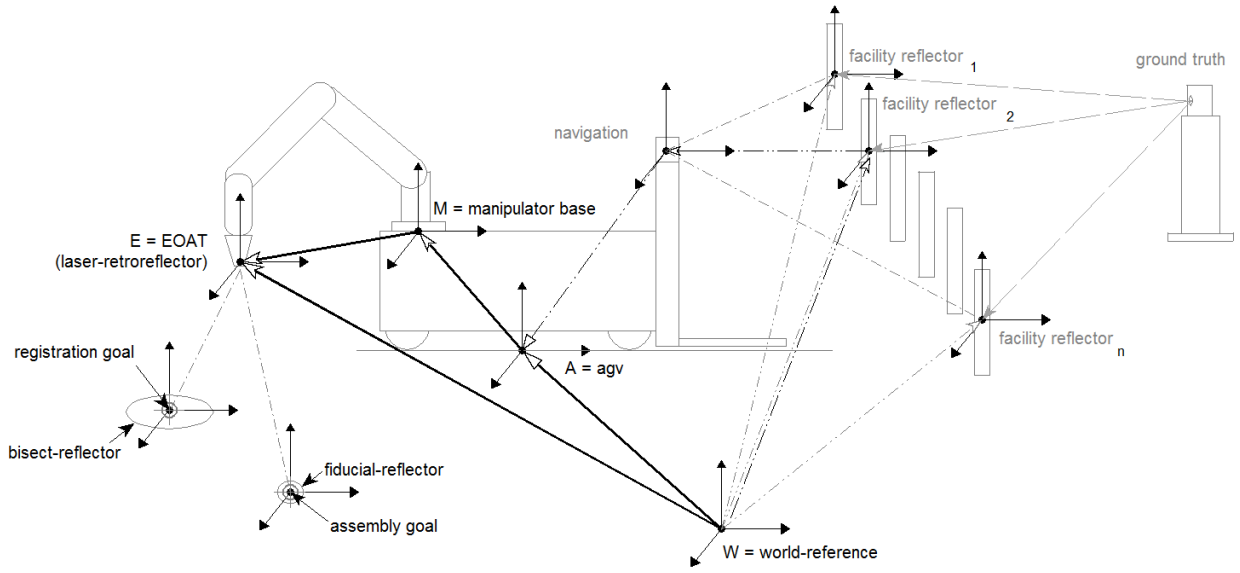

Figure 97. Drawing showing the uncertainty propagation for performance measurement of a mobile manipulator.

Figure 98 shows, using a SysML package diagram, blocks within packages of the world, mobile base, manipulator, and the RMMA for their associated components. Additionally, the end-of-arm-tool which carries the laser retroreflector is shown. The links between each of the blocks mimics the drawing in Figure 97 with the addition of a link from the RMMA to the world which, for verification of the RMMA location, was also measured with respect to the world reference frame used by the AGV. Within each block, values and constraints are also shown.

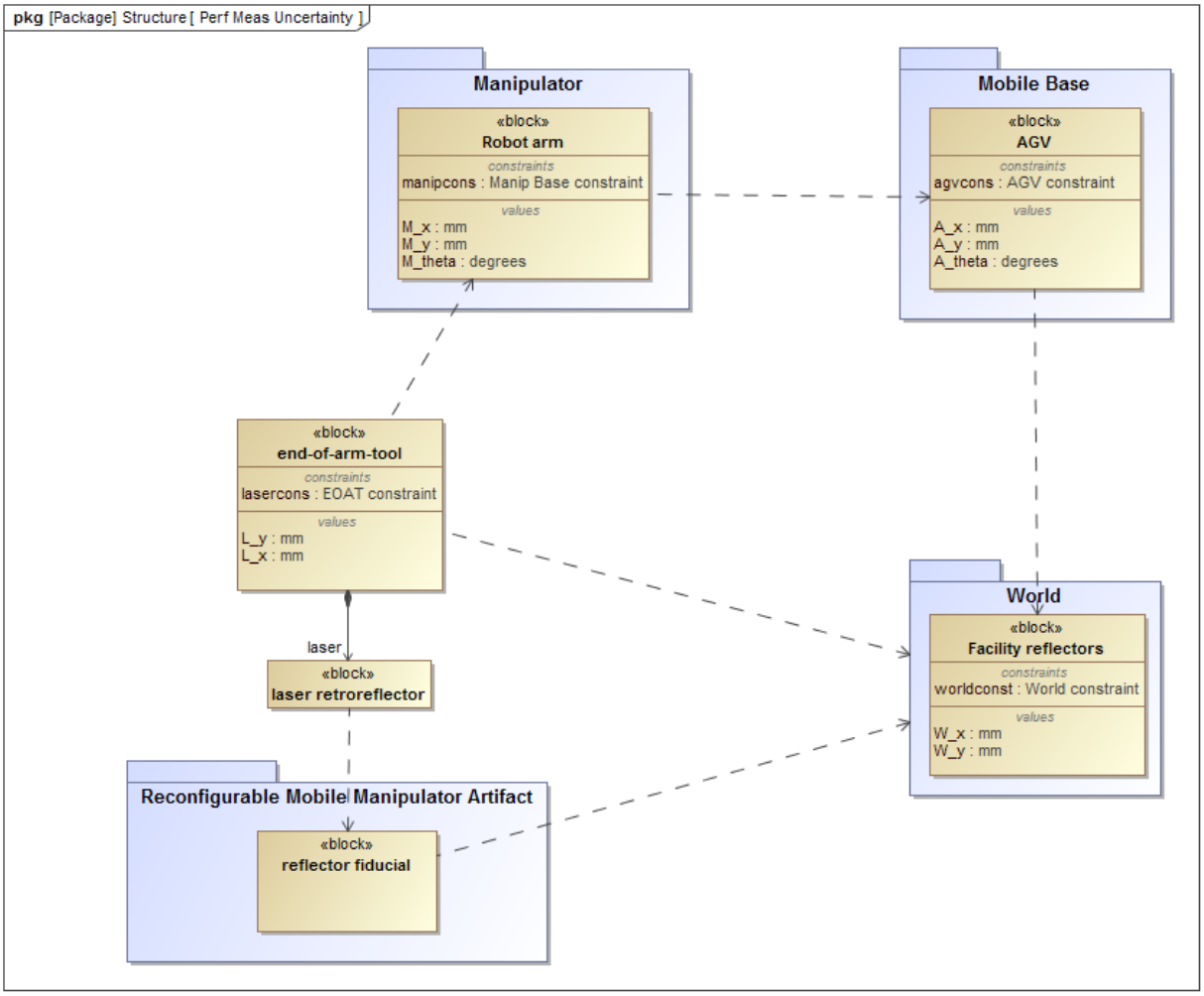

Figure 98. SysML package diagram showing the mobile manipulator and RMMA components that add to performance measurement uncertainty.

Each of the constraint labels (i.e., World, AGV, Manipulator Base, and EOAT constraints) can then be modeled in a block definition diagram, as shown in Figure 99, that allows each of their constraint parameters to be clearly displayed. Also, the parameters for each of the constraints is shown and the interconnect, that mimics the uncertainty propagation previously described, are also shown with the AGV, Manipulator Base, and EOAT all connected to the World constraint. This block definition diagram of constraints provides the basis for the parametric diagram shown in Figure 100. The parameters for each of the constraints and interconnects that produce the uncertainty propagation are shown in Figure 100 which can be described in the matrix equation:

$$ {}_{W}P_{E} = {}_{W}H_{A} * {}_{A}H_{M} * {}_{M}P_{E} \quad (14) $$

or

$$ \begin{pmatrix} X_E^W \\ Y_E^W \\ 1 \end{pmatrix} = \begin{pmatrix} \cos\Theta_A^W & -\sin\Theta_A^W & T_{X_A^W} \\ \sin\Theta_A^W & \cos\Theta_A^W & T_{Y_A^W} \\ 0 & 0 & 1 \end{pmatrix} \begin{pmatrix} \cos\Theta_M^A & -\sin\Theta_M^A & T_{X_M^A} \\ \sin\Theta_M^A & \cos\Theta_M^A & T_{Y_M^A} \\ 0 & 0 & 1 \end{pmatrix} \begin{pmatrix} X_E^M \\ Y_E^M \\ 1 \end{pmatrix} \quad (15) $$

$$ \begin{pmatrix} X_E^W \\ Y_E^W \\ 1 \end{pmatrix} = \begin{pmatrix} \cos\Theta_A^W & -\sin\Theta_A^W & T_{X_A^W} \\ \sin\Theta_A^W & \cos\Theta_A^W & T_{Y_A^W} \\ 0 & 0 & 1 \end{pmatrix} \begin{pmatrix} X_E^M\cos\Theta_M^A - Y_E^M\sin\Theta_M^A + T_{X_M^A} \\ X_E^M\sin\Theta_M^A + Y_E^M\cos\Theta_M^A + T_{Y_M^A} \\ 1 \end{pmatrix} \quad (16) $$

$$ \begin{pmatrix} X_E^W \\ Y_E^W \\ 1 \end{pmatrix} = \begin{pmatrix} \cos\Theta_A^W\,(X_E^M\cos\Theta_M^A - Y_E^M\sin\Theta_M^A + T_{X_M^A}) - \sin\Theta_A^W\left(X_E^M\sin\Theta_M^A + Y_E^M\cos\Theta_M^A + T_{Y_M^A}\right) + T_{X_A^W} \\ \sin\Theta_A^W\left(X_E^M\cos\Theta_M^A - Y_E^M\sin\Theta_M^A + T_{X_M^A}\right) + \cos\Theta_A^W\left(X_E^M\sin\Theta_M^A + Y_E^M\cos\Theta_M^A + T_{Y_M^A}\right) + T_{Y_A^W} \\ 1 \end{pmatrix} \quad (17) $$

where: P represents a 2D point, H represents a 2D homogeneous matrix, W = World, E = EOAT, A = AGV, and M = Manipulator. A SysML parametric diagram, not included here, can then be used to further display the equations within a model. If the RMMA were to be tilted to an angle other than parallel with the manipulator base, the point ${}_{M}P_{E}$ would change to a 3 x 3 homogeneous matrix ${}_{M}H_{E}$. Similarly, if the AGV reference was not parallel with the world reference, ${}_{W}P_{E}$ would change into a 3 x 3 homogeneous matrix ${}_{W}H_{E}$. In our case, the robot base height above the floor is relatively equal in height to the RMMA height thereby eliminating the need to include z in calculations.

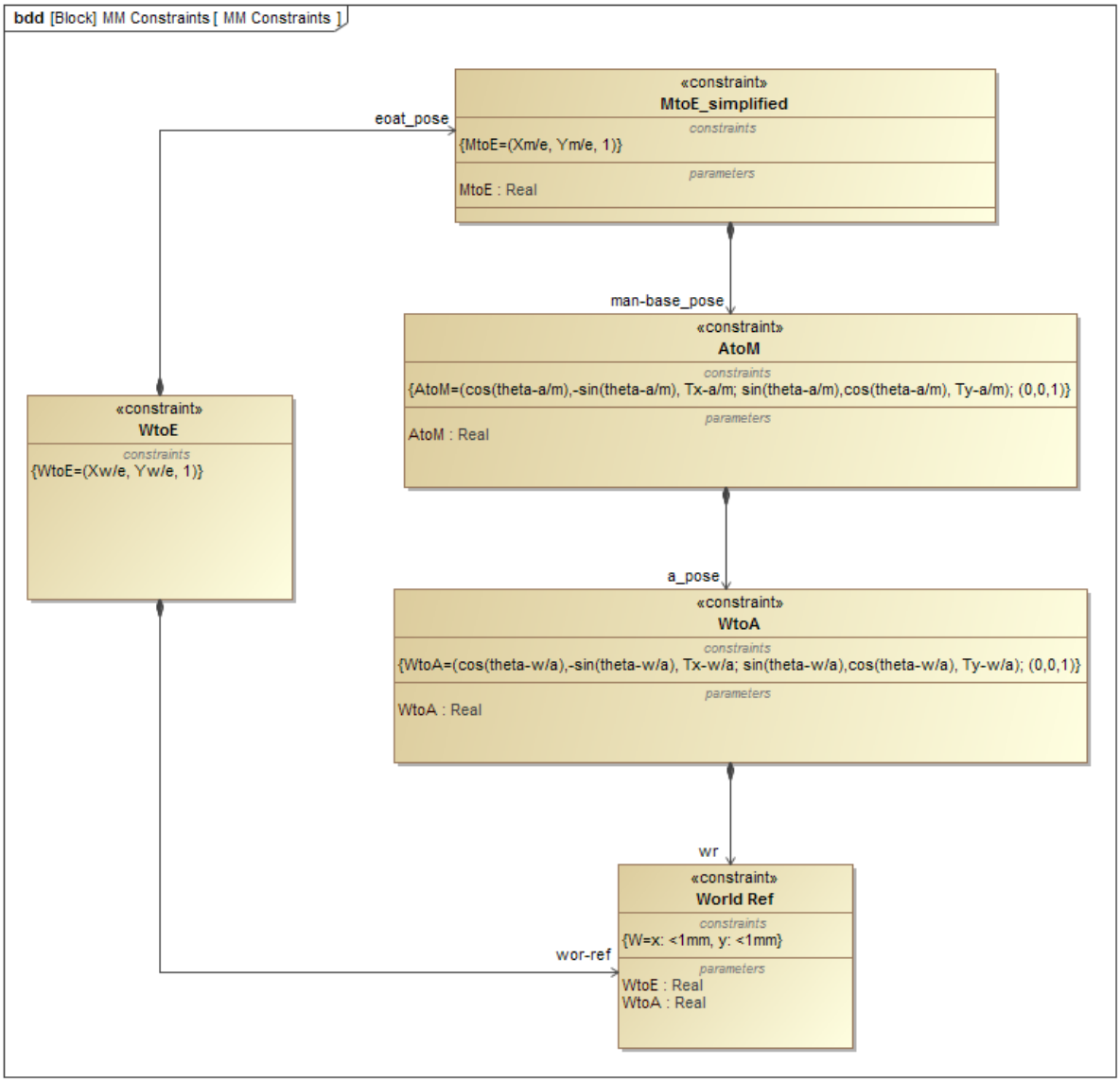

Figure 99. SysML block definition diagram applying equation 15 showing the constraints for the AGV, Manipulator Base, and EOAT that reference to the World constraint.

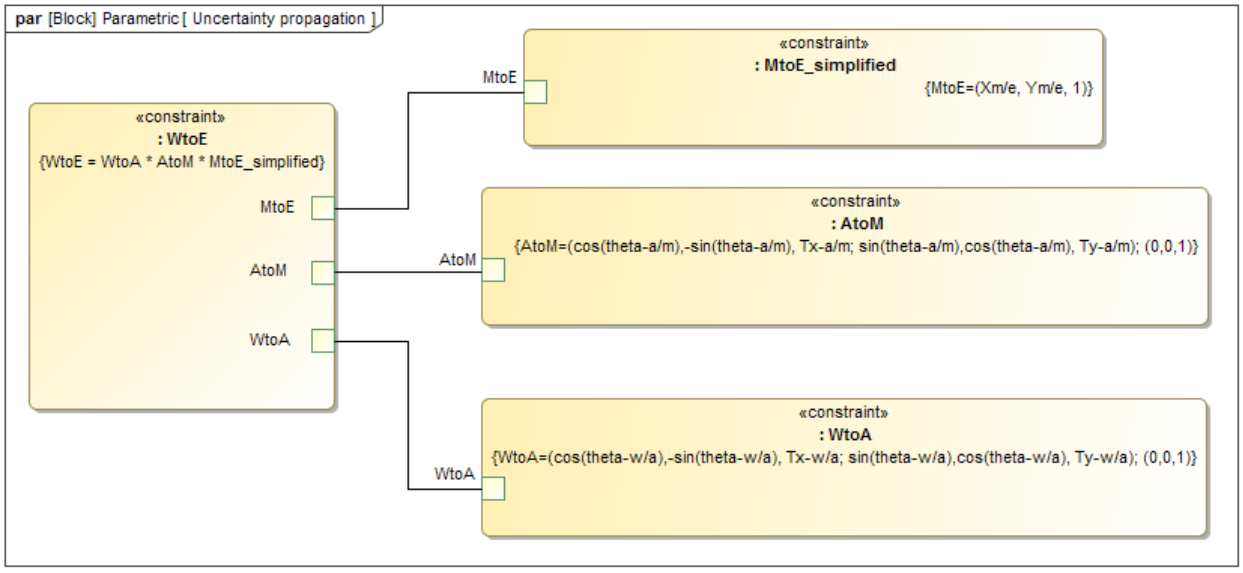

Figure 100. SysML parametric diagram showing the uncertainty propagation for a mobile manipulator.

The parametric diagram describes the mathematical equation of the uncertainty propagation transformation from the world to AGV, the AGV to the manipulator base, and manipulator base to the laser. Because of the difficulty to measure from the AGV reference location to the manipulator base ${}_{A}H_{M}$ and from the world reference to the EOAT ${}_{W}P_{E}$, they are considered unknowns.

6.4. Performance Measurement of Mobile Manipulators Use Case

This section describes the application of the mobile manipulator performance measurement concept using the RMMA. Figure 101 shows a SysML use case diagram [160] modeling the process that represents a production facility where a mobile manipulator is: systematically sent from the production area to a calibration area (MM (mobile manipulator) System and Measurement Systems package), adjusted upon calibration (violet task), and then returned to 'Continue normal production operations'. To be thorough, the addition of the three actors (with blue heads) were also needed to perform tests during the author's experimental research. The parallel tracks for the optical tracking system (green tasks) and the use of the RMMA (yellow tasks) provide comparable methods. Both systems, as explained in sections 3.2.1 and 3.2.2, are useful measurement methods and are dependent upon the stakeholder's requirements for mobile manipulator accuracy and cost. One or the other would be chosen as the ideal measurement method while simplifying the use case models by removing method not chosen.

In the research use case, not only are the initial number of operators increased to perform the research experiments, there is no initial optical tracking power-on nor mobile manipulator power-on to steady state tasks and after adjustment of the mobile manipulator to peak performance, there is no return of the system back into production as is shown in Figure 101. It is also expected that the 'Adjust MM (mobile manipulator) parameters based on performance tests' task would be

performed automatically for the in-situ use case in Figure 101 and may be either manually or automatically adjusted for the research experiment case.

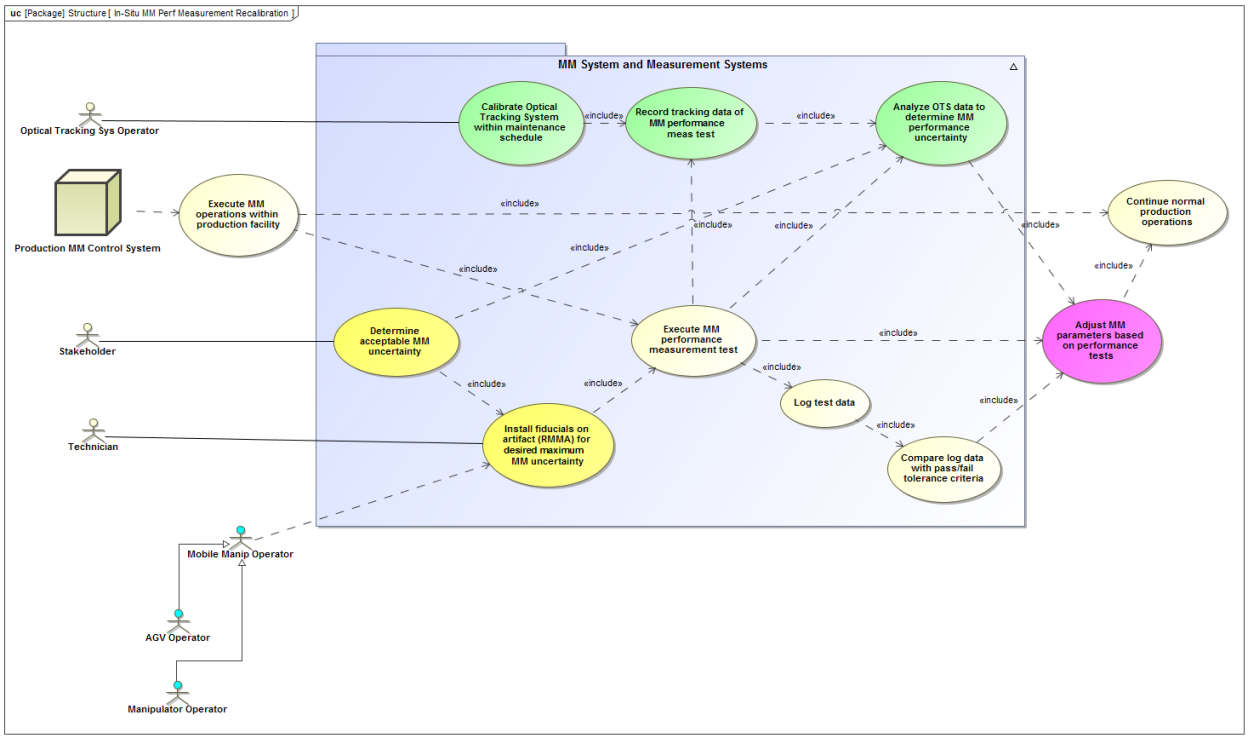

Figure 101. SysML use case diagram of an optical tracking system (green tasks) in parallel with the RMMA (yellow tasks) used to measure performance of a mobile manipulator as may be found in a production facility during operation. The addition on the three blue head actors were required during research and are not required for a production case.

6.5. Conclusions

Three manipulator base positioning methods by the mobile base were described including: static, index, and dynamic. Static allows the manipulator to reach all target locations. Index allows the manipulator to reach all locations by moving the manipulator base by the mobile base to poses within the manipulator work volume. Dynamic allows the manipulator to reach all target locations with simultaneous mobile base motion and this method is left for future research since it is less useful to current applications (e.g., peg-in-hole assembly) than static and index. However, a second RMMA was produced for when this concept becomes more useful. Static and index control methods were described.

Mobile manipulator registration methods were then described narrowing in on the search methods typically used for assembly. The alignment of the laser retroreflector to a fiducial reflector is similar to robot assembly where an EOAT staging point above the target is typical prior to part insertion/extraction. Fine search methods were discussed and the circular and square search methods were programmed into the manipulator control for experimentation. However, the RMMA concept is versatile where any search method could be used. Due to long search times resulting from high uncertainty AGV pose, an additional search registration method, called the Bisect with Fine Search Method, was developed and then used during this thesis research.

Several experiments the tested the circular and square search methods and the bisect with fine search method. Results are shown in Table 23. Clearly, using only the fine search causes good detection results but with a large search time. Alternatively, including a bisect on a large reflector that is larger than the overall system uncertainty, the search time dramatically lowers and the success rate improves. When using the bisect method prior to the fine search, the total bisect plus fine search steps/time was a maximum of 184 steps/86 s or nearly 90% less time than using only the fine search method.

To allow other researchers to develop better search methods, control schemes, etc., data sets were published and are available for download from NIST. A final experiment was performed by NIST researchers with participation by the author of this thesis using augmented reality software, tags and a camera. The results are promising as a comparable registration method to the laser method. However, tradeoffs are that relatively rapid registration can occur with AR although through use of a relatively high resolution camera costing potentially more than the laser retroreflector and more complex software algorithms.

Table 23. Summary of experimental results for measuring the performance of a mobile manipulator.

Experiment	Setup Parameters	Results
1	Square pattern of fiducials	
	Four 6.3 mm fiducials	
	Circular fiducial search	
	3.1 mm diameter x 15^0 increment step search for fine search	
	Metric: registration, detect/non-detect, time, repeatability	
	average success rate	28%
	average search time/steps	78 s/159 steps
2	Square pattern of fiducials	
	Two 1 mm fiducials	
	3 mm fiducials for two remaining square fiducials	
	Square fiducial search	
	0.5 mm step search for fine search	
	Metric: registration steps/time, detect/non-detect, repeatability	
	average success rate	91%
	average search time/steps	397 s/794 steps
3	Square and circle pattern of fiducials	
	Large bisect fiducials	
	3 mm step search for bisect	
	Two 1 mm fiducials on each pattern	
	6 mm diameter fiducials for two remaining square pattern fiducials and 3 mm fiducials for all remaining circle fiducials	
	Square fiducial search	
	0.5 mm step search for fine search	
	Metrics: registration, detect/non-detect, repeatability	
	average success rate	99%
	average search time/steps	310 s/621 steps
4	Square and circle pattern of fiducials	
	Large 30 mm diameter, large prism, bisect fiducials	
	3 mm step search for bisect	
	Two 1 mm fiducials on each pattern	
	3 mm fiducials for all remaining square and circle fiducials	
	Square fiducial search	
	0.5 mm step search for fine search	
	Metric: registration steps/time, detect/non-detect	
	average success rate	92%
	average search time/steps	6 s/11 steps
5	Square and circle pattern of fiducials	
	Large 42 mm diameter, micro-prism, bisect fiducials	
	1 mm step search for bisect	
	Two 1 mm fiducials on each pattern	
	3 mm fiducials for all remaining square and circle fiducials	
	Square fiducial search	
	0.5 mm step search for fine search	
	Metrics: registration, detect/non-detect, repeatability	
	average success rate	98%
	average search time/steps	not recorded
6	Square and circle pattern of fiducials	
	Large 42 mm diameter, micro-prism, bisect fiducials	
	1 mm step search for bisect	
	Two 1 mm fiducials on each pattern	
	2 mm fiducials for all remaining square and circle fiducials	
	Square fiducial search	
	0.5 mm step search for fine search	
	Metrics: registration, detect/non-detect, repeatability	
	average success rate	96%
	average search time/steps	0.8 s/1.8 steps

As described in chapters 4 through 6.2.3 Experiments, there is uncertainty in the independent systems that make up the mobile manipulator as a system. And as uncertainties are within each subsystem, they can add to form a greater uncertainty for the combined mobile manipulator system. The propagation of uncertainty was referenced, described, and generically modeled for the use of the RMMA. Mathematical equations describe the uncertainties in a generic way through matrix mathematics and SysML modeling to provide theoretical basis for the performance measurement of mobile manipulators.

Lastly, a use case for the performance measurement of mobile manipulators was shown in a SysML model and described. The use case modeled provides a scenario that allows mobile manipulator measurement in a parallel process to the assembly process whereby periodic system performance can be measured and fed back into the production system for known system uncertainty.

7. THESIS CONTRIBUTIONS AND FUTURE WORK

The objective of this thesis research was to address a currently non-existent research and implementation area - to measure the performance of mobile manipulators. The following summary describes the research performed to address this new critical area. Also, the research described provides additional work beyond this thesis research extending to even more complex measurements of performance, standards, and even cross-industry extension of mobile manipulator performance measurement methods to exoskeletons worn by humans. Some of this work is already being considered as this thesis author attempts to expand the use of the research described herein.

7.1. Summary of Thesis Contributions

An advanced approach to flexible manufacturing is to move robotic manipulators, using an AGV or mobile robot, called mobile manipulators, between workstations. The use of mobile manipulators can be advantageous in a number of situations. It can result in cost savings when a single mobile manipulator can be used to replace several stationary manipulators. Expert researchers reported in 2005: "Autonomous mobile manipulation is a relatively young discipline within robotics." [66] An extensive literature review of the research leading to commercial mobile manipulators and mobile robots was performed. The performance measurement of mobile manipulators, including a mobile base with an onboard robot arm, is virtually non-existent. However, mobile manipulators are beginning to appear in manufacturing, healthcare, and possibly other industries and therefore, a method to measure their performance is critical to both manufacturers and users of these relatively complex systems. Measurements of mobile manipulators performing standard tasks (poses and motions) are also non-existent except for simply ensuring that the task has been more or less completed. The task chosen for this thesis case is assembly due to its requirement for relatively precise system posing. Peg-in-hole insertion was demonstrated by Hamner et al. [5], and other mobile manipulators were demonstrated by Aalborg University [68], [69], Flannigan [70], and several others, although the focus was mainly on control strategies and completing tasks instead of the performance measurement itself.

The literature also described the unified motion of the mobile manipulator treating the two component (mobile base and manipulator) as one. Further on control research, trajectory planning, optimizing the system configuration were also researched. And the aspects of tasking by performing multiple tasks, being stable, avoiding obstacles, and even using mobile manipulators outdoors was also surveyed providing a broad perspective of these complex systems. However, performance measurements still lag in the research with few papers on calibration where Elatta et al. [128] only discusses the mathematical model of the mobile manipulator and Greenway [130] discusses string-pull and laser-based measurement systems, although string-pull is a cumbersome, in-flexible method and the laser system used was based on laser tracking, a relatively expensive measurement technique. Attempts at using sensors combined with the mobile manipulator were also researched but, provide even more complexity to the system being measured.

Performance test methods have lagged behind safety test methods for mobile manipulators which is progressing towards development of a new safety standard in the US [16]. Metrics for safety

and performance of mobile manipulators include many areas, such as: safe operation, task completion, time to complete the task, quality, and quantity (i.e., accuracy and repeatability, respectively) of tasks completed. Prior to industrial acceptance and standards development for mobile manipulators, users of these new systems will expect manufacturers to provide real performance data to guide their procurement and assure suitability for given application tasks. Motion capture systems are useful and as measured in this thesis research, provide appropriate ground truth measurement for the thesis case. Due to the relatively high cost to procure and setup motion tracking systems to measure systems performance, an alternative method for use by manufacturers and users is ideal. A new test method concept that uses an artifact, called the Reconfigurable Mobile Manipulator Artifact (RMMA), was described in this thesis and compared to an optical tracking system (OTS) that was used as ground truth for the RMMA and mobile manipulator. Research for performance measurements of robot arms, mobile bases and mobile manipulators is again minimal in the literature mainly discussing task-based measures (i.e., completion of tasks).

The complexity of the mobile manipulator, which typically has at least nine degrees-of-freedom, can be difficult to comprehend and is compounded by the many control languages used today. System modeling the mobile manipulator system, components, and the associated measurements can help to improve the understanding of system complexity. Just as there is a need for a standard performance measurement test method for measuring mobile manipulators, there should also be a standard robot modeling and control language for use within the test method. Systems Modeling Language (SysML) was chosen and used throughout this thesis because SysML has reusable software modules for structure, behavior, requirements, and parametrics of the mobile manipulator. Modeling the application domain, as Rahman, et al. [158], in this case performance measurement of mobile manipulators, shows the flexibility of SysML describing the many perspectives of the modeling language. Shown in this thesis were package, block definition and internal block diagrams, activity and sequence diagrams, and parametric and use case diagrams that fully describe the application with detail or generality to apply to other mobile manipulators.

Two measurement systems were modeled using SysML showing their interconnected components, - the OTS and the RMMA. OTSs measure the 3D, static and dynamic pose of multiple markers attached to objects within a measurement space and is ideally suited for measuring mobile manipulators. Prior to using the OTS for these measurements, the OTS was measured with a new method of using an artifact to determine the OTS capability for use as ground truth to other measurements. The concept was accepted to be standardized in ASTM E3064 where the system used in this thesis has a static measurement uncertainty of 0.022 mm and 0.046° and dynamic measurement uncertainty of 0.26 mm and 0.20°. The RMMA concept includes posing a mobile manipulator next to an artifact as well as posing the EOAT attached to the manipulator at specific locations above the RMMA to digitally detect reflective fiducials with known uncertainty. The performance evaluation criteria can include the:

- Time to register the mobile manipulator to the artifact
- Time to move from the registration points to the assembly points
- Repeatability after registration
- Number of search steps equating to the initial distance from registration/assembly points
- Detection of reflectors with varying diameters

The reflector material itself is critical as is the movement of the AGV, manipulator, RMMA, when they are statically posed for measurement, although the uncertainty can be greatly decreased by delaying the measurement allowing the system to reach a steady state.

The mobile base, whether an AGV or mobile robot, is relatively complex in components that make up the mobile base, as well as its performance. The mobile base SysML internal block diagram model of the AGV described in this thesis shows the interconnect of the AGV components as a generic model describing passing signals, reference to system constraints (e.g. AGV and Facility reflectors) and the vehicle itself, and the internal controller (AGVBrain) that inputs and outputs the signals for expected vehicle performance. The same model for the AGV can be readily extended to the mobile robot or any other autonomous industrial vehicle since the components are similar. Differing among systems are the referenced, designated by the dashed boxes, AGV and Facility reflectors constraints that can be changed to match the mobile base being modeled. Due to the AGV potential uncertainties, measurements describing its performance were required and performed, including: calibration; navigation, docking, and stability performance; and obstacle avoidance. The OTS system can aid in these measurements towards calibration. However, more cost effective manual methods can also provide appropriate calibration. Hence, a method for calibrating an AGV with multi-wheel steering was developed and implemented providing an order of magnitude better AGV performance. AGV navigation and docking performance measurements experiments were conducted using simple, geometrical, path-navigation experiments. Results show path deviation from commanded paths. Analysis of the AGV tracked data as compared to ground truth system data shows that the AGV could track to within approximately 3 mm and 5 mm uncertainty, for both the circle and square navigation tests, while moving at 0.25 m/s. Uncertainty in docking improved to 5 mm for the calibrated AGV tests. Stability of the mobile base, AGV or advanced mobile base (i.e., mobile robot), was shown to be affected by onboard manipulator motion, to approximately 0.15 mm in X and 0.25 mm in Y for a relatively heavy AGV. The test method was extended to the lighter mobile robot resulting in approximate uncertainty of 2.5 mm in X and 2.8 mm in Y.

Performance measurement for robot arms has been standardized in ISO 9283:1998 [44] with no suggested improvements from the world over nearly 20 years. A SysML internal block diagram was developed to include the robot arm controller, manipulator controller-offboard, as used for this thesis research, and robot arm. Precision measurements of the robot arm were required since the specified uncertainty was ± 1 mm repeatability and the measured uncertainty was approximately 0.6 mm. However, the angular offset to the AGV varied from 1.28° to 2.18° and when the associated pose offset angles were applied to the translational measurements, offset error from a 457.2 mm square pattern was between 0.32 and 4.67 mm.

A critical component of the mobile manipulator performance description is the manipulator-to-mobile base adjustment determination, where a manual calibration method, a calibration method using Ceres Solver, and a closed-form vs. iterative solution method were described and evaluated. The Ceres Solver method proved to be a valuable tool in calibrating a variety of hard to measure constants. The main issues that were observed are that the Ceres Solver model cannot be either

over or under constrained to allow proper convergence. The manual calibration method generated a base offset of (x = 831.5, y = - 7.5) mm and a rotation of 90.6°, yielding a mean square error of 1.25 mm and a maximum residual of 6.3 mm. The Ceres Solver showed an offset of (x =833.637, y = -8.22) mm and a rotation of 90.53°, yielding a mean square error of 1.19 mm and a maximum residual (cost function) of 10.7 mm. Shah, et al. [230] then used data from this thesis research to develop closed-form solutions for the offset between the manipulator base and the AGV by constructing a robot-world/hand-eye calibration problem AX = YB. Uncertainty was calculated to be 0.09 mm for the iterative solution and 0.04 mm for the closed form solution.

Three manipulator base positioning methods by the mobile base were described including: static, index, and dynamic. Static allows the manipulator to reach all target locations. Index allows the manipulator to reach all locations by moving the manipulator base by the mobile base to poses within the manipulator work volume. Dynamic allows the manipulator to reach all target locations with simultaneous mobile base motion and this method is left for future research since it is less useful to current applications (e.g., peg-in-hole assembly) than static and index. However, a second RMMA was produced for when this concept becomes more useful. Static and index control methods were evaluated in this thesis.

Mobile manipulator registration methods, using fine search and bisect with fine search, were then described. The alignment of the laser retroreflector to a fiducial reflector is similar to robot assembly where an EOAT staging point above the target is typical prior to part insertion/extraction. The RMMA concept is versatile such that any search method could be used. Due to long search times resulting from high uncertainty AGV pose, the bisect with fine search was developed and then tested. Several experiments tested the circular and square search methods and the bisect with fine search method. Results clearly showed that using only the fine search causes good detection results but with a large search time. Alternatively, including a bisect on a large reflector that is larger than the overall system uncertainty, the search time dramatically lowers and the success rate improves. When using the bisect method prior to the fine search, the total bisect plus fine search steps/time was a maximum of 184 steps/86 s or nearly 90% less time than using only the fine search method. Augmented reality registration also shows promise as an alternative to using the laser retroreflector method. However, tradeoffs are that relatively rapid registration can occur with AR although through use of a relatively high resolution camera costing potentially more than the laser retroreflector and more complex software algorithms.

As described in this thesis, there is uncertainty in the independent systems that make up the mobile manipulator as a system. And as uncertainties are within each subsystem, they can add to form a greater uncertainty for the combined mobile manipulator system. The propagation of uncertainty was referenced, described, and generically modeled for the use of the RMMA. Mathematical equations describe the uncertainties in a generic way through matrix mathematics and SysML modeling to provide theoretical basis for the performance measurement of mobile manipulators. Lastly, a use case for the performance measurement of mobile manipulators was shown in a SysML model and described. The use case modeled provides a scenario that allows mobile manipulator measurement in a parallel process to the assembly process whereby periodic system performance can be measured and fed back into the production system for known system uncertainty.

Associated adjustments to the production process can then be performed or at a minimum, mobile manipulator uncertainties can be equated to the production time to allow comparison of effects on products made between scheduled performance measurements.

7.2. Beyond This Thesis

7.2.1. Non-horizontal RMMA Performance Measurement of Mobile Manipulators

This thesis described the concept of using the RMMA as a tool for measuring performance of mobile manipulators tasked for assembly applications. As described in section 4.1.2, the RMMA is capable of being raised, lowered, and tilted to match more complex assembly scenarios that may occur in real factory environments. Therefore, a future task beyond this thesis is to measure mobile manipulators using these more complex RMMA configurations. Raising and lowering the RMMA may be a simple extension of this thesis research whereby the manipulator would simply be given a higher or lower Z-axis value to achieve, potentially without dramatic changes to system performance. However, rotating the RMMA to angles other than horizontal will force manipulator wrist and perhaps other joint rotations that did not occur in this thesis research. Hence, the complexity will dramatically extend this thesis research using the same artifact and test methods.

7.2.2. Dynamic Performance Measurement of Mobile Manipulators

Extending the efforts described in this thesis, especially section 6.2.3, the author recommended that NIST provide a grant to develop dynamic mobile manipulator performance measurement. The grant was provided to Marquette University in 2016. To the date of this thesis, Marquette had developed: initial theory, mobile manipulator control algorithms using the Fine Search Method described in this thesis, and had initially simulated dynamic performance measurement and physically demonstrated index performance measurement, with a 1/3rd scaled, relatively inaccurate, mobile manipulator and mock RMMA-2. Much of this early research is described in [249]. Figure 102 (a) shows their simulation that receives manipulator move commands to each fiducial position, spiral searches, and upon fiducial detection, the mobile base moves (in this case slides) to the next location while measuring motion-planning time for the mobile base.

Figure 102 (b) shows a stationary spiral search evaluation using the proof-of-concept platform towards dynamic mobile manipulator performance measurement by Marquette University. In their experiment, the mobile manipulator was positioned so that the laser beam was approximately orthogonal to the ground plane and 20 cm away from the fiducial marker under consideration. They similarly used the OTS (upper right corner) to qualitatively evaluate the spiral search procedure with a proof-of-concept platform (white boxes with reflectors on top). For this early step, a mock-up artifact was used instead of the 3D printed RMMA to facilitate robot alignment and marker position reconfiguration. Figure 102 (c) trajectory of the end effector as observed by the optical tracking system for one run of the experiment. Although in this experiment the based was stationary during each search (i.e., the index test), the platform successfully performed the spiral search at each of the locations and eventually localize the markers. As indicated in the figure, although the trajectory is somewhat noisy due to physical limitations of the proof-of-concept platform, the spiral search was successfully executed.

Marquette is planning to demonstrate the dynamic performance measurement method. They also plan to procure the Lynx mobile robot and UR5 to duplicate the authors-described, NIST mobile manipulator (see Figure 57 (a, c, e)) and to demonstrate relatively increased accuracy, dynamic performance measurement using a full-scale RMMA-2.

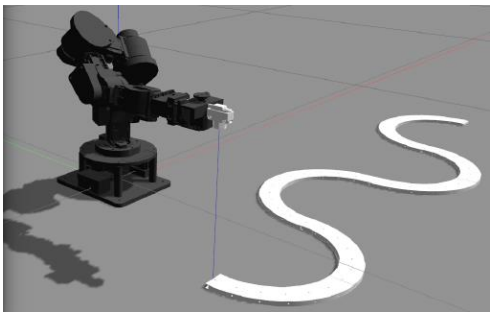

a

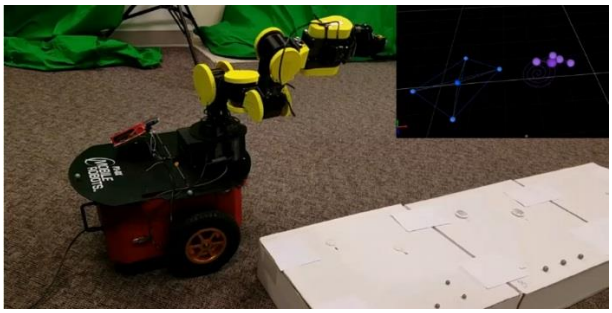

b

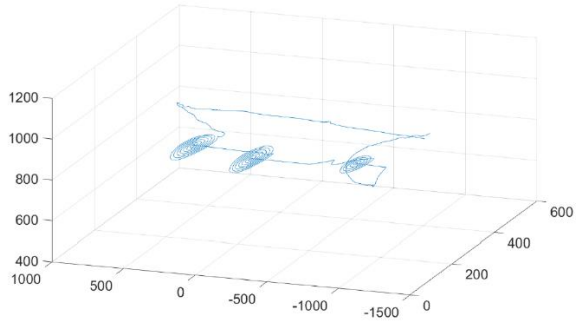

c

Figure 102. (a) Gazebo simulation snapshot of the Marquette dynamic mobile manipulator performance measurement. Note the sinusoidal markers on the ground. (b) Snapshot of the spiral search evaluation using the proof-of-concept platform towards dynamic mobile manipulator performance measurement by Marquette University. (c) Plotted trajectory of the end effector as observed by the optical tracking system in an experiment.

7.2.3. Standards

ASTM F45.02 has also started working document WK57000 [250] on docking industrial vehicles with the environment. Nearly, if not all, vehicles require navigation followed by docking with varying types of precision. The author proposed [251] the generic docking method described in Section 4.4.1 and shown in Figure 46. The standard concept would be to provide a test method to measure the mobile base docking accuracy and repeatability. Extended from this concept is to apply the research from this thesis into docking onboard equipment, such as a manipulator, with an apparatus, such as the RMMA. The concept is proposed as a follow-on to the current working document effort.

7.2.4. Cross-Industry Test Methods – Wearable Robots

Wearable robots or passive exoskeletons that allow human arms to move and hold tools for longer periods of time at intended locations could be measured using the RMMA. [252] The human can instead, carry a laser retroreflector or insert pegs in holes on such an artifact using a variety of geometric patterns and RMMA configurations. Also, similar to the mobile manipulator, as shown

in Figure 1 (b), fiducials detectable by an optical tracking system can measure the wearable robot motion if higher precision measurement data is required. This fine motion detection data can be used to further refine wearable robot motor tuning.

Figure 103 depicts the same RMMA, previously described for measuring performance of industrial robot arms and mobile manipulators, being used to measure the performance of an exoskeleton. The figure shows a human wearing arm exoskeletons and aligning a laser retroreflector to reflectors. The same RMMA could instead include holes in which the human could insert pegs or screws as potentially required for precision assembly applications. The RMMA is shown in Figure 103 (a) horizontal, (b) vertical-low, (c) vertical-high, and (d) over-head-angled configurations.

Both navigation and docking can be combined for full-body exoskeleton (i.e., legs and arms) access and dexterity tests. For example, the human in exoskeleton would repeatedly move from a different location to the RMMA, similar to tests for the mobile manipulator. Once at the RMMA, the same docking test would be administered. The results of this test could show the time for a human, wearing leg and arm exoskeletons, to repeatedly move to and be positioned to reach the RMMA (using leg exoskeletons) followed by the time to transition from full-body motion to arm-only motion (using arm exoskeletons) when controlled by the exoskeleton.

Dynamic tests can also be administered with the RMMA moving relative to the human and the same alignment task performed as previously described. Additionally, both the human with exoskeleton and RMMA can be moving while alignment or peg insertion tasks are performed.

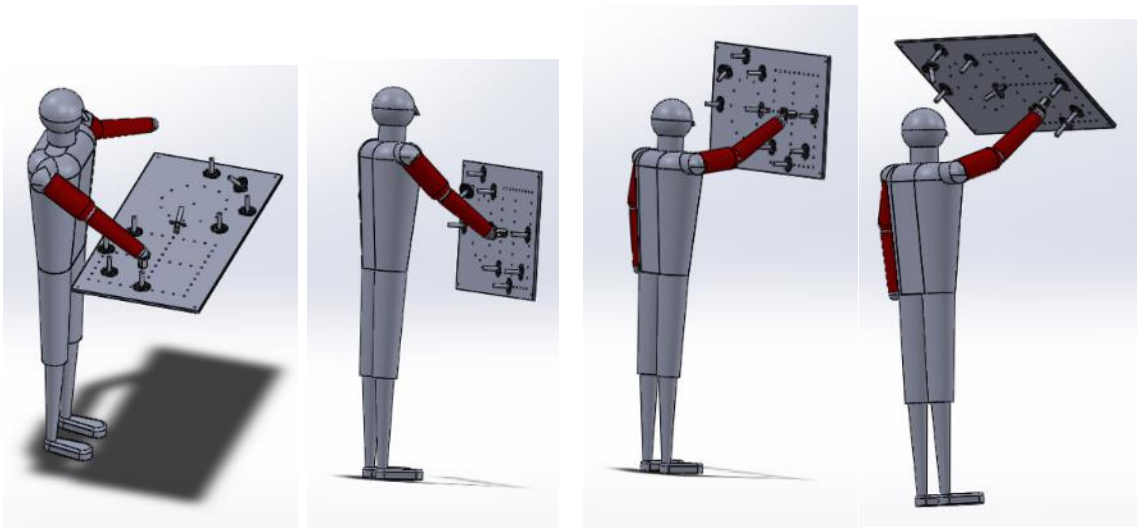

a b c d

Figure 103. Graphics of a human wearing arm exoskeletons (red) testing its performance using the RMMA for precision assembly applications when the RMMA is in (a) horizontal, (b) vertical-low, (c) vertical-high, and (d) overhead-angled configurations.

8. BIBLIOGRAPHY

[1] B. Hamner, S. Koterba, J. Shi, R. Simmons, and S. Singh, “Mobile robotic dynamic tracking for assembly tasks,” IEEE/RSJ International Conference on Intelligent Robots and Systems, pp. 2489-2495, 2009.

[2] R. Bostelman, T. Hong, and G. Cheok, "Navigation Performance Evaluation for Automated Guided Vehicle," 2015 IEEE International Conference on Technologies for Practical Robot Applications (TePRA), pp. 1-6 , 2015.

[3] R. E. Mandapat, “Development and evaluation of positioning systems for autonomous vehicle navigation,” Florida University Gainesville Center for Intelligent Machines and Robotics, pp. 1-277, 2001.

[4] A. Kelly, B. Nagy, D. Stager, and R. Unnikrishnan, "Field and service applications an infrastructure free automated guided vehicle based on computer vision an effort to make an industrial robot vehicle that can operate without supporting infrastructure." IEEE Robotics & Automation Magazine, pp.24-34, 2007.

[5] B. Hamner, S. Koterba, J. Shi, R. Simmons, and S. Singh, “An autonomous mobile manipulator for assembly tasks,” Autonomous Robot, pp.131-149 , 2010.

[6] J. Vannoy and J. Xiao, “Real-time Adaptive Motion Planning (RAMP) of mobile manipulators in dynamic environments with unforeseen changes,” in IEEE Trans. on Robotics, pp.1199-1212 , 2008.

[7] H. Martínez-Barberá and D. Herrero-Pérez, "Autonomous navigation of an automated guided vehicle in industrial environments." Robotics and Computer-Integrated Manufacturing, pp.296-311, 2010.

[8] R. C. Arkin and R. Murphy, "Autonomous navigation in a manufacturing environment," IEEE Transactions on Robotics and Automation, pp.445-454 ,1990.

[9] H. F. Durrant-Whyte, "An autonomous guided vehicle for cargo handling applications." The International Journal of Robotics Research, pp.407-440, 1996.

[10] S. Bøgh, M. Hvilshøj, M. Kristiansen, and O. Madsen, "Autonomous industrial mobile manipulation (AIMM): from research to industry." In 42nd International Symposium on Robotics. Pp. 1-9, 2011.

[11] M. Shneier and R. Bostelman, “Literature Review of Mobile Robots for Manufacturing,” NIST Internal Report #8022, 2014.

[12] “Yaskawa Motoman MH80 robot unloading trucks - from Wynright Corporation,” http://www.youtube.com/watch?v=8wngL0BnF_4, June 18, 2013.

[13] E. Guizzo, “Meka Robotics, Announces Mobile Manipulator With Kinect and ROS,” http://spectrum.ieee.org/automaton/robotics/humanoids/meka-robotics-announces-mobile-manipulator-with-kinect-and-ros, 16 Feb 2011.

[14] T. Green, “KUKA Falls First, Buys Swisslog for $335M. Who’s Next?,” Robotics Business Review, Sept 29, 2014.

[15] Marvel, Jeremy A., and Roger Bostelman. "Test Methods for the Evaluation of Manufacturing Mobile Manipulator Safety." Journal of Robotics and Mechatronics Vol. 28.2 (2016), pp 199-214.

[16] Machinery Safety Standards-ANSI B11, “RIA 15.08”, http://b11standards.org/event/2017/2/28/ria-1508, accessed May 2017.

[17] E. Saggini, E. Zereik, M. Bibuli, G. Bruzzone, M. Caccia and E. Riccomagno, “Performance Indices for Evaluation and Comparison of Unmanned Marine Vehicles' Guidance Systems,” 19th World Congress The International Federation of Automatic Control Cape Town, South Africa. August 24-29, 2014.

[18] F. Lizarralde, J. T. Wen and L. Hsu, "Quaternion-based coordinated control of a subsea mobile manipulator with only position measurements." Proceedings of the 34th IEEE Conference on Decision and Control, vol. 4, pp. 3996-4001. IEEE, 1995.

[19] E.J. Van Henten, B.A.J. Van Tuijl, J. Hemming, J.G. Kornet, J. Bontsema and E.A. Van Os, “Field Test of an Autonomous Cucumber Picking Robot,” Biosystems Engineering 86 (3), 305–313, 2003.

[20] B. Hannaford, L.Wood, D. McAffee and H. Zak. "Performance evaluation of a six-axis generalized force-reflecting teleoperator." Systems, Man and Cybernetics, IEEE Transactions on 21, no. 3: 620-633, 1991.
[21] W. Miksch and D. Schroeder, "Performance-Functional Based Controller Manipulator Design for a Mobile," Robotics and Automation, 12-14 May 1992.
[22] Daniel Konderman, "Ground Truth Design Principles, An Overview" VIGTA '13, St. Petersburg, Russia, July 15, 2013.
[23] Albus JS (2002) Metrics and performance measures for intelligent unmanned ground vehicles. In Proceedings of the Performance Metrics for Intelligent Systems (PerMIS) Workshop (National Institute of Standards and Technology, Gaithersburg, MD).
[24] Hägele M, Pfeiffer K (2007) Report on State of the Art on Benchmarks for Mobile Manipulation and Service Robots (Fraunhofer IPA), RoSta Deliverable D 4.1.
[25] Edan Y, Friedman L, Mehrez A, Slutski L (1998) A three-dimensional statistical framework for performance measurement of robotic systems. Robot Cim-Int Manuf 14(4):307-315. http://dx.doi.org/10.1016/S0736-5845(98)00006-4
[26] Wong SC, Middleton L, MacDonald BA, Auckland N (2002) Performance metrics for robot coverage tasks. In Proceedings of Australasian Conference on Robotics and Automation, vol 27, pp 29.
[27] Sprunk C, Röwekämper J, Parent G, Spinello L, Tipaldi GD, Burgard W, Jalobeanu M (2014) An Experimental Protocol for Benchmarking Robotic Indoor Navigation. In Proceedings of the International Symposium on Experimental Robotics (ISER).
[28] Ioan S, Kavraki LE (2010) On the implementation of single-query sampling-based motion planners. In Proceedings of the 2010 IEEE International Conference on Robotics and Automation, pp 2005-2011. http://dx.doi.org/10.1109/ROBOT.2010.5509172
[29] Bonsignorio F, Hallam J, del Pobil A (2009) Defining the requisites of a replicable robotics experiment. RSS2009 Workshop on Good Experimental Methodologies in Robotics (Seattle, WA).
[30] Jacoff A, Messina E, Weiss BA, Tadokoro S, Nakagawa Y (2003) Test arenas and performance metrics for urban search and rescue robots. In Proceedings of the 2003 IEEE/RSJ International Conference on Intelligent Robots and Systems, vol 3393, pp 3396-3403. http://dx.doi.org/10.1109/IROS.2003.1249681
[31] Lampe A, Chatila R (2006) Performance measure for the evaluation of mobile robot autonomy. In Proceedings of the 2006 IEEE International Conference on Robotics and Automation, pp 4057-4062. http://dx.doi.org/10.1109/ROBOT.2006.1642325
[32] Steinfeld A, Fong T, Kaber D, Lewis M, Scholtz J, Schultz A, Goodrich M (2006) Common metrics for human-robot interaction. In Proceedings of the 1st ACM SIGCHI/SIGART Conference on Human-robot Interaction, pp 33-40.
[33] Canfield SL, Langley D, Shibakov A (2013) Developing Metrics for Comparison of Mobile Robots Performing Welding Tasks. In Proceedings of the ASME 2013 International Design Engineering Technical Conferences and Computers and Information in Engineering Conference (Portland, Oregon).
[34] Eastman R, Hong T, Shi J, Hanning T, Muralikrishnan B, Young S, Chang T (2010) Performance Evaluation and Metrics for Perception in Intelligent Manufacturing. Performance Evaluation and Benchmarking of Intelligent Systems, eds Madhavan R, Tunstel E, Messina E (Springer US), pp 269-310.
[35] Ilnicki R, Zadarnowska K (2009) Efficiency of double nonholonomic mobile manipulators. In Proceedings of the 14th International Conference on Methods and Models in Automation and Robotics, vol 14, pp 641-646. http://dx.doi.org/10.3182/20090819-3-PL-3002.00111
[36] Shiakolas PS, Conrad KL, Yih TC (2002) On the Accuracy, Repeatability, and Degree of Influence of Kinematics Parameters for Industrial Robots. International Journal of Modelling and Simulation 22(4):245-254. http://dx.doi.org/10.1080/02286203.2002.11442246
[37] MasterCal, http://www.americanrobot.com/products_mastercal.html, 2005.
[38] C B. Atcheson, F. Heide, and W. Heidrich, "CALTag: High Precision Fiducial Markers for Camera Calibration," Vision, Modeling, and Visualization, 2010.

[39] Dainis A, Juberts M (1985) “Accurate remote measurement of robot trajectory motion”. Proceedings 1985 IEEE International Conference on Robotics and Automation, pp 92-99. http://dx.doi.org/10.1109/ROBOT.1985.1087317
[40] Jose Mauricio, S. T. Motta, “Robot Calibration: Modeling Measurement and Applications,” Industrial Robotics: Programming, Simulation and Applications, Low Kin Huat (Ed.), ISBN: 3-86611-286-6, InTech, 2006
[41] K. Lau, R. Hocken and L. Haynes, "Robot performance measurements using automatic laser tracking techniques." Robotics and computer-integrated manufacturing 2, no. 3, pp 227-236, 1985.
[42] Kevin L. Conrad, Panayiotis S. Shiakolas, T. C. Yih, “Robotic Calibration Issues: Accuracy, Repeatability, and Calibration,” Proceedings of the 8th Mediterranean Conference on Control & Automation (MED 2000), Rio, Patras, Greece, 17-19 July 2000.
[43] Gerent J, Hong D, Duportal T, Granger R, inventors; Hexagon Metrology, Inc., assignee. Portable coordinate measurement machine. United States patent US D599,226. 2009 Sep 1.
[44] ISO 9283:1998 Manipulating industrial robots - Performance criteria and related test methods, www.iso.org.
[45] Choi JP, Min BK, Lee SJ (2004) Reduction of machining errors of a three-axis machine tool by on-machine measurement and error compensation system. J Mater Process Tech 155:2056-2064. http://dx.doi.org/10.1016/j.jmatprotec.2004.04.402
[46] Liu H, Darabi H, Banerjee P, Liu J (2007) Survey of Wireless Indoor Positioning Techniques and Systems. IEEE Transactions on Systems, Man, and Cybernetics, Part C (Applications and Reviews) 37(6):1067-1080. http://dx.doi.org/10.1109/TSMCC.2007.905750
[47] Angeles J, Park FC (2008) Performance Evaluation and Design Criteria. Springer Handbook of Robotics, eds Siciliano B, Khatib O (Springer Berlin Heidelberg, Berlin, Heidelberg), pp 229-244.
[48] ASTM E2919-14 (2014) Standard Test Method for Evaluating the Performance of Systems that Measure Static, Six Degrees of Freedom (6DOF), Pose, ASTM International, West Conshohocken, PA. http://dx.doi.org/10.1520/E2919-14
[49] ASTM WK49831 (2015) Standard Test Method for Evaluating the Performance of Systems that Measure Static and Dynamic, Six Degrees of Freedom (6DOF), Pose Working Document.
[50] Bostelman R, Falco J, Hong T (2015). “Performance Measurements of Motion Capture Systems used for AGV and Robot Arm Evaluation”. 6th Computer Vision in Vehicle Technology Workshop (CVVT) at CVPR 2015 (Boston, MA).
[51] Virtual Reality Design Lab, University of Minnesota, http://vr.design.umn.edu/technology/, 2015.
[52] Murray D, Basu A (1994) “Motion tracking with an active camera”. IEEE Transactions on Pattern Analysis and Machine Intelligence 16(5):449-459. http://dx.doi.org/10.1109/34.291452
[53] Foxlin E (2002) “Motion tracking requirements and technologies”. Handbook of virtual environment technology 8:163-210.
[54] Foxlin EM (2001, 2008) Motion tracking system. (U.S. Patent 6,176,837, US Patent 7,395,181).
[55] Prenninger JP (1993) Contactless position and orientation measurement of robot end-effectors. In Proceedings of the 1993 IEEE International Conference on Robotics and Automation, vol 181, pp 180-185. http://dx.doi.org/10.1109/ROBOT.1993.291980
[56] Estler WT, Edmundson KL, Peggs GN, Parker DH (2002) Large-Scale Metrology – An Update. CIRP Annals - Manufacturing Technology 51(2):587-609. http://dx.doi.org/10.1016/S0007-8506(07)61702-8
[57] Qiao H (2015) Advanced Sensing, Automation, and Manufacturing Information Integration, Automated Precision, Inc. Lecture at the National Institute of Standards and Technology (Gaithersburg, MD).
[58] Mayer JRR, Parker GA (1994) A portable instrument for 3-D dynamic robot measurements using triangulation and laser tracking. IEEE Transactions on Robotics and Automation 10(4):504-516. http://dx.doi.org/10.1109/70.313100
[59] Slamani M, Nubiola A, Bonev I (2012) Assessment of the positioning performance of an industrial robot. Ind Robot 39(1):57-68. http://dx.doi.org/10.1108/01439911211192501

[60] Tso SK, Wang TW, Xu WL, Sun ZQ (2003) Vibration control for a flexible-link robot arm with deflection feedback. Int J Nonlin Mech 38(1):51-62. http://dx.doi.org/10.1016/S0020-7462(01)00040-3
[61] Schmitt R, Nisch S, Schönberg A, Demeester F, Renders S (2010) Performance evaluation of iGPS for industrial applications. In Proceedings of the 2010 International Conference on Indoor Positioning and Indoor Navigation, pp 1-8. http://dx.doi.org/10.1109/IPIN.2010.5647630
[62] Nikon Metrology (2014) iGPS System. http://www.nikonmetrology.com/en_US/Products/Large-Volume-Applications/iGPS/iGPS/(key_features)
[63] National Institute of Standards and Technology (NIST) Robotic Systems for Smart Manufacturing Program, https://www.nist.gov/programs-projects/robotic-systems-smart-manufacturing-program, accessed February 8, 2017.
[64] K. Zadarnowska and K. Tchoń, "Kinematic Motion Patterns of Mobile Manipulators." In Robot Motion and Control 2007, pp. 209-217. Springer London, 2007.
[65] Roger Bostelman, Tsai Hong, and Jeremy Marvel, "Survey of Research for Performance Measurement of Mobile Manipulators", Volume 121 (2016) Journal of Research of the National Institute of Standards and Technology, http://dx.doi.org/10.6028/jres.121.015, 2016.
[66] D. Katz, E. Horrell, Y. Yang, B. Burns, T. Buckley, A. Grishkan, V. Zhylkovskyy, O. Brock, and E. Learned-Miller, "The UMass mobile manipulator UMan: An experimental platform for autonomous mobile manipulation." Workshop on Manipulation in Human Environments, at Robotics: Science and Systems, 2006.
[67] O. Madsen, S. Bogh, C. Schou, R. S. Andersen, J. S. Damgaard, M. R. Pedersen and V. Kruger, "Integration of Mobile Manipulators in an Industrial Production," Ind. Rob.: An Int. J., vol. 42, 201, 18 December 2014.
[68] M. Hvilshøj and S. Bøgh, "Little Helper," An Autonomous Industrial Mobile Manipulator Concept. International Journal of Advanced Robotic Systems, 8(2), pp.80-90, 2011.
[69] C. Caroe, K. Hvilshoj and C. Schou, "Rotor Shaft Assembly using the KUKA LWR," http://www.youtube.com, 2012.
[70] C. Flannigan, "Mobile Manipulation Robotics & Automation Engineering," Southwest Research Institute, http://www.swri.org/4org/d10/msd/automation/mobile-manipulator.htm, 2012.
[71] Y. Chen, L. Liu, M. Zhang and H. Rong, "Study on coordinated control and hardware system of a mobile manipulator," In Intelligent Control and Automation, 2006. WCICA 2006. The Sixth World Congress on, vol. 2, pp. 9037-9041. IEEE, 2006.
[72] L Peterson, D Austin, D Kragic, "High-level control of a mobile manipulator for door opening," IEEE/RSJ International Conference on Intelligent Robots and Systems (IROS), Volume:3, Takamatsu, 2000.
[73] K. Nagatani and S. Yuta, "Designing strategy and implementation of mobile manipulator control system for opening door." In Robotics and Automation, 1996. Proceedings., IEEE International Conference on, vol. 3, pp. 2828-2834. IEEE, 1996.
[74] S. Chitta, B. Cohen, and M. Likhachev. "Planning for autonomous door opening with a mobile manipulator." In Robotics and Automation (ICRA), IEEE International Conference on, pp. 1799-1806, 2010.
[75] F. Pin and J.Culioli, "Optimal positioning of combined mobile platform-manipulator systems for material handling tasks," Journal of intelligent and Robotic Systems 6, no. 2-3: 165-182, 1992.
[76] J. Advait and C. Kemp, "EL-E: an assistive mobile manipulator that autonomously fetches objects from flat surfaces." Autonomous Robots 28, no. 1: 45-64, 2010.
[77] A. Agah and K. Tanie, "Human interaction with a service robot: Mobile-manipulator handing over an object to a human," In Robotics and Automation, Proceedings IEEE International Conference on, vol. 1, pp. 575-580. IEEE, 1997.
[78] T. Tomizawa, A. Ohya and S. Yuta, "Remote book browsing system using a mobile manipulator," In Robotics and Automation, 2003. Proceedings. ICRA'03. IEEE International Conference on, vol. 1, pp. 256-261. IEEE, 2003.

[79] L. Bort and A. P. del Pobil, "Using speech to guide a mobile robot manipulator," In Systems, Man, and Cybernetics, 2000 IEEE International Conference on, vol. 4, pp. 2356-2361. IEEE, 2000.
[80] R. Holmberg and O. Khatib, "Development and control of a holonomic mobile robot for mobile manipulation tasks," The International Journal of Robotics Research 19, no. 11: 1066-1074, 2000.
[81] O. Khatib, K. Yokoi, K. Chang, D. Ruspini, R. Holmberg and A. Casal, "Vehicle/Arm Coordination and Multiple Mobile Manipulator Decentralized Cooperation," Proceedings of the 1996 IEEE/RSJ International Conf. on Intelligent Robots and Systems (IROS) '96, Osaka, Japan, November 1996.
[82] O. Khatib , K. Yokoi , K. Chang , D. Ruspini , R. Holmberg , A. Casal and A. Baader, "Force Strategies for Cooperative Tasks in Multiple Mobile Manipulation Systems," Int. Symp. of Robotics Research, Munich, October 1995.
[83] H. Osumi, M. Terasawa and H. Jojiri, "Cooperative control of multiple mobile manipulators on uneven ground," Proc. IEEE Int. Conf. On Robotics and Automation, pp.3198-3203, 1998.
[84] T. Sugar and V. Kumar, "Decentralized control of cooperating mobile manipulators," Proc. IEEE Int. Conf. On Robotics and Automation, pp.2916-2921, 1998.
[85] A. Stroupe, T. Huntsberger, A. Okon, H. Aghazarian and M. Robinson, "Behavior-based multi-robot collaboration for autonomous construction tasks," Proc. IEEE/RSJ Int. Conf. Intell. Rob. Syst., 2005, pp. 1495-1500.
[86] J. Gardner and S.Velinsky, "Kinematics of mobile manipulators and implications for design," Journal of Robotic Systems 17, no. 6: 309-320, 2000.
[87] E. Papadopoulos and J. Poulakakis, "Planning and Model-Based Control for Mobile Manipulators," IROS 2000 Conference on Intelligent Robots and Systems, Takamatsu, Japan, 2000.
[88] J.. Kim, W. K. Chung, Y. Youm and B. H. Lee, "Real-time ZMP compensation method using motion for mobile manipulators," ICRA vol. 2, pp. 1967-1972. IEEE, 2002.
[89] K. Nagatani, T. Hirayama, A. Gofuku and Y. Tanaka, "Motion planning for mobile manipulator with keeping manipulability", IEEE/RSJ International Conference on Intelligent Robots and Systems, Lausanne, Switzerland, October 2002. DOI: 10.1109/IRDS.2002.1043994
[90] M. Mailah, E. Pitowarno and H. Jamaluddin, "Robust motion control for mobile manipulator using resolved acceleration and proportional-integral active force control," arXiv preprint cs/0601057, 2006.
[91] M. W. Chen and A. M. S. Zalzala, "Dynamic modelling and genetic-based trajectory generation for non-holonomic mobile manipulators," Control Engineering Practice 5, no. 1, pp 39-48, 1997.
[92] H. G., Tanner, and K. J. Kyriakopoulos, "Mobile manipulator modeling with Kane's approach." Robotica 19, no. 06, pp 675-690, 2001.
[93] A. Mohri, S. Furuno, and M. Yamamoto, "Trajectory planning of mobile manipulator with end-effector's specified path," In Intelligent Robots and Systems, 2001. Proceedings. 2001 IEEE/RSJ International Conference on, vol. 4, pp. 2264-2269, 2001.
[94] D. H. Shin, B. S. Hamner, S. Singh and M. Hwangbo, "Motion planning for a mobile manipulator with imprecise locomotion," In Intelligent Robots and Systems, 2003.(IROS 2003). Proceedings. 2003 IEEE/RSJ International Conference on, vol. 1, pp. 847-853. IEEE, 2003.
[95] C. P. Tang, P. T. Miller, V. N. Krovi, J.-C. Ryu and S. K. Agrawal. "Differential-flatness-based planning and control of a wheeled mobile manipulator—Theory and experiment," Mechatronics, IEEE/ASME Transactions on 16, no. 4: 768-773, 2011.
[96] Y. Yamamoto and X. Yun, "Coordinating locomotion and manipulation of a mobile manipulator," Proceedings of the 31st IEEE Conference on Decision and Control, Tucson, AZ, 1992.
[97] M. Chen and A. Zalzala, "A genetic approach to motion planning of redundant mobile manipulator systems considering safety and configuration," Journal of Robotic Systems, Volume 14, Issue 7, pages 529–544, July 1997.
[98] F. G., Pin, J. C. Culioli, and D. B. Reister, "Using minimax approaches to plan optimal task commutation configurations for combined mobile platform-manipulator systems," Robotics and Automation, IEEE Transactions on 10, no. 1: 44-54, 1994.
[99] J.-K. Lee, and H. S. Cho, "Mobile manipulator motion planning for multiple tasks using global optimization approach," Journal of Intelligent and Robotic Systems 18, no. 2: 169-190, 1997.

[100]S. Dubowsky and E. Vance, “Planning mobile manipulator motions considering vehicle dynamic stability constraints,” Proceedings IEEE International Conference on Robotics and Automation, Scottsdale, AZ14-19 May 1989.
[101]S. Dubowski, P-Y. Gu and J. F. Deck, “The dynamic analysis of flexibility in mobile robotic manipulator systems,” Proceeding of the Eighth World Congress on the Theory of Machines and Mechanisms, page , Prague, Czechoslovakia, August 1991.
[102]Q. Huang, S. Sugano and I. Kato, "Stability control for a mobile manipulator using a potential method," Proceedings of the IEEE/RSJ/GI International Conference on, vol. 2, pp. 839-846. IEEE, 1994.
[103]Q. Huang and S. Sugano, “Manipulator motion planning for stabilizing a mobile-manipulator,” IEEE/RSJ International Conference, Vol. 3, pp. 467-472, 1995.
[104]Huang Q, Sugano S, “Motion planning of stabilization and cooperation of a mobile manipulator-vehicle motion planning of a mobile manipulator,” Proceedings of the 1996 IEEE/RSJ International Conference (Vol. 2, pp. 568-575). IEEE, 1996.
[105]S. Sugano, Q. Huang and I. Kato, “Stability criteria in controlling mobile robotic systems,” Proceedings of the 1993 IEEE/RSJ International Conferenc, July 1993.
[106]Q. Huang, S. Sugano and K. Tanie, “Motion planning for a mobile manipulator considering stability and task constraints,” InRobotics and Automation, 1998. Proceedings. 1998 IEEE International Conference, 1998.
[107]Q. Huang Q, K. Tanie and S. Sugano, “Stability compensation of a mobile manipulator by manipulator motion: feasibility and planning,” Advanced robotics, 1998.
[108]Q. Huang, K. Tanie and S. Sugano, “Coordinated motion planning for a mobile manipulator considering stability and manipulation,” International Journal of Robotics Research, vol. 19, no. 8, pp 732-742, August 2000.
[109]F. Inoue, T. Muralami, and K. Ihnishi, "A motion control of mobile manipulator with external force," Mechatronics, IEEE/ASME Transactions on 6, no. 2: 137-142, 2001.
[110]S. Furuno, M. Yamamoto and A. Mohri, “Trajectory planning of mobile manipulator with stability considerations,” Proceedings IEEE International Conference on Robotics and Automation, (ICRA) 2003.
[111]T. Shibata, and T. Murakami, "A Null Space Control of Two Wheels Driven Mobile Manipulator Using Passivity Theory," IEEJ Transactions on Industry Applications 127, 1109-1116, 2007.
[112]E. G., Papadopoulos, and D. A. Rey, "A new measure of tipover stability margin for mobile manipulators," In Robotics and Automation, 1996. Proceedings., IEEE International Conference on, vol. 4, pp. 31S11-3116. 1996.
[113]E. Papadopoulos, and D. A. Rey, "The force-angle measure of tipover stability margin for mobile manipulators," Vehicle System Dynamics 33, no. 1: 29-48, 2000.
[114]B. J. Thibodeau, P. Deegan, and R. Grupen, "Static analysis of contact forces with a mobile manipulator," Proceedings IEEE International Conference on Robotics and Automation, ICRA., pp. 4007-4012. 2006.
[115]O. Khatib, "Real-time obstacle avoidance for manipulators and mobile robots," The International Journal of Robotics Research 5, no. 1, pp 90-98, 1986.
[116]Y. Yamamoto and Xiaoping Yun, "Coordinated obstacle avoidance of a mobile manipulator," Proceedings IEEE International Conference on Robotics and Automation, vol. 3, pp. 2255-2260. 1995.
[117]Y. Yamamoto and S. Fukuda, "Trajectory planning of multiple mobile manipulators with collision avoidance capability," Proc. IEEE Int’l Conf. on Robotics and Automation, ICRA, vol. 4, pp. 3565-3570. IEEE, 2002.
[118]W. Nowak, A. Zakharov, S. Blumenthal, and E. Prassler, "Benchmarks for mobile manipulation and robust obstacle avoidance and navigation," BRICs Deliverable, 2010.
[119]N.A.M. Hootsmans, S. Dubowsky and P.Z. Mo, “The experimental performance of a mobile manipulator control algorithm,” Proceedings, IEEE International Conference Robotics and Automation, 12-14 May 1992.

[120]H. Najjaran and A. Goldenberg, "Real-time motion planning of an autonomous mobile manipulator using a fuzzy adaptive Kalman filter," Robotics and Autonomous Systems 55, no. 2: 96-106, 2007.
[121]P. Wells, D. Deguire, “TALON: a universal unmanned ground vehicle platform, enabling the mission to be the focus,” Proc. SPIE 5804, Unmanned Ground Vehicle Technology VII, 747, June 02, 2005.
[122]Y. Yang and O. Brock, “Elastic roadmaps: Globally task-consistent motion for autonomous mobile manipulation,” In Proceedings of Robotics: Science and Systems (RSS), Philadelphia, USA, August 2006.
[123]T. J. Graettinger, and B. H. Krogh, "The acceleration radius: a global performance measure for robotic manipulators," Robotics and Automation, IEEE Journal of 4, no. 1: 60-69, 1988.
[124]J. H. Chung and S. A. Velinsky, "Modeling and control of a mobile manipulator," Robotica 16, no. 06 (1998): 607-613.
[125]K. Watanabe, K. Sato, K. Izumi and Y. Kunitake, "Analysis and control for an omnidirectional mobile manipulator," Journal of Intelligent and Robotic Systems 27, no. 1-2: 3-20, 2000.
[126]J. B. Mbede, P. Ele, C.-M. M. Abia, Y. Toure, V. Graefe, and S. Ma. "Intelligent mobile manipulator navigation using adaptive neuro-fuzzy systemsm," Information Sciences 171, no. 4: 447-474, 2005.
[127]M. H. Korayem and H. Ghariblu, "Analysis of wheeled mobile flexible manipulator dynamic motions with maximum load carrying capacities." Robotics and Autonomous Systems 48, no. 2, pp 63-76, 2004.
[128]A.Y. Elatta, Li Pei Gen, Fan Liang Zhi, Yu Daoyuan and Luo Fei, “An Overview of Robot Calibration,” Information Technology Journal 3 (1): 74-78, ISSN Asian Network for Scientific Information 1682-6027, 2004.
[129]F. Hidalgo and P. Brunn, "Robot metrology and calibration systems-a market review." Industrial Robot: An International Journal 25, no. 1: 42-47, 1998.
[130]B. Greenway, "Robot accuracy." Industrial Robot: An International Journal 27, no. 4, pp257-265, 2000.
[131]NIST Robot Calibrator, http://www.nist.gov/el/isd/robot-calibrator.cfm, August 25, 2011.
[132]M. R., Driels and W. E. Swayze. "Automated partial pose measurement system for manipulator calibration experiments." Robotics and Automation, IEEE Transactions on 10, no. 4 (1994): 430-440.
[133]V. Pradeep, K. Konolige and E. Berger, “Calibrating a multi-arm multi-sensor robot: A Bundle Adjustment Approach,” 12th International Symposium on Experimental Robotics, Delhi, India, 2010.
[134]H. Zhuang, K. Wang and Z. S. Roth, "Simultaneous calibration of a robot and a hand-mounted camera." IEEE Transactions on Robotics and Automation, 11, no. 5: 649-660, 1995.
[135]B. Preising and T. C. Hisa, "Robot performance measurement and calibration using a 3D computer vision system." Robotica 13, no. 04, pp 327-337, 1995.
[136]International Organization of Standardization, ISO 10218-1. Robots and robotic devices – Safety requirements – Part 1 and Robots, ISO 10218-2. Robots and robotic devices – Safety requirements – Part 2: Industrial robot sys-tems and integration, 2011.
[137]ANSI/RIA R15.06, American National Standard for Industrial Robots and Robot Systems- Safety Requirements, 2012.
[138]Industrial Truck Standards Development Foundation, ANSI/ITSDF B56.5-2012, Safety Standard for Driverless, Automatic Guided Industrial Vehicles and Automated Functions of Manned Industrial Vehicles, 2012.
[139]European Standards, BS EN1525: Safety of industrial trucks. Driverless trucks and their systems, 1998.
[140]ANSI/RIA R15.05. Evaluation of Point-to-Point and Static Performance Characteristics of Industrial Robots and Robot Systems. 1999.
[141]ASTM F45: 2014 Driverless Automatic Industrial Vehicles, www.astm.org, January 2015.
[142]J. Marvel and R. Bostelman, “Towards Mobile Manipulator Safety Standards,” Proceedings of the IEEE International Symposium on RObotic and Sensors Environments (ROSE), October 2013.
[143]R. Bostelman and J. Marvel, “Control fusion for safe multi-robot coordination,” Proc. SPIE 9121, Multisensor, Multisource Information Fusion: Architectures, Algorithms, and Applications 2014, May 22, 2014.
[144]A. Bowling and O. Khatib, "The dynamic capability equations: a new tool for analyzing robotic manipulator performance." IEEE Transactions on Robotics, 21, no. 1: 115-123, 2005.

[145]K.-T. Park, C.-H. Park and Y.-J. Shin, “Performance Evaluation of Industrial Dual-Arm Robot,” International Conference on Smart Manufacturing Application, KINTEX, Gyeonggi-do, Korea, April. 9-11, 2008,
[146]S. Balakirsky, C.Scrapper, S. Carpin and M. Lewis, "USARSim: providing a framework for multi-robot performance evaluation." In Proceedings of PerMIS, vol. 2006.
[147]D. Calisi and D. Nardi, “Performance evaluation of pure-motion tasks for mobile robots with respect to world models,” Auton Robot, Vol 27: 465–481, 2009.
[148]J. Baltes, “A Benchmark Suite for Mobile Robots,” Proceedings of the 2000 IEEE/RSJ International Conference on lntelligent Robots and Systems, 2000.
[149]N. M. Ceballos, J. Valencia and A. A. Giraldo, “Simulation and Assessment Educational Framework for Mobile Robot Algorithms,” Journal of Automation, Mobile Robotics & Intelligent Systems, Vol. 8, No. 1, 2014.
[150]Duckett, Tom and Ulrich Nehmzow. "Mobile robot self-localisation and measurement of performance in middle-scale environments." Robotics and Autonomous Systems 24, no. 1, pp 57-69, 1998.
[151]R. Bostelman, E. Messina and P. Picariello, “Towards Development of an Automated Guided Vehicle Intelligence Level Performance Standard,” to appear in *Autonomous Industrial Vehicles: From the Laboratory to the Factory Floor*, ASTM Selected Technical Publication 1595, ASTM International, 2016.
[152]RoCKIn Competition, http://rockinrobotchallenge.eu/index.php, 2013 RoCKIn project, European Union contract no. FP7-ICT-601012, 2013
[153] “Robots for the Battlefield: 12 Finalists in Worldwide Competition Go for the Prize in 2010,” http://www.robotics.org/, November 2009.
[154]Y. Yamamoto and X. Yun. "Modeling and compensation of the dynamic interaction of a mobile manipulator." Proceedings IEEE International Conference on Robotics and Automation, pp. 2187-2192. 1994.
[155]K. Zadarnowska and K. Tchoń, "A control theory framework for performance evaluation of mobile manipulators," Robotica 25, no. 06: 703-715, 2007.
[156]Object Management Group Systems Modeling Language (OMG SysML) Tutorial, http://www.omgsysml.org/INCOSE-OMGSysML-Tutorial-Final-090901.pdf, September, 2009, accessed December 19, 2016.
[157]John R. Palmer, Michael E. Crow, Ronald S. Carson, “Model-Based Systems Engineering without SysML”, Boeing presentation to National Defense Industrial Association Systems Engineering Conference, October 24-27, 2011, accessed December 19, 2016.
[158]Mohd Azizi Abdul Rahman, Katsuhiro Mayama, Takahiro Takasu, Akira Yasuda, and Makoto Mizukawa. “Model-driven development of intelligent mobile robot using systems modeling language (SysML).” In Mobile Robots - Control Architectures, Bio-Interfacing, Navigation, Multi Robot Motion Planning and Operator Training. InTech, 2011.
[159]Roger Bostelman, Sebti Foufou, Tsai Hong, “Modeling Performance Measurement of Mobile Manipulators” 7th Annual IEEE Int. Conf. on CYBER Technology in Automation, Control, and Intelligent Systems, Waikiki, HA, July 31-August 4, 2017.
[160]Roger Bostelman, Sebti Foufou, Tsai Hong, Mili Shah, “"Model of Mobile Manipulator Performance Measurement using SysML", Journal of Intelligent & Robotic Systems, in-process, April 5, 2017.
[161]Warren WH, Kay BA, Zosh WD, Duchon AP, Sahuc S. Optic flow is used to control human walking. Nature neuroscience. 2001 Feb 1;4(2):213-6.
[162]OptiTrack for Movement Sciences, http://www.optitrack.com/motion-capture-movement-sciences/, 2016.
[163]Bostelman, R., Falco, J., Shah, M. and Hong, T., “Dynamic Metrology Performance Measurement of a Six Degree-of-Freedom Tracking System Used in Smart Manufacturing”, ASTM International STP1594: Autonomous Industrial Vehicles: From the Laboratory to the Factory Floor, R. Bostelman and E. Messina, Eds., Ch. 7, pp. 91-105, 2016.

[164]Shackleford, W., Cheok, G., Hong, T-H, Saidi, K., and Shneier, M., "Performance Evaluation of Human Detection Systems for Robot Safety," Journal of Intelligent & Robotic Systems, Jan. 2016.
[165]IBIS World, "Motion Capture Software Developers in the US: Market Research Report", 2014.
[166]Moeslund, T. B., Hilton, A, and Krüger, V.,"A survey of advances in vision-based human motion capture and analysis," Computer Vision and Image Understanding, vol. 104, no. 2, 2006.
[167]Field, M., Stirling, D., Naghdy, F., Pan, Z., "Motion Capture in Robotics Review," 6th IEEE International Conference on Control &Automation, New Zealand, Dec 2009.
[168]Roger Bostelman, Joe Falco, Tsai Hong, "Performance Measurements of Motion Capture Systems used for AGV and Robot Arm Evaluation", Editors: Roger Bostelman, Elena Messina, "Autonomous Industrial Vehicles: From the Laboratory to the Factory Floor", STP1594, Book Chapter 7, May 2016.
[169]Roger Bostelman, Sebti Foufou, Tsai Hong, Mili Shah, "Dynamic Metrology and ASTM E57.02 Dynamic Measurement Standard", Journal of the Coordinate Metrology Society 2016, June 2017.
[170]R. Bostelman, T. Hong, and J. Marvel, "Performance Measurement of Mobile Manipulators", SPIE 2015, Multisensor, Multisource Information Fusion: Architectures, Algorithms, and Applications, Baltimore, MD, Vol. 9498, pp. 1-9, April 2015.
[171]R. Bostelman, T. Hong, and S. Legowik, "Mobile Robot and Mobile Manipulator Research Towards ASTM Standards Development", SPIE 2016, Baltimore, MD, pp. 98720F-98720F, 2016.
[172]R. Bostelman, S. Foufou, S. Legowik, and T. Hong "Mobile Manipulator Performance Measurement Towards Manufacturing Assembly Tasks", 13th IFIP International Conference on Product Lifecycle Management (PLM16), Columbia, SC, July 11-13, Vol. 9892, pp. F1-F10, 2016.
[173]NaturalPoint, https://www.naturalpoint.com/, accessed May 2017.
[174]ASTM E3064 Standard Test Method for Evaluating the Performance of Optical Tracking Systems that Measure Six Degrees of Freedom (6DOF) Pose, www.astm.org, 2016.
[175]Taylor, B. N., and C. E. Kuyatt. "Guidelines for Evaluating and Expressing the Uncertainty of NIST Measurement Results", NIST Technical Note 1297, National Institute of Standards and Technology, Gaithersburg, MD. (1994).
[176]Burge, James H., Peng Su, Chunyu Zhao, and Tom Zobrist. "Use of a commercial laser tracker for optical alignment." In Optical Engineering+ Applications, pp. 66760E-66760E. International Society for Optics and Photonics, 2007.
[177]Nelson, David; Munoz Ceballos; Jaime Alejandro Valencia; and Nelson Londono Ospina (2010). "Quantitative Performance Metrics for Mobile Robots Navigation," Mobile Robots Navigation, Alejandra Barrera (Ed.), ISBN: 978-953-307-076-6, InTech.
[178]Khatib, O. (1986). "Real-Time Obstacle Avoidance for Manipulators and Mobile Robots," Journal of Robotics Research, Vol. 5, pp. 90-98.
[179]Krogh, B.H. & Thorpe, C.E. (1986). "Integrated Path Planning and Dynamic Steering control for Autonomous Vehicles," Proceedings of IEEE International Conference on Robotics and Automation, San Francisco, CA, pp. 1664–1669.
[180]Borenstein, J. & Koren, Y. (1991). "The Vector Field Histogram–Fast Obstacle Avoidance for Mobile Robots," Proceedings of IEEE Transactions on Robotics and Automation, pp. 278– 288.
[181]Quinlan, S. & Khatib, O. (1993). "Elastic Bands: Connecting Path Planning and Control," Proceedings of IEEE International Conference on Robotics and Automation, Vol. 2, pp. 802–807, Atlanta, GA.
[182]Fox, D., Burgard, W. & Thrun, S. (1997). "The Dynamic Window Approach to Collision Avoidance," Proceedings of IEEE Robotics and Automation Magazine. Vol. 4, Num. 1, 1997.
[183]Simmons, R. (1996). "The Curvature-Velocity Method for Local Obstacle Avoidance," Proceedings of IEEE International Conference on Robotics and Automation, pp. 3375– 3382, Minneapolis, MN.
[184]Minguez, J., Osuna, J. & Montano, L. (2004). "A Divide and Conquer Strategy to Achieve Reactive Collision Avoidance in Troublesome Scenarios," Proceedings of IEEE International Conference on Robotics and Automation, Minneapolis, MN.
[185]Minguez, J. (2008). "Robot Obstacle Avoidance Papers Using Experiments, In: Good experimental methodology guidelines, Bonsignorio, F.; Hallam J., & del Pobil, A. P. (Ed), Special Interest Group on

Good Experimental Methodology in Robotics European Robotics Research Network (EURON), Tech. Rep., 2008.
[186] Dae Hee Won, Sebum Chun, Sangkyung Sung, Taesam Kang and Young Jae Lee, (2008) "Improving Mobile Robot Navigation Performance using Vision based SLAM and Distributed Filters," Int'l Conf. on Control, Automation and Systems 2008, Oct. 14-17, Korea
[187] Troy Gray, Daniel Orf, Greg Adams, "Mobile Automated Robotic Drilling, Inspection, and Fastening," SAE International, https://www.electroimpact.com/WhitePapers/2013-01-2338.pdf, 2012.
[188] NAV300 Laser Positioning Sensor, www.sick.com, 2008.
[189] Evans, J. & Messina, E. (2000). "Performance Metrics for Intelligent Systems," Proceeding of the Performance Metrics for intelligent Systems Workshop, August, 2000, Gaithersburg, MD.
[190] Harsha Kikkeri and Gershon Parent and Mihai Jalobeanu and Stan Birchfield, (2014) "An Inexpensive Method for Evaluating the Localization Performance of a Mobile Robot Navigation System," Proc. IEEE Int'l Conf. on Robotics and Automation (ICRA), May 2014.
[191] Hui-Min Huang, Kerry Pavek, Mark Ragon, Jeffry Jones, Elena Messina, James Albus; "Characterizing unmanned system autonomy: contextual autonomous capability and level of autonomy analyses". Proc. SPIE 6561, Unmanned Systems Technology IX, 65611N, May 02, 2007.
[192] Roger Bostelman, Will Shackleford, "Obstacle Detection and Avoidance from an Industrial Automatic Guided Vehicle," IROS 2014.
[193] ASTM International, Committee F45 on Driverless Automatic Guided Industrial Vehicles, www.astm.org/COMMITTEE/F45.htm, 2014.
[194] NDC8 AGV Control System, http://www.kollmorgen.com/en-us/products/vehicle-controls/electrical-vehicle-controls/ndc8/, 2015.
[195] Total Station – Wikipedia, https://en.wikipedia.org/wiki/Total_station, accessed June 2017.
[196] Steven Legowik, Roger Bostelman, Tsai Hong, Elena Messina, "Guideline for Automatic Guided Vehicle Calibration", NIST Interagency/Internal Report (NISTIR) 8168, February 2017.
[197] Jeremy A. Marvel, Elena Messina, Brian Antonishek, Karl Van Wyk, and Lisa Jean Fronczek, "Tools for Robotics in SME Workcells: Challenges and Approaches for Calibration and Registration," NISTIR 8093, 2015.
[198] Johann Borenstein, Hobart R. Everett, Liqiang Feng, and David Wehe, "Mobile Robot Positioning -- Sensors and Techniques," Invited Paper for the Journal of Robotic Systems, Special Issue On Mobile Robots. 1997 Vol. 14 No. 4, pp. 231 – 249, 1997.
[199] L. Ailes, M. D. Keitz, S. L. McCulley, S. Y. Seidel, M. Deisenroth, and T. S. Rappaport, "Development of an Autonomous Guided Vehicle for Indoor Propagation Measurements", IEEE VTC 90, May 7, Orlando, FL
[200] T. J. W. Bentvelsen, "On Calibration of Model AGVs", Report number 2015.TEL.7946, Faculty Mechanical, Maritime and Materials Engineering, Delft University of Technology, Delft, Netherlands, June 23, 2015.
[201] Eliana P. L. Aude, Ernesto P. Lopes, Julio T. C. Silveira, and Henrique Serdeira, "CONTROLAB AGV: Control and Calibration", Multibody Dynamics 2007, ECCOMAS Thematic Conference, Milano, Italy, 25-28 June 2007.
[202] Mariolino De Cecco, "Self-Calibration of AGV Inertial-Odometric Navigation Using Absolute-Reference Measurements," IEEE Instrumentation and Measurement, Technology Conference, Anchorage, AK, USA, 21-23 May 2002
[203] Thomas Dall Larsen, Martin Bak, Nils A. Andersen, and Ole Ravn, "Location Estimation for an Autonomously Guided Vehicle using an Augmented Kalman Filter to Autocalibrate the Odometry," In FUSION98 SPIE, July 1998.
[204] Mariolino De Cecco, Luca Baglivo, E. Ervas, and E. Marcuzzi, "Asynchronous and Time-Delayed Sensor Fusion of a Laser Scanner Navigation System and Odometry," XVIII IMEKO World Congress, Metrology for a Sustainable Development, Rio de Janeiro, Brazil. pp.17-22, September 2006.

[205] Carlos Garcia-Saura, "Self-calibration of a Differential Wheeled Robot using only a Gyroscope and a Distance Sensor," Imperial College London Department Of Computing, September 2015.
[206] Walter Gander, Gene H. Golub and Rolf Strebel, "Least-Squares Fitting of Circles and Ellipses," BIT Numerical mathematics, Springer, 1994.
[207] S. Agarwal and K. Mierle, "Ceres solver," http://ceres-solver.org [retrieved August, 2016].
[208] Roger Bostelman, Tsai Hong, and Elena Messina, "Intelligence Level Performance Standards Research for Autonomous Vehicles", FinE-R 2015 The Path to Success: Failures in Real Robots Workshop, Intelligent Robot Systems (IROS) 2015, Hamburg, Germany, October 2, 2015
[209] ASTM F45.02 Subcommittee, "Standard Test Method for Navigation: Defined Area", Working Document WK48955, www.astm.org, May 2017.
[210] Adept Lynx Handler-Semi, http://www.adept.com/products/mobile-robots/mobile-transporters/handler-semi/general
[211] TOA SE, Inc., http://toa-se.com/category/news/ , January, 12, 2017, accessed May 2017.
[212] Bostelman R, Falco J, Hong T (2015) Performance Measurements of Motion Capture Systems used for AGV and Robot Arm Evaluation. 6th Computer Vision in Vehicle Technology Workshop (CVVT) at CVPR 2015 (Boston, MA).
[213] Roger Bostelman, Tsai Hong, "Mobile Manipulator Stability Measurements", NIST Technical Note 1955, https://doi.org/10.6028/NIST.TN, February 2017
[214] Universal Robots A/S UR10 User Manual, UR10/CB3, Version 3.0 (rev. 15167), 2014.
[215] F. Dornaika and R. Horaud, "Simultaneous robot-world and hand-eye calibration, "IEEE Transactions on Robotics and Automation, pp.617-622 ,1998.
[216] H. Zhuang, Z. Roth, and R. Sudhakar, "Simultaneous robot/world and tool/flange calibration by solving homogeneous transformation of the form AX = YB," IEEE Trans. Robot. Automat, pp.549-554, 1994.
[217] A. Geiger, F. Moosmann, O. Car, and B. Schuster, "Automatic calibration of range and camera sensors using a single shot," ICRA, pp. 3936-3943 , 2012.
[218] H. S. Alismail, D. Baker, and B. Browning, "Automatic calibration of a range sensor and camera system," Second International Conference on 3D Imaging, Modeling, Processing, Visualization & Transmission. IEEE, pp. 286-292 ,2012.
[219] Z. Zhang, "A flexible new technique for camera calibration," IEEE Transactions on pattern analysis and machine intelligence, pp.1330-1334 , 2000.
[220] J-Y. Bouguet, "Camera calibration toolbox for matlab," < http://www.vision.caltech.edu/bouguetj/calib_doc/> [retrieved August, 2016].
[221] J. Weng, P. Cohen, and M. Herniou. "Camera calibration with distortion models and accuracy evaluation," IEEE Transactions on pattern analysis and machine intelligence 14.10, pp.965-980, 1992.
[222] O. D. Faugeras, Q.-T. Luong, and S. J. Maybank, "Camera self-calibration: Theory and experiments," European conference on computer vision, Springer Berlin Heidelberg, pp. 321-334, 1992.
[223] Y. Huang, X. Qian, and S. Chen, "Multi-sensor calibration through iterative registration and fusion, " Computer-Aided Design, pp.240-255, 2009.
[224] S. Spiess, V. Vincze, and M. Ayromlou, "On the calibration of a 6D laser tracking system for contactless, dynamic robot measurements," Instrumentation and Measurement Technology Conference, pp. 1203-1208 ,1997.
[225] M. Shah, R. D. Eastman, and T. Hong, "An overview of robot-sensor calibration methods for evaluation of perception systems," In Proceedings of the Workshop on Performance Metrics for Intelligent Systems, pp. 15-20, ACM, 2012.

[226] M. Shah, “Solving the Robot-World/Hand-Eye Calibration Problem Using the Kronecker Product,” ASME Journal of Mechanisms and Robotics, Vol. 5, 031007, pp. 1-7, 2013.
[227] M. Shah, R. D. Eastman, and T. Hong, “An overview of robot-sensor calibration methods for evaluation of perception systems,” In Proceedings of the Workshop on Performance Metrics for Intelligent Systems, pp. 15-20, ACM, 2012.
[228] R. Hartley, J. Trumpf, Y. Dai, and H. Li, “Rotation averaging,” International journal of computer vision, 103(3), pp.267-305 , 2013.
[229] F. L. Markley, Y. Cheng, J. L. Crassidis, and Y. Oshman, “Averaging quaternions,” Journal of Guidance, Control, and Dynamics, pp.1193-1197, 2007.
[230] Mili Shah, Steven Legowik, Roger Bostelman, Tsai Hong, “Sensor Calibration of Mobile Manipulators”, Journal of the International Societies for Precision Engineering and Nanotechnology, Submitted June 2017.
[231] K. Strobl, G. Hirzinger, Optimal hand-eye calibration, in: IEEE/RSJ International Conference on Intelligent Robots and Systems, 2006, pp. 4647 – 4653.
[232] Steven Legowik, Roger Bostelman, and Tsai Hong, “Sensor Calibration and Registration for Mobile Manipulators”, The Fifth International Conference on Advances in Vehicular Systems, Technologies and Applications (VEHICULAR 2016), Barcelona, Spain, November 13-17, 2016.
[233] ProMat 2015, Material Handling Ind. of America, Chicago, IL, March 2015.
[234] Modex 2016, Material Handling Ind. of America, Atlanta, GA, April 2016
[235] Jim Camillo, “Moving Ahead With MR. ROAM”, Assembly, http://www.assemblymag.com/blogs/14-assembly-blog/post/90914-moving-ahead-with-mr-roam, February 4, 2013, Accessed May 24, 2017.
[236] Jeremy Marvel, Roger Bostelman, Joe Falco, “Multi-Robot Assembly Strategies and Metrics”, submitted to ACM Transactions on Embedded Computing Systems, December 13, 2016.
[237] R. Andersen, O. Madsen, T. Moeslund, “Hand-Eye of Depth Cameras based on Planar Surfaces”, Abstract from Int’l Workshop on Intell. Robot Assistants, Padova, Italy, 2014.
[238] Wikipedia-Ulam Spiral, https://en.wikipedia.org/wiki/Ulam_spiral, accessed May 2017.
[239] R. Andersen, J. Damgaard, O. Madsen, T. Moeslund, "Fast calibration of industrial mobile robots to workstations using QR codes." 44th Int’l Symp. Robotics (ISR), pp. 1-6. IEEE, 2013.
[240] M. Meggiolaro, G. Scriffignano, S. Dubowsky, “Manipulator Calibration Using A Single Endpoint Contact Constraint”, Proceedings of DETC2000: 2000 ASME Design Engineering Technical Conference, DETC2000/MECH-14129, Baltimore, MD, September 2000.
[241] S. Chatpar, M. Branicky, “Localization for Robotic Assemblies Using Probing and Particle Filtering”, Proc. of the 2005 IEEE/ASME Int’l Conf. on Advanced Intelligent Mechatronics, Monterey, CA, USA, 24-28 July 2005.
[242] Y. Taguchi, T. Marks, J. Hershey, “Entropy-Based Motion Selection for Touch-Based Registration Using Rao-Blackwellized Particle Filtering”, TR2011-067, September 2011.
[243] Roger Bostelman, Roger Eastman, Tsai Hong, Omar Aboul Enein, Steven Legowik, Sebti Foufou, “Comparison of Registration Methods for Mobile Manipulators”, Proceedings Book: “Advances in Cooperative Robotics”, CLAWAR 2016, London, England, UK, September 2016.
[244] M. Mesko, S. Toth, “Laser Spot Detection”, Journal of Information, Control and Management Systems, 11, No. 1 (2013).
[245] A. Krstinic, K. Skein, I. Milatic, “Laser Spot Tracking Based On Modified Circular Hough Transform and Motion Pattern Analysis”, Sensors, 14, 20112-20133; ISSN 1424-8220, (2014).
[246] N. Macias, J. Wen, “Vision guided robotic block stacking”, IEEE/RSJ Int’l Conf. Intelligent Robots and Systems (IROS 2014), pp. 779-784, 2014.

[247] Roger Bostelman, Ya-Shian Li-Baboud, Steve Legowik, Tsai Hong, Sebti Foufou, "Mobile Manipulator Performance Measurement Data", NIST Technical Note 1965, May 2017.
[248] NIST MIDAS, https://inet.nist.gov/nvl/midas-management-institutional-data-assets, accessed May, 2017.
[249] Henry Medeiros, "Stochastic Search methods for Mobile Manipulators", unpublished Interim Report for Grant 70NANB16H196 to Marquette University, August 2016 – July 2017.
[250] ASTM F45.02 Subcommittee, "Standard Test Method for A-UGV Docking", Working Document WK57000, www.astm.org, May 2017.
[251] Roger Bostelman, "Recommendations for Autonomous Industrial Vehicle Performance Standards", Editors: Roger Bostelman, Elena Messina, "Autonomous Industrial Vehicles: From the Laboratory to the Factory Floor", STP1594, Book Chapter 8, May 2016.
[252] Roger Bostelman, Elena Messina, Sebti Foufou, "Cross-Industry Standard Test Method Developments – from Manufacturing to Wearable Robots", Frontiers of Information Technology & Electronic Engineering Journal, Vol. 1998, No.-1, P 1, October 2017.